Sede Amministrativa: Università degli Studi di Padova

Dipartimento di Scienze del Farmaco

SCUOLA DI DOTTORATO DI RICERCA IN BIOLOGIA E MEDICINA DELLA RIGENERAZIONE

CICLO XXVI

MICROTECHNOLOGY-AIDED DIFFERENTIATION OF HUMAN PLURIPOTENT STEM CELLS INTO HEPATOCYTE-LIKE CELLS

Direttore della Scuola: Chiar.ma Prof.ssa Maria Teresa Conconi

Supervisore: Chiar.ma Prof.ssa Annarosa Floreani

Co-supervisore: Dott. Nicola Elvassore

Dottorando: Giovanni Giuseppe Giobbe

Table of contents

SOMMARIO

Vi è un crescente interesse fra la comunità scientifica internazionale, le compagnie farmaceutiche e la ricerca clinica nel trovare delle valide alternative ai modelli standard nello sviluppo di nuove strategie terapeutiche e di processi di scoperta di nuovi farmaci. I ricercatori si basano tuttora sull'utilizzo di linee cellulari immortalizzate, cellule primarie estratte da organi e su modelli animali. Queste metodiche sono valide e largamente utilizzate per scopi generali, ma il più delle volte presentano dei limiti evidenti. Le linee cellulari e cellule primarie spesso non riproducono fedelmente le esatte caratteristiche dei tessuti in vivo, poiché perdono alcune caratteristiche fisiche e funzionali quando sono coltivate in vitro. D'altra parte, i modelli animali sono ancora necessari per lo studio di patologie specifiche e nel test di nuovi composti, ma risultano essere dispendiosi in termini di tempo e denaro e spesso mostrano una scarsa capacità predittiva nei confronti degli effetti sull'uomo. Quindi, le cellule staminali pluripotenti umane rappresentano una valida alternativa ai modelli esistenti, grazie alle loro capacità di essere espanse in vitro indefinitamente e di poter differenziare in tutti i tipi cellulari derivanti dai tre foglietti germinali. Negli ultimi anni l'attenzione si è concentrata sui tessuti ingegnerizzati, differenziati a partire da cellule pluripotenti. Questi hanno la possibilità di trasformare radicalmente il modo in cui studiamo in vitro la fisiologia e la patofisiologia umana. Ciò non di meno, vi sono ancora problemi nei processi di differenziamento di cellule staminali embrionali e pluripotenti indotte umane in vitro. Questo perché si riscontra difficoltà nel dirigere specificamente il destino cellulare verso un determinato tipo cellulare in modo robusto, e per la scarsa riproducibilità delle condizioni fisiologiche in cui questi processi hanno normalmente luogo in vivo. In questo ambito, le nuove micro-tecnologie possono dare un aiuto nell'oltrepassare queste limitazioni, poiché permettono di lavorare in micro-scala in maniera difficilmente riproducibile in condizioni di coltura standard. In questo contesto, lo scopo di questa tesi di dottorato è quello di differenziare efficacemente cellule staminali pluripotenti umane per riuscire ad ottenere rilevanti tipi cellulari, quali cardiomiociti ed epatociti. La strategia applicata per l'ottenimento di questi modelli umani in vitro si basa sull'applicazione di tecnologie in micro-scala per permettere la riproduzione in vitro delle nicchie fisiologiche, che guidano il differenziamento e permettono lo sviluppo

funzionale. In particolare sono stati utilizzati dei micro-pozzetti tridimensionali per modulare l'accumulo di fattori endogeni in corpi embrioidi umani in differenziamento, per studiare lo sviluppo dei tre foglietti germinali guidato da diversi microambienti cellulari. È stata poi imposta una modulazione delle proprietà meccaniche dei nuclei di cellule pluripotenti tramite utilizzo di substrati micro-strutturati, per lo studio della capacità peculiare di deformazione nucleare di tali cellule e si è valutato l'effetto sulla pluripotenza e il differenziamento precoce. Inoltre sono state utilizzate tecnologie micro-fluidiche per modulare selettivamente il microambiente cellulare solubile, in modo da ottimizzare il mantenimento della pluripotenza in chip micro-fluidici, nonché lo sviluppo cellulare precoce e il differenziamento funzionale in cardiomiociti ed epatociti. È stata ottenuta un'alta percentuale di cardiomiociti contrattili nei chip che mostravano risposte funzionali corrette a stimoli di calcio. La tecnologia micro-fluidica ha permesso poi di ottenere un'alta percentuale di epatociti in chip rispetto alle condizioni di coltura standard. Queste cellule mostravano caratteristiche fenotipiche e funzionali corrette, che sono state poi analizzate in condizioni più fisiologiche sotto un gradiente stabile di ossigeno, mimando le condizioni in vivo. Questi tipi cellulari specifici, generati in chip da cellule staminali pluripotenti umane tramite un approccio multi-stadio, mostrano un differenziamento funzionale specifico, che apre a nuove prospettive per test multi-parametrici su larga scala basati su tessuti funzionali umani.

INTRODUZIONE

Lo sviluppo di nuovi modelli in vitro di tessuti umani, in cui le cellule umane si sviluppano in un microambiente fisiologico, offre straordinarie opportunità di studiare la fisiologia e la patofisiologia umana in un contesto organo-specifico (Huh et al. 2012).

Tale prospettiva potrebbe fornire una soluzione effettiva ai limiti delle colture cellulari convenzionali, che non riescono a ricapitolare effetti e caratteristiche di malattie umane complesse, e potrebbe inoltre contribuire efficacemente all'uso di test animali dispendiosi che spesso offrono uno scarso potere predittivo della fisiologia umana.

In questa direzione, la comunità scientifica e le agenzie governative riconoscono l'enorme importanza dello sviluppo di nuovi modelli, che diano la possibilità di svolgere test multi-parametrici economici per studi ad hoc di sviluppo, malattie e patogenesi, o per testare nuove e specifiche strategie terapeutiche.

I saggi fisiologici in vitro aiuterebbero a migliorare il grado di trasferimento delle scoperte pre-cliniche alla clinica, ma da questo punto di vista, un componente critico per tali test sarebbe l'uso di modelli cellulari affidabili che riescano a catturare la complessità della situazione clinica in esame (Engle and Puppala, 2013). Per questo motivo vengono subito in mente le cellule primarie umane, dati i loro vantaggi maggiori rispetto alle linee cellulari, quali l'espressione di importanti proteine target nel loro normale ambiente normale. Però anche questi tipi cellulari presentano svantaggi significativi (Eglen et al. 2008). In primis, la scarsa disponibilità data dalla difficile reperibilità di tessuti estratti da pazienti. Le cellule differenziate in modo terminale poi non sono proliferanti e risulta impossibile una loro espansione in coltura (Goldbard, 2006). Le cellule primarie mostrano spesso in coltura un fenotipo instabile de-differenziato dopo l'isolamento dal tessuto, il che rende l'interpretazione dei dati difficile e limita la finestra temporale disponibile per la sperimentazione (Sahi et al. 2010). Per alcuni tessuti, gli attuali protocolli di coltura sono incapaci di ricapitolare lo stato cellulare di interesse. La generazione di cellule staminali embrionali umane (hESCs) e di cellule staminali pluripotenti indotte umane (hiPSCs) ha offerto una valida alternativa all'uso di cellule primarie nello sviluppo di farmaci e nella generazione di modelli di tessuti umani (Engle and Puppala, 2013). Queste cellule possono essere espanse in coltura indefinitamente in

opportune condizioni, e possono essere fatte differenziare nei tipi cellulari terminali derivanti dai tre foglietti germinali, ectoderma, endoderma e mesoderma. Il processo di differenziamento in vitro ricapitola gli aspetti del normale sviluppo cellulare, offrendo quindi un'opportunità di compiere studi di sviluppo e processi rigenerativi.

Il tessuto cardiaco ed il tessuto epatico sono due dei maggiori tessuti di interesse nel processo di sviluppo di modelli patologici e sviluppo di farmaci. La fase di sviluppo pre-clinico dei farmaci presenta un alto grado di fallimento a causa di effetti cardiaci indesiderati. Inoltre, tossicità cardiache non riconosciute preoccupano sempre più, non solo in test clinici, ma anche per quanto riguarda farmaci già in commercio. Da qui risulta l'importanza dello sviluppo di modelli in vitro rilevanti, che rispecchino la funzionalità normale del tessuto cardiaco (Agarwal et al., 2013).

Al momento anche gli epatociti primari umani costituiscono un modello comune per saggi in vitro. Sfortunatamente, proteine e funzioni chiave vengono perse quando queste cellule sono mantenute in coltura. Per queste ragioni vi è una impellente necessità di studiare nuovi modelli che riescano a mimare cellule epatiche umane e che possano predire gli effetti di molecole candidate nello sviluppo di nuovi composti o farmaci (Sartipy and Björquist, 2011).

Il Capitolo 1 si focalizzerà sull'introduzione dei modelli di cellule staminali umane adottati in questo lavoro di dottorato, con una descrizione delle caratteristiche più importanti, incluso un focus sul microambiente e i maggiori pathway proteici coinvolti nel mantenimento della pluripotenza. Sarà discusso lo stato dell'arte di diverse micro-tecnologie applicate alla biologia cellulare e sarà introdotto lo scopo generale di questa tesi.

Il Capitolo 2 introduce le metodologie applicate per lo sviluppo in laboratorio degli strumenti micro-ingegneristici utilizzati nelle colture cellulari, quali i micro-pozzetti di idrogel di poliacrilammide, i substrati micro-strutturati e le piattaforme micro-fluidiche. Saranno inoltre presentate le metodiche per la coltura di cellule staminali e il loro differenziamento in tipi cellulari specifici.

Il Capitolo 3 si focalizzerà sui risultati ottenuti nella modulazione del microambiente cellulare tramite l'uso di idrogel tridimensionali e il suo effetto sugli stadi precoci del differenziamento. Inoltre saranno presentati i risultati sul controllo meccanico della morfologia dei nuclei di cellule staminali e sarà presentata una analisi degli effetti della deformazione durante la pluripotenza in diversi tipi cellulari e durante il differenziamento precoce in cellule pluripotenti.

Nel Capitolo 4 saranno descritti i risultati sul controllo del microambiente solubile cellulare durante lo stato di pluripotenza e come il mantenimento di cellule staminali possa essere ottimizzato in colture in micro-fluidica, tramite cambi medium a intervalli definiti.

Il Capitolo 5 si focalizzerà poi sull'utilizzo di piattaforme microfluidiche per dirigere lo sviluppo precoce dei foglietti germinali. In questo Capitolo saranno poi presentati i risultati sull'utilizzo di questa tecnologia per l'obbiettivo principale di dirigere selettivamente il differenziamento di cellule staminali pluripotenti umane in cardiomiociti ed epatociti funzionali.

Nel Capitolo 6 saranno presentate la discussione generale e le conclusioni del lavoro, insieme ad un caso particolare di studio, esposto come prospettiva futura del lavoro, del gradiente di ossigeno generato nel chip micro-fluidico per riuscire a mimare le condizioni di un microambiente fisiologico in cui gli epatociti si trovano in vivo all'interno del lobulo epatico.

Referenze

Dongeun Huh, Daniel C. Leslie, Benjamin D. Matthews, Jacob P. Fraser, Samuel Jurek, Geraldine A. Hamilton, Kevin S. Thorneloe, Michael Allen McAlexander, Donald E. Ingber. A Human Disease Model of Drug Toxicity–Induced Pulmonary Edema in a Lung-on-a-Chip Microdevice. SciTransl Med 7 November 2012: Vol. 4, Issue 159, p. 159ra147

Engle SJ, Puppala D. Integrating human pluripotent stem cells into drug development. Cell Stem Cell. 2013 Jun 6;12(6):669-77. doi: 10.1016/j.stem.2013.05.011.

Eglen RM, Gilchrist A, Reisine T. The use of immortalized cell lines in GPCR screening: the good, bad and ugly. Comb Chem High Throughput Screen. 2008 Aug;11(7):560-5.

Goldbard S. Bringing primary cells to mainstream drug development and drug testing. Curr Opin Drug Discov Devel. 2006 Jan;9(1):110-6.

Sahi J, Grepper S, Smith C. Hepatocytes as a tool in drug metabolism, transport and safety evaluations in drug discovery. Curr Drug Discov Technol. 2010 Sep;7(3):188-98.

Agarwal A, Goss JA, Cho A, McCain ML, Parker KK. Microfluidic heart on a chip for higher throughput pharmacological studies. 2013 Sep 21;13(18):3599-608.

Sartipy P, Björquist P. Concise review: Human pluripotent stem cell-based models for cardiac and hepatic toxicity assessment. Stem Cells. 2011 May;29(5):744-8. doi: 10.1002/stem.631.

SUMMARY

There is a growing interest by scientific community, together with pharmaceutical companies and clinical researcher on finding valid alternatives to standard models in the development of new therapeutic strategies and robust drug screening processes. Research still relies on the use of immortalized cell lines, primary cell extracted from living organs and animal models. These methodologies are valid and still mainstream for general purposes, but most of the times present evident limits. Cell lines and primary cells often fail to reproduce the exact characteristics of the tissue found in vivo, because they lose some of the features and functionalities when grown in culture. On the other hand, animal models, even if necessary for the study of specific diseases and new compound testing, are expensive and time-consuming, and often show poor predictive capacity and scarce reproducibility of the human condition. Hence, human pluripotent stem cells could represent a valid alternative to the existing models, thank to their capacity to be expanded indefinitely and differentiate into almost all cell types found in vivo. In the recent years, there has been a growing attention on engineered tissues differentiate from pluripotent cells. They have the capacity to transform the way to study human pathophysiology and physiology in vitro. Nevertheless, there are still major problems in the process of differentiating human embryonic and induced pluripotent stem cell in vitro. This is because of the difficulty to specifically direct cell fate to a particular cell type in a robust way, and for the poor reproduction of the physiological conditions under which these processes take place. In this direction, new microtechnologies could help overcome these major limitations, because they allow working on microscales, in a way that cannot be reproduced by standard culture conditions. In this context, the aim of this PhD thesis is to efficiently differentiate human pluripotent stem cells in order to obtain functional relevant cell types, such as cardiomyocytes and hepatocytes. The strategy applied for the obtainment of these human in vitro models rely on the application of microscale technologies for reproducing in vitro the main physiological cues, which guide differentiation and allow functional development. In particular, three-dimensional microwell were used for modulating endogenous factor accumulation on differentiating human embryoid bodies, to screen for selective germ layer commitment guided by a differential microenvironment around the differentiating cells. Furthermore, a mechanical modulation of the pluripotent nuclei mechanical properties was

imposed with the use of microstructured substrate, for the study of the peculiar capacity of nuclear cell deformation, and its effect in pluripotency and early differentiation. Moreover, microfluidic technologies were used to selectively modulate cell soluble microenvironment, in order to optimize pluripotency maintenance, early germ layer commitment, and functional differentiation into cardiomyocytes and hepatocytes. A high percentage of spontaneously beating cardiomyocytes on chip was obtained, showing proper functional response to calcium stimuli. On the other hand, microfluidic technology allowed to obtain a higher percentage of hepatocytes compared to standard culture conditions. These cells showed proper phenotypic and functional characteristics, which were also analyzed in a more physiological condition under a defined oxygen gradient, mimicking in vivo physiological conditions. These specific cell types generated on chip from human pluripotent stem cells through a multi-stage approach show specific functional differentiation, which opens a new perspective for multi-parametric and large scale human tissue-based screening assays.

INTRODUCTION

The development of new in vitro human tissue models, in which cultured human cells recapitulate the whole living organ microenvironment, offers an extraordinary opportunity to study human physiology and pathophysiology in an organ-specific context (Huh et al. 2012).

This perspective could provide an effective solution to the limitations of conventional cell cultures, which fail to recapitulate complex, organ-level disease processes in humans, and it could efficiently contribute to the use of expensive and time-consuming animal testing, which often shows poor predictive power of human physiology.

In this direction, also the scientific community, the major pharmaceutical companies and the government agencies are recognizing the paramount importance of developing new models, which would allow to perform cost effective and multi-parametric assays for ad hoc studies in development, disease and pathogenesis, or for screening specific therapeutic strategies.

If physiologically relevant in vitro assays are to improve the success in translating preclinical discoveries to the clinic, a critical component will be the use of more relevant cellular systems, which capture the complexity of the clinical situation (Engle and Puppala, 2013). For this reason one would immediately think of primary human cells, because of their major advantages over cell lines, such as the expression of target proteins functioning in their normal environment. However, primary cells present some significant disadvantages (Eglen et al. 2008). First of all there is a limited availability caused by the shortage of tissues extracted from patients. Further differentiated cells do not proliferate, so their expansion in culture is impossible (Goldbard, 2006). Primary cells often exhibit an unstable, dedifferentiated phenotype in culture after isolation, which makes data interpretation difficult and limits the available time window for experimentation (Sahi et al. 2010).

For some tissues, the current culture protocols are incapable of recapitulating the cellular state of interest. The generation of human embryonic stem cells (hESCs) and human induced pluripotent stem cells (hiPSCs) has offered a valid alternative to human primary cells for use in drug development and human tissue model generation (Engle and Puppala, 2013). Under proper conditions, these cells can be expanded in culture indefinitely and eventually directed to differentiate into a variety of terminal cell types within the three

germ layers, ectoderm, endoderm and mesoderm. The in vitro differentiation process recapitulates aspects of normal development, opening up the opportunity to study developmental and regenerative processes.

Two of the major tissues of interest in the process of disease modeling and drug development are cardiac and hepatic tissues. Preclinical drug development is severely hampered by high failure rates due to cardiac side effects. In addition, unforeseen cardiac toxicities are also a growing concern not only for clinical trials but also for already marketed drugs. Hence, the importance of developing relevant in vitro models which recapitulate cardiac tissue level functionality (Agarwal et al., 2013). Accordingly, at present, primary human hepatocytes constitute a common model for in vitro safety assessment. Unfortunately, key proteins and functions are missing in these cells when kept in culture. For these reasons there is a urgent need for new model systems that better mimic human liver cells and that are able to predict effect of candidate molecules in the development of new drugs or chemicals (Sartipy and Björquist, 2011).

Chapter 1 will focus on the introduction of the human stem cell models adopted during the PhD project, with a description of their most important characteristics, including a focus on their microenvironment and main pathways involved in maintenance of pluripotency. The state of the art of different microtechnologies applied to cell biology will be discussed, together with the general aim of the thesis.

Chapter 2 introduces the methodologies applied in order to set up the microengineering tools used for cell culture, such as polyacrylamide hydrogel microwells, microstructures substrates and microfluidic platforms. It will be also presented the methodology for stem cell culture and differentiation into specific cell lines.

Chapter 3 will focus on the results obtained in the modulation of the cell microenvironment through the use of the three-dimensional hydrogels, and its effect on early differentiation stages. Further results on a mechanical control of stem cell nuclei morphology will be presented, and there will be an analysis on the effect of the deformation during pluripotency in different cell types and during early germ layer commitment in pluripotent cell types.

Chapter 4 will describe the results on the control of the cell soluble microenvironment during pluripotency state and how stem cell maintenance can be optimized in microfluidic cell culture through intermittent medium perfusion.

Chapter 5 will focus next on the use of microfluidic platforms to drive stem cell early germ layer commitment. This chapter presents then the results on this technology used for its main goal of selectively directing human pluripotent stem cell differentiation into functional cardiomyocyte and hepatocyte-like cells.

Chapter 6 will present the general discussion and conclusions, together with a case study as a future perspective of an oxygen gradient generated in the microfluidic chip in order to better mimic physiological microenvironment condition in which hepatocytes are found in vivo in the liver lobules.

References

Dongeun Huh, Daniel C. Leslie, Benjamin D. Matthews, Jacob P. Fraser, Samuel Jurek, Geraldine A. Hamilton, Kevin S. Thorneloe, Michael Allen McAlexander, Donald E. Ingber. A Human Disease Model of Drug Toxicity–Induced Pulmonary Edema in a Lung-on-a-Chip Microdevice. SciTransl Med 7 November 2012: Vol. 4, Issue 159, p. 159ra147

Engle SJ, Puppala D. Integrating human pluripotent stem cells into drug development. Cell Stem Cell. 2013 Jun 6;12(6):669-77. doi: 10.1016/j.stem.2013.05.011.

Eglen RM, Gilchrist A, Reisine T. The use of immortalized cell lines in GPCR screening: the good, bad and ugly. Comb Chem High Throughput Screen. 2008 Aug;11(7):560-5.

Goldbard S. Bringing primary cells to mainstream drug development and drug testing. Curr Opin Drug Discov Devel. 2006 Jan;9(1):110-6.

Sahi J, Grepper S, Smith C. Hepatocytes as a tool in drug metabolism, transport and safety evaluations in drug discovery. Curr Drug Discov Technol. 2010 Sep;7(3):188-98.

Agarwal A, Goss JA, Cho A, McCain ML, Parker KK. Microfluidic heart on a chip for higher throughput pharmacological studies. 2013 Sep 21;13(18):3599-608.

Sartipy P, Björquist P. Concise review: Human pluripotent stem cell-based models for cardiac and hepatic toxicity assessment. Stem Cells. 2011 May;29(5):744-8. doi: 10.1002/stem.631.

FOREWORD

During these three years of PhD work, I have been able to learn how to work in an interdisciplinary environment, merging my industrial biotechnology background with clinical expertise, and chemical engineering knowhow. The opportunity to work in a multidisciplinary laboratory gave me the possibility to explore new frontiers in scientific research and open my mind to challenging situations. I would like to thank my PhD supervisor, Prof. Annarosa Floreani, for her dedication to this project, for the trust she put in me and for introducing me to new academic experiences. I would also like to thank my PhD co-tutor Dr. Nicola Elvassore for giving me this chance and always believing in me, and for all the things I learned thank to him.

The author is grateful to the Università degli Studi di Padova, Fondo Sociale Europeo, Progetti di Eccellenza Cariparo, Progetti di Eccellenza Giovani Ricercatori of Ministero della Salute, for financial support to the research activity.

During the period of the PhD program, the following publication have been produced:

- *Giobbe GG, Zagallo M, Riello M, Serena E, Masi G, Barzon L, Di Camillo B, Elvassore N. Confined 3D microenvironment regulates early differentiation in human pluripotent stem cells. Biotechnol Bioeng. 2012 Dec;109(12):3119-32.*
- *Giobbe GG, Michielin F, Martewicz S, Giulitti S, Luni C, Floreani A, Elvassore N. Integrated multi-stage tissue on a chip generation from human pluripotent stem cells. Nat Methods. (under revision).*
- *Zatti S, Martewicz S, Serena E, Uno N, Giobbe GG, Kazuki Y, Oshimura M & Elvassore N. Complete restoration of multiple dystrophin isoforms in genetically corrected Duchenne muscular dystrophy patient–derived cardiomyocytes. Molecular Therapy - Methods & Clinical Development. doi:10.1038/mtm.2013.1. Published online 08 January 2014.*
- *Grespan E, Giobbe GG, Badique F, Anselme K, Rühe J, Elvassore N. Human pluripotent stem cell nuclear self-deformation in pluripotency and differentiation. (to be submitted).*

Numerous abstracts were submitted to several international conferences during the PhD program, for oral presentations and poster presentations, including: Italian Association For The Study of the Liver (AISF); European Association for the Study of the Liver (EASL); American Assiociation for the Study of Liver Diseases (AASLD); International Society for Stem Cell Research (ISSCR).

CHAPTER 1

MICROTECHNOLOGIES FOR THE DEVELOPMENT OF STEM CELL DERIVED IN VITRO MODELS

1.1 Human pluripotent stem cells

Stem cells are undifferentiated cells, which do not show any specific characteristic in terms of morphology, antigenicity and function, and they have the capacity to self-renew and differentiate into specialized cells. Self-renewal allows stem cells to replicate indefinitely while maintaining an undifferentiated state. Plasticity, instead, allows them to differentiate into a wide range of cells, which maintain the original hereditary information but reduce the potential of their genome to specialize and acquire defined functions. The self-maintenance capacity is given by the peculiar characteristics of division regulated by two main mechanisms. Symmetric proliferative division gives rise to two identical cells from the mother cells, while symmetric differentiative division generates two identical cells but more differentiated. These two mechanisms maintain a constant percentage of stem cell in an organism. Stem cells allow the tissues to maintain an proper architectural, cytological and biochemical structure in order to guarantee the correct functionality of the different organs (Potten and Loeffler, 1990).

Particular types of stem cells are the pluripotent cells. The first report of human embryonic stem cells was on 1998 (Thomson et al. 1998). This was a breakthrough among the international scientific community and the whole society still recognize huge potentiality to the applications of stem cells for models development, screening and disease therapies. On the other side, a large debate took place on whether hESCs use was ethical or not. In fact, they derive from the inner cell mass (ICM) of a 5-days fertilized blastocyst (Fig. 1.1), which is extracted and grown in culture with, or without, feeder layer cells. When the clonal expansion begins, only the cell colonies showing undifferentiated state, high clonal capacity, pluripotency and normal karyotype are kept and expanded.

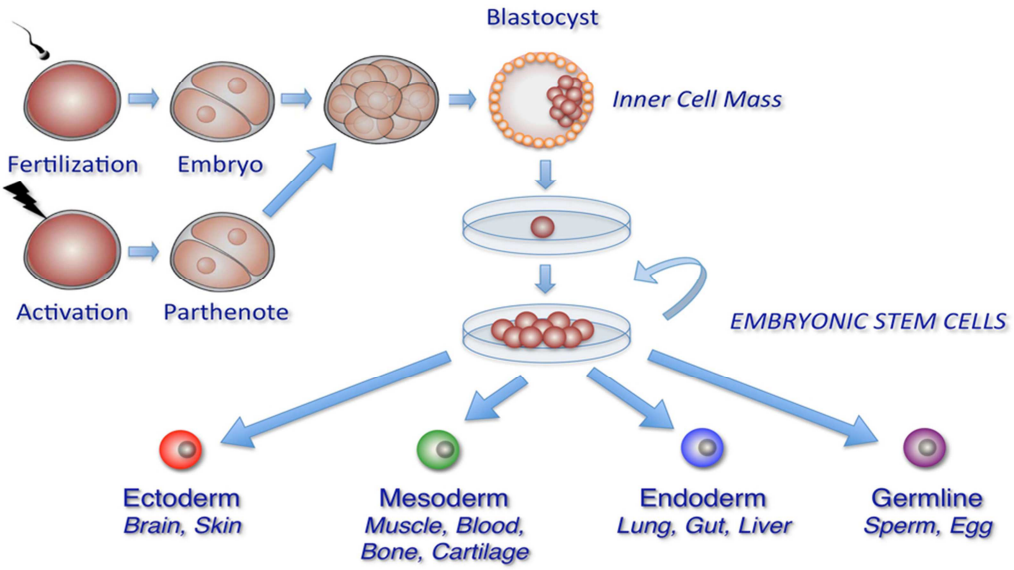

Figure 1.1.*Generation of human embryonic stem cell lines. Donor embryos are first obtained after in vitro fertilization or by egg activation (parthenogenetic embryos), and allowed to develop in vitro. Pluripotent cells are then isolated either from the inner cell mass of pre-implantation blastocysts or from 4, 8, or 16 -cell stage morulae. Finally, isolated cells are plated in defined hESC medium with or without feeder cell layers to propagate and select for pluripotent cell populations. These processes have resulted in hESC lines able to generate tissues from all three embryonic germ layers and the germline (adapted from Yabut and Bernstein, 2011).*

Pluripotency state is verified by the capacity to form spontaneous cell aggregates under appropriate culture conditions, the embryoid bodies (EB), in which cells start to differentiate spontaneously into various cell types. Moreover, when hESCs are injected in an immunocompromised mouse they generate a teratoma, in which cells differentiate spontaneously into several cells types. Therefore, hESCs can originate all the derivates of the three germ layers and are a precious tool for the development of in vitro models and therapeutic screening.

The proof of pluripotency properties opened new and promising perspectives in fields such as developmental biology, genomics, pathophysiological studies, drug screening and development. It is worth underlying how many of the most common diseases (heart failure, liver diseases, neurodegenerative disorders, diabetes, etc.) result from cellular deficiencies or dysfunctions. In this sight, having the possibility of generating relevant numbers of defined cell populations, may allow the development of novel cell therapies or, in parallel, to perform studies on specialized human cells that would permit the obtainment of more significant data aimed at the development of the necessary therapeutic strategies.

The ethical issues centered on the use of embryos for the obtainment of human embryonic cells, have been a driving force towards the development of alternative strategies for obtaining similar and such powerful cells. In 2007 (Takahashi et al. 2007) another breakthrough in science, first on mouse and then on human cells, was reported. Dr. Yamanaka found a way to overcome the ethical issues raised by hESCs, by reprogramming adult somatic cells to a pluripotent state, with selective induction of specific pluripotency factors Oct4, Sox2, cMyc, and Klf4 (Fig. 1.2).

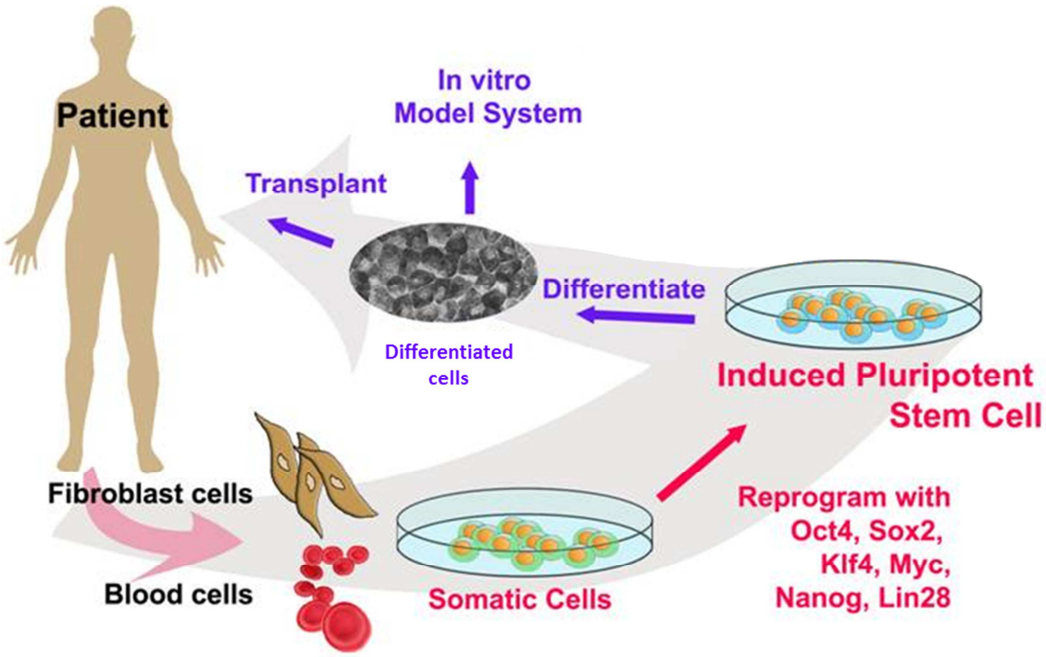

Figure 1.2.*Generation of human induced pluripotent stem cell lines. Adult somatic cells, i.e. skin fibroblasts, are taken from patient, cultured in vitro and reprogrammed with specific factors i.e. Oct4, Sox2, Klf4, Myc, Nanog, Lin28. Reprogramming can be done by viral vectors, modified mRNAs etc. Pluripotent cells colonies are selected and and expanded in culture and can be differentiated to specific cell types (modified from Carr et al. 2013).*

HiPSCs share equal or similar characteristics with hESCs, but this groundbreaking methodology opened new perspectives especially toward a patient-specific medicine. Many human diseases (metabolic, genetic, multifactorial diseases) are difficult to study in animal models. Thus, the reprogrammed cells would give scientists a new tool for studying genetic and molecular basis on a much relevant model. It is important to underline that all the technologies and studies that will be presented in this thesis, have been performed both on hES and hiPS cells, in order to develop more relevant in vitro models.

1.2.1 Major pathways involved in pluripotency maintenance and differentiation

Mechanisms controlling pluripotency and differentiation of pluripotent cells have been extensively studied, but many aspects remain still unknown. It has been clearly demonstrated that activin/nodal signaling maintains the pluripotent status of hPSCs (Vallier et al. 2009). Pluripotency is regulated by a combination of extrinsic and intrinsic factors. FGF (Fibroblast Growth Factor) signaling and a balance between TGF-Beta (Transforming Growth Factor-Beta)/Activin and BMP (Bone Morphogenic Protein) signaling are central to hPSCs self-renewal. Intrinsic factors regulating pluripotency include transcription factors such as Nanog and Oct4 (Octamer Binding Transcription Factor-4) (Biswas and Hutchins, 2007).

TGF-Beta ligand superfamily, plays a major role in maintaining the self-renewal capacity. TGF-Beta signals through two main branches: the SMAD1/5 branch, which transduces on behalf of BMP and GDF (Growth Differentiation Factor), and the TGF-Beta/Activin/Nodal branch, which involves the activation of SMAD2/3. There are also two inhibitory SMADs: SMAD6, which selectively inhibits SMAD1/5, and SMAD7, which inhibits both branches of TGF-Beta signaling, that provide a repressive input on the pathway. Upon activation by phosphorylation and association with a common SMAD4, the receptor-activated SMADs translocates to the nucleus and, with other transcription factors, regulates gene expression. Activation of the TGF-Beta/Activin/Nodal branch through SMAD2/3 is associated with pluripotency and is required for the maintenance of the undifferentiated state in hPSCs (Xiao et al. 2006, James et al. 2005).

In contrast, BMP signaling is unable to support self-renewal and it is associated with differentiation to trophoblast or extraembryonic endoderm cells. In hPSCs, BMP4 induces differentiation into mesoderm and ectoderm, whereas BMP2 promotes extraembryonic endoderm differentiation. Repression of BMP signaling in by Noggin and FGF supports long term self-renewal. FGF2 is known as the best known factor promoting self-renewal in hPSCs and is capable of maintaining pluripotent cells in the absence of serum and feeder cells. FGF2 promote self-renewal of Human ESCs by activating the PI3K pathway (Xu et al. 2005).

Nanog is another member of the group of transcription factors whose functions are deemed essential for the process of self-renewal in hPSCs. The

binding of Oct3/4 and SOX2 to its promoter regulates transcription of Nanog. Oct3/4, SOX2, and Nanog co-occupy the promoters of a large range of genes, many of which encode developmentally important transcription factors. HPSCs exhibit a number of signaling pathways involved in self-renewal and pluripotency that are interdependent and display a range of cross-talk mechanisms (Boyer et al. 2005, Pan and Thomson, 2007). The understanding of the exogenous and endogenous factors determining cell fate will facilitate the use of these cells in cell-based therapies and will allow further understanding of early developmental processes.

1.2.2 Human pluripotent stem cell microenvironment

The cell microenvironment is a dynamic structure, defined as the "niche" where the cell grows and develops. During embryonic development, various microenvironment factors act on embryonic stem cells to alter gene expression, and induce their proliferation or differentiation for the development of the fetus. Within the human body, stem cell niches maintain adult stem cells in a quiescent state, but after tissue injury, the surrounding micro-environment actively signals to stem cells to either promote self-renewal or differentiation to form new tissues. Several factors are important to regulate stem cell characteristics within the niche: growth factors, cytokines, stem cell-cell interactions, interactions with nearby differentiated cells, adhesion molecules, extracellular matrix components, oxygen tension, physiochemical nature of the environment (i.e. pH, ionic strength and metabolites) (Fig. 1.3). The stem cells and microenvironment may induce each other during development, and reciprocally communicate to maintain each other during adulthood (Scadden, 2006).

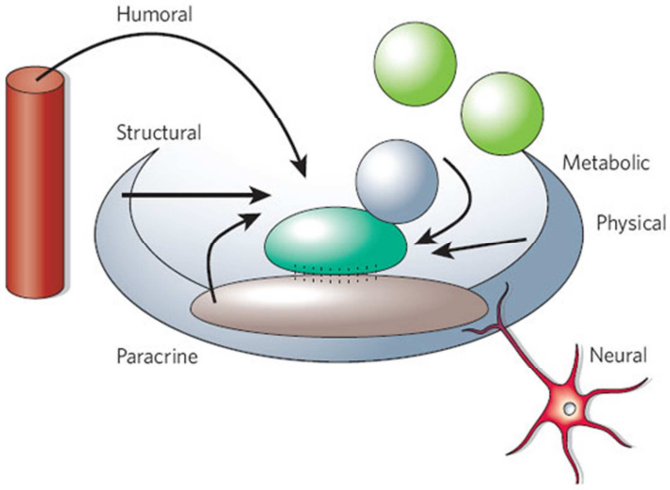

Figure 1.3.*Components of the local microenvironment, which participate in regulating the system of a stem cell in its tissue site (adapted from Scadden, 2006).*

A pluripotent stem cell can be considered "naked" without its own microenvironment, and may not behave as expected during pluripotency and differentiation. For this reason, scientific community has been trying to recreate in vitro the various components of the niche found in vivo. For regenerative therapies, models and drug screening purposes, cell proliferation and differentiation must be accurately controlled.

1.2.3 Human pluripotent stem cell limitations

Both human embryonic and induced pluripotent stem cells have high potential in basic science and clinical application, but this is hindered by the impossibility to perfectly control them in vitro through their microenvironment. Some limitations during differentiation protocols to a particular cell type come as a consequence of this problematic:

Non robust differentiation protocols, especially between different stem cell lines;

Differentiated cells do not have an homogenous phenotype;

Inability to reach adult cell phenotype;

Relative low expression, or partial expression, of functional proteins defining a particular cell type;

Only partial expression of functional properties;

Partial expression of structural properties like polarization, interaction, architecture, vascularization, tissue structure.

Coupling stem cells with microengineering technologies could help overcome these current limitations, in order to possibly reproduce some features of adult tissue types.

1.2 Micro-technologies in pluripotent cell culture and tissue development

Human pluripotent stem cells secrete numerous endogenous factors, which constitute the soluble microenvironment around cells, together with exogenous molecules and metabolites. In order to manipulate the microenvironment it is necessary to work on dimensions of micrometers. It is almost impossible to do

this in standard Petri dish culture plates. For this reason, in this PhD project, microengineering technologies have been applied to manipulate such small dimensions.

Efficient control of the differentiation of hES and hiPS cells is a prerequisite for obtaining phenotypically homogenous populations. However, thus far, accurate expansion and differentiation processes of hPSC remained an open challenge. Multiple methods have been used to induce human pluripotent stem cells differentiation, including use of specific growth factors, co-culture with specific cell lines, culture on extracellular matrix proteins, and embryoid body formation (Dvash and Benvenisty, 2004; Itskovitz-Eldor et al., 2000; Keller, 2005; Odorico et al., 2001). EB differentiation method recapitulates the early stages of human embryonic development and provides a three-dimensional structure, most similar to in vivo conditions, where gradients of secreted factors are present. Recent developments in EB formation techniques have enabled more controlled systems capable of modulating EB shape and size, as these parameters have been recognized to contribute to the control of the resulting cell population. Non-adhesive polyethylene glycol (PEG) microwell arrays have been used to control the homogeneity of EB size and shape (Karp et al., 2007; Moeller et al., 2008). Recent studies on PEG microwell-mediated control of EB size have also investigated the effects on hES cell fate determination, specifically addressing cardiogenesis and vasculogenesis via WNT signaling pathways (Hwang et al., 2009). Micro-contact printing techniques have also been developed to regulate EB size-dependent hES cell differentiation and to investigate the stem cell biology (Lee et al., 2009; Park et al., 2007; Peerani et al., 2007, 2009). Concave (Choi et al., 2010; Park et al., 2009), convex-based (Park et al., 2009) thin PDMS membrane arrays and stimuli-responsive microwells (Tekin et al., 2010) for culturing the cells and better mimic the contour of EBs have also been developed. All these studies analyze the effect of factors or EB size and shape in regulating hPSC differentiation. The importance of growth factors in media during differentiation is clear, but little information about the role of secreted molecules during early differentiation stages has been reported, and this process will be further discussed in Chapter 3.

During differentiation processes, stem cells are subjected to numerous stimuli, chemical, physical or mechanical. A growing number of studies try to analyze nuclear mechanics behavior, and there is an emergent topic in scientific research, which investigates the possible relationship between nuclear

properties and cancer, pluripotency and mechanotransduction responses (Zink et al. 2004,Davidson et al. 2009 and 2010, Chalut et al. 2012). Nuclear stiffness has been evaluated and compared in healthy and pathological cells, and a connection between disease and nuclear stiffness was reported (Lombardi et al. 2010, De Vos et al. 2010). Nuclear stiffness seems to increase from human embryonic stem cells to differentiated cells and chromatin is shown to be less condensed in the pluripotent stage (Pajerowski et al. 2007). Few studies consider nuclear mechanics as a property of the nucleus in the cell in connection with the cytoskeleton. Studies on cancer cells show a strong deformation of the cell, and in particular of the nucleus, which adapts to the surrounding micro-topography. Despite such large nuclear deformation, cancer cells are still capable to divide, proliferate and differentiate. It has been demonstrated that this capability to self-deform depends on substrate topography, cell phenotype and cytoskeleton organization (Badique et al. 2013). Nuclear self-deformation due to geometric constraints on human pluripotent stem cells during differentiation will be analyzed in Chapter 3.

1.2.1 Microfluidic technology and cell culture

Microfluidics is a microengineering tool with application crossing from biology to chemistry, physics and medicine, which deal with fluids within micrometer scale devices (Whitesides 2006). This microtechnology gives major advantages in term of high throughput analyses, automatization of the systems, and the possibility to manipulate at micron scale the cell culture microenvironment, in terms of controlling the balance between endogenous and exogenous soluble factors.

Microscale technologies were designed for applications ranging from studies at a single cell level to the recreation of more complex three-dimensional structures (Gottwald et al. 2007, Kim et al. 2007). Successful examples of tissue-on-chip development have been provided (Huh et al. 2010, Lee et al. 2013), however, they were obtained from primary animal cells and, in few cases, from primary human cells. The possibility of developing tissue-on-chips from hPSCs could overcome the limited availability of human primary cells, such as human hepatocytes or cardiomyocytes. Cell differentiation and tissue generation are complex developmental processes starting from germ layer specification and phenotypic differentiation to tissue morphogenesis. Biomimetic scale down of

this multi-stage developmental process could take advantage of the intrinsic properties of micro-technologies and microfluidics that allow accurate control of cell culture microenvironment, of temporal evolution of chemical gradients and of mechanical features, which support specific tissue differentiation (Discher et al. 2009). Few studies reported on mouse embryonic stem cell cultures using microfluidic systems and highlight the importance of accurate soluble microenvironment regulation to maintain pluripotency and self-renewal (Przybyla and Voldman, 2012).

The microtechnology-aided culture of pluripotent cells will be further discussed in Chapter 4, while functional differentiation into cells of interest will be discussed in Chapter 5. Cardiomyocytes and hepatocytes have been chosen as differentiation tissue models in the microfluidic chip, for their importance on in vitro model development and translational research.

In particular, liver tissue shows a high degree of structural complexity, with perfectly interconnected different cell types. The smallest functional working unit of the human liver is the hepatic lobule. It is a small hexagonal division defined at histological scale, divided into concentric centrilobular, midzonal, periportal parts. Between two liver lobules there is a metabolic unit defined as the acinus. This elliptical region is divided into zone I (periportal), zone II (transition zone), and zone III (pericentral). Hepatocytes develop under a constant oxygen gradient, from the oxygenated blood of hepatic artery (pO2 60-70 mmHg) to the less oxygenated blood of the central vein (pO2 25-35 mmHg) (Fig. 1.4). Functionally, a metabolic zonation is present: zone I hepatocytes are specialized for oxidative liver functions such as gluconeogenesis, β-oxidation of fatty acids and cholesterol synthesis, while zone III cells are more important for glycolysis, lipogenesis and cytochrome P-450-based drug detoxification (Schiff et al., 2007; Usynin and Panin, 2008).

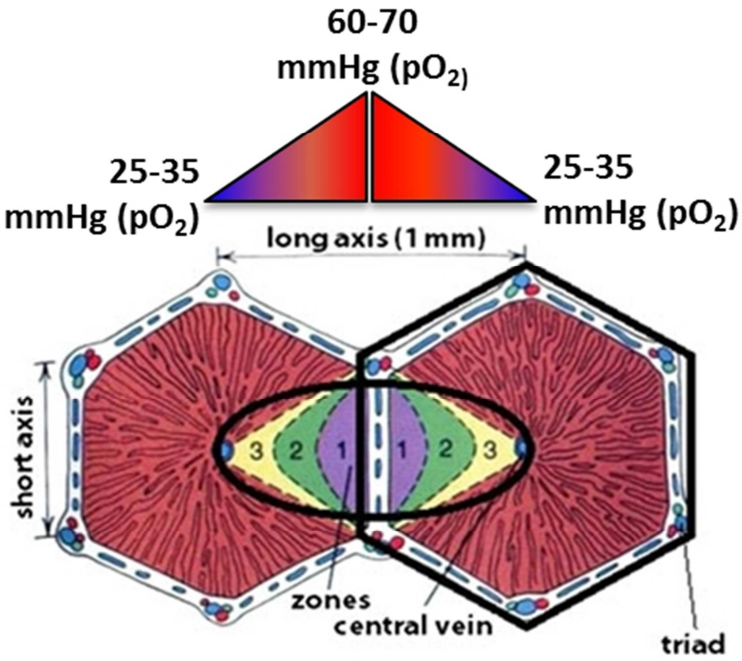

***Figure 1.4**. Schematic representation of two adjacent hexagonal liver lobules, with the central acinus region within the elliptic line. Note the subdivision into the three metabolic regions, and the scheme of the oxygen gradients direction from the branch of the hepatic artery to the central veins.*

When differentiating in vitro hepatocytes, the liver structure complexity is lost, and this is one of the reasons why is difficult to obtain mature hepatocytes from pluripotent cells. As it will be discussed in Chapter 6, microfluidic techniques could help reconstruct some of the features of this complexity, such as the oxygen gradient, under which hepatocytes from hPSCs can differentiate under a more physiological condition.

1.3 Aim of the thesis

The aim of this PhD thesis is to efficiently differentiate human pluripotent stem cells through the use of microtechnologies, into functional cardiomyocytes and hepatocytes, which can be possibly used as in vitro models for drug and therapy development, disease modeling, physiological studies and improve quality of clinical trials.

To this end, the application of microengineering techniques can help to overcome the major limitations of conventional cell cultures, in order to optimize pluripotency maintenance and functional differentiation.

The coupling of pluripotent stem cell potential with ad hoc microtechnologies, would ultimately allow the development of high throughput drug and therapy screenings.

References

Takahashi K, Tanabe K, Ohnuki M, Narita M, Ichisaka T, Tomoda K, Yamanaka S. Induction of pluripotent stem cells from adult human fibroblasts by defined factors. Cell. 2007 Nov 30;131(5):861-72.

Carr AJ, Smart MJ, Ramsden CM, Powner MB, da Cruz L, Coffey PJ. Development of human embryonic stem cell therapies for age-related macular degeneration. Trends Neurosci. 2013 Jul;36(7):385-95. doi: 10.1016/j.tins.2013.03.006.

Potten CS, Loeffler M., Stem cells: attributes, cycles, spirals, pitfalls and uncertainties. Lessons for and from the crypt. Development. 1990 Dec;110(4):1001-20.

Thomson JA, Itskovitz-Eldor J, Shapiro SS, Waknitz MA, Swiergiel JJ, Marshall VS, Jones JM. Embryonic stem cell lines derived from human blastocysts. Science. 1998 Nov 6;282(5391):1145-7.

Yabut O, Bernstein HS. The promise of human embryonic stem cells in aging-associated diseases. Aging. 2011 May;3(5):494-508.

Scadden DT. The stem-cell niche as an entity of action. Nature. 2006 Jun 29;441(7097):1075-9.

Dvash T, Benvenisty N. 2004. Human embryonic stem cells as a model for early human development. Best Practice & Research in Clinical Obstetrics &Gynaecology 18(6):929-940.

Itskovitz-Eldor J, Schuldiner M, Karsenti D, Eden A, Yanuka O, Amit M, Soreq H, Benvenisty N. 2000. Differentiation of human embryonic stem cells into embryoid bodies comprising the three embryonic germ layers. Molecular Medicine 6(2):88-95.

Keller G. 2005. Embryonic stem cell differentiation: emergence of a new era in biology and medicine. Genes & Development 19(10):1129-1155.

Odorico JS, Kaufman DS, Thomson JA. 2001. Multilineage differentiation from human embryonic stem cell lines. Stem Cells 19(3):193-204.

Karp JM, Yeh J, Eng G, Fukuda J, Blumling J, Suh K-Y, Cheng J, Mahdavi A, Borenstein J, Langer R and others. 2007. Controlling size, shape and homogeneity of embryoid bodies using poly(ethylene glycol) microwells. Lab on a Chip 7(6):786-794.

Moeller H-C, Mian MK, Shrivastava S, Chung BG, Khademhosseini A. 2008. A microwell array system for stem cell culture. Biomaterials 29(6):752-763.

Hwang Y-S, Chung BG, Ortmann D, Hattori N, Moeller H-C, Khademhosseini A. 2009. Microwell-mediated control of embryoid body size regulates embryonic stem cell fate via differential expression of WNT5a and WNT11. Proceedings of the National Academy of Sciences of the United States of America 106(40):16978-16983.

Lee LH, Peerani R, Ungrin M, Joshi C, Kumacheva E, Zandstra PW. 2009. Micropatterning of human embryonic stem cells dissects the mesoderm and endoderm lineages. Stem Cell Research 2(2):155-162.

Park J, Cho CH, Parashurama N, Li Y, Berthiaume F, Toner M, Tilles AW, Yarmush ML. 2007. Microfabrication-based modulation of embryonic stem cell differentiation. Lab on a Chip 7(8):1018-1028.

Peerani R, Onishi K, Mahdavi A, Kumacheva E, Zandstra PW. 2009. Manipulation of Signaling Thresholds in "Engineered Stem Cell Niches'' Identifies Design Criteria for Pluripotent Stem Cell Screens. Plos One 4(7).

Peerani R, Rao BM, Bauwens C, Yin T, Wood GA, Nagy A, Kumacheva E, Zandstra PW. 2007. Niche-mediated control of human embryonic stem cell self-renewal and differentiation. Embo Journal 26(22):4744-4755.

Choi YY, Chung BG, Lee DH, Khademhosseini A, Kim J-H, Lee S-H. 2010. Controlled-size embryoid body formation in concave microwell arrays. Biomaterials 31(15):4296-4303.

Park JY, Lee DH, Lee EJ, Lee S-H. 2009. Study of cellular behaviors on concave and convex microstructures fabricated from elastic PDMS membranes. Lab on a Chip 9(14):2043-2049.

Tekin H, Anaya M, Brigham MD, Nauman C, Langer R, Khademhosseini A. 2010. Stimuli-responsive microwells for formation and retrieval of cell aggregates. Lab on a Chip 10(18):2411-2418.

Zink D, Fischer A, Nickerson J. Nuclear structure in cancer cells. Nature Reviews Cancer. 2004 SEP;4(9):677-87.

Davidson PM, Ozcelik H, Hasirci V, Reiter G, Anselme K. Microstructured surfaces cause severe but non-detrimental deformation of the cell nucleus. Adv Mater. 2009 SEP 18;21(35):3586.

Davidson PM, Fromigue O, Marie PJ, Hasirci V, Reiter G, Anselme K. Topographically induced self-deformation of the nuclei of cells: Dependence on cell type and proposed mechanisms. Journal of Materials Science-Materials in Medicine. 2010 MAR;21(3):939-46.

Chalut KJ, Hopfler M, Lautenschlager F, Boyde L, Chan CJ, Ekpenyong A, et al. Chromatin decondensation and nuclear softening accompany nanog downregulation in embryonic stem cells. Biophys J. 2012 Nov 21;103(10):2060-70.

Pajerowski JD, Dahl KN, Zhong FL, Sammak PJ, Discher DE. Physical plasticity of the nucleus in stem cell differentiation. ProcNatlAcadSci U S A. 2007 OCT 2;104(40):15619-24.

Badique F, Stamov DR, Davidson PM, Veuillet M, Reiter G, Freund J, et al. Directing nuclear deformation on micropillared surfaces by substrate geometry and cytoskeleton organization. Biomaterials. 2013 4;34(12):2991-3001.

Whitesides GM.The origins and the future of microfluidics.Nature. 2006 Jul 27;442(7101):368-73.

Gottwald E, Giselbrecht S, Augspurger C, Lahni B, Dambrowsky N, Truckenmüller R, Piotter V, Gietzelt T, Wendt O, Pfleging W, Welle A, Rolletschek A, Wobus AM, Weibezahn KF. A chip-based platform for the in vitro generation of tissues in three-dimensional organization.Lab Chip. 2007 Jun;7(6):777-85. Epub 2007 Apr 16.

Kim L, Toh YC, Voldman J, Yu H. A practical guide to microfluidic perfusion culture of adherent mammalian cells. Lab Chip. 2007 Jun;7(6):681-94. Epub 2007 May 11.

Huh D, Matthews BD, Mammoto A, Montoya-Zavala M, Hsin HY, Ingber DE. Reconstituting organ-level lung functions on a chip. Science. 2010 Jun 25;328(5986):1662-8.

Lee SA, No da Y, Kang E, Ju J, Kim DS, Lee SH. Spheroid-based three-dimensional liver-on-a-chip to investigate hepatocyte-hepatic stellate cell interactions and flow effects. Lab Chip. 2013 Sep 21;13(18):3529-37.

Discher DE, Mooney DJ, Zandstra PW. Growth factors, matrices, and forces combine and control stem cells. Science. 2009 Jun 26;324(5935):1673-7

Przybyla LM, Voldman J. Attenuation of extrinsic signaling reveals the importance of matrix remodeling on maintenance of embryonic stem cell self-renewal. Proc Natl Acad Sci U S A. 2012 Jan 17;109(3):835-40.

E.R. Schiff, M.F. Sorrell, W.C. Maddrey, ed. (2007). Schiff's Diseases of the Liver, Tenth Edition. Lippincott William & Wilkins. ISBN 0-7817-6040-2.

I. F. Usynin and L. E. Panin. Mechanisms Determining Phenotypic Heterogeneity of Hepatocytes. Biochemistry, 2008, Vol. 73, No. 4, pp. 367-380.

Vallier L, Touboul T, Brown S, Cho C, Bilican B, Alexander M, Cedervall J, Chandran S, Ahrlund-Richter L, Weber A, Pedersen RA. Signaling pathways controlling pluripotency and early cell fate decisions of human induced pluripotent stem cells. Stem Cells. 2009 Nov;27(11):2655-66. doi: 10.1002/stem.199.

Biswas A, Hutchins R. Embryonic stem cells. Stem Cells Dev. 2007 Apr;16(2):213-22.

Xiao L, Yuan X, Sharkis SJ. Activin A maintains self-renewal and regulates fibroblast growth factor, Wnt, and bone morphogenic protein pathways in human embryonic stem cells. Stem Cells. 2006 Jun;24(6):1476-86.

James D, Levine AJ, Besser D, Hemmati-Brivanlou A. TGFbeta/activin/nodal signaling is necessary for the maintenance of pluripotency in human embryonic stem cells. Development. 2005 Mar;132(6):1273-82.

Xu RH, Peck RM, Li DS, Feng X, Ludwig T, Thomson JA. Basic FGF and suppression of BMP signaling sustain undifferentiated proliferation of human ES cells. Nat Methods. 2005 Mar;2(3):185-90.

Pan G, Thomson JA. Nanog and transcriptional networks in embryonic stem cell pluripotency. Cell Res. 2007 Jan;17(1):42-9.

Boyer LA, Lee TI, Cole MF, Johnstone SE, Levine SS, Zucker JP, Guenther MG, Kumar RM, Murray HL, Jenner RG, Gifford DK, Melton DA, Jaenisch R, Young RA. Core transcriptional regulatory circuitry in human embryonic stem cells. Cell. 2005 Sep 23;122(6):947-56.

CHAPTER 2

MICROTECHNOLOGIES AND STEM CELL CULTURE

2.1 Polyacrylamide hydrogels

Polyacrylamide hydrogels can be polymerized at different concentrations, therefore resulting in a differential permeability to solutes. To evaluate self-diffusivity of molecules in polyacrylamide hydrogels, FRAP experiments were performed. Characterization of the hydrogel permeability was obtained by the estimation of the local diffusion coefficient values for fluorescent probes with a molecular weight of 70 kDa. To perform those experiments, hydrogels obtained from pre-polymeric solutions with different monomer/cross linker molar ratios (acrylamide/bis-acrylamide ratios 29:1; 25:1; 21:1) and different pre-polymer concentrations (10–20%) were used and compared. The experiments were performed with these hydrogel compositions that show diffusional cutoff for 70 kDa fluorescence probes, which have the same order of magnitude of EBs secreted factors. In Figure 2.1 there is an evident trend of the self-diffusion that decreases for higher concentrations of acrylamide solution. From the analysis of these data it is possible to define a decrease in mobility for the 70 kDa dextran in 18–20% acrylamide hydrogels. It is interesting to suppose that soluble molecules with similar molecular weights and comparable hydrodynamic radii with the dextran used in the experiment have similar self-diffusivity in the same hydrogels. Therefore, hydrogels of 20% acrylamide v/w were developed, in order to have a cutoff for molecules with molecular weights within the range 40-70 kDa, with a hydrodynamic radius of 19 nm (for detailed materials and methods see Appendix A).

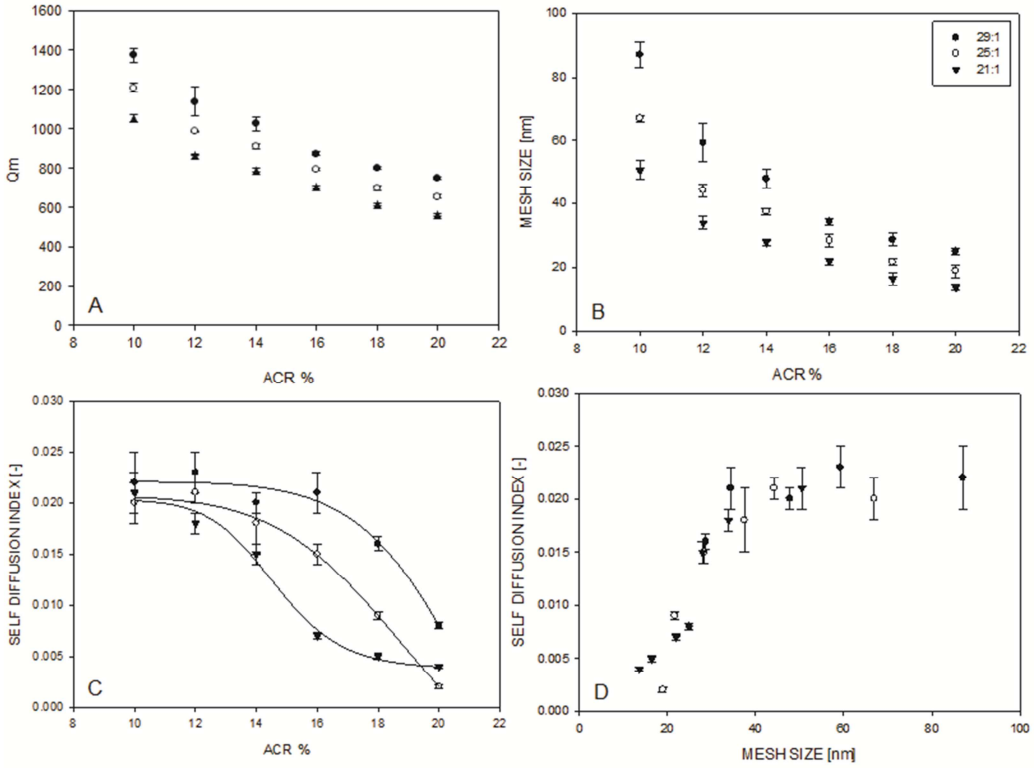

Figure 2.1. A: *Hydrogel mass equilibrium swelling ratio (Qm) decreases as the acrylamide and bis-acrylamide concentration (weight/volume [W/V]) increases in the pre-polimer solution (ACR %).* ***B:*** *From swelling data and Flory-Rehner theory, it is possible to estimate the mesh size of the hydrogel network. The figure shows that the mesh size (in nm) decreases for higher concentrations of acrylamide or bis-acrylamide.* ***C:*** *Self diffusion index (TAU) versus acrylamide concentration, with different cross-linker content. As expected, the self-diffusion decreases as hydrogel network becomes more dense.* ***D:*** *Self diffusion index versus hydrogel network mesh size. Molecular mobility falls to zero for mesh size lower than the molecular radii of the molecular tracer (about 19 nm, MW 70 kDa).*

2.1.1 3D microwells production for embryoid bodies culture

Three-dimensional arrays of microwells with specific dimensions have been produced, through the use of customized photomasks and photopolymerization under UV light (Fig. 2.2A). Acrylamide was polymerized and covalently bound to a pre-treated transparent and thin glass surface (Fig. 2.2B). In order to help cell seeding, concave shape wells were designed. The photomask was designed with a gradient of tone around the 500 µm diameter spot (Fig. 2.2C-D). As the UV light passes through the photomask, it gradually polymerizes the acrylamide, generating a concavity around the microwells (Fig. 2.2E). The diameter of 500 µm was chosen to develop EBs with the best average dimensions for early development (Choi et al. 2010, Mohr et al. 2010, Peerani et al. 2009, Tekin et al. 2010). Microwells with ratio width/depth 1:1 and 1:2 were also chosen to create different culture microenvironments for EBs differentiation.

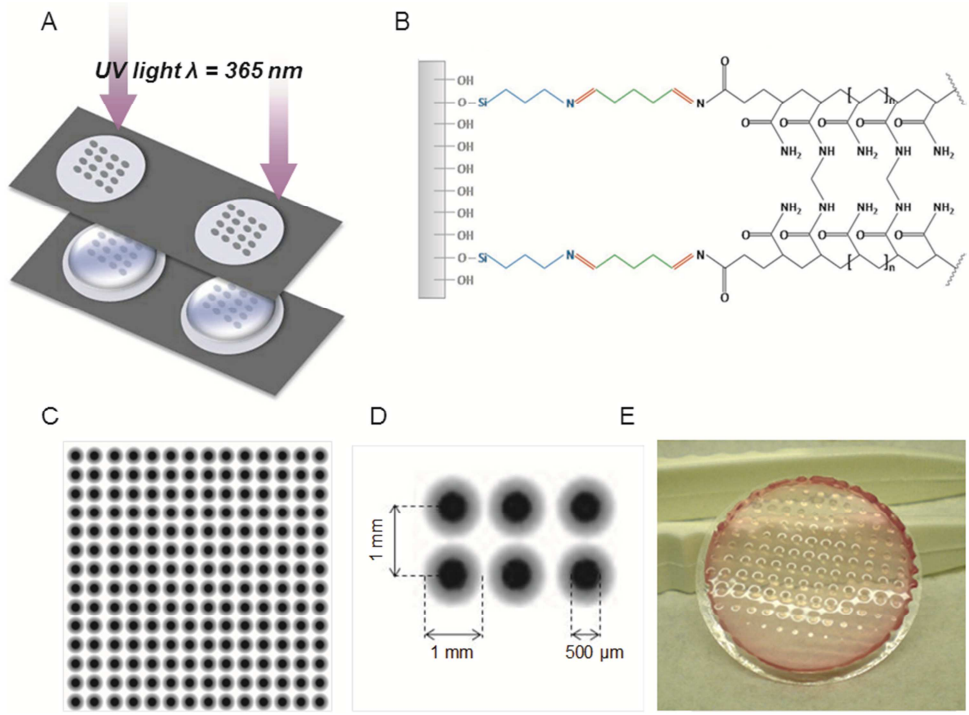

Figure 2.2. *Microstructured PA hydrogel production.* ***A****: The microstructured PA hydrogels are prepared by selective photo-polymerization of the acrylamide/bisacrylamide solution under UV light.* ***B****: The PA hydrogel is covalently bound to a glass coverslip functionalized with 3-aminopropyltriethoxysilane and glutaraldehyde, as shown in the schematic representation of the chemistry.* ***C****: Photomask for selective photopolymerization.* ***D****: Enlargement of a photomask. The shading is realized in order to define the concave shape of the microwells.* ***E****: Microstructured hydrogel, 21 mm in diameter. The color is due to the presence of cell culture medium, which keeps the hydrogel hydrated.*

2.2 Microstructured substrates fabrication

Polydimethylsiloxane (PDMS, Sylgard 184) microstructured substrates were fabricated through a replica-molding process. In the first step, the negative pattern was prepared through standard soft-lithography technique, which is suitable to construct features with measures of micrometer to nanometer scale (Xia et al. 1998, Whitesides et al.2001). Silicon (Si) wafers were spin-coated with AZ-1518 negative photoresist (MicroChemicals) for 30 seconds at 2000 rpm and for 5 minutes at 80°C. The photoresist was illuminated with UV light (λ=365 nm) through a chrome-etched mask that consisted of a square lattice (7 µm width), with a lattice constant of 7 µm. Uncross-linked resist was removed rinsing the wafer in an AZ-1518 developer (MicroChemicals) for 20 s. The obtained microstructured Si-wafers were subsequently silanized by exposure to the vapor of (tridecafluoro-1,1,2,2-tetrahydrooctyl)-1-trichlorosilane in vacuum for 30 minutes, to facilitate PDMS removal during the replica-molding step. PDMS

elastomer was thoroughly mixed with the silicone curing agent in a 10:1 ratio, poured over the microstructured Si-master and kept under vacuum for 1 h to allow the complete filling of the pattern and air bubbles removal. The sample was then cured at 80°C for 3 hours and subsequently peeled off the Si-wafers. The final micropillar topography was characterized by confocal microscopy and scanning electron microscopy (SEM) (Fig. 2.3A). The height of the microstructures was fixed at around 6 µm. PDMS substrates can then be cleaned with 98% ethanol, sterilized in dry autoclave at 121°C and then used as cell substrates. PDMS pillars can be functionalized with matrigel for pluripotent stem cell adhesion and culture (Fig. 2.3B).

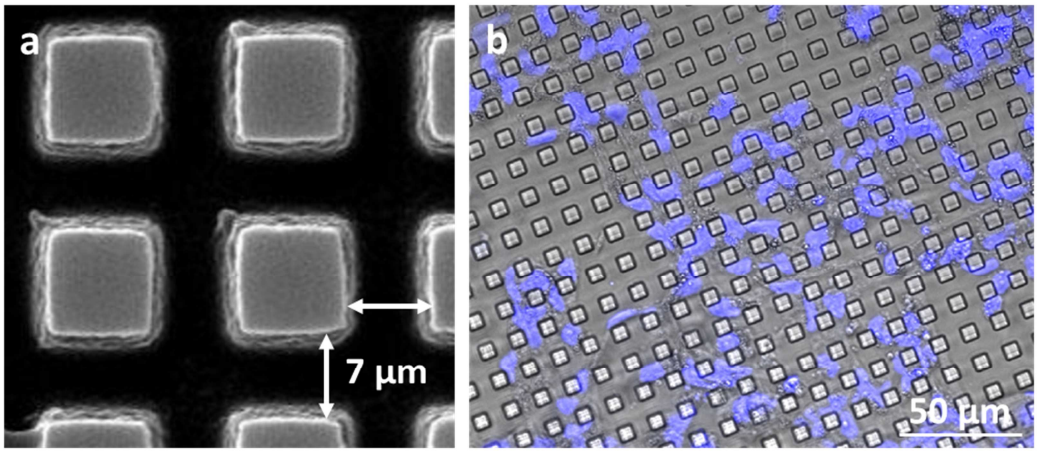

Figure 2.3. A: *PDMS micropillars obtained from a square lattice 7x7 µm.* ***B:*** *HESCs adhering to the micropillar substrate. Note the evident nuclei deformation (stained in blue with Hoechst) of the stem cells adapting to the microstructured geometry.*

2.3 Microfluidic platforms fabrication

Microfluidic devices were fabricated by standard soft-lithography technique. As for micropillar substrates, an elastomeric stamp made PDMS is prepared by replica molding, by casting the liquid prepolymer and the curing agent solution onto a pre-made master with patterned relief structure in its surface. When masters features size are greater than or equal to 20 µm, patterns can be drawn in AutoCAD® and printed onto transparent polymer sheets, through commercially available printers. Photomasks are used to selectively polymerize UV-sensible photoresists, previously spun onto a silicon wafer with defined film-thickness. Parameters such as viscosity of the photoresist, UV-light intensity and baking time should be taken into account in order to achieve selective polymerization of the desired structure. Elastomeric stamps obtained through

soft-lithography technique offer several properties proper to coupling with biological systems. PDMS is chemically inert which makes microfluidic platform biocompatible, and is also highly permeable to gasses (O2, CO2, N2 diffuse rapidly), but not to fluids. It is transparent for detection analysis instruments like fluorescence microscopy. Air or oxygen-base treatments lead to the formation of OH- groups on its surface, which allow covalent bonding between the stamp and glass slides. Photomask in Figure 2.4A was used to produce microfluidic platforms containing 10 parallel microchannels (18 mm long, 1.5 mm wide and 0.2 mm high). PDMS mold was cut and peeled off the Si-wafer, punched to obtain liquid inlets and outlets and sealed to a cleaned glass slide by plasma bonding (Fig. 2.4B). In Figure 2.4C is shown the completed microfluidic platform made of PDMS on a glass surface. Before cell culture integration, microfluidic were rinsed with isopropyl alcohol and sterilized in autoclave. Glass surface has to be opportunely functionalized, with proper adhesion protein solutions (i.e. matrigel), in order to promote cell adhesion.

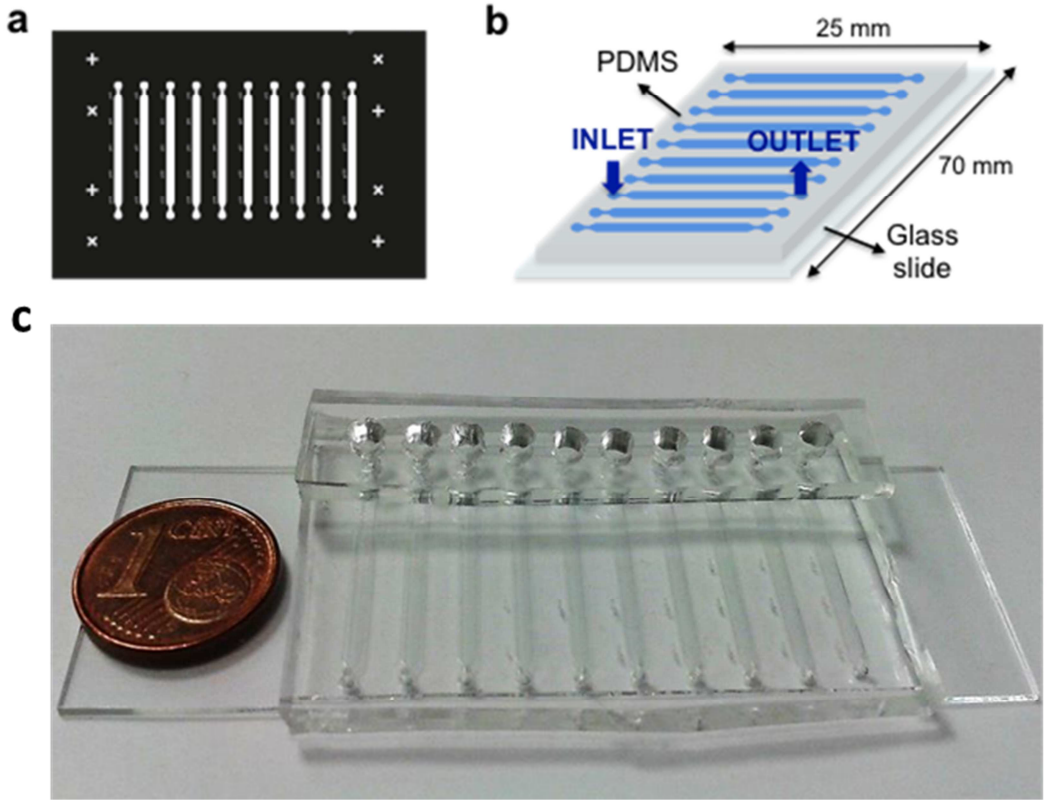

Figure 2.4: *Microfluidic device for cell cultures integration.* ***A:*** *Photomask with microfluidic channels.* ***B:*** *Schematic of microfluidic chip.* ***C:*** *Completed microfluidic chip with 10 independent channels and medium reservoirs at the inlet of the microchannels.*

2.4 Microfluidic oxygen gradient chip

A microfluidic platform was designed to generate a stable O2 gradient inside the microchannels. In order to generate the gradient, it is necessary to have a constant gas flux, with defined gas composition, at the sides of the microchannels. First, a mathematical model was produce before proceeding with platform fabrication (Fig. 2.5A). Next, the design of the photomask was produced, to fabricate a platform with three independent microchannels with defined gradient (Fig. 2.5B). In Figure 2.5C is shown the complete oxygen gradient chip. This platform was produced with the same techniques used for micropillar substrates and 10-channels microchips.

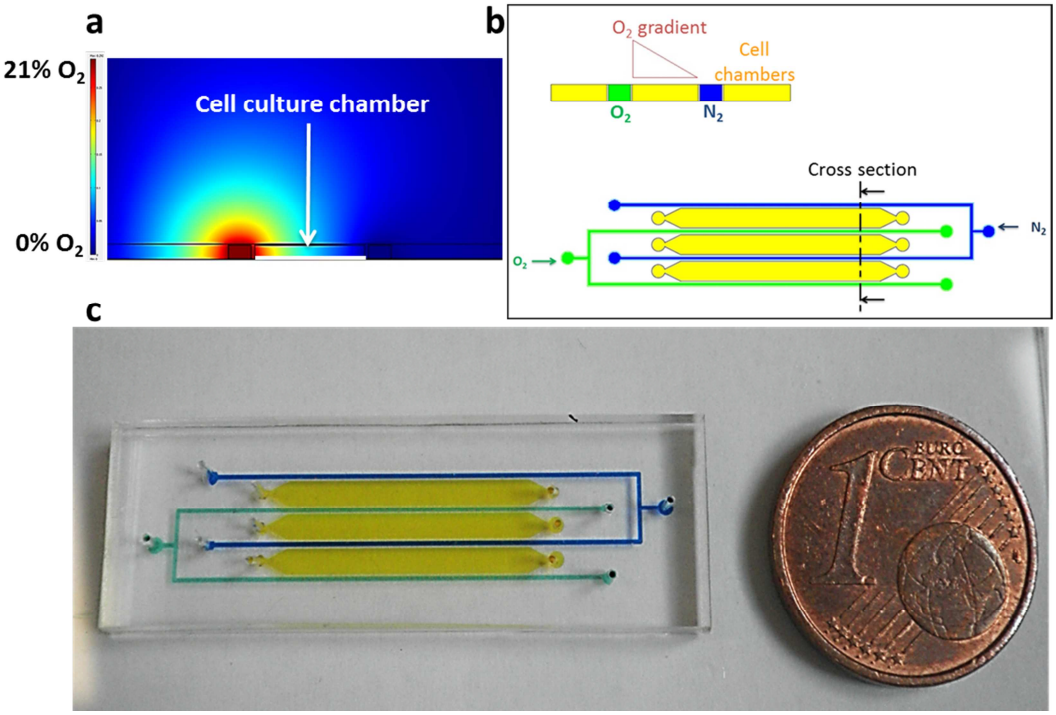

Figure 2.5: A: *Mathematical model of the cross section of the microchannel (cell culture chamber in white) with two gas channels on the sides. One channel with a mixture of air at 21% O_2 and 5% CO_2. In the second gas channel flows a mixture of 95% N_2 and 5% CO_2. The gasses diffuse through the PDMS culture chamber walls, generating an oxygen gradient.* ***B:*** *Microfluidic platform scheme. Three culture chambers (in yellow) and two parallel and opposite gas lines, nitrogen in blue and oxygen in green. Into each single channel, a proper O_2 gradient can be generated.* ***C:*** *Microfluidic oxygen gradient chip. The different channel were colored with standard dyes to make them more visible. Culture chambers (in yellow) and two gas lines (O_2 green, N_2 blue).*

In order to have the defined gas composition, flow meters (Bronkhorst) were used together with software Flow-Bus DDE. To validate oxygen gradient, a

luminescence oxygen sensor based on a Ruthenium (Ru) complex (Sigma-Aldrich) was used. This is a liquid solution, which can be inserted into the culture chambers. Its fluorescence is quenched by oxygen in the medium, and the O2 concentration can be extrapolated by fluorescence measure. Software elaboration (LasAF) was done to measure fluorescence intensity from one side to the other of the channels, both in control without gradient and with the mixture of gasses flowing in the as channels, to see if a stable O2 gradient was achievable (Fig. 2.6). All the measures were done at stationary state, after 5 minutes of fluorescence acquisition. It results that when the two gases flow at the side of the microchannel, they are capable of generating and maintaining on oxygen gradient, as long as the gas flows. This is important because the gradient has to be maintained for days, in order to allow cells to grow and differentiate. Gas flow rate was fixed to 1 mL/min, in order to generate the gradient, but not causing evaporation of medium from the culture chambers.

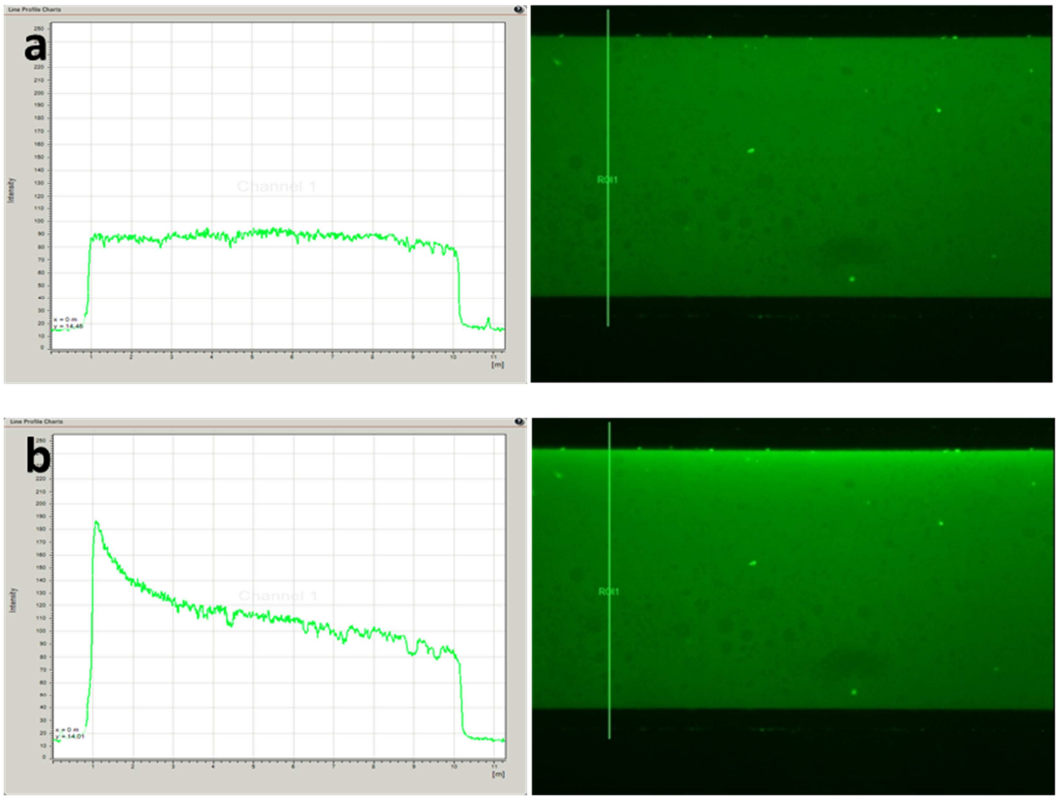

Figure 2.6: A: *Control channel without gas flow. No variation in Ru fluorescence is present.* ***B:*** *Channel with gas flow in the gas lines. At stationary point is present an exponential decay of Ru fluorescence, meaning a presence of a constant oxygen gradient in the cell culture chamber.*

2.5 Cell lines culture and expansion

HESC line HES2 (from National Stem Cell Bank, Madison, WI) was expanded in gelatin-coated Petri dishes (Fig. 2.7) , in co-culture with mouse embryonic fibroblasts (MEF, Chemicon) mitomycin C-inactivated, for various passages. Expansion medium is composed of DMEM F-12 (Invitrogen), 20% KO serum (Invitrogen), 10% MEF conditioned medium, 20 ng/mL basic fibroblast growth factor (b-FGF, Invitrogen), 0.1 mM β-mercaptoethanol (Invitrogen), 1% non-essential amino acid (Invitrogen) and 1% Pen/Strep (Invitrogen). HES2 were passaged to new feeder using trypsin 0.25% (Invitrogen) and disaggregating to single cell solution. For MEFs depletion and cell expansion and differentiation, cells were passaged on matrigel-coated (MRF 50%, BD Biosciences) microchannels.

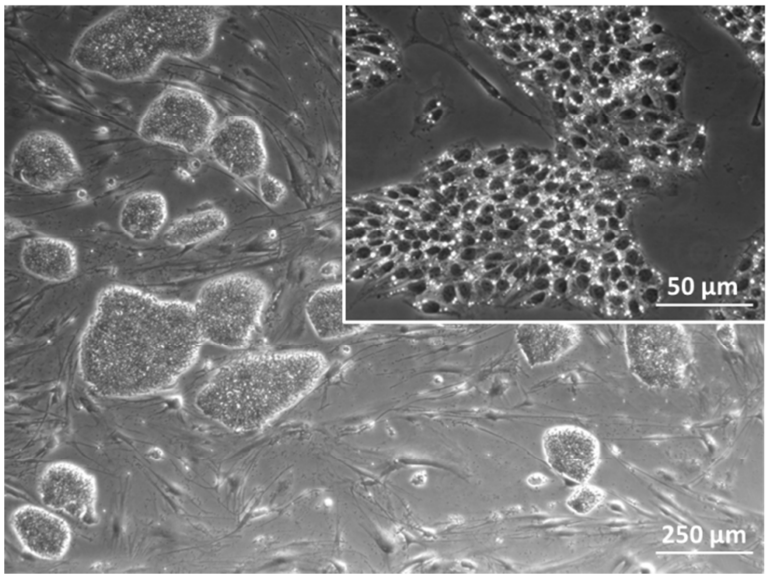

***Figure 2.7**. HES (HES2) cell colonies growing on MEF substrate, with relative enlargement of two adjacent colonies. Note the round shape and the compactness of the cells.*

HiPSC lines ADHF#1 (from Center for iPS Cell Research and Application, iCeMS, Kyoto University) (Fig. 2.8), Send#1 (generated with Sendai viruses), mRNA#1 - #2 (generated with mmRNA technology) were cultured and expanded during this PhD work. Human iPS reprogramming using modified mRNA (mmRNA) was performed according to Warren et al. 2010 (for detailed reprogramming protocol see Appendix B). Cells were cultured in gelatin-coated multiwells with mitomycin c-treated MEFs co-culture, in expansion medium DMEM F-12, 20% KO serum, 10 ng/mL b-FGF, 0.1 mM β-mercaptoethanol, 1% non-essential amino acids and 1% Pen/Strep. HiPSCs were passaged to new feeder using CTK solution (trypsin 0.25% - collagenase IV - Ca2+) and manually

detached by pick to keep technique, under stereoscopic microscope inside biological safety cabinet. For MEFs depletion and cell expansion and differentiation, cells were passaged on matrigel-coated microchannels.

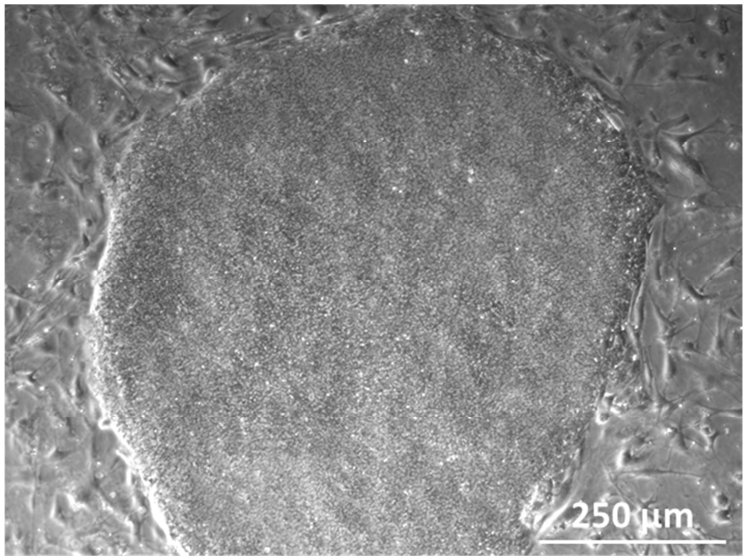

***Figure 2.8**. HiPS (ADHF#1) cell colony growing on MEF substrate. Note the homogeneity and compactness of the pluripotent cells.*

The hPSC suspension was injected into each single channel and the microfluidic chips were incubated overnight at 37°C and 5% CO2 atmosphere without perfusion, to allow cell adhesion to matrigel-treated glass substrate. We used proper cell seeding concentration to achieve 70% confluence cell culture at 24 h after seeding (Fig. 2.9).

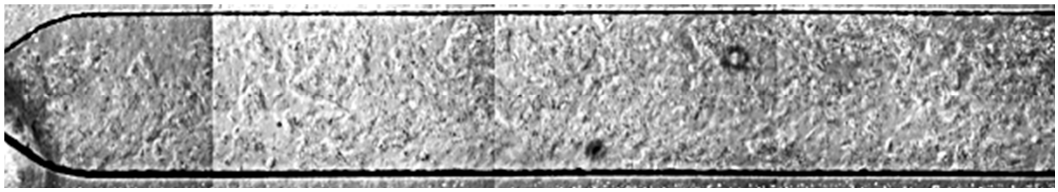

***Figure 2.9**. HES2 cells seeded inside a microchannel (snapshot from inlet to the center of the channel) after 24 h of adhesion to substrate.*

Multiple 9-port pumps (Cavro® XR Rocket pump, TECAN) were used to independently deliver the medium from the reservoirs into each microfluidic channel. Tygon tubing 0.5 ID (Cole-Parmer) and 21 G stainless-steel needles with a polypropylene luer (Microtest) were used to connect the microfluidic chips to the pumps. Discontinuous medium delivery with defined temporal frequencies was achieved by automatically controlling the multi-channel syringe pump through LabView 8.2 (National Instruments).

2.5.1 Cardiac differentiation

Cardiomyocyte differentiation protocol has been adapted from Lian et al. 2012. For cardiac differentiation human pluripotent stem cells were initially cultured with RPMI with 1% B27 supplement without insulin (Invitrogen), and 1% Pen/Strep. After 24 h, the medium was changed to RPMI with 1% B27 supplement w/o insulin, supplemented with 5 ng/mL BMP4 (R&D) and 1% Pen/Strep for another 4 days. After day 5 of differentiation, the medium was changed to RPMI with B27 supplement w/o insulin. At day 7, the cells were transferred to RPMI with B27 supplement complete. Cells were maintained for another 7-8 days in this medium, to obtain cardiomyocyte cells (Fig. 2.10). From day 10 to 15 of the differentiation, cell started to contract spontaneously, firstly isolated spots, then a consistent part of the cell monolayer.

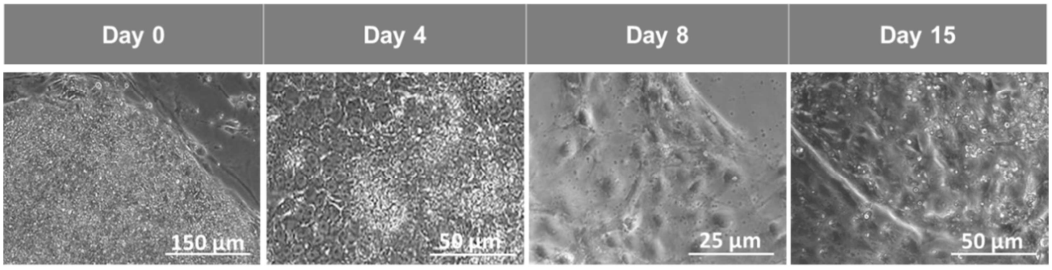

Figure 2.10. *Sequential morphological changes from human embryonic stem cells (day 0), through mesoderm stages (days 4 and 8) to cardiomyocyte cells (day 15).*

2.5.2 Hepatic differentiation

Hepatic differentiation protocol has been adapted from (Hay et al. 2008). For endoderm differentiation cells were treated with RPMI with B27 supplement 1% (both Invitrogen) 100 ng/ml activin A (Peprotech), 1 mM NaB (Sigma-Aldrich) and Pen/Strep 1% for 1 day. After 24h medium was changed to RPMI with B27 supplement 1% (both Invitrogen) 100 ng/ml activin A (Peprotech), 0.5mMNaB(Sigma-Aldrich) and Pen/Strep 1% for 2-3 days. After these first two media, dramatic cell death was observed, and only the survived cells were endoderm committed. Medium was then changed to hepatic endoderm commitment medium to KO-DMEM, 20% KO serum, 1 mM L-glutamine, 1% NEAA, 0.1 mM β-mercaptoethanol (all from Invitrogen), 1% DMSO (Sigma-Aldrich) and Pen/Strep 1% for 6-7 days. Cells were then maturated with L15 medium (Sigma-Aldrich) supplemented with 8.3% FBS, 8.3% tryptose phosphate

broth (both Invitrogen), 10 µM hydrocortisone 21-hemisuccinate, 1 µM insulin (all from Sigma-Aldrich) and 2 mM L-glutamine containing 10 ng/ml hepatocyte growth factor and 20 ng/ml oncostatin M (both from R&D) and Pen/Strep 1% for 7 days (Fig. 2.11). Hepatocyte-like cells were then kept in this medium for another 7 days, while doing the specific analyses and tests.

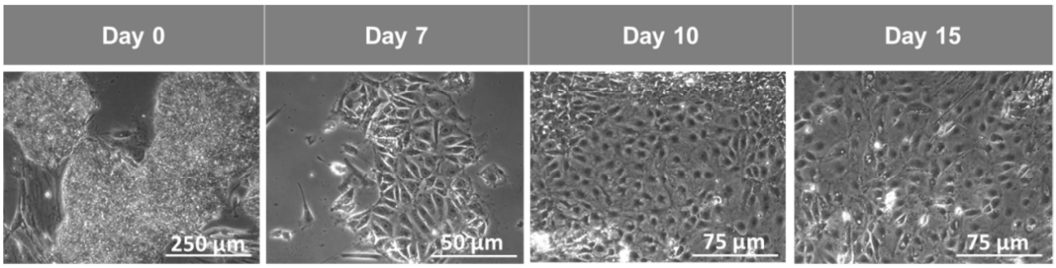

Figure 2.11. *Sequential morphological changes from human embryonic stem cells (day 0), through endoderm stages (days 7 and 10) to hepatocyte-like cells (day 15).*

References

Choi YY, Chung BG, Lee DH, Khademhosseini A, Kim J-H, Lee S-H. 2010. Controlled-size embryoid body formation in concave microwell arrays. Biomaterials 31(15):4296-4303.

Mohr JC, Zhang J, Azarin SM, Soerens AG, de Pablo JJ, Thomson JA, Lyons GE, Palecek SP, Kamp TJ. 2010. The microwell control of embryoid body size in order to regulate cardiac differentiation of human embryonic stem cells. Biomaterials 31(7):1885-1893.

Peerani R, Onishi K, Mahdavi A, Kumacheva E, Zandstra PW. 2009. Manipulation of Signaling Thresholds in "Engineered Stem Cell Niches'' Identifies Design Criteria for Pluripotent Stem Cell Screens. Plos One 4(7).

Tekin H, Anaya M, Brigham MD, Nauman C, Langer R, Khademhosseini A. 2010. Stimuli-responsive microwells for formation and retrieval of cell aggregates. Lab on a Chip 10(18):2411-2418.

Xia, Y. & Whitesides, G. M. Soft Lithography. Angew. Chem. Int. Ed. 37, 550–575 (1998).

Whitesides, G. M., Ostuni, E., Takayama, S., Jiang, X. & Ingber, D. E. Soft Lithography in Biology and Biochemistry. Annu. Rev. Biomed. Eng. 3, 335–373 (2001).

Warren L, Manos PD, Ahfeldt T, Loh YH, Li H, Lau F, Ebina W, Mandal PK, Smith ZD, Meissner A, Daley GQ, Brack AS, Collins JJ, Cowan C, Schlaeger TM, Rossi DJ. Highly efficient reprogramming to pluripotency and directed differentiation of human cells with synthetic modified mRNA. Cell Stem Cell. 2010 Nov 5;7(5):618-30.

Hay DC, Fletcher J, Payne C, Terrace JD, Gallagher RC, Snoeys J, Black JR, Wojtacha D, Samuel K, Hannoun Z, Pryde A, Filippi C, Currie IS, Forbes SJ, Ross JA, Newsome PN, Iredale JP. Highly efficient differentiation of hESCs to functional hepatic endoderm requires ActivinA and Wnt3a signaling. Proc Natl Acad Sci U S A. 2008 Aug 26;105(34):12301-6.

Hay DC, Zhao D, Fletcher J, Hewitt ZA, McLean D, Urruticoechea-Uriguen A, Black JR, Elcombe C, Ross JA, Wolf R, Cui W.Lian, X. et al. Proc. Natl. Acad. Sci. 109, E1848–E1857 (2012). Efficient differentiation of hepatocytes from human embryonic stem cells exhibiting markers recapitulating liver development in vivo. Stem Cells. 2008 Apr;26(4):894-902.

Lian X, Hsiao C, Wilson G, Zhu K, Hazeltine LB, Azarin SM, Raval KK, Zhang J, Kamp TJ, Palecek SP. Robust cardiomyocyte differentiation from human pluripotent stem cells via temporal modulation of canonical Wnt signaling. Proc Natl Acad Sci U S A. 2012 Jul 3;109(27):E1848-57

CHAPTER 3

MICROENVIRONMENT AND HUMAN PLURIPOTENT STEM CELL EARLY DIFFERENTIATION

3.1 Microenvironment modulation through hydrogel microwells

In order to manipulate pluripotent cell culture microenvironment, polyacrylamide hydrogels we used, because they are highly tunable in molecule permeability, and highly tunable in shape through photo-polymerization. Such hydrogels have been used to generate microwells to culture single differentiating embryoid bodies (EBs) derived from human pluripotent stem cells. The importance of growth factors in media during differentiation is well-known, but little information about the role of endogenous secreted molecules during early differentiation stages has been reported. When cultured in the absence of specific growth factors in medium, embryoid bodies can self-regulate their own differentiation through secretion of endogenous factors (Keller, 2005). In this perspective, a biomaterial that can locally accumulate soluble secreted molecules in a confined microenvironment has been designed. Two different heights of three-dimensional hydrogel microwells with defined diffusional properties have been produced and compared with suspension EBs as a control, to have three different microenvironment conditions for analyzing effects on early stem cell differentiation (Fig. 3.1). Embryoid bodies cultured in the three differentiation niches were examined through transcriptomic and proteomic analyses, in order to assess differential expressions of genes involved in early embryonic development, in the different culture conditions.

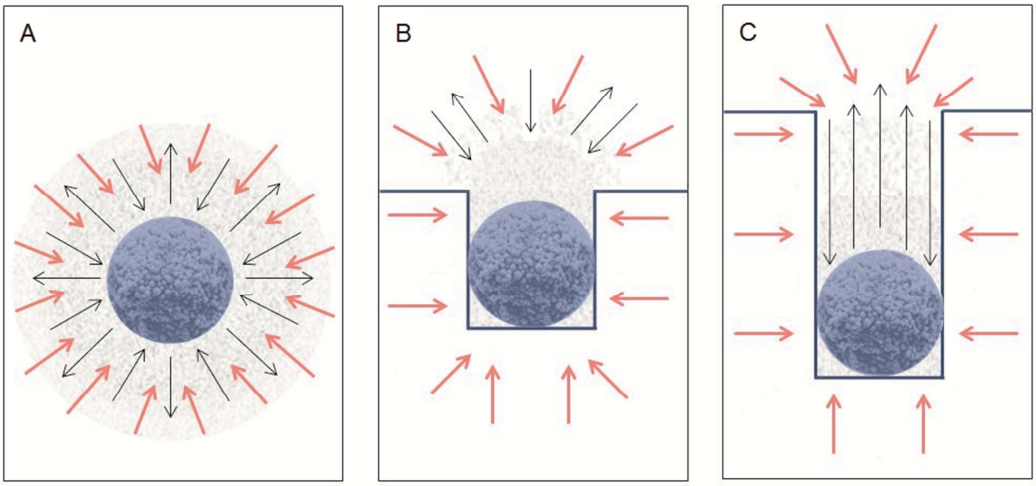

Figure 3.1. *Schematic of embryoid bodies in standard cell culture dishes and compartmentalized into the two types of microwells.* ***A****: EBs in suspension;* ***B****: EBs in microwells 500 µm × 450 µm, 1:1 ratio;* ***C****: 500 µm × 1 mm, 1:2 ratio. Black arrow represent endogenous factors diffusion, pink arrows indicate medium diffusion. In standard cell culture dishes, molecules secreted by differentiating embryoid bodies are rapidly distributed in the bulk medium. In microwells, molecules with different diffusivities will distribute in the EB microenvironment and into the surrounding medium by diffusion.*

A seeding of 4 × 105 cells per well was defined. Figure 3.2A shows an array of approximately 180 independent microwells, which are used for cell aggregation and culture. The concave microwell array allows a consistent cell seeding, which results in homogenous distribution of cells in all the microwells. Figure 3.2B and C shows that modulation of UV light intensity through use of photomasks and different lamps results in efficient modulation of microwell heights, with low standard deviation (Fig. 3.2D). The biocompatibility of polyacrylamide hydrogels was tested at day 10 to see if there was any toxic effect of unpolymerized PA monomers. With the use of Live and Dead essay cell vitality was assessed. It was not affected by embryoid body confinement, and viability was comparable with suspension embryoid bodies. These results indicate that all the PA monomers are washed during the washing procedures, thus the hydrogel is a hydrated and compatible biomaterial for cell culture.

In Figure 3.2E–G are shown the histograms representing the distribution of EBs diameters in suspension, 1:1 and 1:2 µwells, during three time points at 4, 8, and 12 days of culture. In suspension culture the distributions are dispersed in a wider range, showing less uniformity in dimensions during all time points. On the other hand, both microstructured cultures show more symmetric distributions. Average EB diameters are similar both in suspension and hydrogels after 8 days, even if EB cultures in the microwells are more homogenous. It has been

previously demonstrated how important the size homogeneity of embryoid bodies is during cell differentiation (Bauwens et al. 2008, Hwang et al. 2009, Karp et al. 2007, Moeller et al. 2008). Experimental data in Figure 3.2 show that is possible to compare the three different culture conditions, assuming that the effect of EB diameter do not override the influence of local EB microenvironment.

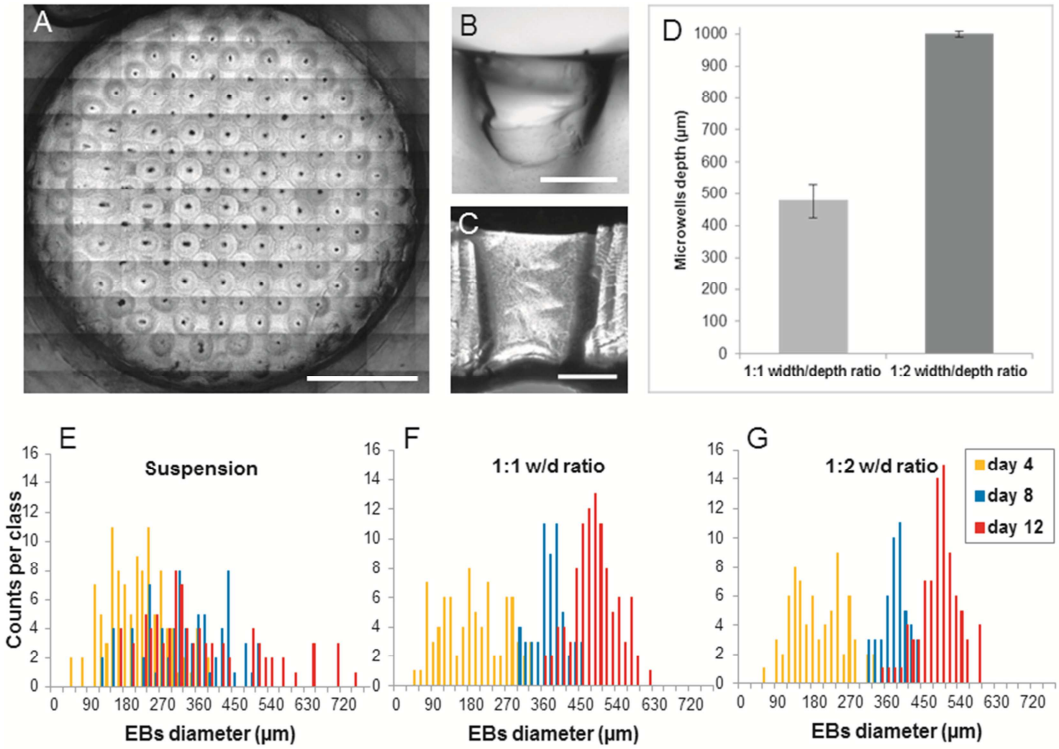

***Figure 3.2. A**: Array of EBs in the microwells of 1 mm depth (scale bar is 0.5 cm). Single EBs can easily be collected with a micropipette without disrupting the culture. **B**,**C**: Show enlargements of the vertical sections of the PA microwells of 450 µm and 1 mm depth, respectively. Scale bars in B and C are 250 µm. **D**: Measurements of the microwell depths. Panels (**E**–**G**) show quantitative distribution of suspension and microwell EBs diameter. E: Measurements of EBs diameters in suspension culture. F: Measurements of EBs diameters cultured in 500 µm width microwells and 450 µm depth (1:1). G: Measurements of EBs diameters cultured in 500 µm width microwells and 1 mm depth (1:2). The average embryoid body diameters (±standard deviation) after 4 days were 312 ± 148 µm (suspension), 210 ± 80 µm (500 µm Ø microwells 1:1) and 225 ± 98 µm (500 µm Ø microwells 1:2); after 8 days were 375 ± 155 µm (suspension), 385 ± 77 µm (500 µm Ø microwells 1:1) and 400 ± 68 µm (500 µm Ø microwells 1:2); after 12 days were 463 ± 191 µm (suspension), 504 ± 102 µm (500 µm Ø microwells 1:1), and 495 ± 84 µm (500 µm Ø microwells 1:2). Note the dispersion of diameter in the suspension culture condition during all time points, while data collected from the two types of microwell cultures have more symmetric distributions.*

3.1.1 EB differentiation in microwells and analysis

The expression patterns of embryoid bodies were assessed through transcriptomic analyses. Whole genome microarrays were used in order to have a complete overview of the gene expression in the different culture conditions.

The differential gene expression was tested at day 8 in HES2-derived EBs, in order to show early differentiation and commitment into the three germ layers (Keller, 2005). The same batches of cells were expanded and used to form EBs for the three different culture conditions, in order to have reliable results. Furthermore, three replicates for each microarray for consistent statistical analyses were done.

In the multiclass analysis 418 probes were selected, corresponding to 380 unique gene IDs and 8 ESTs. Among the 388 genes significantly differentially expressed, 189 resulted upregulated in suspension EBs compared to the cultures of microwell EBs. Other 203 genes were upregulated in the microstructured EB cultures and downregulated in suspension culture. A cluster analysis of the results was done with genes involved in early embryogenesis, which were grouped as reported in the microarray heat map in Figure 3.3. From data analysis it can be seen how the repetition of independent experiments and replicates show comparable results. There is a marked difference between gene expressions in suspension EBs compared to microwell EBs. It is also clear that the different ratio in 1:1 and 1:2 μwells do not influence gene expression, and therefore they have been grouped into a single category and confronted with suspension.

The expression of selective genes in endoderm, mesoderm and ectoderm was analyzed. There is a clear effect of the confinement in the differentiation patterns shown by the color graduation in the heat map. Results show that mesoderm specification and heart development is significantly upregulated in suspension EB, with expression of genes such as WIF1, BOC, MYH6, and TNNT2. On the other hand, genes such as NKX6-2, WNT3, GLI2, GDF3, and NRG1 involved in pattern specification process and regionalization, brain development, endoderm and ectoderm are consistently upregulated in microwell confined embryoid bodies. The microarray analysis thus highlights a significant difference in the differentiation patterns of standard and confined embryoid bodies.

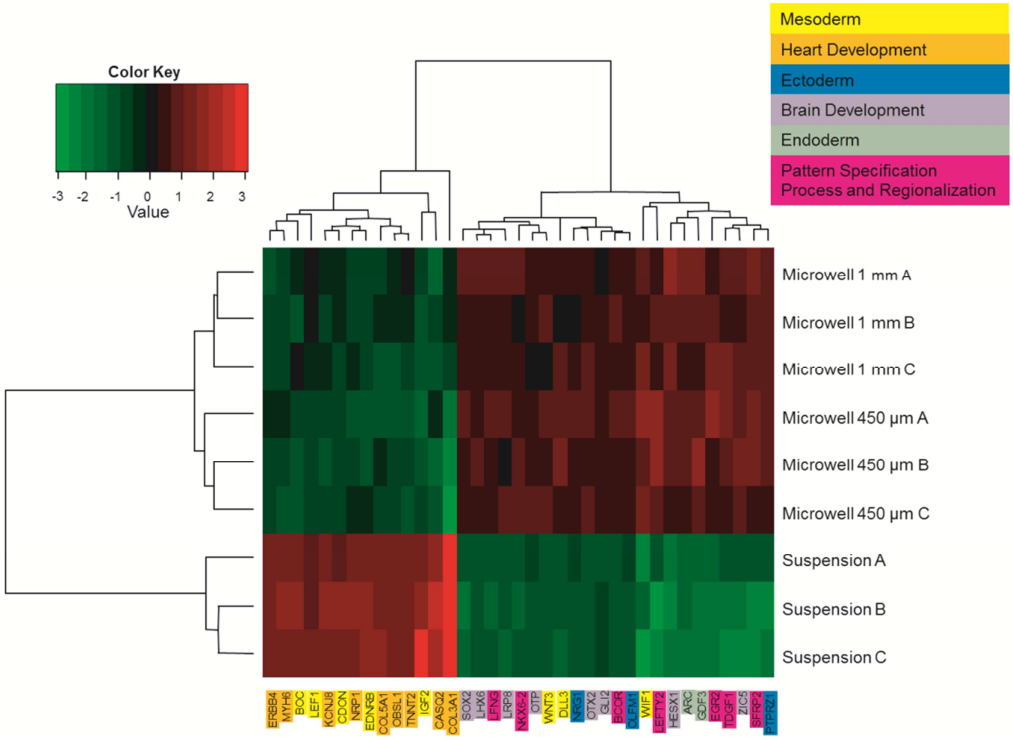

Figure 3.3. *Microarray analysis. The panel shows the heat map of the gene expression values of a subset of genes associated to the Gene Ontology enriched terms "mesoderm," "heart development," "ectoderm," "brain development," "endoderm," "pattern specification process and regionalization," in the different growing conditions and replicates. Mesoderm and heart development genes are significantly upregulated in EBs cultured in suspension. Ectoderm, brain development, endoderm, pattern specification process, and regionalization genes are significantly upregulated in EBs cultured in hydrogel microwells. The genes are grouped using a hierarchical agglomerative clustering (average linkage—Euclidean distance). Heat map showing the same gene expressions scaled with respect to genes average value, and heat map showing the expressions of the all the 388 genes, are shown in the supplementary material.*

After microarray experiments, immunofluorescence analyses were conducted to evaluate the expression of specific embryonic differentiation markers, and to investigate any possible influence of the different culture conditions onto early commitment to the three germ layers. Alpha-fetoprotein was used to mark early endoderm specification. Brachyury T marks the early embryonic mesoderm, while Beta-III Tubulin is used to mark the primary ectoderm. The immunofluorescence of the HES2-derived EBs sections is represented in Figure 6. AFP marking the endoderm is noticeably more expressed in EBs cultured in 1:1 and 1:2 µwells and less expressed in suspension EBs (Fig. 3.4A–C). The same result is observable for β-III Tub marking the ectoderm (Fig. 3.4F–H). On the other hand, brachyury T marking the mesoderm results more expressed in standard suspension EBs and less expressed in

microwell condition (Fig. 3.4K–M). Similar results are observed for hiPS-derived EBs at day 8.

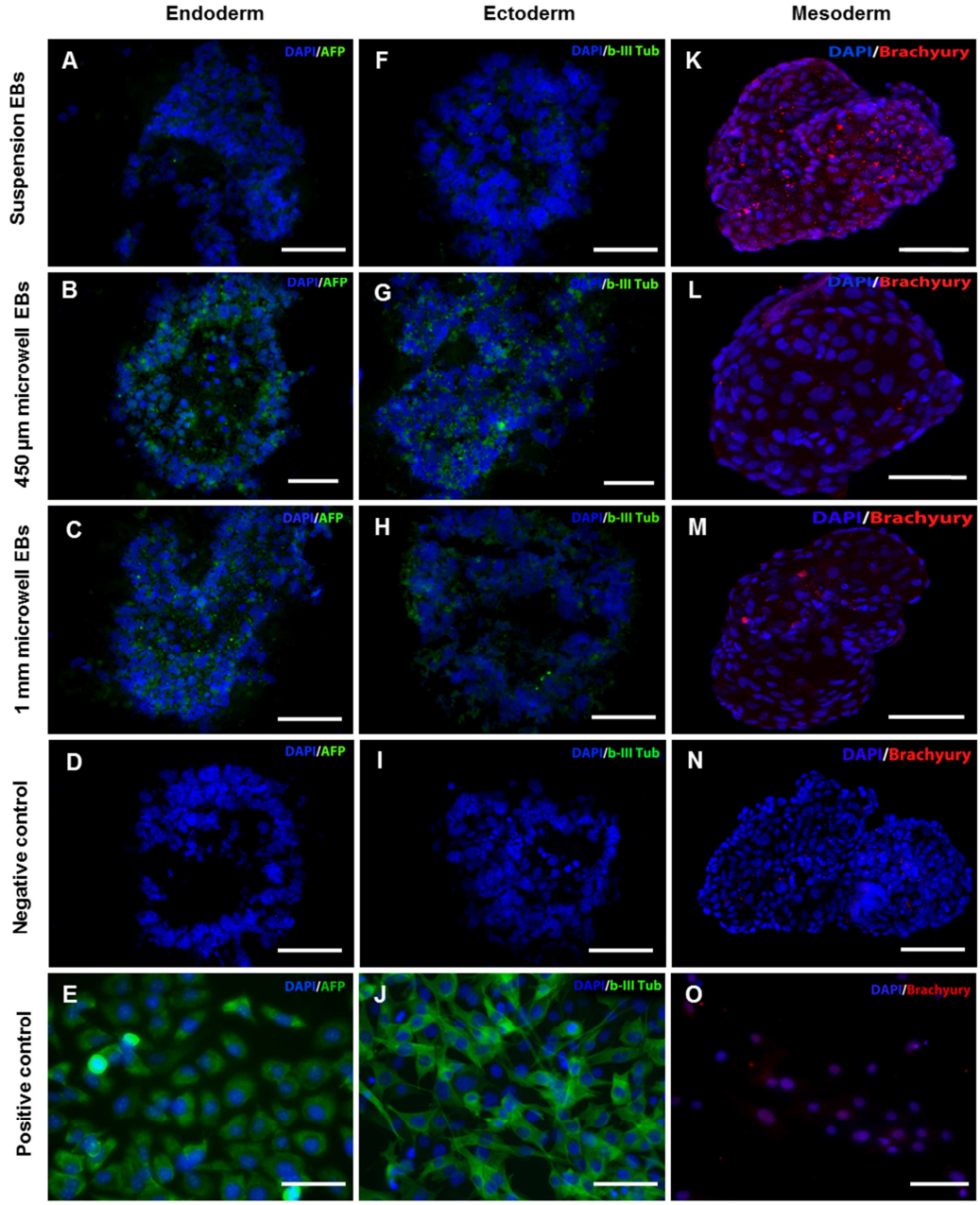

Figure 3.4. *Immunofluorescence analysis of the three germ layers on cryosections (20 µM thick) of 8 days hES-derived EBs cultured in the three conditions. Panels (**A–D**) show immunolabeling with alpha-fetoprotein (green), which marks the endoderm, and nuclei are stained with DAPI (blue). A major expression of this marker is shown by the microwell culture conditions. Panel (**E**) shows HepG2 cell line expressing high levels of AFP. Panels (**F–I**) show the expression of the ectoderm marker beta-III tubulin (green), which results more expressed in the 450 µM and 1 mm µwell conditions. C2C12 expressing b-III Tub are shown in panel (**J**). Panels (**K–N**) show labeling for Brachyury T (red), which recognizes the mesoderm. This marker is more expressed in EBs cultured in suspension. Panel (**O**) show the expression of Brachyury T in cardiomyocytes derived with a high-efficient mesoderm differentiation protocol of EBs. Scale bar is 100 µM.*

Quantification of immunofluorescence analyses was performed through cytospinned cells, and it clearly shows a difference in expression of the three germ layer markers among the different EB cultures. AFP and β-III Tub are significantly more expressed in both microwell cultures compared to suspension. On the other hand, brachyury T is significantly overexpressed in suspension EBs rather than microwells (Fig. 3.5). In order to confirm the results obtained with 8 days old EBs, the same immunofluorescence experiments were performed on adherent EBs at two different time points, days 4 and 12, both for hES and hiPS cells. The expression of differentiation markers agrees with the results observed in day 8 EBs.

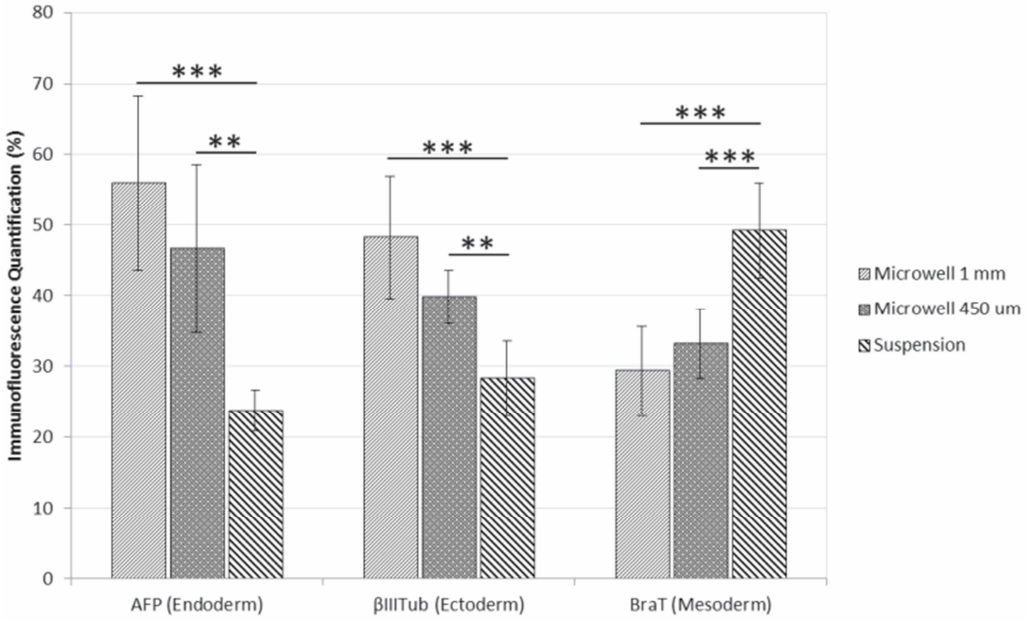

Figure 3.5. *The graph shows the immunofluorescence quantification by cytospin counts of 8 days hES-disaggregated EBs. Alpha-fetoprotein and beta-III tubulin are more expressed in the two microwell conditions, and show high significant difference compared to suspension culture. Brachyury T is higher expressed in suspension culture with high significant difference from 450 µm and 1 mm microwell cultures. Error bars are ±SD. Significativity is calculated with unpaired t-test. ***P < 0.001, **P < 0.01.*

From the analysis of the immunofluorescences, it is noticeable that there is no evident difference between the two types of microwell culture conditions. Microwell depth could still influence differentiation patterns, even though this was not noticed in these microwell geometries. However, it could be interesting to verify if exogenous molecules could restore mesodermal germ layer differentiation, which was downregulated in microstructured cultures. To this purpose, an experiment was performed in which 5 ng/mL of activin A, a mesoderm inducing factor at low concentrations, was added in the 1 mm

microwell culture medium. Surprisingly, at all the time points measured, the expression of mesoderm marker (brachyury T) in HES2-derived EBs was enhanced if compared with non-treated microwell EBs as shown in Figure 3.6.

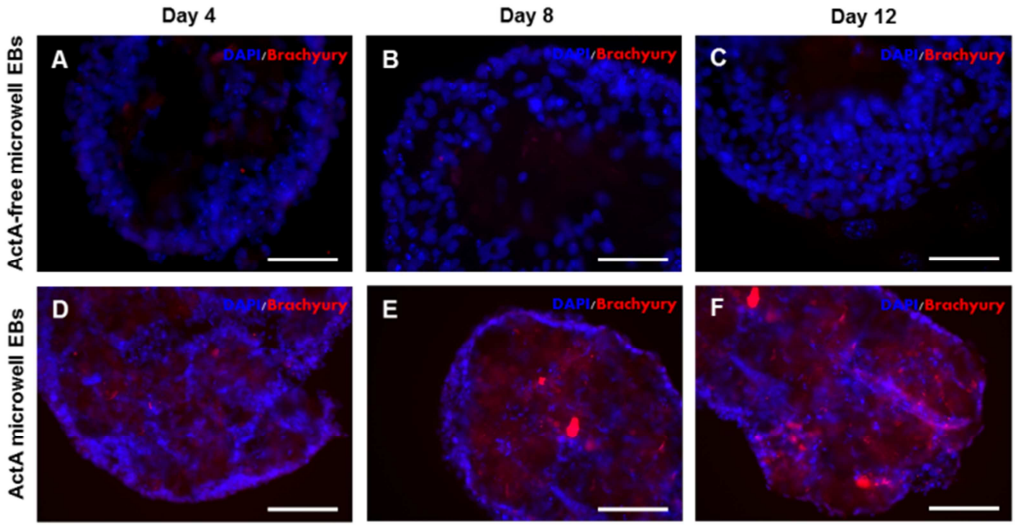

Figure 3.6. *Immunofluorescence analysis on adhered hES-derived EBs. Panels (**A–C**) show immunofluorescence of Brachyury T in 1 mm microwell EBs non-treated with exogenous factors. Panels (**D–F**) show immunolabeling with Brachyury T in 1 mm microwells EBs treated with Activin A (5 ng mL^{-1}), at three different time points, 4, 8, and 12 days. Treatment with exogenous ActA show induction of mesoderm germ layer in microwells culture of embryoid bodies. Scale bar is 300 µM.*

These outcomes on differentiation marker expression and gene expression can be correlated with an analysis of the relative dimensions (according to UniProt Database http://www.uniprot.org/) of the main secreted factors by the EBs, which are involved in the regulation of the differentiation patterns (Aberger et al., 1998; Clark et al., 2003; Germain and Littlefield, 1986; Stennard et al., 1997). The data of the molecular weights of the endogenous factors are shown in Figure 3.7. From these data, it can be seen that mesoderm is more expressed in suspension culture, therefore it can be hypothesized that mesoderm-inducing factors are relatively small compared to the cutoff of the polyacrylamide, so that they diffuse away from the cell niche in the microwells. At the same time, mesoderm-inhibiting factors should be relatively larger molecules that overstay in the microwells and diffuse slowly from the EBs. These hypotheses have a confirmation in the dimensions of secreted factors that influence or inhibit mesoderm formation (see Fig. 3.7). In the same table the data of the endogenous factors referring to ectoderm and endoderm are shown. Endoderm factors are not clearly defined in number and molecular weight, and not much can be discussed for this germ layer, even though immunofluorescence and

microarray experiments confirm that these factors are more expressed in the microwell EBs. Ectoderm-inducing factors have higher molecular weight compared to mesoderm-inducing factors, and therefore have lower diffusional times through the PA mesh and remain longer in the EBs microenvironment. In fact, ectoderm result more expressed in embryoid bodies cultured in the microwells. Interestingly, these results show that a mesoderm-inducing factor could override the effect of endogenous factors in 1 mm microwell culture, restoring mesodermal commitment.

These findings could indicate that the locally controlled availability of endogenous factors elicits significant differences in hPSC differentiation and may provide new insights into the mechanisms involved in cell differentiation.

Secreted Factor	Molecular Weight [kDa]	Regulation			References
		Endoderm	Mesoderm	Ectoderm	
Egf	6.4		Induction		(Stennard et al., 1997)
b-Fgf	18		Induction		(Stennard et al., 1997)
Ecdgf	18	Induction			(Germain et al., 1986)
Dkk-1	28		Induction	Inhibition	(Clark et al., 2003)
Noggin	30			Induction	(Aberger et al., 1998)
Scgf	33.9	Induction			(Germain et al., 1986)
FrzB	37		Inhibition		(Stennard et al., 1997)
Follistatin	39			Induction	(Aberger et al., 1998)
Wnt	40 - 46		Inhibition	Induction	(Aberger et al., 1998)
Tgf-b	50 (dimer)		Induction		(Stennard et al., 1997)
Bmp-4	60 (dimer)		Induction	Inhibition	(Germain et al., 1986)
Chordin	120			Induction	(Aberger et al., 1998)

Figure 3.7. *The chart shows some of the main germ layers secreted factors involved in embryogenic processes. The red parenthesis at the left side of the chart indicates the molecular weight cutoff of the PA hydrogel (around 40–70 kDa). The factors are ordered by growing molecular weight to show the correlation between dimensions and effect on the germ layers, to correlate with the data shown in the microarray and immunofluorescence analyses. Data referred to UniProt Database http://www.uniprot.org/.*

HPSC cultured in the three-dimensional system synthesize their own endogenous repertoire of factors and contribute to create a microenvironment suitable for cell growth and differentiation. Results show that the accumulation of endogenous factors has a deep effect on hPSC differentiation. This study could provide insights to the relationship between the confined cell niche and stem cell behavior during differentiation. In addition it sheds light on the potential effects of the diffusion of soluble factors and related effects on differentiation patterns in microenvironments, relevant to the emerging use of microstructured culture systems. Further experiments are required in order to study the regionalization

process in the EBs. It is also necessary to further study the possibility to modulate the microenvironment in a more accurate way, both in 3D and 2D cell cultures, in order to address specific differentiation.

3.2 Nuclear self-deformation in pluripotency and differentiation

To further evaluate effects of microenvironment variation during differentiation, an intrinsic property of hPSCs was considered, which has still to be deeply investigated and understood. This property is nuclei self-deformation capacity under defined geometrical constraints.

Nuclear shape and structure in eukaryotic cells are recognized to be deeply related with cell function during developmental, physiological and pathological modifications (Lombardi et al. 2010, De Vos et al. 2010, Dahl et al. 2010,). The nucleus, while regulating cell division and transcription processes, is exposed to mechanical stimuli from inside and outside the cell. Mechanical stimuli are transmitted by the cytoskeleton to the highly specialized nuclear membrane. The nuclear envelope connects to and interacts with the inner nucleus through the nuclear lamina, a dense protein network also connected to chromatin structure and gene regulatory complexes, which is crucial for structural support of the nucleus. Mechanics of the interphase cell nucleus is of paramount importance for the biological function of healthy cells and it is related to several pathologies (Lee et al. 2007, Hale et al. 2008, Lammerding et al. 2004,).

Nuclear plasticity and self-nuclear arrangement due to geometric constraints on human pluripotent stem cells during differentiation has never been reported and the comparison between pluripotent cells and cancer cells has not yet been performed.

In this part of the project, the aim was to study human pluripotent stem cell nuclear capacity to self-deform under defined geometrical constraints, meant as the spontaneous nuclear response to the morpho-topological environment. Here is reported how nuclei of human pluripotent stem cells have a high capability to deform and adapt their shape to the geometry of the substrate. Give this, the interest focused on understanding if this strong nuclear deformability could affect pluripotency and it was shown that pluripotency is not affected by a highly deformed nucleus. Furthermore, an investigation was done on how highly deformed nucleus can have an influence in the process of early germ layer

differentiation. Results show that the strong nuclear deformation of the nuclei when seeded in microstructured substrates affects the process of differentiation.

Studies on stem cells can represent an effective model to evaluate transitions in nuclear plasticity from the pluripotent to the differentiated stage and to elucidate the underlying mechanisms.

3.2.1 Pluripotency maintenance in micropillar cell culture

To evaluate how nuclear deformability changes in different cell lines, osteosarcoma cells (SaOs-2), hESCs, hiPSCs, cord blood mesenchymal stem cells (CBMSCs) and human epithelial renal cells (hERC) were seeded on matrigel-coated microstructured polymeric substrates characterized by square micropillars with a width of 7 micrometers, an inter-axial distance of 14 micrometers and a height of 7 micrometers. The substrates were fabricated both in polydimethylsiloxane (PDMS) and poly-l-lactic acid (PLLA). PDMS substrates were fabricated through replica molding technique and PLLA substrates through hot embossing technique. Substrate morphology was then characterized by SEM measurements (Fig. 3.8B). The geometrical structure of the substrates has been designed in order to impose a geometrical constrain to cell body and nucleus: the available space among micropillars is smaller than the average diameter both of cells and cell nuclei (for detailed materials and methods used in the work of nuclear deformation see Appendix D).

HOECHST stained cell nuclei of all cell lines were observed through fluorescent microscopy after two days of culture (Fig. 3.8A). A qualitative analysis of nuclear morphology show how SaOs-2, hESC and hiPSC nuclei strongly deform and assume very unusual shapes, to adapt to the morphology of the environment. HERCs keep a rounder shape, while CBMSCs are characterized by an intermediate behavior, with some nuclei showing concave shape. For each cell line the distribution of the number of concavities (Nc) was also evaluated (Figure 3.8D): cells that have a lot of concave nuclei that present only one concavity have to be considered less deformable than cells where high number of nuclei show three or four concavities. Lightly deformable cells as CBMSC and hERCs are characterized by nuclei that never present three or four concavities. To quantify this deformability two parameters were calculated, which are related respectively to nuclear penetration below pillar height and to nuclear shape: nuclear deformability (ND) and nuclear concavity (NC). ND has been calculated

as the percentage of the nuclear volume that lies below pillar height (Fig. 3.8C). NC is the percentage of nuclei that present at least one concavity. A concavity is defined as a concave curvature in cell nucleus: concave shapes appear only in deformable nuclei to adapt to pillar interspaces. The calculation of ND show a higher degree of deformability of SaOs-2, hESCs and hiPSCs compared to CBMSCs. HERCs show low deformability (Fig. 3.8E). These data are consistent with results obtained through the calculation of NC (Fig. 3.8F). Again, SaOs-2, hESCs and hiPSCs are the cells whose nuclei adapt the most to the morphological environment.

All together these results show that hPSCs have highly deformable nuclei, and this behavior can be compared to results found for cancer cell line SaOs-2. Nuclear deformability is much lower in mesenchymal cells and very strongly reduced in adult somatic cells.

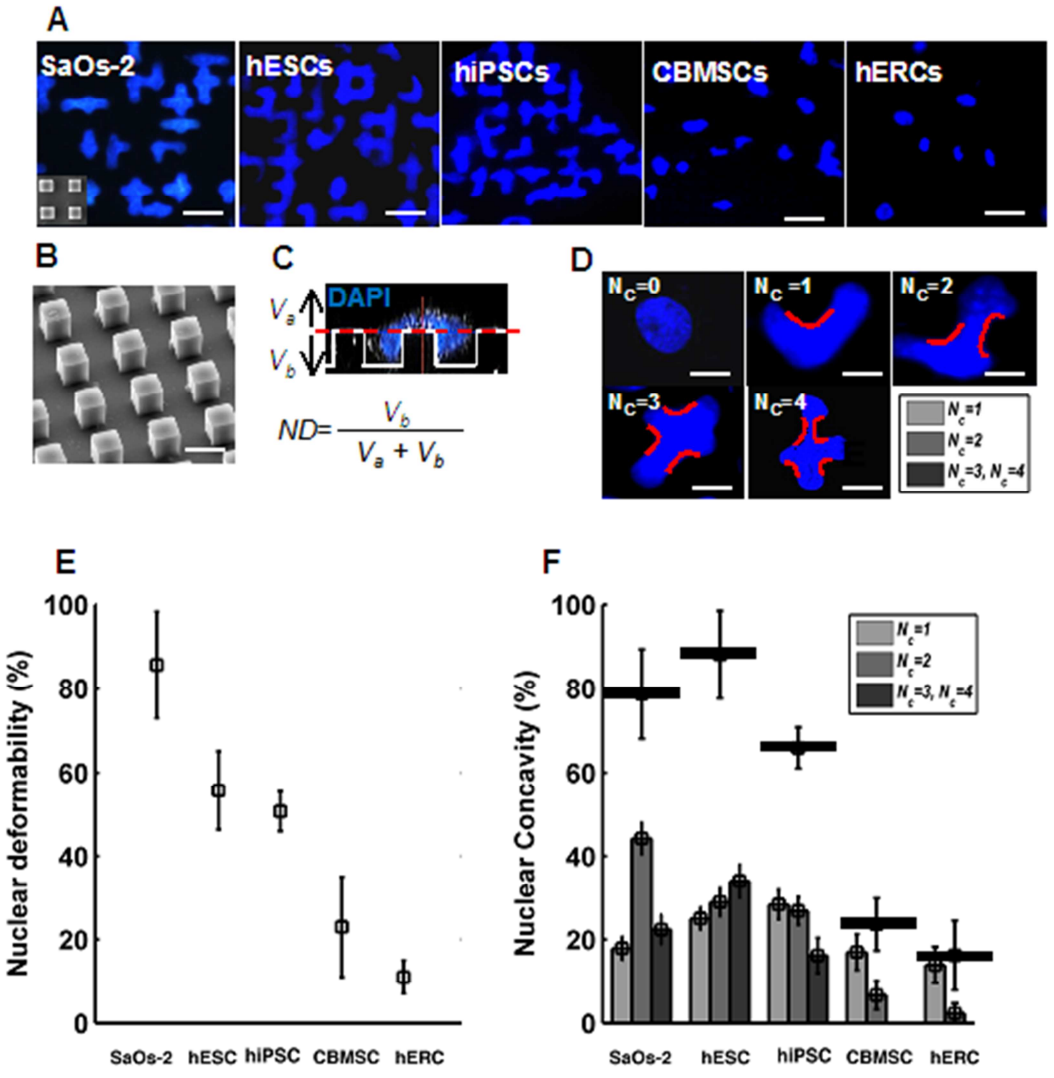

Figure 3.8. *Evaluation of nuclear deformability for different cell lines.* ***A:*** *HOECHST stained nuclei of SaOs-2, hiPSCs, hESCs, and CBMSCs acquired through fluorescent microscopy at day 2. Images*

show very deformed nuclei that assume unusual concave and sometimes branched shapes in hESCs, hiPSCs and SaOs-2. hERCs keep a round shape and CBMSCs show an intermediate behavior. ***B:*** *SEM image of the PDMS microstructured substrates were cells are seeded.* ***C:*** *Confocal image of a fluorescent labeled deformed nucleus: V_b (volume below) is the part of the nucleus which penetrates among pillar interspaces; V_a (volume above) is the part of the nucleus which stays above pillar height. Nuclear deformability (ND) is defined as $ND=(V_b/(V_a+V_b))*100$.* ***D:*** *Examples of nuclei with 0 concavities (Number of concavities=N_c=0), 1 concavity (Nc=1), 2 concavities (N_c=2), 3 concavities (Nc=3) and 4 concavities (N_c=4). The presence of such concavities in the nucleus is related to nuclear capability to deform.* ***E:*** *Plot of the nuclear deformability values calculated respectively for SaOs-2, hESCs, hiPSCs, CBMSCs and hERCs after fixing the cells at day 2. hESCs , hiPSCs and SaOs-2 present a nuclear deformability above 50%.* ***F:*** *Plot of nuclear concavity, meant as the percentage of cells having N_c>= 1. The histograms show the distribution of the number of nuclear concavities (1 concavity N_c=1, 2 concavities N_c=2, 3 or more concavities N_c=3, N_c=4) calculated among all the concave nuclei for each cell line. This graph show that hESCs, hiPSCs and SaOs-2 present the more deformable nuclei, in particular hESCs and SaOs-2 cell lines.*

After assessing how hESCs have a highly deformable nucleus, an investigation was done to see if morphologically deformed nuclei can affect pluripotent cell behavior. First, an evaluation of the possible effects on pluripotency maintenance was done. HESCs were seeded both in flat (Ctrl) and microstructured (μP) matrigel-coated PDMS substrates, and cultured in expansion medium. After 6 days cells were fixed and immunofluorescence analysis of pluripotency markers Oct-4, Nanog and SSEA4 was performed (Fig. 3.9A). The analysis shows a comparable expression of the markers between cells expanded in Ctrl and μP substrates. To confirm these data, quantitative real time PCR of pluripotency markers Nanog and Oct-4 was also performed (Fig. 3.9B). The results from qRT-PCR demonstrate that there is not a significant difference of marker expression between cells expanded on Ctrl and on μP. Pluripotency is maintained by hPSCs also when the expansion is performed in μP substrates, where cell nuclei present very deformed shapes. Consequently, self-deformation does not affect maintenance of pluripotency. The same experiments were performed on PLLA flat (Ctrl-PLLA) and microstructured (μP-PLLA) substrates and the same results were obtained (data not shown).

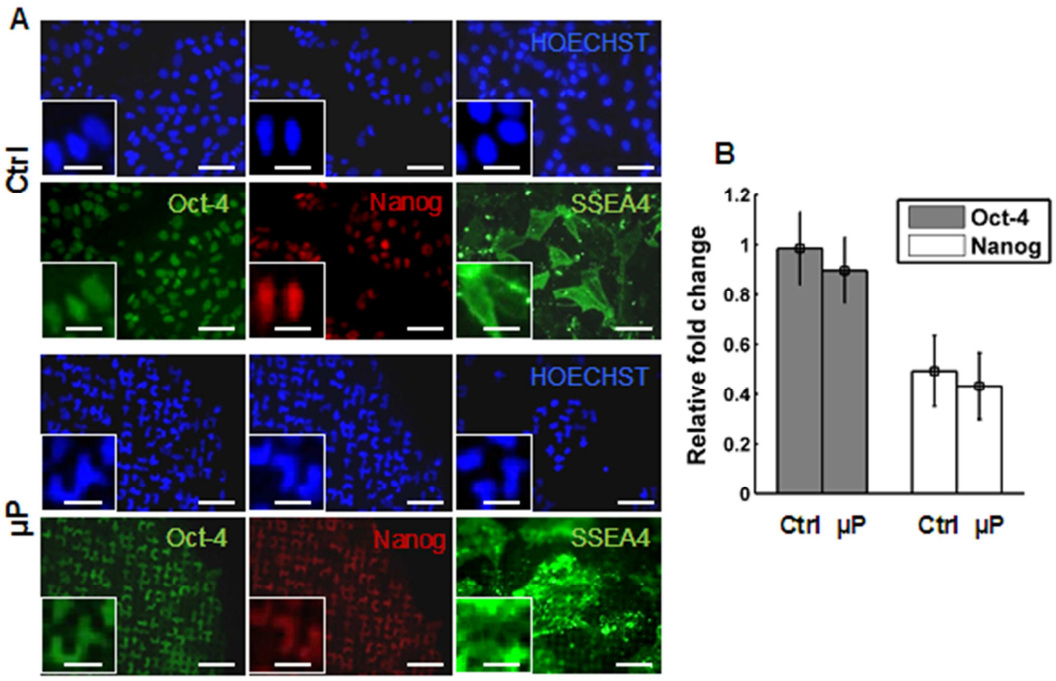

Figure 3.9. *HESC pluripotency maintenance on microstructured substrates.* ***A:*** *Immunofluorescence panel of cells cultured on flat PDMS substrates (Ctrl), showing pluripotency marker expression of Oct-4, Nanog and SSEA4. Cells cultured on PDMS microstructured substrates (μP). Marker expression between Ctrl and μP is similar. These panels show how nuclear deformation have no effect on pluripotency maintenance.* ***B:*** *qRT-PCR of Oct-4 and Nanog expression in hESCs cultured on flat PDMS (Ctrl) and pillar PDMS substrates (μP), which show comparable expression of pluripotency transcripts between the two conditions. Relative fold expression normalized on GAPDH (n=3).*

3.2.2 Effects of self-deformation during early differentiation

Next, an analysis was done to prove if the reorganization of the nuclei morphology can influence the process of differentiation into the three germ layers. Again, hESCs were seeded both in flat (Ctrl) and microstructured (μP) matrigel-coated PDMS substrates. The scheme in Figure 3.10A shows all the steps that lead to the commitment of the cells into early germ layers. Cells were first expanded for two days in expansion medium to achieve 70-80% cell confluence. Early germ layer specification was induced for 5 days, after which fluorescent labeled nuclei were observed through fluorescent microscopy. Interestingly, nuclei from ectoderm germ layer tend to escape from pillar interspaces and assume a round shape, whereas nuclei from mesoderm and endoderm germ layers still lies among the microstructures keeping deformed shapes. To understand if early germ layer specification took place, an immunolabeling was done on specific markers for each germ layer: β-III tubulin for ectoderm, brachyury T for mesoderm and α-fetoprotein for endoderm (Fig.

3.10B). Immunofluorescence early differentiation markers seems normally expressed in μP cells, compared to flat controls, and both in deformed nuclei (meso, endo) and de-deformed nuclei (ecto). To quantitatively assess changes in gene expression due to nuclear deformation, qRT-PCR was performed to quantify the expression of β-III Tub, Bra-T and AFP for each germ layer, both for ctrl and μP substrates (Fig. 3.10C). The analysis shows that the expression of β-III Tub and AFP is comparable between ctrl and μP substrates, whereas there is a significant difference between Bra-T expression in ctrl and μP substrates. Bra-T is very lowly expressed both in ectoderm and endoderm early germ layers when the protocol of early germ layers specifications are applied on cells cultured on flat substrates (ctrl) whereas there is an usual and significant expression of Bra-T on endoderm germ layer obtained from cells cultured and differentiated on microstructured substrates (μP).

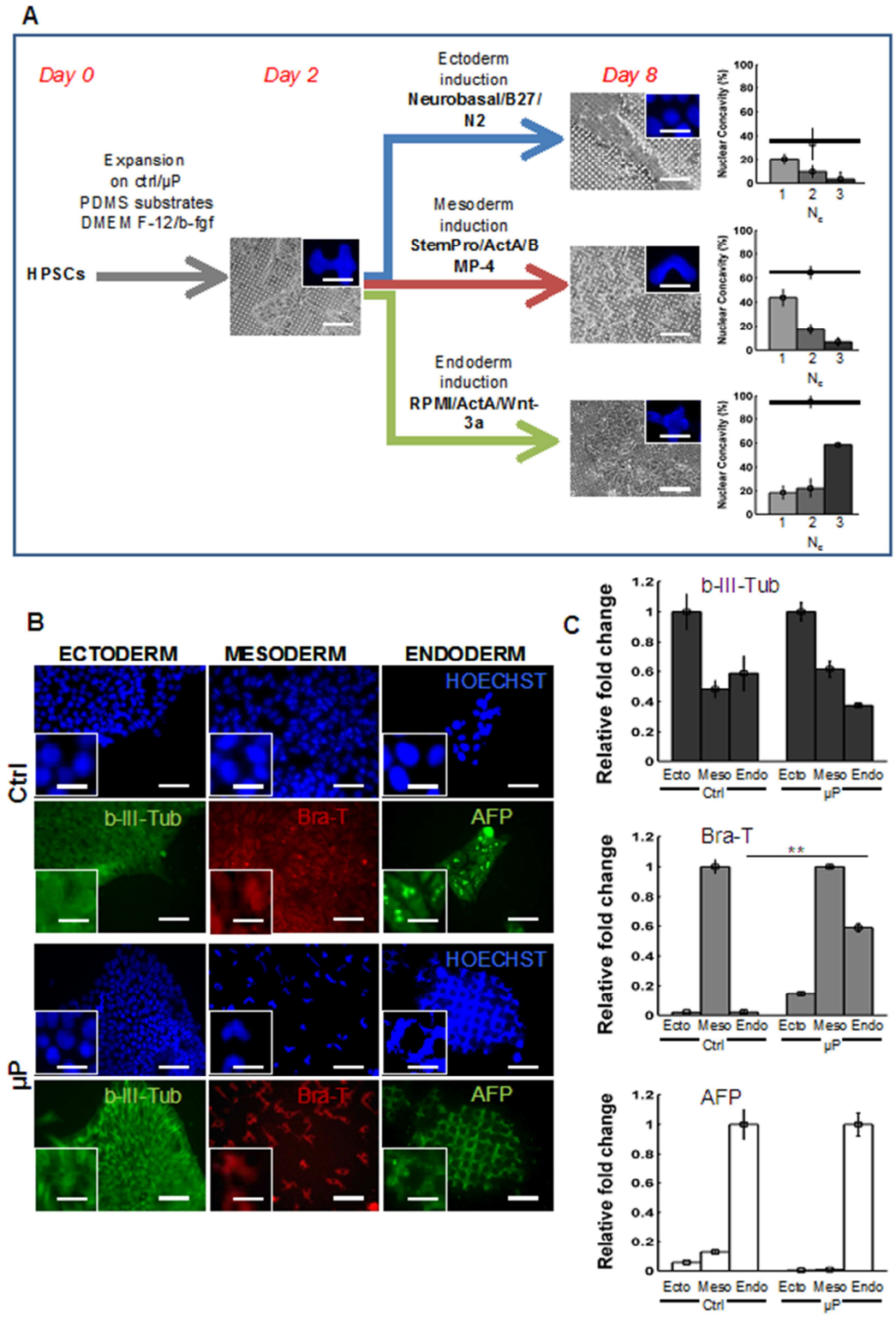

Figure 3.10. *HESC differentiation on microstructured substrates.* ***A:*** *Schematic showing experimental procedure of early germ layer commitment in hESCs with self-deformed nuclei. Cell are passaged on microstructured PDMS substrates and expanded for 2 days. Different replicates are then induced with specific media into 3 germ layers for 5 days* ***B****: Immunofluorescence panel showing differentiated hESCs on flat PDMS substrates (Ctrl) and on PDMS substrates (μP). Cells are marked with beta III tubulin for ectoderm, brachyury for mesoderm and alpha-fetoprotein for endoderm. Notably, ectoderm cell nuclei tend to homogeneously emerge from the pillars and gain round shape. Mesoderm and endoderm cells tend to differentiate while maintaining highly*

deformed nuclei. ***C:*** *qRT-PCR of early germ layer markers, β-III tub, bry and AFP in the 3 differentiation protocols in both flat (Ctrl) and microstructured substrates (μP) . β-III tub is significantly higher expressed in ectoderm flat and pillar differentiation. Bry is significantly higher expressed in mesoderm flat and pillar differentiation, and notably, in endoderm pillar differentiated cells. AFP is significantly high in endoderm flat and pillar differentiation. Relative fold expression normalized on GAPDH (n=3). Student* t *test p-values P ≤ 0.01 (**).*

The nuclear deformation induced by microstructured substrates does not affect mesoderm specification, despite cell nuclei keep a high level of deformation during the all process of differentiation. Ectoderm specification can also take place when cells are seeded on microstructured substrates, but is associated to a strong loss of nuclear deformability by the cells. Endoderm germ layer specification is characterized by strongly deformed nuclei that do not lost their deformability, but this nuclear reorganization hinders the physiological process of differentiation.

Being ectoderm the only germ layer showing major nuclear morphological changes, it was decided to further investigate nuclear behavior during differentiation. In Figure 3.11A is shown a time-course of live-stained HES2 nuclei from pluripotent state at day 0, with highly deformed shapes, to ectodermal commitment ad day 4, with almost entirely round-shaped nuclei. Figure 3.11B shows nuclear concavity quantification following a day by day measure of percentage concavity. Notably, major shape changes happen between day 1 and day 2, with almost all cells losing self-deformation capacity. It will be necessary to further analyze this results, mainly studying what happens when cells start changing morphology during ectodermal commitment. This will be done through cytoskeletal analyses, with chemical and biological selective inhibitors of specific proteins though to be involved in nuclear and cytoskeletal organization. New results will help to understand how important is nuclear deformation during differentiation and if these properties have specific relevant applications.

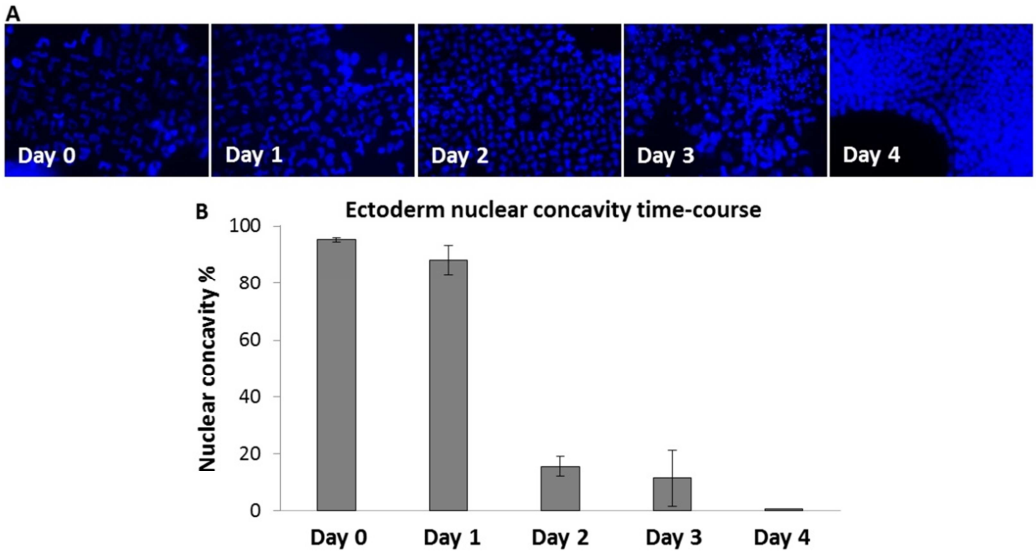

Figure 3.11. *HESC ectoderm differentiation on microstructured substrates.* ***A:*** *Nuclear morphology evolution from pluripotent state (Day 0) to ectoderm germ layer (Day 4). Nuclei progressively pass from deformed shapes to rounder morphology. B: Nuclear concavity time-course of pluripotent cells (Day 0) induced to ectoderm commitment (Day 4). Major drop of NC % in between day 1 and day 2 of differentiation.*

These first results on pluripotent nuclei self-deformation capacity are important to understand the mechanisms of nuclear properties and plasticity. Further and detailed work has to be done in order to understand how this intrinsic property is important for pluripotency, early germ layer commitment and functional maturation, and to understand if there is a strict connection between pluripotent cells and cancer cells properties.

Concluding, in this chapter it has been provided a strong evidence that cell endogenous niche is fundamental in order to modulate cell differentiation and fate. The methodologies presented give the possibility to modulate different aspects of the stem cell niche, such as endogenous factors accumulation in the three-dimensional hydrogel microwells, or geometrical cues, and how superimposed mechanical constraints influence cell behavior during early commitment. These strategies give the opportunity to study particular aspects in stem cell culture and differentiation, but they cannot be tuned during these processed. There is the need to find a methodology, which allows a deeper control over cell culture microenvironment, in order to address cell fate in a more precise way.

References

Keller G. 2005. Embryonic stem cell differentiation: emergence of a new era in biology and medicine. Genes & Development 19(10):1129-1155.

Bauwens CL, Peerani R, Niebruegge S, Woodhouse KA, Kumacheva E, Husain M, Zandstra PW. 2008. Control of human embryonic stem cell colony and aggregate size heterogeneity influences differentiation trajectories. Stem Cells 26(9):2300-2310.

Hwang Y-S, Chung BG, Ortmann D, Hattori N, Moeller H-C, Khademhosseini A. 2009. Microwell-mediated control of embryoid body size regulates embryonic stem cell fate via differential expression of WNT5a and WNT11. Proceedings of the National Academy of Sciences of the United States of America 106(40):16978-16983.

Karp JM, Yeh J, Eng G, Fukuda J, Blumling J, Suh K-Y, Cheng J, Mahdavi A, Borenstein J, Langer R and others. 2007. Controlling size, shape and homogeneity of embryoid bodies using poly(ethylene glycol) microwells. Lab on a Chip 7(6):786-794.

Moeller H-C, Mian MK, Shrivastava S, Chung BG, Khademhosseini A. 2008. A microwell array system for stem cell culture. Biomaterials 29(6):752-763.

Aberger F, Weidinger G, Grunz H, Richter K. 1998. Anterior specification of embryonic ectoderm: the role of the Xenopus cement gland-specific gene XAG-2. Mechanisms of Development 72(1-2):115-130.

Clark HF, Gurney AL, Abaya E, Baker K, Baldwin D, Brush J, Chen J, Chow B, Chui C, Crowley C and others. 2003. The Secreted Protein Discovery Initiative (SPDI), a large-scale effort to identify novel human secreted and transmembrane proteins: A bioinformatics assessment. Genome Research 13(10):2265-2270.

Germain EL, Littlefield JW. 1986. Endoderm-Secreted Factor Stimulates Growth of Embryonal Carcinoma Stem-Cells. In Vitro Cellular & Developmental Biology 22(2):107-112.

Stennard F, Ryan K, Gurdon JB. 1997. Markers of vertebrate mesoderm induction. Current Opinion in Genetics & Development 7(5):620-627.

Lombardi ML, Lammerding J. Altered mechanical properties of the nucleus in disease. Nuclear Mechanics and Genome Regulation. 2010;98:121-41.

Dahl KN, Booth-Gauthier EA, Ladoux B. In the middle of it all: Mutual mechanical regulation between the nucleus and the cytoskeleton. J Biomech. 2010 JAN 5;43(1):2-8.

De Vos WH, Houben F, Hoebe RA, Hennekam R, van Engelen B, Manders EM, et al. Increased plasticity of the nuclear envelope and hypermobility of telomeres due to the loss of A-type lamins. Biochim Biophys Acta. 2010 Apr;1800(4):448-58.

Lee JSH, Hale CM, Panorchan P, Khatau SB, George JP, Tseng Y, et al. Nuclear lamin A/C deficiency induces defects in cell mechanics, polarization, and migration. Biophys J. 2007 OCT;93(7):2542-52.

Hale CM, Shrestha AL, Khatau SB, Stewart-Hutchinson PJ, Hernandez L, Stewart CL, et al. Dysfunctional connections between the nucleus and the actin and microtubule networks in laminopathic models. Biophys J. 2008 DEC 1;95(11):5462-75.

Lammerding J, Schulze P, Takahashi T, Kozlov S, Sullivan T, Kamm R, et al. Lamin A/C deficiency causes defective nuclear mechanics and mechanotransduction. J Clin Invest. 2004 FEB;113(3):370-8.

CHAPTER 4

MICROFLUIDIC TECHNOLOGY AND HUMAN PLURIPOTENT STEM CELL MICROENVIRONMENT MODULATION

4.1 Stem cell culture and expansion in microfluidic chip

Micro-engineering human "tissues-on-chips" remains an open challenge from both scientific and technological points of view. In this part of the PhD project, I describe an efficient microfluidic-based approach for the differentiation of human pluripotent stem cells into functional cells, in order to generate human cardiomyocytes and hepatocytes on chip. This technology opens a new perspective for multi-parametric and large scale human organ-based screening assays.

In this chapter, cell microenvironment will be analyzed with a different technology, which can help controlling in a more accurate way the balance between endogenous and exogenous factors, rather than just utilizing diffusional properties as in polyacrylamide hydrogel microwells. An exploration was done to see whether is possible to control stem cell expansion of hESCs and hiPSCs through a multi-stage microfluidic-based technology. (Discher et al., 2009; Dupont et al., 2011; Wan et al., 2011). Pluripotency maintenance during stem cell expansion would require an accurate balance between extrinsic and intrinsic cell signaling, through optimal in vitro delivery of exogenous factors and removal of endogenous cell-secreted factors (Korin et al., 2006; Villa-Diaz et al., 2009). Continuous microfluidic flow perfusion has been recently shown to generate soluble factor spatial gradients along the microfluidic channel that lead to heterogeneous cell phenotype. Here, is shown how a discontinuous periodic medium delivery with stage-dependent frequency (number of cycles of medium change per day) is an effective strategy for modulating stem cell niche specification in vitro (Fig. 4.1). Cell growth in continuous perfusion appears more inhomogeneous after 48 h of culture, compared to homogenous distribution of cell colonies under discontinuous medium change, which also show homogenous expression of pluripotency markers. Also quantification of cell colony diameters from inlet, center and outlet of the microchannels shows high homogeneity in periodic perfusion compared to continuous perfusion.

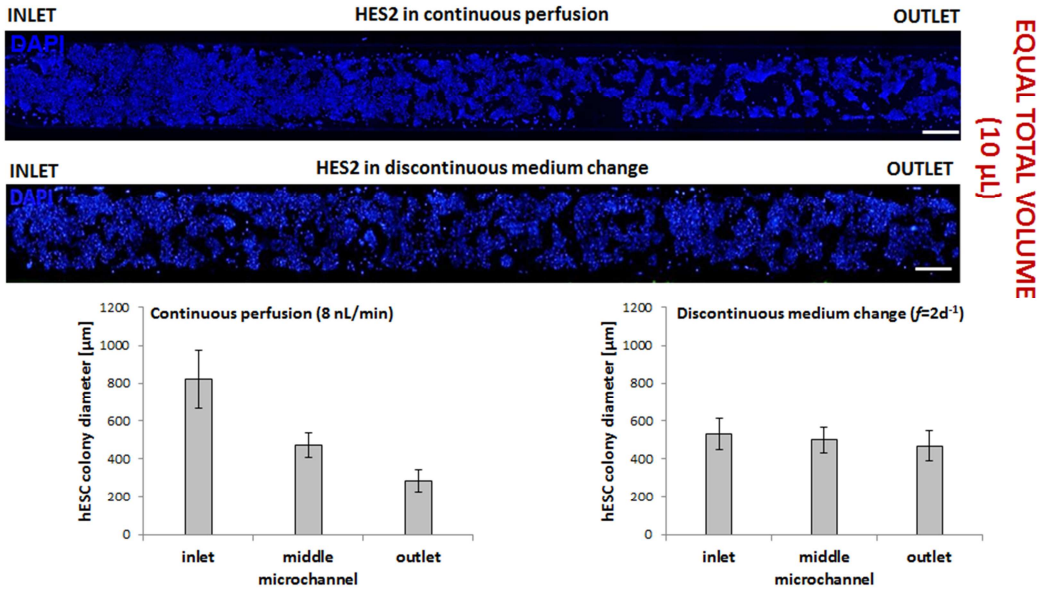

Figure 4.1. *Microchannels with cells cultured in continuous perfusion compared with discontinuous medium change with a frequency of medium change of $f=2d^{-1}$. Diameters ± S.D. of cell colonies have been quantified through LAS AF software with a minimum of 6 measures for each single position, in three independent channels for each culture condition.*

The identification of the role of extrinsic autocrine-paracrine factors in pluripotency and self-renewal and germ layer commitment (see Chapter 3), suggests a synergic mechanism of specific exogenous and endogenous factors in promoting transcriptional activity of pluripotency genes (Fig. 4.2A). The computational investigations on extrinsic signaling model revealed that frequency of periodic medium delivery strongly affects accumulation of exogenous and endogenous factors, thus regulating transcriptional activity of target genes. A frequency increase reduces the amplitude of temporal fluctuations of both exogenous and endogenous factors (Fig. 4.2B), thus maintaining sustained transcriptional activity of the associated target genes. However, higher frequencies of medium change produce decreased expression of gene transcript, due to continuous endogenous secreted factors wash-out. This simple schematic modeling reveals high correlation between frequency of medium change and extrinsic signaling regulation (for detailed materials and methods used in this work of hPSCs on-a-chip see Appendix B).

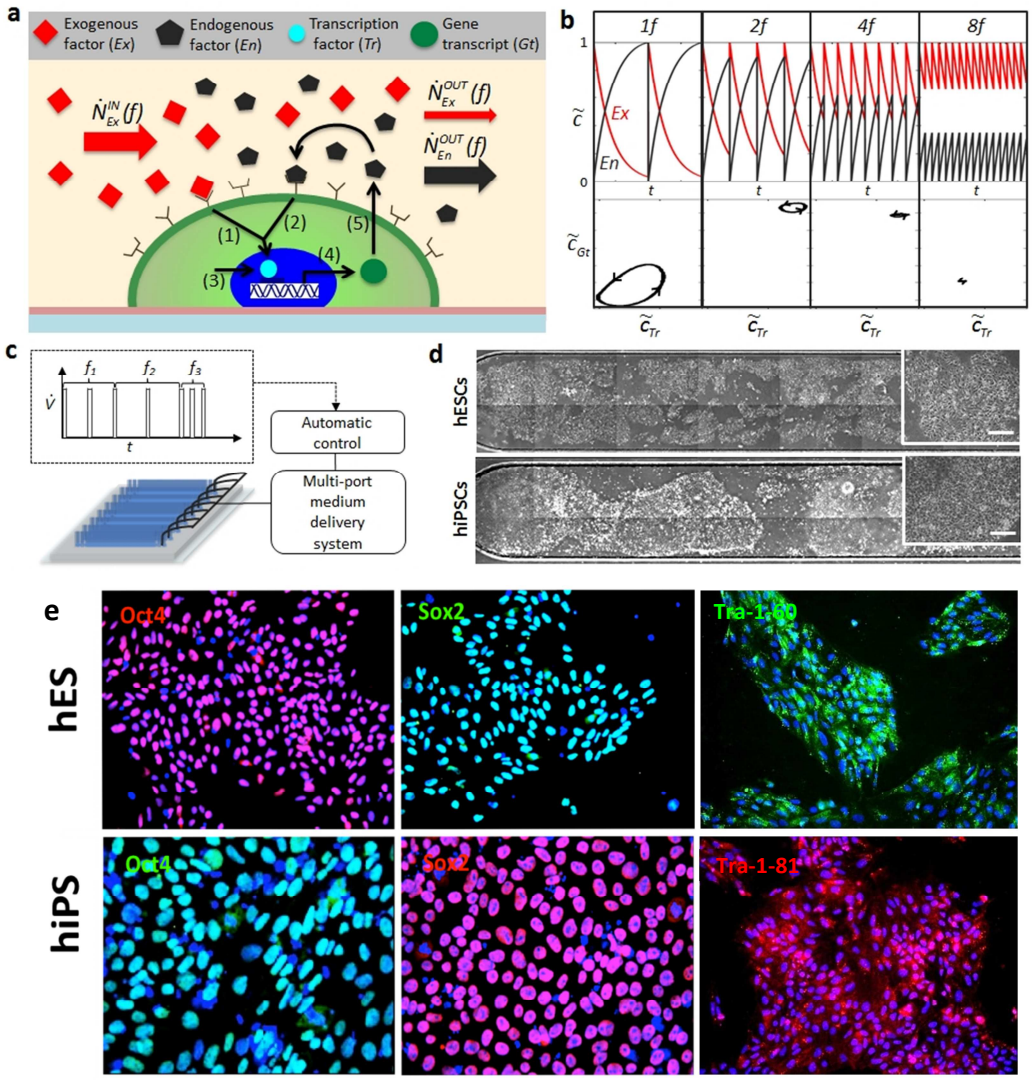

Figure 4.2. *Pluripotent stem cell culture on-a-chip.* ***A:*** *Pluripotency signaling model in microfluidic stem cell culture. Both exogenous (Ex) and endogenous (En) factors contribute to transcriptional activity of pluripotency genes through activation of target transcription factors (Tr).* ***B:*** *Signaling model output. Temporal profiles of normalized Ex and En factor concentrations in the microfluidic channel at increasing frequencies (up). Gene transcript (Gt) concentration profile plotted versus corresponding Transcription factor (Tr) variation during a single medium perfusion at increasing frequencies.* ***C:*** *Experimental set-up. Periodic medium delivery in microfluidic channels (200 μm high, 1.5 mm width, 1.8 mm length and 6 μL volume) is controlled through a multi-port delivery system. Different frequencies sequences are automatically programmed through Labview software.* ***D:*** *Microfluidic hPSCs culture. Half channel views showing hESCs and hiPSCs expanded for 6 days in microfluidic conditions with* $f=2d^{-1}$*. Insets show typical morphology of stem cells colonies. Scale bar 50 μm.* ***E:*** *Immunofluorescence analysis of pluripotency markers Oct-4, Sox2, Tra-1-60 and Tra-1-81 for hESCs and hiPSCs after 6 days in microfluidic channels.*

An investigation was done on the best condition for both hESC and hiPSC expansion in microfluidic channels to maintain high stemness and homogeneous morphology among colonies at different regions along the channels. HPSCs were injected into multiple microfluidic platforms, each containing 8 independent

channels and connected to a multi-port syringe pump, for software-automatize medium change (Fig. 4.2C). Cells were then cultured with defined frequency up to 6 days (Fig. 4.2D). Immunofluorescence staining revealed that both hESCs (HES2) and hiPSCs (ADHF#1) homogeneously express pluripotency markers such as Oct-4, Sox2, Tra-1-60 and Tra-1-81 (Fig. 4.2E).

4.2 Pluripotency maintenance optimization

Next, optimization of hESC microfluidic culture was performed to maintain high pluripotency in the channels, comparable to standard static conditions. The qRT-PCR analysis of pluripotency marker Oct-4 and Nanog after 6 days of culture, showed optimal frequencies of f=1.5d-1 and f=2d-1 (Fig. 4.3). Significant two-fold higher expression compared to lower (f=1d-1) and higher frequencies (f=3d-1 f=4d-1 f=8d-1 and continuous perfusion) was observed. These results are consistent with the hypothesis that an appropriate balance of exogenous molecules and endogenous cell-secreted factors has to be provided.

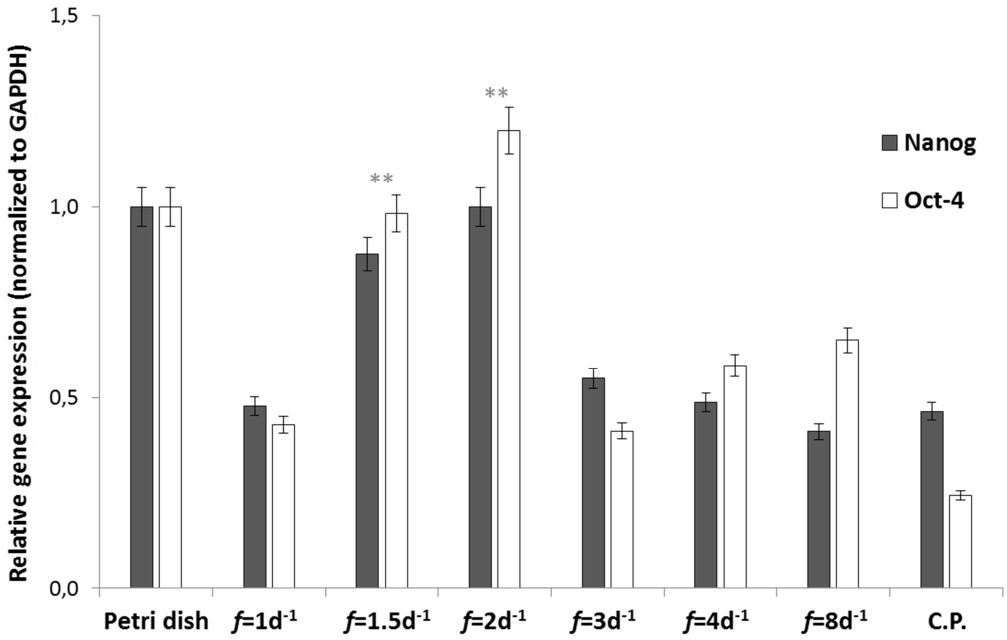

Figure 4.3. *Frequency-dependent pluripotency marker expression. QRT-PCR analysis of pluripotency markers Oct-4 and Nanog in hESCs at different frequencies, f, compared to standard static culture control (Petri dish) and continuous perfusion (C.P.). p-value **P≤0.01. Data are shown as mean ± s.d. (n=6).*

In order to ensure that the depletion of metabolites within the small microfluidic volume is not reaching critical values (especially for low frequencies 1d-1), quantitative detection of glucose depletion at different conditions was

performed. Figure 4.4 shows, first of all, that glucose concentration in the medium kept inside a microfluidic channel is the same as in the fresh medium, meaning that no evaporation effects, which could increase metabolites concentration, are present. Moreover, glucose concentration was measured inside microfluidic channels, in the presence of cells, at the end of the cycle of medium perfusion for three different f, i.e. f=8-2-1d-1, showing that there are no statistical differences, or minimal differences (only by using f=1d-1), compared to glucose concentration measured in Petri dish after 24h of culture.

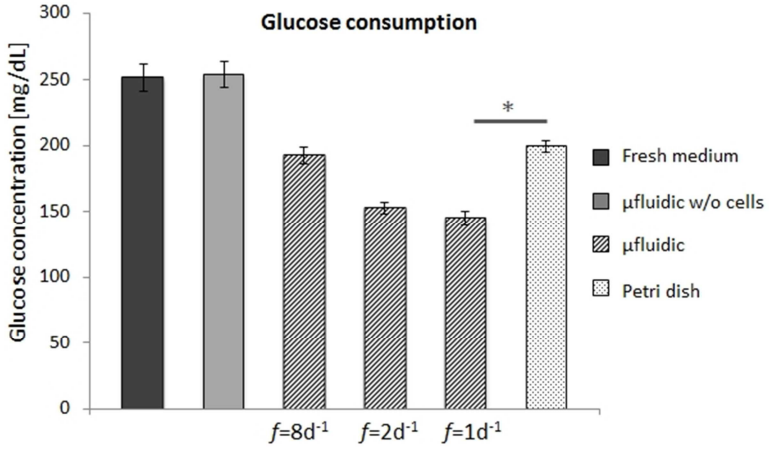

Figure 4.4. *Glucose uptake in microfluidic channel compared to Petri dish culture. Glucose concentration of medium inside a microfluidic channel (with no cells seeded) is equivalent to that of fresh medium. Glucose concentration of medium in microfluidic channel collected at the end of the cycle of perfusion is reported for three different frequencies of medium change. Only with* $f=1d^{-1}$*, glucose concentration results statistically decreased compared to standard condition in Petri Dish. Student* t *test p-values* $P \leq 0.05$ *(*).*

The presented data show a crucial effect of medium change frequency on hPSC pluripotency maintenance and homogeneity in microfluidics, to allow proper factor supply, while avoiding up/downstream effects throughout the channels (Fig. 4.5).

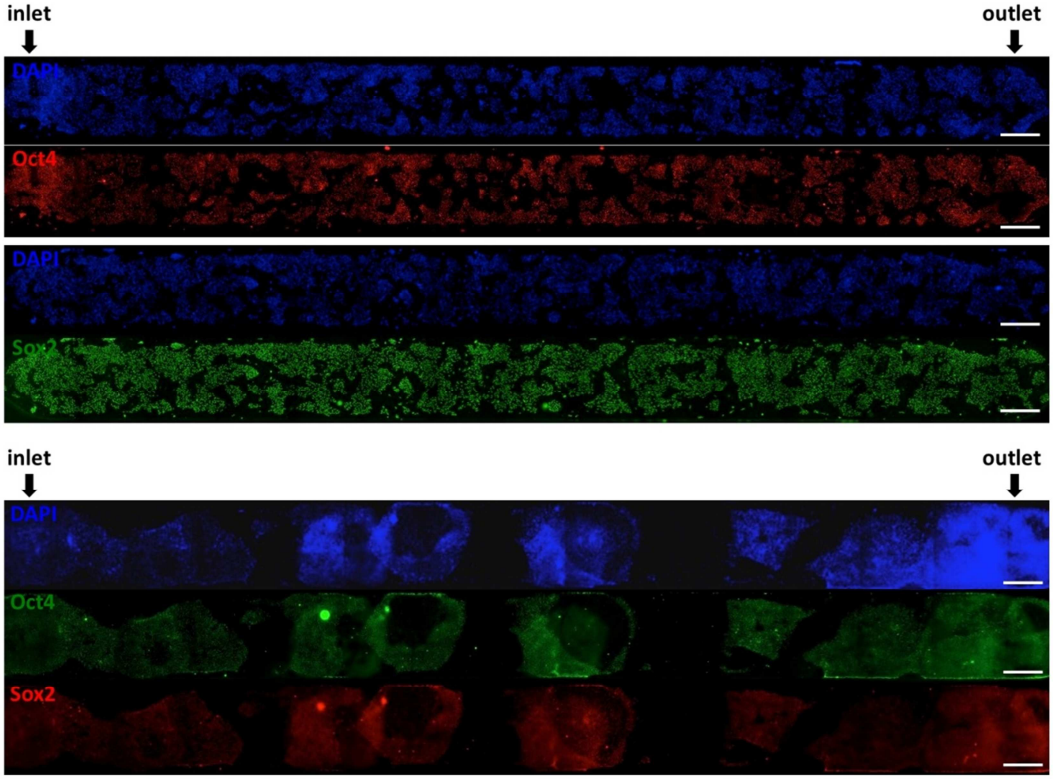

Figure 4.5. *Pluripotency marker expression at day 6 in human pluripotent stem cells cultured in microchannels with f=2d^{-1}. First "HES2" hES cell line showing Oct-4 and Sox2 expression. Next "ADHF#1" hiPS cell line showing Oct-4 and Sox2 expression. High homogeneity in expression is shown along the microchannels with no upstream and downstream effects.*

4.3 Pluripotency rescue with conditioned media

Pluripotency optimization experiment in microfluidic chip (see Fig. 4.3) showed how is possible to modulate frequency up to the best condition for cell culture. With this in mind, the aim was to provide strong experimental evidence that frequency of medium change could be used as an additional variable to control pluripotent stem cell microenvironment by regulating the level of endogenous factors within low-volume system. It is worth to underline that the level of extrinsic exogenous factors, could be independently regulated by tuning the fresh media composition, delivered within the microfluidic volume. An experiment was designed to analyze the rescue of pluripotency of cells under non-optimal culture condition (f=8d-1), using conditioned media collected from microfluidic optimized hESC culture (f=2d-1) (Fig. 4.6).

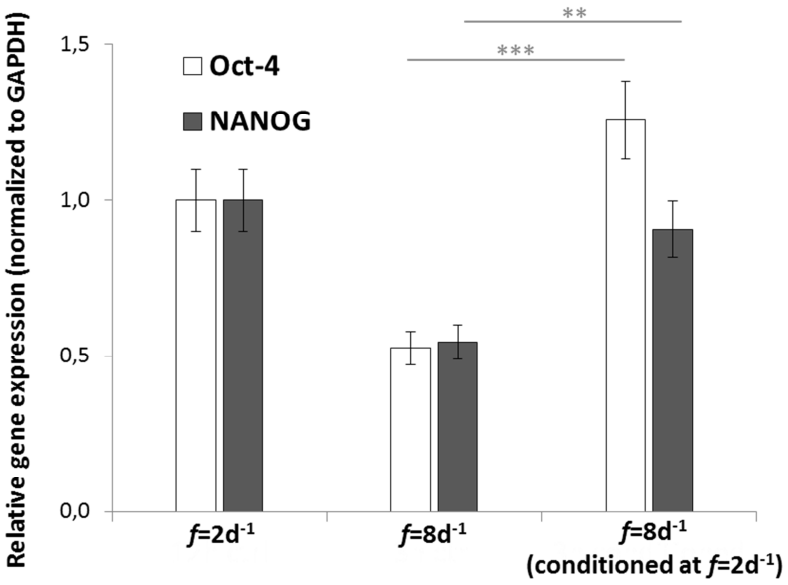

Figure 4.6. *Rescue of pluripotency. QRT-PCR on pluripotency markers Oct-4 and Nanog was performed on f=2d^{-1} for positive control, f=8d^{-1} for negative control and f=8d^{-1} cultured with f=2d^{-1} cells conditioned medium. Cells cultured for 6 days at high f with conditioned medium show pluripotency marker expression comparable with positive control. Normalization on GAPDH. Data are shown as mean ± s.d. (n=3). Significativity is calculated with unpaired t-test. ***P < 0.001, **P < 0.01.*

These experiment gives a proof that frequency itself is affecting stem cell function through the modulation of endogenous factor concentration, and that an optimal frequency (i.e. f=2d-1 in this microfluidic setup) allows accumulations of essential factors for pluripotency maintenance in microfluidics channels.

References

Discher DE, Mooney DJ, Zandstra PW. Growth factors, matrices, and forces combine and control stem cells. Science. 2009 Jun 26;324(5935):1673-7

Dupont S, Morsut L, Aragona M, Enzo E, Giulitti S, Cordenonsi M, Zanconato F, Le Digabel J, Forcato M, Bicciato S, Elvassore N, Piccolo S. Role of YAP/TAZ in mechanotransduction. Nature. 2011 Jun 8;474(7350):179-83. doi: 10.1038/nature10137.

Wan CR, Chung S, Kamm RD. Differentiation of embryonic stem cells into cardiomyocytes in a compliant microfluidic system. Ann Biomed Eng. 2011 Jun;39(6):1840-7.

Korin N, Bransky A, Dinnar U, Levenberg S. Periodic "flow-stop" perfusion microchannel bioreactors for mammalian and human embryonic stem cell long-term culture. Biomed Microdevices. 2009 Feb;11(1):87-94.

Villa-Diaz LG, Torisawa YS, Uchida T, Ding J, Nogueira-de-Souza NC, O'Shea KS, Takayama S, Smith GD. Microfluidic culture of single human embryonic stem cell colonies. Lab Chip. 2009 Jun 21;9(12):1749-55.

CHAPTER 5

HUMAN PLURIPOTENT STEM CELL FUNCTIONAL DIFFERENTIATION IN MICROFLUIDIC CHIP

5.1 Early germ layer differentiation in microfluidic chip

In this chapter, an analysis is done on whether is possible to control selective germ layer commitment and derive functional tissue-specific cells on a chip from hESCs and hiPSCs through the multi-stage microfluidic-based technology. The different developmental stages require cell niche specification in terms of accurate balance between extrinsic and intrinsic cell signaling, through optimal in vitro delivery of exogenous factors and removal of endogenous cell-secreted factors.

5.1.1 Frequency controlled spontaneous differentiation

HESCs were expanded for 3 days and differentiated for 4 days at different frequencies in spontaneous differentiating conditions, with no specific differentiation factor (for detailed materials and methods used in this work of hPSC differentiation on-a-chip see Appendix B). Expression levels of early germ layers markers were analyzed through qRT-PCR analysis of β-III Tub and OTX2 (ectoderm), Bra T, GATA4 and αSMA (mesoderm), AFP, EOMES and FOXA2 (endoderm). Under these conditions, the static Petri dish control showed mainly ectoderm expression. On the other hand, frequency-dependent germ layer enrichment was observed in microfluidic culture (Fig. 5.1). Ectoderm resulted highly expressed at lower frequencies (f=1d-1 and f=2d-1) and it is completely down regulated at higher frequency (f=8d-1) whereas mesoderm and endoderm expression are enhanced at higher frequency (f=8d-1). Gene expression is associated with cell morphology changes. These experimental observations are consistent with the hypothesis that ectoderm differentiation requires high accumulation of extrinsic endogenous factors (Chapter 3; Przybyla and Voldman, 2012). Whereas strong endoderm enrichment is only possible with exogenous factor delivery. All together, these results suggest that periodic perfusion frequency is an additional player in directing early germ layer commitment.

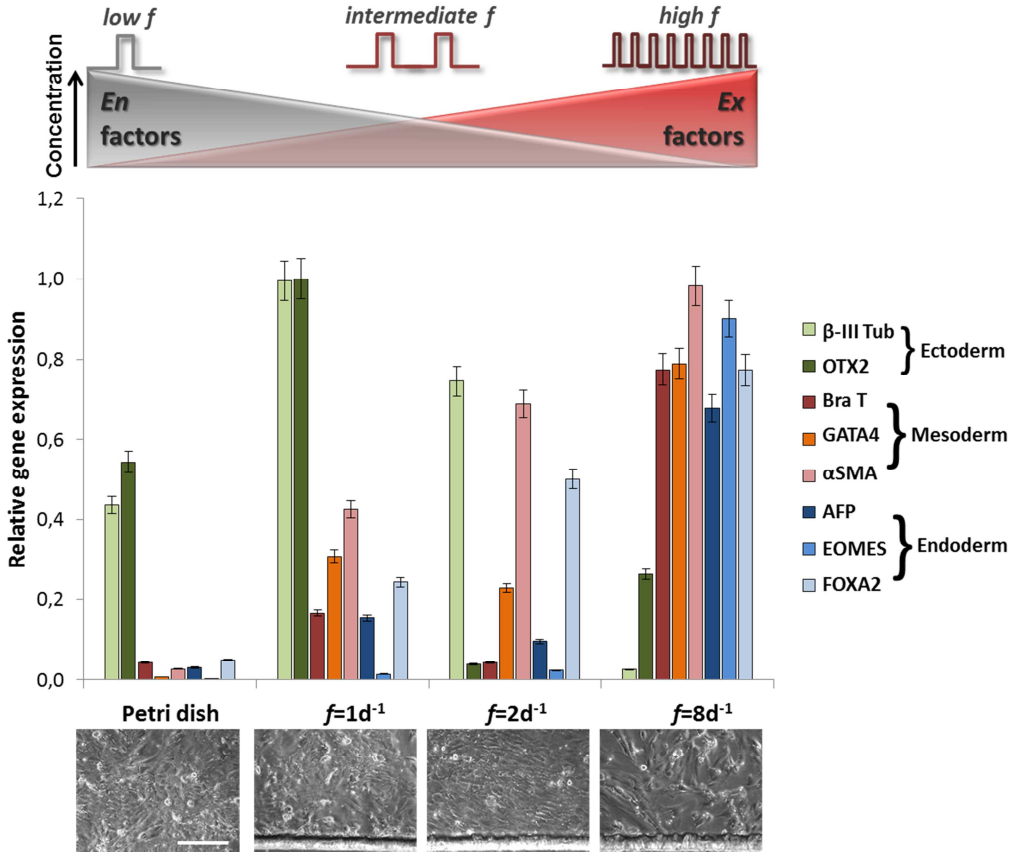

***Figure 5.1**. Early germ layer induction of hESCs on-a-chip. Schematic of frequency-dependent differentiation with f and its correlation to En and Ex factors balance (up). QRT-PCR analysis of β-III tubulin and OTX2 for ectoderm; brachyury T, GATA4 and alpha smooth muscle actin for mesoderm; alpha-fetoprotein, EOMES and FOXA2 for endoderm, in hESC spontaneous differentiation on chip, under different f. Cell morphology in phase contrast for each differentiation condition. Scale bar 50 µm. Normalization on GAPDH. Data are shown as mean ± s.d. (n=6).*

5.1.2 Specific differentiation and mesoderm optimization

To verify whether an efficient and selective induction of the three germ layers could be achieved, hESCs were induced to ectoderm, mesoderm and endoderm by specific differentiation media and with ad hoc frequency (Fig. 5.2A). Particularly, according to previous results, f=1d-1 was used for ectoderm specification whereas f=2d-1 and f=3d-1 for mesoderm and endoderm, respectively. Selective germ layer commitment was successfully obtained as reported by qRT-PCR analysis, which showed high expression of specific germ layer genes for each differentiation protocol. All other non-specific germ layer genes are down regulated.

Next, an analysis was done to see if perfusion frequency can be further adjusted for optimizing germ layer microfluidic induction when specific

differentiation protocols are used. As proof of concept, results in Figure 5.2B show how selective induction of mesoderm was achieved by adjusting frequency of periodic perfusion. In particular, it resulted a 3 fold higher brachyury T expression at f=2d-1 and 3d-1, compared to f=1d-1 and almost null expression at f=12d-1.

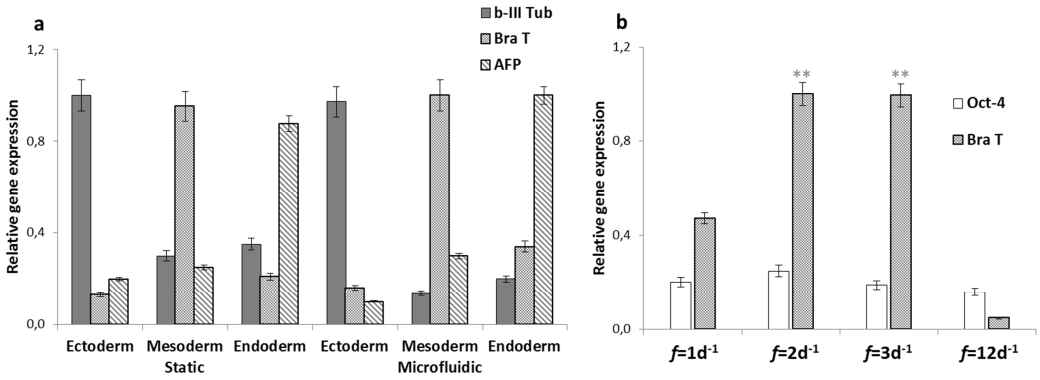

Figure 5.2. *Early germ layer induction of hESCs on-a-chip.* ***A:*** *Early germ layer induction with specific media. The qRT-PCR analysis of β-III tubulin, brachyury T and AFP, and comparison between standard static control and microfluidic differentiation. Data are shown as mean ± s.d. (n=3).* ***B:*** *Mesoderm optimization. The qRT-PCR analysis of Oct-4 and brachyury T expression in different frequencies of medium change for germ layer commitment optimization. Bra T expression is comparable between f=3d^{-1} and f=2d^{-1}, while there is a significantly lower expression at high and low frequencies. Normalization on GAPDH. Student's t-test p-values **P≤0.01. Data are shown as mean ± s.d. (n=3).*

5.1.3 Homogeneity during differentiation

Next question was to see if cell culture homogeneity, already shown during pluripotent stem cell expansion (Fig. 4.5) was also maintained during the differentiation processes inside the chip. As shown in Figure 5.3, periodic perfusion ensures maintenance of homogenous culture and marker expression along microchannels also during germ layer commitment and differentiation. In both early and late endoderm, cell distribution appears uniform, and also marker expression is intense and homogenous, with no signs of upstream and downstream effects due to local factors accumulation or washout.

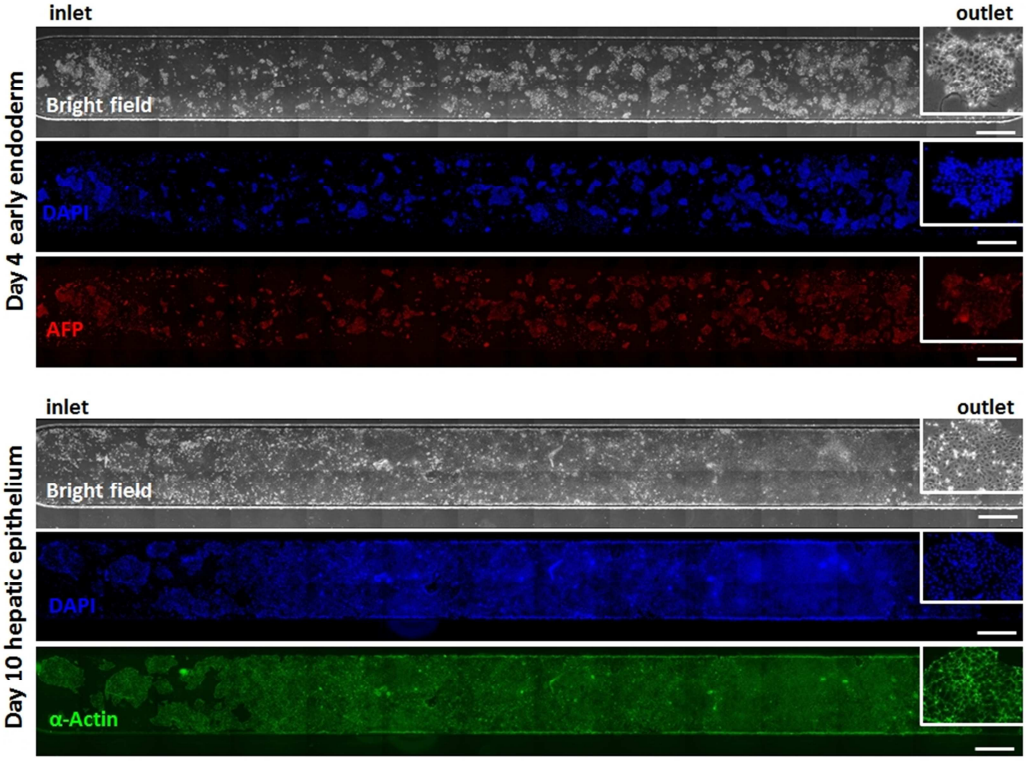

Figure 5.3. *Cell homogeneity during differentiation. Hepatic differentiation at f=2d^{-1} in microchannels at day 4 of early endoderm, and day 10 of definitive endoderm commitment. Cells show homogenous expression of alpha-fetoprotein at day4, and polygonal epithelial cell shape at day 10 along microfluidic channel.*

Collectively, these findings indicate that the frequency of periodic perfusion is an additional parameter to enhance robustness and efficiency of early germ layer specification. Mesoderm differentiation seems to require a proper balance between exogenous and endogenous molecules that can be achieved by frequency optimization, although dependent on cell culture density and media composition. Ectoderm commitment is mainly driven by endogenous stimulations and microfluidic differentiation can reproduce the results obtained with conventional cell culture methods. From technological point of view, small-scale microfluidic volume leads to extremely reduced medium consumption (few microliter per day per channel) and rapid and accurate perturbation of medium composition that is an important prerequisite for multi-stage differentiation process.

5.2 Functional differentiation and tissue-on-a-chip generation

Lastly, the major goal of the use of microfluidic technology together with stem cell culture, is to demonstrated whether functional tissue-specific cell

generation on chip can be achieved. The focus was on cardiac and hepatic cells, as already explained at the beginning of the PhD thesis, which are derived from mesoderm and endoderm germ layers, respectively. These cell types are extremely relevant for tissue-on-a-chip applications. Cell differentiation was achieved by combining ad hoc hPSC differentiation stages, germ layer specification and mature differentiation with proper frequencies of periodic perfusion and chemical regulation of soluble microenvironment.

5.2.1 Cardiac differentiation on chip

First, I report how cardiac cells on chip were derived after 15 days of frequency-dependent multi-stage differentiation protocol (Fig. 5.4A), consisting on mesoderm induction (by Wnt induction), early cardiac commitment (by Wnt inhibition) and functional cardiac maturation (by pro-cardiac factors supply). Typically 5 to 10 thousands cells per channel were obtained. Almost 65% of cardiac troponin-T positive cells were obtained, from both hESC- (HES2) and hiPSC- (ADHF#1) derived cardiomyocytes (Fig. 5.4B). HPSC-derived cardiomyocytes show spontaneous calcium transients and excitation contraction coupling. In the line scan magnification in Figure 5.4C both calcium transients and spark-like spontaneous activity are presented. Analyzing calcium handling of hPSC-CM in microchannels, a functional response is present to 0.5 µM Verapamil with reduced calcium release after L-type channel inhibition, and response to 10 mM caffeine with cytosolic calcium increase after ryanodine channel activation (Fig. 5.4D).

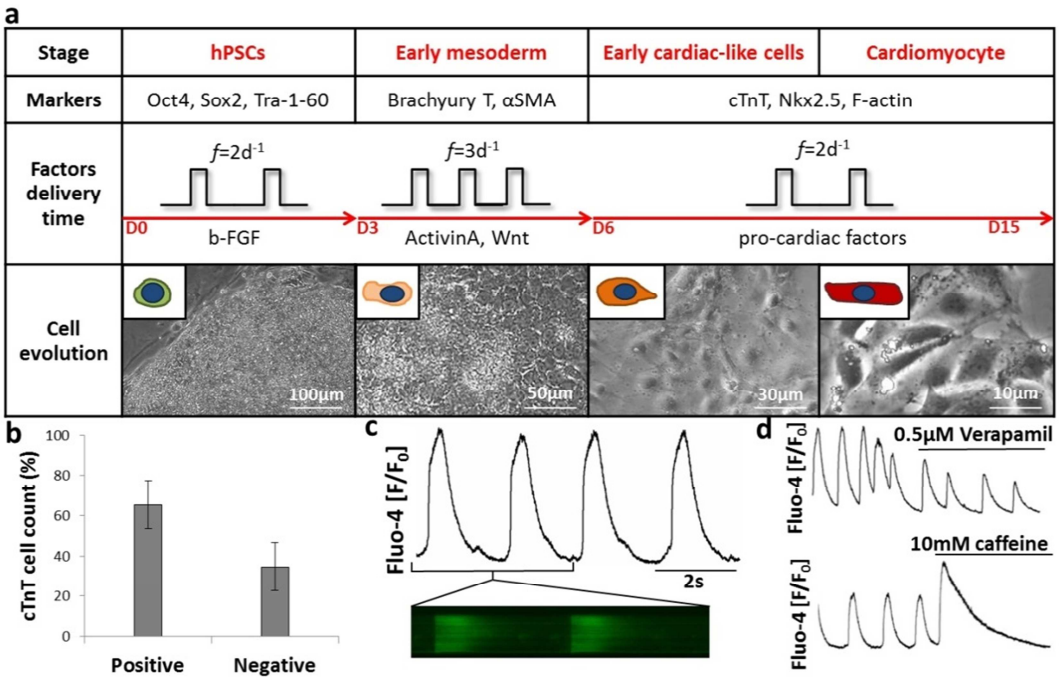

Figure 5.4*. Cardiac functional differentiation on-a-chip from both hESCs and hiPSCs.* ***A:*** *Microfluidic cardiomyocyte differentiation protocol and morphology changes from pluripotent state to differentiated cell type.* ***B:*** *Cardiac troponin T positivity cell count percentage.* ***C:*** *Microfluidic calcium dynamics. Spontaneous calcium transients in hPSC-cardiomyocytes recorded with Fluo-4 indicator.* ***D:*** *Functional cardiomyocytes response to 0.5 µM Verapamil with reduction in calcium release, and to 10 mM caffeine with increase in cytosolic calcium.*

The cardiac tissue obtained in the microchannels show cardiac troponin T positive cells with defined sarcomeric organization (Fig. 5.5A). In every microchannel replicate homogenous monolayers of cells with spontaneous contractile activity were obtained, as shown in the video frame shot in Figure 5.5B. These results have been replicated both with human embryonic and human induced pluripotent stem cells.

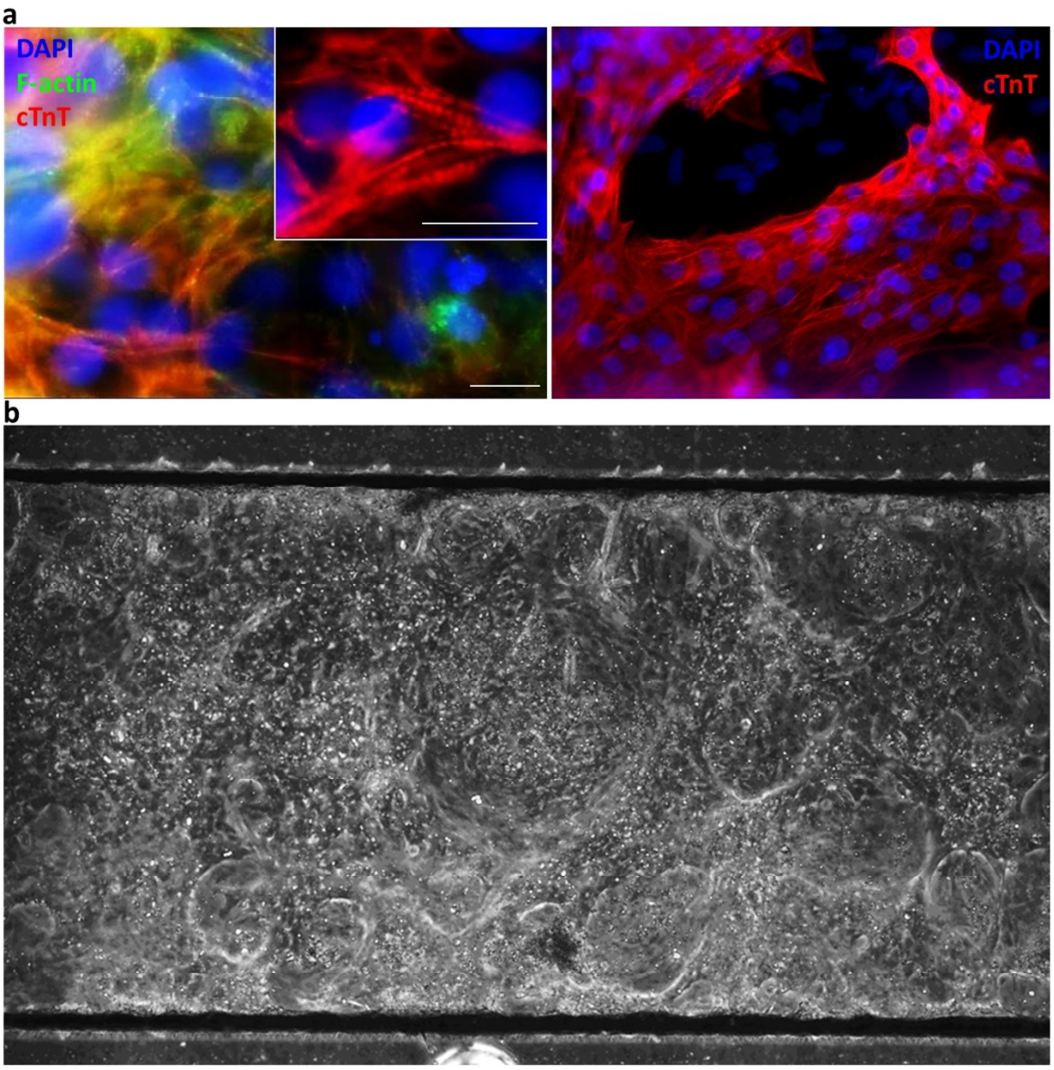

Figure 5.5. A: *Immunofluorescence of hESC-derived CM showing f-actin and cardiac troponin-t sarcomeric organization. Scale bars 20 µm.* ***B:*** *Video frame shot of the central section of a microchannel with spontaneous contractile monolayer of hESC-CMs.*

It was successfully shown that it is possible to generate functional cardiac cells on chip and to directly perform dynamic biochemical stimulations taking advantage of the microfluidic environment, which allows robust, accurate, fast, and cost-effective spatio temporal control of cell microenvironment (Disher et al., 2009).

5.2.2 Hepatic differentiation on chip

Next, this methodology was applied to derive hepatocytes on chip. Hepatic cells were obtained from both hESCs and hiPSCs by early endoderm commitment, definitive endoderm specification and hepatocyte-like cell maturation steps, driven by specific periodic medium delivery (Fig. 5.6A). In

order to assess the robustness of the method, in addition to hESCs (HES2) and retrovirus-derived hiPSCs (ADHF#1), 3 different hiPSC lines were generated by non-integrating methods: Sendai viruses (Send#1) and modified mRNAs (RNA#1, RNA#2). Characteristic polygonal-shaped hepatocyte-like cells are obtained, with presence of bi-nucleate cells at the late stage, characteristic resembling in vivo hepatocytes. Compared to static Petri dish control differentiation, a shortening of the time required for differentiation was obtained, from ~16 days to ~14 days. ELISA was performed to analyze functional human albumin secretion in the medium by hepatocyte-like cells. At the last day of maturation, a 40% higher albumin secretion rate is present in microfluidic cells compared to Petri dish control (Fig. 5.6B). Also quantification of immunofluorescence of late stage albumin and CYP-3A in hESCs shows higher expression in microfluidic differentiated cells compared to static control (Fig. 5.6C). Albumin quantification shows comparable results also for all other 4 different hiPSCs lines, confirming the robustness of the method (Fig. 5.6D).

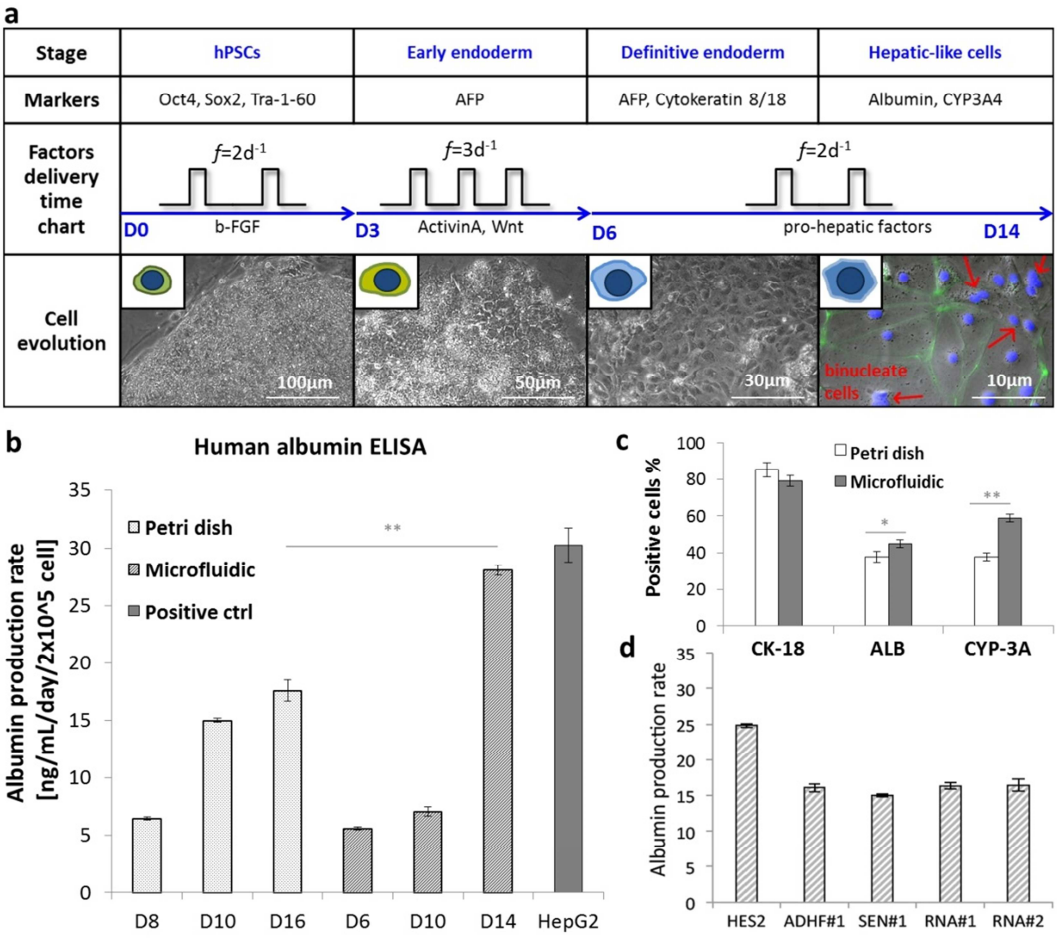

Figure 5.6. *Hepatic functional differentiation on-a-chip from both hESCs and hiPSCs.* ***A:*** *Hepatic differentiation protocol and cell change in morphology up to hepatocyte-like cells. Red*

arrows indicate binucleate cells in late stages. ***B:*** *ELISA albumin secretion quantification. Microfluidic-derived hepatocyte-like cells secrete 40% more albumin compared to static control at the last day of differentiation. Student's t-test p-values **P≤0.01. Data are shown as mean ± s.d. (n=3).* ***C:*** *Quantification of immunofluorescence markers. Microfluidic hepatic cells show significant higher expression of ALB and CYP-3A compared to static control. Data are shown as mean ± s.d. (n=10).* ***D:*** *Comparison of Albumin production at Day 14 for different hiPSCs derived cell lines differentiated into hepatocytes-like cells. Levels of albumin secretion comparable to HES2-hESC line-derived hepatocytes were obtained for hiPSCs lines ADHF#1, derived with retroviruses, Send#1, derived with Sendai viruses and RNA#1-2, derived with mRNA technology. Albumin production rate is expressed as ng/mL/day/2x10^5 cells.*

The hepatic tissue on chip has been characterized with immunofluorescence staining for cholangiocyte marker cytokeratin-19, hepatocyte marker cytokeratin-19, late hepatocyte markers albumin and cytochrome P450-3A (Fig. 5.7A). The tissue has been also tested for functional activity such as glycogenesis, an important metabolic function of the liver to maintain normal levels of circulating glucose in the blood. Periodic acid oxidizes vicinal diols in the glycogen, creating a pair of aldehydes, which then react with the Schiff reagent to give a magenta color. PAS staining in Figure 5.7B shows high glycogen storage capacity (75% of total cells) of hESC-hepatocytes. Cells show also breakdown capacity of specific compounds, such as indocyanine green. Absorbed ICG is metabolized in the functional liver cells and excreted after few hours (Yamada et al. 2002). These functions are extremely relevant for hepatic drug metabolism studies.

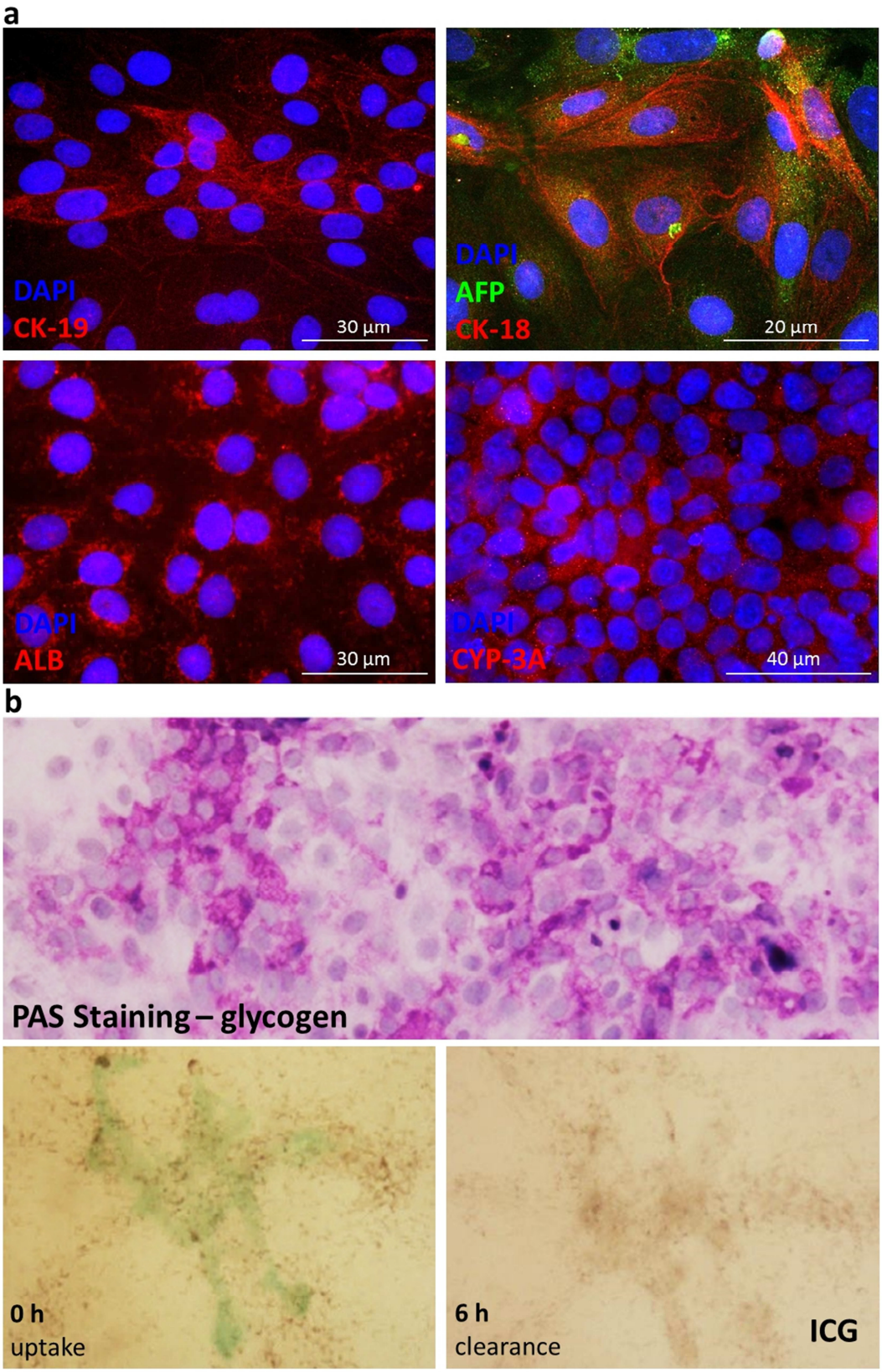

Figure 5.7. A: *Immunofluorescence analysis for cytokeratin-19 in red, alpha-fetoprotein in green, cytokeratin-18 in red, albumin in red, cytochrome P450-3A in red.* ***B:*** *Functional tests. Periodic acid–Schiff (PAS) stain. Pink-magenta cells retain high levels of glycogen in the cytoplasm. Completely white cell retain no glycogen. Nuclei are stained in purple-*

blue with haematoxylin. Indocyanine green (ICG) test. Functional hepatocyte-like cells incubated with ICG internalize the cyanine dye (O h) and metabolize and excrete it (6 h).

The microfluidic environment together with optimized periodic perfusion frequency provide an effective methodology for generating hepatic-like tissues on a chip with remarkable functional differentiation also compared to conventional cell culture methods.

References

Przybyla LM, Voldman J. Attenuation of extrinsic signaling reveals the importance of matrix remodeling on maintenance of embryonic stem cell self-renewal. Proc Natl Acad Sci U S A. 2012 Jan 17;109(3):835-40.

Discher DE, Mooney DJ, Zandstra PW. Growth factors, matrices, and forces combine and control stem cells. Science. 2009 Jun 26;324(5935):1673-7

Yamada T, Yoshikawa M, Kanda S, Kato Y, Nakajima Y, Ishizaka S, Tsunoda Y. In vitro differentiation of embryonic stem cells into hepatocyte-like cells identified by cellular uptake of indocyanine green. Stem Cells. 2002;20(2):146-54.

CHAPTER 6

FUTURE PERSPECTIVES AND CONCLUSIONS

6.1 Future perspectives

The results obtained during this PhD project shed a little light on the deep effects that cell soluble microenvironment have on pluripotency homeostasis, and cell differentiation processes. Much has still to be done in order to deeply understand how all the single components of the surrounding microenvironment cooperate actively in pluripotency and functional maturation. One of the major goal of scientists working in the stem cell fields, regenerative medicine, in vitro therapeutics and screenings, is to reach the complex features of the most complicated biological machine, the human body.

6.1.1 Hepatic differentiation under oxygen gradient

As a proof of concept, an attempt has been made to better mimic in vivo conditions during cell differentiation.

With this in mind, a microfluidic chip, which can create and maintain a stable oxygen gradient, has been developed (see Chapter 2). For experimental reasons, it was not adopted the physiological pO2 range found in the liver lobule (Fig. 1.4), but the range was enlarged from 21% oxygen to 0% oxygen, to see in the first experimental trials if it was possible to obtain a biological response to a larger gradient range. When all the experimental procedures are set up and robust, then it will be possible to reduce the gradient to mimic the physiological one.

First, hESCs were differentiated into hepatocytes like cells in the microchannels with the stable gradient. The first time point was at day 9, when cells are committed to hepatic endoderm. Cells have been fixed and stained for alpha-fetoprotein (Fig. 6.1A). As a first result, qualitative analysis of the immunofluorescence gives a gradient of marker expression between the two extremes of the gradient. It results a higher expression of AFP in the oxygenated side of the channel (21% O2), compared to lower expression in the deoxygenated side (<5% O2).

In order to quantify the qualitative analysis, a series of region of interest (ROI) was selected in each fluorescence image at the extremes of the gradient, in the channel extremities. Same exposure time and 20X magnification was used for all the acquired images. The mean fluorescence of the oxygenated and deoxygenated sides was compared (Fig. 6.1B). A significant difference in marker fluorescence was obtained at the extremes of the gradient. The same analysis procedure was applied on images taken in the length of the gradient, and mean quantities were plotted against channel width. It results an exponential decay of the fluorescence from oxygenated to deoxygenated side (Fig. 6.1C). This is a first proof that it is possible to obtain a biological response to an imposed physical gradient.

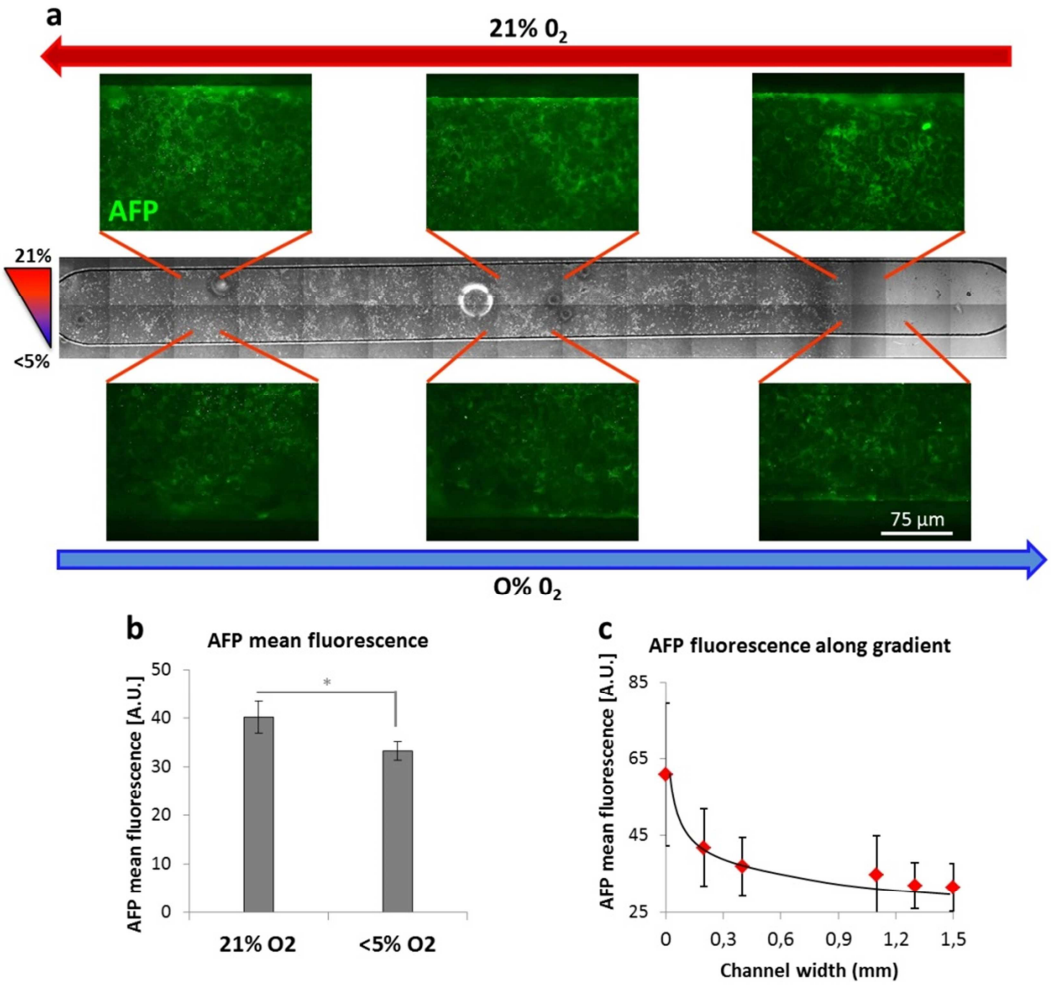

***Figure 6.1**. **A:** Schematic representation of air (21% O_2) and nitrogen (0% O_2) lines creating the oxygen gradient in the cell culture microchannel. HESC-derived endoderm cells at day 9 of differentiation stained with AFP in green. **B:** Graph showing mean fluorescence in arbitrary units of selected ROIs in the two sides of the microchannel. Data shown ±s.d. (n=12). Student's t-test p-value *P≤0.05. **C:** Graph showing mean fluorescence in arbitrary units of selected ROIs along the width of the microchannel. Data shown ±s.d. (n=3).*

As a second experiment, a differentiation protocol was completed inside the oxygen gradient chip. This was done to evaluate if a biological effect was also present at mature stage. A control experiment was done on cells put under oxygen gradient from day 8, to see if eventual metabolic zonation could be induced also starting from endoderm committed cells, as it happens in vivo in new hepatocytes originating from adult liver stem cells (Forbes et al., 2002). HESC-derived hepatocyte-like cells were fixed at day 15 and stained for glycogen, in order to analyze metabolic differences. As shown in Figure 6.2, the cells subjected to oxygen gradient, both from the beginning of the experiment and starting from endoderm, show a qualitative difference in glycogen storage. It appears more present in the oxygenated side (corresponding to in vivo zone I hepatocytes) compared to lower glycogen storage in deoxygenated side (corresponding to in vivo zone III hepatocytes). In the control cells, cultured with no O2 gradient, glycogen storage is more homogenous.

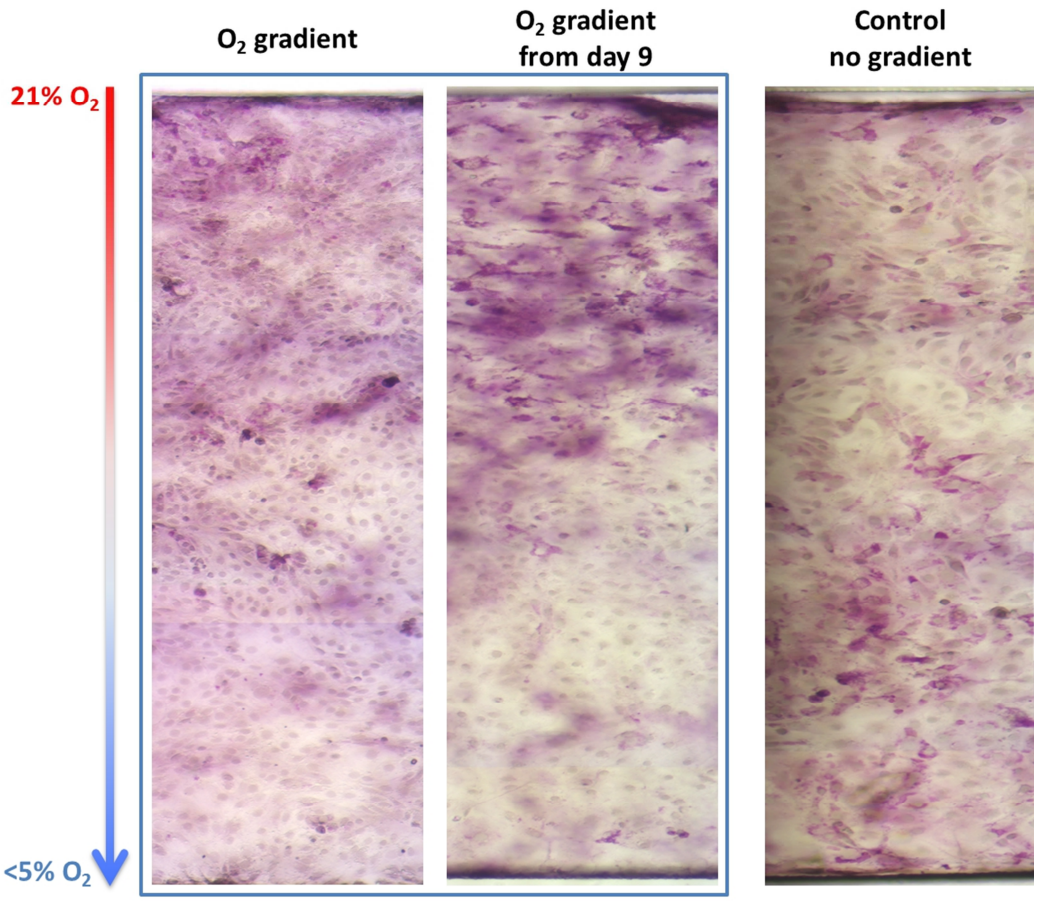

***Figure 6.2**. Periodic acid–Schiff(PAS) stain of hESC-derived hepatocyte-like cells at day 15 of differentiation. The first image on the left show cells subject to O_2 gradient from first day of differentiation. Central stain show cells subject to O_2 gradient from day 8 of*

differentiation. Last stain on the left shows control differentiation w/o gradient. Stain of cells under gradient show a glycogen (magenta-pink) decreasing gradient from high O_2 to low O_2.

This result is consistent to in vivo functions of gluconeogenesis in zone I (high O2) and glycolysis in zone III (low O2). It means that portal hepatocytes (zone I) tend to store higher quantities of glycogen, while central hepatocytes (zone III) tend to store less and use more glucose (Kudryavtseva et al., 1996).

Much work has still to be done in order to better imitate physiological conditions, such as the accurate screening of functional enzymes distribution, i.e. all the different isoforms of cytochromes P450 (Usynin and Panin, 2008). These results obtained with an imposed oxygen gradient are very promising for what concerns tissue development, and the need of in vitro models to gradually reach the complexity of living tissue and organs.

6.2 Conclusions

The development of in vitro human tissues is hindered by the difficulty to give perfect chemical and physical stimuli to cells, and perfectly control cell culture microenvironment.

Understanding the mechanisms that underlie stem cell self-renewal and differentiation is central to realizing this potential, and efforts have increasingly focused on elucidating the signals that regulate cell function in the tissues where they reside, i.e. the endogenous stem cell niche. The governing principle of this niche, first proposed 30 years ago, is that stem cell fate decisions are influenced by cells' interactions with components of their microenvironment, and these cell extrinsic factors include soluble and immobilized factors, the extracellular matrix, and signals presented by neighboring cells. Thus, recreating or simulating this microenvironment may be critical for properly expanding and controlling the differentiation of stem cells outside the body, for both basic biological study and therapeutic translation (Eshghi and Schaffer, 2008). In standard in vitro cell cultures is still missing biomimesis. The regular Petri dish lacks of physiological stimuli reproducing the correct cell microenvironment, while in vivo animal models are not fully representative of the human physiology. Tissue engineering research field has deeply inspired by biomimetic concepts, and in the last years several strategies and technologies were developed in this perspective, to generate and improve engineered tissues as alternative in vitro models.

To this end, this PhD thesis focused on the development of functional tissues, starting from human pluripotent stem cells, for a possible use as in vitro models. The work started with the initial understanding on how a modulation of the soluble microenvironment is capable of affecting differentiation patterns in pluripotent cells (Chapter 3). In particular, polyacrylamide hydrogels were characterized and used for their highly selective diffusional properties. Three-dimensional microwell allowed the obtainment of homogenous embryoid bodies, critical to obtain a standardize cell culture. This potential improvement in homogeneity may be beneficial to the reproducibility of differentiation protocols into specific lineages for potential tissue engineering and organ regeneration applications. Furthermore, hPSC cultured in the three-dimensional system synthesize their own endogenous repertoire of factors and contribute to create a microenvironment suitable for cell growth and differentiation. The results showed how the accumulation of endogenous factors has a deep effect on hPSC differentiation. The study could provide insights to the relationship between the confined cell niche and stem cell behavior during differentiation. In addition it sheds light on the potential effects of the diffusion of soluble factors and related effects on differentiation patterns in microenvironments, relevant to the emerging use of microstructured culture systems.

Next step of the PhD work was the production of functional hepatic and cardiac tissues with the use of ad hoc microtechnologies. The first critical step was the choice of a suitable cell source, which can replace standard immortalized cells lines, lacking many of the adult cell characteristics and functionalities, and primary cell lines, difficult to extract, if not almost impossible in large quantities (i.e. human cardiomyocytes and human hepatocytes), and difficult to maintain and expand in culture for many passages. To this end, human pluripotent stem cells were chosen. Human embryonic stem cell lines have the possibility to be expanded in culture almost indefinitely, while maintaining their characteristics of stemness and potency. These cells are extremely versatile as they can be differentiated into all derivates of the three germ layers, giving the possibility to generate a high number of mature cells of interest (Thomson et al., 1998). Secondly, human induced pluripotent stem cells were produced and used as cell source. This is one of the major discoveries in the last decade, confirmed also by the Nobel Prize in Physiology or Medicine 2012 awarded to Prof. Shinya Yamanaka (Nobelprize.org, 2013). The hiPSCs are adult somatic cell reprogrammed to an embryonic state, which can then be differentiate to any cell

type (such as hESC) but overcomes the ethical issues involving the use of embryos (Takahashi et al., 2007). They have all the characteristics of hESCs, and they also give the possibility to derive patient-specific cell lines, in order to develop ad hoc models for specific in vitro therapeutic studies.

Despite their high sensitivity to environmental conditions and their time-demanding cell culture, different lines of hPSCs were successfully cultured and expanded during this study. One of the major problems of these cell types is the difficulty to homogenously differentiate them and maturate them to obtain completely functional adult cells. These problems are difficult to address in a standard cell culture in Petri dish, because of the impossibility to accurately monitor and manipulate cell microenvironment.

Microtechnologies can help overcome the problems resulting by the poor control on standard Petri dish cell cultures. For this reason, microfluidic technology was applied to hPSCs culture in order to better control expansion and differentiation processes, to achieve functional tissues on chip. With this technology it has been possible to control cell soluble microenvironment to optimize hESC culture in the microfluidic channels. It was also demonstrated how the frequency of medium change is essential in directing early differentiation, and how a change in f during spontaneous differentiation results in dramatic changes in the germ layer commitment. Therefore, frequency has been adopted as a new variable to consider during stem cell microfluidic culture.

The differentiation of hPSCs into cardiomyocytes and hepatocytes was achieved by standardized protocols (Hay et al., 2008; Lian et al., 2012) combined with microfluidic cell culture, through hESC and hiPSC stimulation with defined temporal sequences of soluble factors, finely controlled by automatized media changes. By this, a high percentage of cardiomyocyte cells were obtained (65% of the cells positive to cardiac troponin t). Cardiac tissue showed remarkable self-contraction capacity and correctly responded to functional tests, such as proper calcium dynamics and correct response to Verapamil and caffeine drugs. Also hepatic tissue showed high functional activity, such as proper albumin secretion, expression of functional cytochrome P450 enzyme, high levels of glycogen storage and metabolic function in breakdown of chemical compound indocyanine. Moreover, hepatic cells obtained in microfluidic channels showed higher percentage of hepatic markers and albumin secretion compared to standard differentiated Petri dish cells.

The micro-technologies used in this thesis are reproducible, completely customizable, inexpensive and extremely versatile. They were designed and developed with the intent of being used in the development of an in vitro model, able to lower cost and time of drug and therapy development, which could be easily used by biological researchers. The coupling of biological science with engineering tools offer new possibilities, otherwise not easily accessible, as demonstrated by the promising results obtained in this PhD thesis. Microengineered cell-culture systems that mimic complex organ physiology have the potential to be used for the development of human-relevant disease models that are more predictive of drug efficacy and toxicity in patients, while also providing greater insight into drug mechanism of action. More predictive in vitro assays incorporating cultured human cells also will protect public health by identifying environmental toxins and providing a better understanding of their mechanisms of action, as well as improving our ability to predict risks for specific compounds. In addition, the organ-on-chip microdevices could be integrated to study the interplay of different organs in determining pharmacokinetic properties of compounds at a higher level of functionality than was possible in the past (Huh et al., 2011).

Concluding, in this PhD work, functional tissue-specific cells on a chip were derived through a robust multi-stage microfluidic technology, which allows accurate spatio-temporal control of cell soluble microenvironment through regulation of periodic-perfusion frequencies. Moreover, functionally differentiated cells derived in the microfluidic channels can be directly used for dynamic multi-parametric and large-scale drug screening or for developing micro-engineered human organ models. It will be important to ensure that appropriate biomarkers and assays are developed for use with these microsystems, and to validate the extrapolation of in vitro results to the human situation. This technology opens a new perspective in generating organs-on-chips from hPSCs overcoming the issues related to the limited availability of human primary cell sources. This last aspect will require strong scientific and technological efforts for further mimicking the organogenesis in vitro.

References

Stuart Forbes, Pamela Vig, Richard Poulsom, Howard Thomas, Malcolm Alison, Hepatic stem cells, The Journal of Pathology. Volume 197, Issue 4, pages 510–518, July 2002

M.V. Kudryavtseva, G.A. Sakuta, A.D. Skorina, G.I. Stein, A.V. Emelyanov, B.N. Kudryavtsev, Quantitative analysis of glycogen content in hepatocytes of portal and central lobule zones of normal human liver and in patients with chronic hepatitis of different etiology, Tissue and Cell, Volume 28, Issue 3, June 1996, Pages 279–285.

I. F. Usynin and L. E. Panin. Mechanisms Determining Phenotypic Heterogeneity of Hepatocytes. Biochemistry, 2008, Vol. 73, No. 4, pp. 367-380.

Eshghi, S. and Schaffer, D.V., Engineering microenvironments to control stem cell fate and function (September 15, 2008), StemBook, ed. The Stem Cell Research Community, StemBook, doi/10.3824/stembook.1.5.1, http://www.stembook.org.

Thomson JA, Itskovitz-Eldor J, Shapiro SS, Waknitz MA, Swiergiel JJ, Marshall VS, Jones JM. Embryonic stem cell lines derived from human blastocysts. Science. 1998 Nov 6;282(5391):1145-7.

Takahashi K, Tanabe K, Ohnuki M, Narita M, Ichisaka T, Tomoda K, Yamanaka S. Induction of pluripotent stem cells from adult human fibroblasts by defined factors. Cell. 2007 Nov 30;131(5):861-72.

Hay DC, Zhao D, Fletcher J, Hewitt ZA, McLean D, Urruticoechea-Uriguen A, Black JR, Elcombe C, Ross JA, Wolf R, Cui W.Lian, X. et al. Proc. Natl. Acad. Sci. 109, E1848–E1857 (2012). Efficient differentiation of hepatocytes from human embryonic stem cells exhibiting markers recapitulating liver development in vivo. Stem Cells. 2008 Apr;26(4):894-902.

"Shinya Yamanaka - Facts". Nobelprize.org. Nobel Media AB 2013. Web. 26 Jan 2014. <http://www.nobelprize.org/nobel_prizes/medicine/laureates/2012/yamanaka-facts.html>

Huh D, Hamilton GA, Ingber DE. From 3D cell culture to organs-on-chips. Trends Cell Biol. 2011 Dec;21(12):745-54. doi: 10.1016/j.tcb.2011.09.005.

APPENDIX A

CONFINED 3D MICROENVIRONMENT REGULATES EARLY DIFFERENTIATION IN HUMAN PLURIPOTENT STEM CELLS

Giovanni G. Giobbe[1,2], Monica Zagallo[1,2], Massimo Riello[1], Elena Serena[1,2], Giulia Masi[3], Luisa Barzon[3], Barbara Di Camillo[4], Nicola Elvassore[1,2]

[1]Department of Industrial Engineering (DII), University of Padua, via Marzolo 9, 35131 Padua, Italy; telephone: +39-049-8275469; fax: +39-049-8275461; e-mail: nicola.elvassore@unipd.it
[2]Venetian Institute of Molecular Medicine (VIMM), via Orus 2, 35129 Padua, Italy
[3]Department of Histology, Microbiology and Medical Biotechnologies, via Gabelli 63, 35131 Padua, Italy
[4]Department of Information Engineering (DEI), University of Padua, via Gradenigo 6B, 35131 Padua, Italy

Article first published online: 20 JUN 2012
DOI: 10.1002/bit.24571
Biotechnology and Bioengineering
Volume 109, Issue 12, pages 3119–3132, December 2012

Keywords: human embryonic stem cells; human induced pluripotent stem cells; differentiation; embryoid bodies; microenvironment; hydrogel microwells; endogenous factors

Abstract

The therapeutic potential of human pluripotent stem (hPS) cells is threatened, among various problems, by the difficulty to homogenously direct cell differentiation into specific lineages. The transition from hPSC into committed differentiated cells is accompanied by secretome activity, remodeling of extracellular matrix and self-organization into germ layers. In this work, we aimed to investigate how different three-dimensional microenvironments regulate the early differentiation of the three germ layers in human embryonic stem (hES) cells derived embryoid bodies. In particular, a permeable, biocompatible, hydrogel microwell array was specifically designed for recreating a confined niche in which EB secreted molecules accumulate in accordance with hydrogel diffusional cut-off. Fluorescence recovery after photobleaching technique was performed to accurately evaluate hydrogel permeability, mesh size and diffusional cutoff for soluble molecules. Three different culture conditions of EB culture were analyzed: suspension, confinement in microwells of width/depth ratio 1:1 and 1:2. Results show that EBs cultured in microwells are viable and have comparable average size after 8 days culture. Whole genome microarrays show that significative differential gene expression was observed between suspension and confined EBs culture. In particular, EBs culture in microwells promotes the expression of genes involved in pattern specification processes, brain development, ectoderm and endoderm differentiation. On the contrary, suspension EBs express instead genes involved in mesoderm specification and heart development. These results suggest that local accumulation of EBs secreted molecules drives differentiation patterns, as confirmed by immunofluorescence of germ layer markers, in hydrogel confined EB culture from both hES cells and human induced pluripotent stem (hiPS) cells. Our findings highlight an additional potential role of biomaterial in controlling hPSC differentiation through secreted factor niche specification.

Introduction

Human pluripotent stem cells, and in particular human embryonic stem cell lines derived from the inner cell mass of blastocyst stage human embryos and human induced pluripotent stem cells

derived by reprogramming of human somatic cells, are capable of unlimited proliferation and differentiation into the three embryonic germ layers (Odorico et al., 2001; Reubinoff et al., 2000; Thomson et al., 1998). Efficient control of the differentiation of hES and hiPS cells is a prerequisite for obtaining phenotypically homogenous populations, useful in clinically relevant therapeutic applications. However, thus far, accurate expansion and differentiation processes of hPSC remains an open challenge.

Multiple methods have been used to induce human pluripotent stem cells differentiation, including use of specific growth factors, co-culture with specific cell lines, culture on extracellular matrix proteins, and embryoid body formation (Dvash and Benvenisty, 2004; Itskovitz-Eldor et al., 2000; Keller, 2005; Odorico et al., 2001; Schuldiner et al., 2000). Of all the approaches, EB formation is a simple and straightforward methodology. Aggregation of cells is imposed with particular culture techniques, which prevent cell adhesion to a substrate. EBs are formed from hPSC colonies chemically or mechanically detached from their substrate, then cultured in suspension in the absence of mouse embryonic fibroblasts (MEFs) or MEF-conditioned medium (Keller, 2005; Schuldiner et al., 2000; Tian et al., 2004; Wang et al., 2004). After some days after aggregation, cells start a spontaneous and anisotropic differentiation into lineages of the three germ layers. This differentiation method recapitulates the early stages of human embryonic development (Keller, 2005; Kurosawa, 2007; Tian et al., 2004; Wang et al., 2004). It provides a three-dimensional structure, most similar to in vivo conditions, where gradients of secreted factors are present.

In the cell aggregate, the first germ layer to develop is the endoderm, which surrounds a pluripotent ectoderm zone and a primitive mesoderm. Primitive endoderm seems to be induced by the signaling of fibroblast growth factor. This germ layer differentiates into parietal and visceral endoderm, and deposit a basal membrane composed mainly by laminin and collagen IV. Endoderm promotes the differentiation of adjacent mesoderm into cardiac lineages. On the other hand, ectoderm secretes factors (such as Wnt), which inhibit cardiac differentiation and promote formation of the neural tube (Bauwens et al., 2008). As differentiation continues, cells acquire typical phenotypes of committed differentiated cells of the three germ lineages (Bratt-Leal et al., 2009). Therefore, when cultured in the absence of specific growth factors in medium, embryoid bodies can self-regulate their own differentiation through secretion of endogenous factors (Keller, 2005).

Several protocols have been established to promote an efficient and reproducible obtainment of the cell types of interest. Modification of medium composition, conditioning medium with specific cell types, and addition of growth factors are methodologies used to induce specific cell lineages. The most common growth factors used for these purposes are activin-A, BMP-4, bFGF, TGFβ, HGF, NGF, EGF, and retinoic acid (Kurosawa, 2007). Other ways to induce desired cell types are EB size-dependent differentiation methods. Recent developments in EB formation techniques have enabled more controlled systems capable of modulating EB shape and size, as these parameters have been recognized to contribute to the control of the resulting cell population. Non-adhesive polyethylene glycol (PEG) microwell arrays have been used to control the homogeneity of EB size and shape (Karp et al., 2007; Moeller et al., 2008). Recent studies on PEG microwell-mediated control of EB size have also investigated the effects on hES cell fate determination, specifically addressing cardiogenesis and vasculogenesis via WNT signaling pathways (Hwang et al., 2009). Micro-contact printing techniques have also been developed to regulate EB size-dependent hES cell differentiation and to investigate the stem cell biology (Lee et al., 2009; Park et al., 2007; Peerani et al., 2007, 2009). Concave (Choi et al., 2010; Park et al., 2009), convex-based (Park et al., 2009) thin PDMS membrane arrays and stimuli-responsive microwells (Tekin et al., 2010) for culturing the cells and better mimic the contour of EBs have also been developed. Three-dimensional cuboidal microwell systems have also been realized to culture hES colonies of defined dimension for the further study of cardiac differentiation (Mohr et al., 2010). In order to study the spatial and temporal organization of germ layers during the early stages of differentiation, eight hES cell lines have been compared through the analysis of expression of mesoderm, endoderm and ectoderm markers in order to evaluate whether the differences in EB characteristics would correlate with cardiac differentiation (Pekkanen-Mattila et al., 2010).

All these studies analyze the effect of factors or EB size and shape in regulating hPSC differentiation. The importance of growth factors in media during differentiation is clear, but little information about the role of secreted molecules during early differentiation stages has been reported. In this perspective, we designed a biomaterial that can locally accumulate soluble secreted molecules in a confined microenvironment.

In conventional in vitro culture dishes any molecule is rapidly distributed over the total volume of medium. We designed three-dimensional hydrogel microwells with defined diffusional properties. Different heights of microwells are used in order to vary the extent of factors accumulation (Fig. 1). For this goal, we need a hydrated, biocompatible, long-term stable in vitro culture system suitable for suspension culture, characterized by a non-adhesive surface, and above all, selectively permeant to molecules in the cell culture medium. Polyacrylamide hydrogel is chosen for the research purposes because it addresses the cited requirements and, in addition, its geometry is tunable, thus allowing for easy microwells depth modulation. The culture within the physically separated hydrogel microwells is also expected to increase EB size homogeneity in the population, preventing the formation of random cell aggregates. Embryoid bodies cultured in the diverse differentiation niches are examined through transcriptomic and proteomic analyses, in order to assess differential expressions of genes involved in early embryonic development, in the different culture conditions.

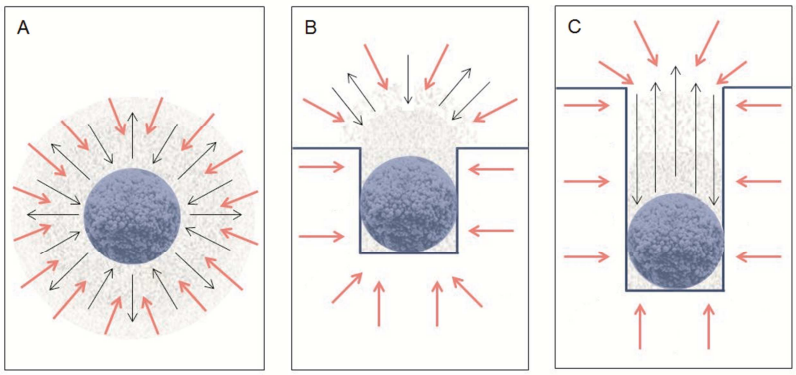

Figure 1. *Schematic of embryoid bodies in standard cell culture dishes and compartmentalized into the two types of microwells.* ***A****: EBs in suspension;* ***B****: EBs in microwells 500 µm × 450 µm, 1:1 ratio;* ***C****: 500 µm × 1 mm, 1:2 ratio. Black arrow represent endogenous factors diffusion, pink arrows indicate medium diffusion. In standard cell culture dishes, molecules secreted by differentiating embryoid bodies are rapidly distributed in the bulk medium. In microwells, molecules with different diffusivities will distribute in the EB microenvironment and into the surrounding medium by diffusion.*

Materials and Methods

Microstructured Hydrogel Production

Hydrogels were prepared as previously described (Cimetta et al., 2009). Briefly, clean and dry glass slide surfaces were chemically modified by deposition of a solution of 3-aminopropyltriethoxysilane (Sigma–Aldrich, St. Louis, MO) and glutaraldehyde 0.5% (Sigma–Aldrich) in phosphate buffered saline (PBS; Sigma–Aldrich); this results in the formation of a hydrophobic coating ensuring covalent binding of the hydrogel films. Acrylamide/bis-acrylamide 29:1 solution 40% (Sigma–Aldrich) was diluted in PBS 1× to the final concentrations of 20%. The photoinitiator (Irgacure 2959; Ciba Specialty Chemicals) was dissolved in methanol at 200 mg mL^{-1} and added to the acrylamide/bis-acrylamide solution in order to obtain a final concentration of 20 mg mL^{-1}.

Four Hundred Fifty Micrometer Depth Hydrogel Microwells

Five hundred microliter of the prepolymer solution were dropped over the functionalized glass surface, confined by a polydimethylsiloxane ring. Hydrogel polymerization occurred by exposing the prepolymer solution to UV light for 4 min (high-pressure mercury vapor lamp, Philips HPR 125 W, emitting at 365 nm with an incident light intensity of 20 mW cm^{-2}). Selective photo-polymerization of acrylamide solutions on the glass surface was achieved by interposing the photomask with the desired geometry between the light source and the glass slide.

One Millimeter Depth Hydrogel Microwells

This hydrogel array was prepared with two different layers. Hydrogel polymerization occurred first by exposing 30 µL of prepolymer solution to UV light for 3 min (Philips HPR 125 W) to obtain a thin film of hydrogel. Second, it was covered by 500 µL of prepolymer solution enclosed by a polydimethylsiloxane ring, to be exposed UV light (UV-vis lamp, Dymax Bluewave-50, 3 W, with filter at 366 nm) for 50 s for selective photopolymerization. Non-polymerized acrylamide was removed using distilled water. Such procedures resulted in homogeneous 3D hydrogels with 21 mm diameter and an average thickness of 1 mm (Fig. 2). Hydrogels were immersed in ultra-pure milliQ water for 4 days to ensure complete removal of the unreacted monomeric units or photoinitiator, and then the bottom of the glass slides were soaked in pure ethanol. After rinsing with ultra-pure distilled water, final sterilization occurred with 20 min exposure to UV light under a sterile hood.

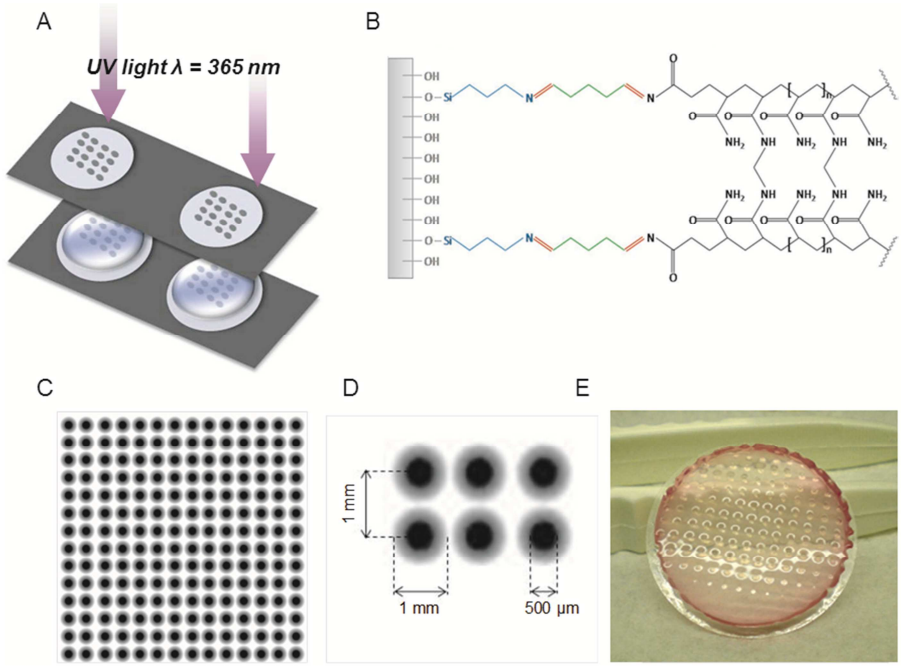

Figure 2. *Microstructured PA hydrogel production.* ***A****: The microstructured PA hydrogels are prepared by selective photo-polymerization of the acrylamide/bisacrylamide solution under UV light.* ***B****: The PA hydrogel is covalently bound to a glass coverslip functionalized with 3-aminopropyltriethoxysilane and glutaraldehyde, as shown in the schematic representation of the chemistry.* ***C****: Photomask for selective photopolymerization.* ***D****: Enlargement of a photomask. The shading is realized in order to define the concave shape of the microwells.* ***E****: Microstructured hydrogel, 21 mm in diameter. The color is due to the presence of cell culture medium, which keeps the hydrogel hydrated.*

Fluorescence Recovery After Photobleaching Analysis

The FRAP method has been adapted to estimate the mobility of a fluorescent probe, with a defined hydrodynamic radius (TRITC-Dextran, 70 kDa) (Invitrogen, Grand Island, NY), in hydrogels

of PA made with different concentrations of acrylamide and bis-acrylamide. To perform FRAP technique the fluorescent diffusion tracer is introduced at a suitable concentration (2 mg mL^{-1}) into the prepolymer solution. After UV polymerization, it is possible to conduct the FRAP analysis on a hydrated hydrogel. A concentration gradient is created by photobleaching the fluorescence in a small circular region (5 μm). The molecules can move in the hydrogel by means of self-diffusion if the hydrogel mesh size is large enough, and the recovery of fluorescence is detected by monitoring of the signal, using low intensity excitation. FRAP was performed using a confocal laser scanning microscope, equipped with a laser source at 561 nm. The intensity of the fluorescence signal was monitored between 570 and 600 nm with a 20× objective and 5× optical zoom. The laser output power was set to 10 μW for a pre-bleaching period of 30 s to record the initial fluorescence, then to 60 μW for 20 s to achieve sufficient photobleaching for FRAP measurements. Fluorescence recovery was monitored for 450 s with a scansion of the bleached area every 10 s, decreasing the laser output power to 10 μW. To assess the fluorescence recovery kinetics, the intensity of fluorescence measured in the target area before photobleaching was set as the reference value to express the recovery of fluorescence. Then, for each time point, the fluorescence intensity value measured in the photobleached target area was divided by the intensity value recorded in a reference region located at a suitable distance from the target area. For each experiment, the reference region was only slightly affected by the laser bleach and this ratio allowed us to correct for artificial changes in fluorescence intensity due primarily to photobleaching caused by the exposure of the field to the excitation obtain FRAP curves light source. These ratios were plotted against time and fitted using a single exponential function to obtain FRAP curves (Fig. 1 supplementary).

HES and hiPS Cell Culture

HES cells (cell line HES2; National Stem Cell Bank, Madison, WI) and hiPS cells (cell line ADHF#1; Center for iPS Cell Research and Application, iCeMS, Kyoto University) were grown on MEFs (Chemicon, Temecula, CA) inactivated with mitomycin C, in growth medium consisting of DMEM F-12 (Gibco, Grand Island, NY), supplemented with 20% knockout serum replacement (Invitrogen), 10% MEF conditioned medium (not used for hiPS), 20 ng mL^{-1} basic fibroblast growth factor for HES2, 10 ng mL^{-1} for hiPS (b-FGF; Invitrogen), 0.1 mM β-mercaptoethanol (Gibco), 1% non-essential amino acid stock (Invitrogen) and 1% Penicillin/Streptomicin (Invitrogen). HPSC were passaged to new feeder using 1 mL trypsin 0.25% for HES2 (Invitrogen), and CTK solution (trypsin 0.25%–collagenase IV–Ca^{2+}) for hiPS. To induce the formation of human EBs, undifferentiated hPSC were treated with 1 mL trypsin 0.25% and CTK, and then transferred to matrigel coated dishes for MEF depletion. 24–48 h later, undifferentiated hPSC were treated with 1 mg mL^{-1} type I collagenase (Invitrogen) for 20 min followed by 1 mL trypsin 0.25% in PBS for 30 s and then transferred to ultra-low adhesion plates containing EB medium: 80% knockout Dulbecco's modified Eagle medium (Gibco) supplemented with 20% defined fetal bovine serum (Hyclone), 1 mM L-glutamine, 1% non-essential amino acid stock (Gibco) and 1% penicillin/streptomycin. Human EBs were cultured at 37°C and 5% CO_2 in a humidified incubator, with changes of medium every 3 days. In order to check the influence of the modulate availability of endogenous factors on cell differentiation, 4–8–12 days old EBs were analyzed.

Microwell Cell Seeding

Prior to seeding cells in microwells, each UV sterilized microstructured hydrogel was placed in a well of a 6-well plate, immersed in cell culture medium and incubated at 37°C for 24 h for equilibration. HPSC were passaged from two wells of a 6-well matrigel coated plates to one microstructured hydrogel in 700 μL of cell culture medium. In order to maximize cell-seeding efficiency, the cell suspension was aliquoted to the top of the microstructured hydrogel, taking care to maintain the entire volume of cell suspension on the hydrogel. Hydrogel were kept at room temperature for at least 15 min to allow cells to settle into microwells and then placed into the incubator for 24 h. Finally, 3 mL $well^{-1}$ of EB medium was added carefully to each well of the 6-well plate to prevent cells from being washed out of microwells. We analyzed the effects of microwell confinement on EBs dimensions at time points of 4, 8, and 12 days after seeding. EB

size distributions were quantified using image analysis by measuring the diameter of each EB at the microscope.

Cell Viability Analysis

To conduct the analyses of cell viability, about 2×10^5 HES2 cells were seeded onto both microstructured hydrogels (microwells of 450 µm and microwells of 1 mm depth) and into ultra-low adhesive dishes for suspension culture. EBs were cultured for days after seeding, and cell viability was analyzed by Live & Dead assay. Cells were incubated for 45 min at room temperature with a solution containing 3 µM ethidium homodimer and 3 µM calcein AM dissolved, in DMEM containing 10% FBS. Living cells stained green, while dead cells stained red, and they were visualized by fluorescence microscopy.

Microarray

HES2-derived EBs collected at day 8 from the three culture conditions were lysed, RNA was extracted and cDNA was retro-transcribed and used for microarray experiments. DNA microarray analysis was carried out on the EBs cultured in the three different culture conditions. Total RNA was isolated using TRIZOL reagent (Invitrogen) coupled to RNeasy Kit (Qiagen) according to the manufacturers' instruction. Labelled cDNAs were synthesized by reverse transcription from the total RNA using the Quick Amp Labeling Kit, one-color (Agilent, Santa Clara, CA). Whole Human Genome Microarray Kit, 4× 44K (Agilent) was used according to the manufacturer's protocol. Each probe, corresponding to a specific gene, is repeated four times in the microarray glass slide for consistent data analysis. For statistical purposes, two independent experiments were performed. For every experiment, a triplicate of each cell culture condition was analyzed.

Immunofluorescence Analysis

After 8 days of culture in the three different conditions, embryoid bodies were carefully collected from suspension and from the microwells. Each batch was included into OCT and cryosectioned into 20 µm thick slices. Cryosections were cut onto poly-L-lysine coated glass microscope slides. EBs of 4, 8, and 12 days were cultured in adherent Petri dishes for 16 h to perform further analyses. Immunocytochemistry was performed as described: cryosections and adhered EBs were first fixed with paraformaldehyde 4% (8 min at room temperature) and then washed in PBS solution. Sections and EBs were then permeabilized in permeabilization buffer (PBS with 0.1% Triton X-100, Sigma) for 8 min at RT. Aspecific binding sites were blocked for 1 h at RT with blocking solution (PBS with 5% decomplemented Horse Serum). Sections and EBs were then washed and incubated with anti-Brachyury T for mesoderm, anti-AFP for endoderm and anti-β-III Tubulin for ectoderm, in blocking solution overnight at 4°C in humid environment, followed by two washes in wash solution and then incubated with secondary antibodies (1:200 in blocking solution) conjugated with Alexa548 or 594, for 1 h at 37°C in humid environment. Sections and EBs were counterstained in DAPI (Invitrogen, 1:1,000 in PBS) for nuclear staining. Slides were mounted with mounting medium and the coverslips were sealed with transparent varnish. The resulting immunostaining was evaluated using fluorescent microscopy imaging.
For immuno-quantification experiments, EBs were enzymatically and mechanically disaggregated with collagenase IV 2 mg mL^{-1} trypsin 0.25% and syringe passage. Single cells were plated in SuperFrost Plus glass slides by cytospin, 800 rpm for 5 min. Cells were fixed and stained with DAPI for total cell count, and for each marker for positive cell count. Six fields (20× magnification) were counted for each marker and condition, and statistical analyses were conducted.

Results

FRAP Analysis of Polyacrylamide Hydrogels

In order to evaluate self-diffusivity of molecules in polyacrylamide hydrogels, FRAP experiments were performed. Characterization of the hydrogel permeability was obtained by the estimation

of the local diffusion coefficient values for fluorescent probes with a molecular weight of 70 kDa. To perform those experiments, hydrogels obtained from pre-polymeric solutions with different monomer/cross linker molar ratios (acrylamide/bis-acrylamide ratios 29:1; 25:1; 21:1) and different pre-polymer concentrations (10–20%) were used and compared. The experiments were performed with these hydrogel compositions that show diffusional cutoff for 70 kDa fluorescence probes, which have the same order of magnitude of EBs secreted factors. Figure 3A shows swelling ratio Qm that decreases as the acrylamide and bis-acrylamide concentration (w/v) increases in the pre-polimer solution. In Figure 3B the mesh size, estimated from swelling data and Flory–Rehner theory, is plotted versus acrylamide percentage (w/v). Estimated mesh size decreases as pre-polymer concentration (w/v) increases, and also decreases as acrylamide/bis-acrylamide molar ratio in the pre-polymer solution increases. Figure 3C shows self-diffusion index, which is the diffusion coefficient of species when the chemical potential gradient equals zero. The coefficient is shown as a function of percentage of acrylamide and mesh size of the hydrogels. Figure 3D shows the diffusion index as a function of mesh size previously evaluated from Figure 3A. There is an evident trend of the self-diffusion that decreases for higher concentrations of acrylamide solution. There is also a unique correlation between diffusion coefficient and mesh size. From the analysis of these data it is possible to define a decrease in mobility for the 70 kDa dextran in 18–20% acrylamide hydrogels. It is interesting to suppose that soluble molecules with similar molecular weights and comparable hydrodynamic radii with the dextran used in the experiment have similar self-diffusivity in the same hydrogels. Therefore, we developed hydrogels of 20% acrylamide v/w, in order to have a cutoff for molecules with molecular weights within the range 40–70 kDa, with a hydrodynamic radius of ∼19 nm.

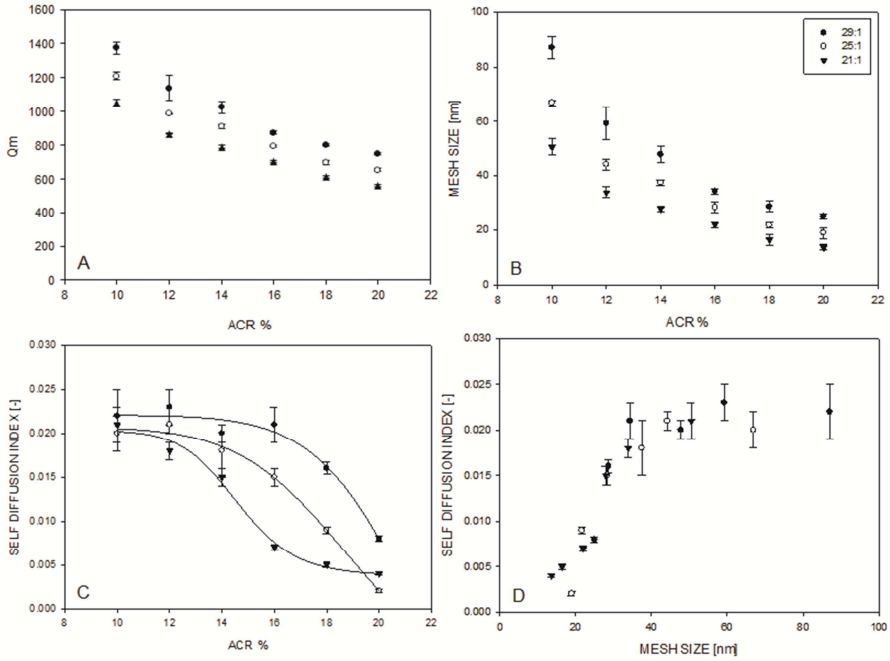

Figure 3. A*: Hydrogel mass equilibrium swelling ratio (Qm) decreases as the acrylamide and bis-acrylamide concentration (weight/volume [W/V]) increases in the pre-polimer solution (ACR %).* ***B****: From swelling data and Flory-Rehner theory, it is possible to estimate the mesh size of the hydrogel network. The figure shows that the mesh size (in nm) decreases for higher concentrations of acrylamide or bis-acrylamide.* ***C****: Self diffusion index (TAU) versus acrylamide concentration, with different cross-linker content. As expected, the self-diffusion decreases as hydrogel network becomes more dense.* ***D****: Self diffusion index versus hydrogel network mesh size. Molecular mobility falls to zero for mesh size lower than the molecular radii of the molecular tracer (about 19 nm, MW ∼70 kDa).*

Size-Distribution of EBs Cultured in Microwells

In this work, we successfully created a three-dimensional array of microwells, with specific dimensions. A diameter of 500 µm was chosen to develop EBs with the best average dimensions for early development (Choi et al., 2010; Mohr et al., 2010; Peerani et al., 2009; Tekin et al., 2010). We also chose to develop microwells with ratio width/depth 1:1 and 1:2 to create different culture microenvironments for EBs differentiation. Figure 4A shows an array of approximately 180 µwells completely independent, which can be used for cell aggregation. In order to help cell seeding, concave shape wells were designed. The photomask was designed with a gradient of tone around the 500 µm diameter spot (Fig. 2D). As the UV light passes through the photomask, it gradually polymerizes the acrylamide, generating a concavity around the microwell. We theoretically defined a seeding of 4×10^5 cells per well. The concave microwell array allows a consistent cell seeding, which results in homogenous distribution of cells in all the microwells. Figure 4B and C shows that modulation of UV light intensity through use of photomasks and different lamps results in efficient modulation of microwell heights, with low standard deviation. The biocompatibility of polyacrylamide hydrogels was tested at day 10 to see if there was any toxic effect of unpolymerized PA monomers. With the use of Live and Dead essay we observed that cell vitality was not affected by embryoid body confinement, and viability was comparable with suspension embryoid bodies (Fig. 2 supplementary). These results indicate that all the PA monomers are washed during the washing procedures, thus the hydrogel is a hydrated and compatible biomaterial for cell culture.

In Figure 4E–G are shown the histograms representing the distribution of EBs diameters in suspension, 1:1 and 1:2 µwells, during three time points at 4, 8, and 12 days of culture. In suspension culture the distributions are dispersed in a wider range, showing less uniformity in dimensions during all time points. On the other hand, both microstructured cultures show more symmetric distributions. Average EB diameters are similar both in suspension and hydrogels after 8 days, even if EB cultures in the microwells are more homogenous. It has been previously demonstrated how important the size homogeneity of embryoid bodies is during cell differentiation (Bauwens et al., 2008; Hwang et al., 2009; Karp et al., 2007; Moeller et al., 2008). With the experimental data shown in Figure 4, we can compare the three different culture conditions, assuming that the effect of EB diameter do not override the influence of local EB microenvironment.

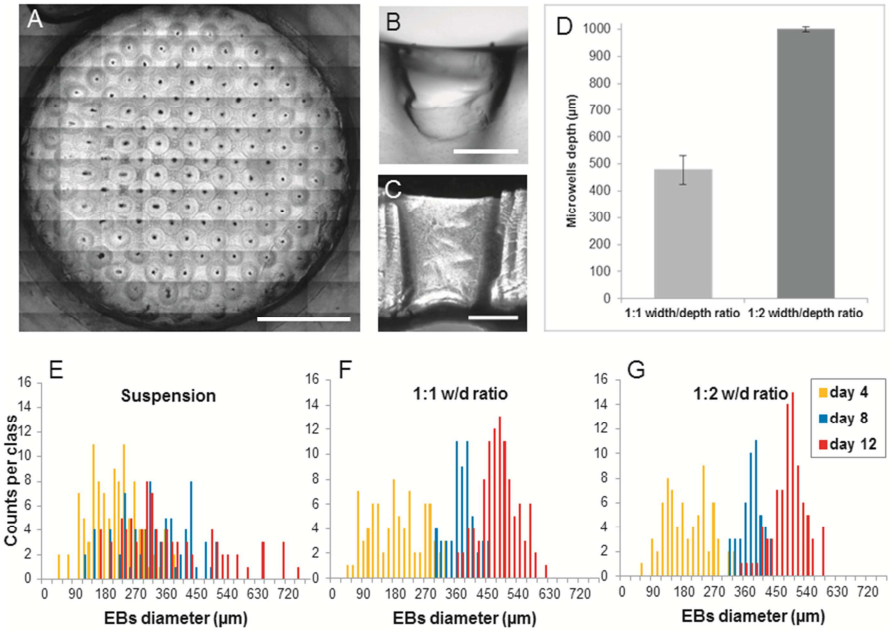

***Figure 4. A**: Array of EBs in the microwells of 1 mm depth (scale bar is 0.5 cm). Single EBs can easily be collected with a micropipette without disrupting the culture. **B,C**: Show enlargements of the vertical sections of the PA microwells of 450 µm and 1 mm depth, respectively. Scale bars in B and C are 250 µm. **D**: Measurements of the microwell depths. Panels (**E–G**) show quantitative*

distribution of suspension and microwell EBs diameter. E: Measurements of EBs diameters in suspension culture. F: Measurements of EBs diameters cultured in 500 µm width microwells and 450 µm depth (1:1). G: Measurements of EBs diameters cultured in 500 µm width microwells and 1 mm depth (1:2). The average embryoid body diameters (±standard deviation) after 4 days were 312 ± 148 µm (suspension), 210 ± 80 µm (500 µm Ø microwells 1:1) and 225 ± 98 µm (500 µm Ø microwells 1:2); after 8 days were 375 ± 155 µm (suspension), 385 ± 77 µm (500 µm Ø microwells 1:1) and 400 ± 68 µm (500 µm Ø microwells 1:2); after 12 days were 463 ± 191 µm (suspension), 504 ± 102 µm (500 µm Ø microwells 1:1), and 495 ± 84 µm (500 µm Ø microwells 1:2). Note the dispersion of diameter in the suspension culture condition during all time points, while data collected from the two types of microwell cultures have more symmetric distributions.

Microarray Functional Analysis

The expression patterns of embryoid bodies were assessed through transcriptomic analyses. Whole genome microarrays were used in order to have a complete overview of the gene expression in the different culture conditions. The differential gene expression was tested at day 8 in HES2-derived EBs, in order to show early differentiation and commitment into the three germ layers (Keller, 2005). The same batches of cells were expanded and used to form EBs for the three different culture conditions, in order to have reliable results. Furthermore, we used three replicates for each microarray for consistent statistical analyses.

During preprocessing of microarray data, Loess pair-wise normalization was applied. Quality reports and MvA plots showed high data quality for all the arrays. In the selection step (univariate analysis), significant analysis of microarrays (SAM) algorithm (Tusher et al., 2001) was used to identify genes with statistically significant changes in expression between different classes. All data were permutated over 1,000 cycles by using the multiclass response format, not considering equal variances. Significant genes were selected based on a false discovery rate (FDR) threshold of 0.05 (Benjamini and Hochberg, 1995). Significant genes were tested using the two-classes response format (suspension vs. 1:1 µwells, suspension vs. 1:2 µwells, 1:1 µwells vs. 1:2 µwells), not considering equal variances, and selected based on a significance level of 0.05/3 (Bonferroni correction). In the functional analysis, the probe sets were functionally annotated and grouped according to their biological function using Gene Ontology (GO) Biological Process descriptions (Ashburner et al., 2000). The functional enrichment analysis to identify the most relevant biological mechanisms was performed using DAVID (Dennis et al., 2003; Huang et al., 2009). GO Fat was used instead of standard GO to filter the broadest terms so that they do not overshadow the more specific terms. *P*-values were corrected for multiple testing using FDR (Ashburner et al., 2000).

In the multiclass analysis 418 probes were selected, corresponding to 380 unique gene IDs and 8 ESTs. Among the 388 genes significantly differentially expressed, 189 resulted upregulated in suspension EBs compared to the cultures of microwell EBs. Other 203 genes were upregulated in the microstructured EB cultures and downregulated in suspension culture (table shown in Fig. 3 supplementary). A cluster analysis of the results was done with genes involved in early embryogenesis, which were grouped as reported in the microarray heat map in Figure 5. From data analysis it can be seen that the repetition of independent experiments and replicates show comparable results. There is a marked difference between gene expressions in suspension EBs compared to microwell EBs. It is also clear that the different ratio in 1:1 and 1:2 µwells do not influence gene expression, and therefore they have been grouped into a single category and confronted with suspension.

We analyzed the expression of genes expressed in endoderm, mesoderm and ectoderm. There is a clear effect of the confinement in the differentiation patterns shown by the color graduation in the heat map (in red and green in Fig. 5). Results show that mesoderm specification and heart development is significantly upregulated in suspension EB, with expression of genes such as WIF1, BOC, MYH6, and TNNT2. On the other hand, genes such as NKX6-2, WNT3, GLI2, GDF3, and NRG1 involved in pattern specification process and regionalization, brain development, endoderm and ectoderm are consistently upregulated in microwell confined embryoid bodies.

The microarray analysis thus highlights a significant difference in the differentiation patterns of standard and confined embryoid bodies (see Figs. 4 and 5 supplementary).

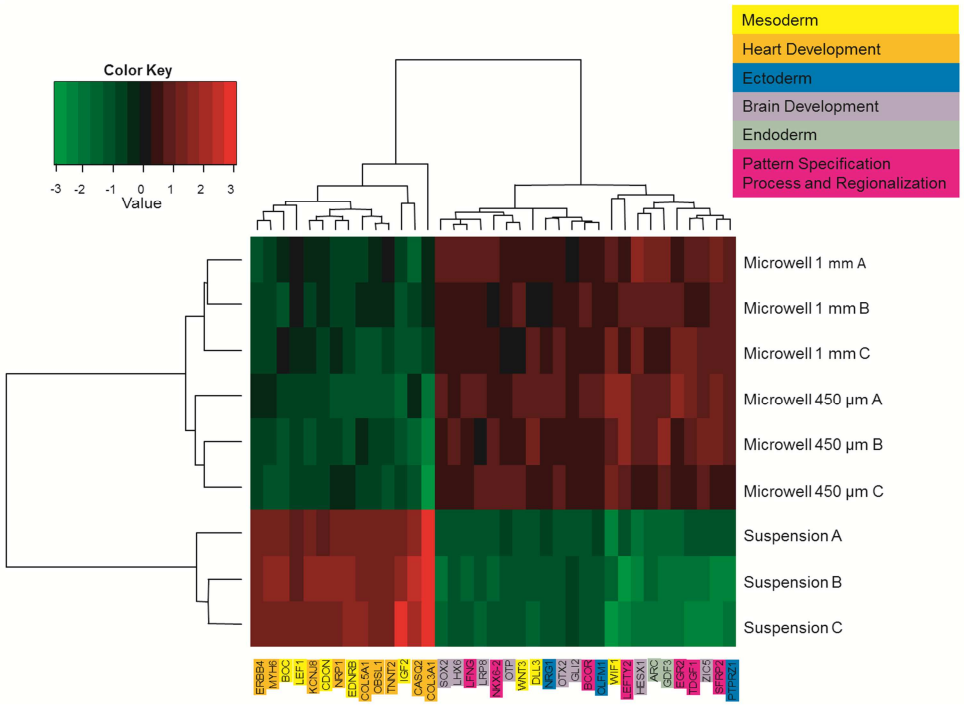

Figure 5. *Microarray analysis. The panel shows the heat map of the gene expression values of a subset of genes associated to the Gene Ontology enriched terms "mesoderm," "heart development," "ectoderm," "brain development," "endoderm," "pattern specification process and regionalization," in the different growing conditions and replicates. Mesoderm and heart development genes are significantly upregulated in EBs cultured in suspension. Ectoderm, brain development, endoderm, pattern specification process, and regionalization genes are significantly upregulated in EBs cultured in hydrogel microwells. The genes are grouped using a hierarchical agglomerative clustering (average linkage—Euclidean distance). Heat map showing the same gene expressions scaled with respect to genes average value, and heat map showing the expressions of the all the 388 genes, are shown in the supplementary material.*

Immunofluorescence of EBs Cryosections

After microarray experiments, we conducted immunofluorescence analyses to evaluate the expression of specific embryonic differentiation markers, and to investigate any possible influence of the different culture conditions onto early commitment to the three germ layers. Alpha-fetoprotein was used to mark early endoderm specification. Brachyury T marks the early embryonic mesoderm, while Beta-III Tubulin is used to mark the primary ectoderm. The immunofluorescence of the HES2-derived EBs sections is represented in Figure 6. AFP marking the endoderm is noticeably more expressed in EBs cultured in 1:1 and 1:2 µwells and less expressed in suspension EBs (Fig. 6A–C). The same result is observable for β-III Tub marking the ectoderm (Fig. 6F–H). On the other hand, brachyury T marking the mesoderm results more expressed in standard suspension EBs and less expressed in microwell condition (Fig. 6K–M). Similar results are observed for hiPS-derived EBs at day 8. Immunofluorescence analysis for induced pluripotent stem cells is shown in Figure 7, where AFP and β-III Tub result more expressed in the two microwell culture conditions (Fig. 7A–C,E–G), while brachyury T is higher expressed in suspension cultures (Fig. 7I–K). Quantification of immunofluorescence analyses was performed through cytospinned cells, and it clearly shows a difference in expression of the three germ layer markers among the different EB cultures. AFP and β-III Tub are significantly more expressed in both microwell cultures compared to suspension. On the other hand, brachyury T is

significantly overexpressed in suspension EBs rather than microwells (Fig. 8). In order to confirm our results obtained with 8 days old EBs, we performed the same immunofluorescence experiments on adherent EBs at two different time points, days 4 and 12, both for hES and hiPS cells. The expression of differentiation markers agrees with the results observed in day 8 EBs (see panels in Figs. 6 and 7 supplementary).

From the analysis of the immunofluorescences, it is noticeable that there is no evident difference between the two types of microwell culture conditions. Microwell dept could still influence differentiation patterns, even though this was not noticed in our microwell geometries. However, it could be interesting to verify if exogenous molecules could restore mesodermal germ layer differentiation, which was downregulated in microstructured cultures. To this purpose, we performed an experiment in which 5 ng mL^{-1} of activin A, a mesoderm inducing factor, was added in the 1 mm microwell culture medium. Surprisingly, at all time points measured, the expression of mesoderm marker (brachyury T) in HES2-derived EBs was enhanced if compared with non-treated microwell EBs as shown in Figure 9.

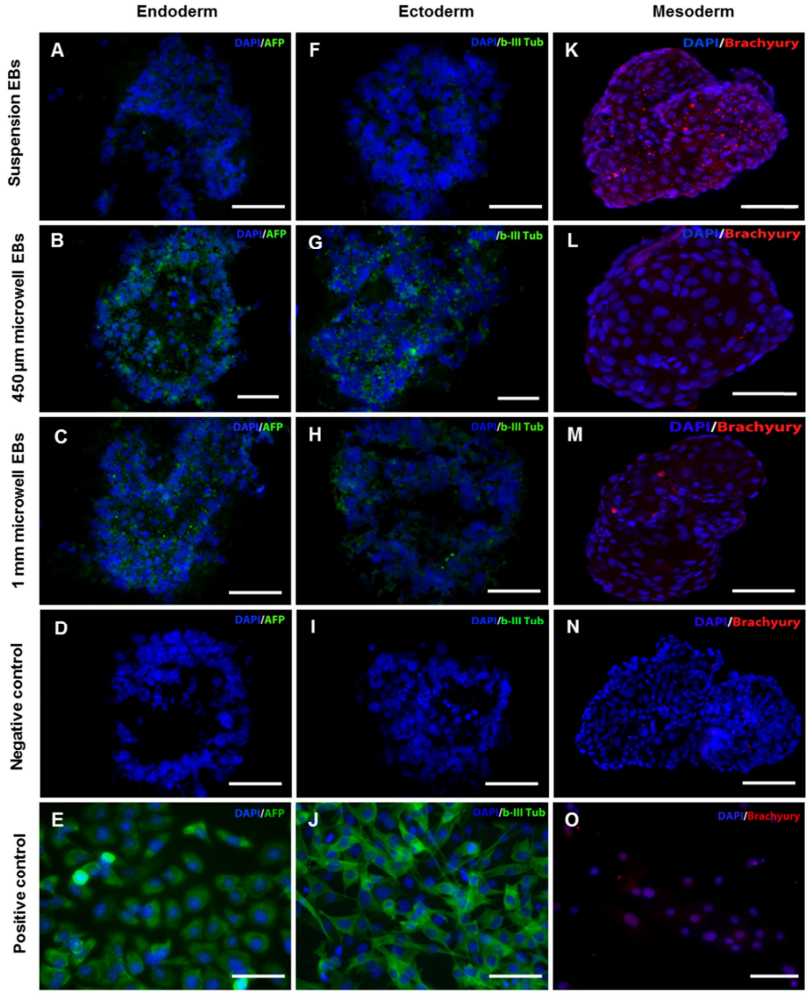

Figure 6. *Immunofluorescence analysis of the three germ layers on cryosections (20 µM thick) of 8 days hES-derived EBs cultured in the three conditions. Panels (**A–D)** show immunolabeling with alpha-fetoprotein (green), which marks the endoderm, and nuclei are stained with DAPI (blue). A major expression of this marker is shown by the microwell culture conditions. Panel (**E)** shows HepG2 cell line expressing high levels of AFP. Panels (**F–I**) show the expression of the ectoderm marker beta-III tubulin (green), which results more expressed in the 450 µM and 1 mm µwell conditions. C2C12 expressing b-III Tub are shown in panel (**J**). Panels (**K–N**) show labeling for Brachyury T (red), which recognizes the mesoderm. This marker is more expressed in EBs cultured*

*in suspension. Panel (**O**) show the expression of Brachyury T in cardiomyocytes derived with a high-efficient mesoderm differentiation protocol of EBs. Scale bar is 100 µM.*

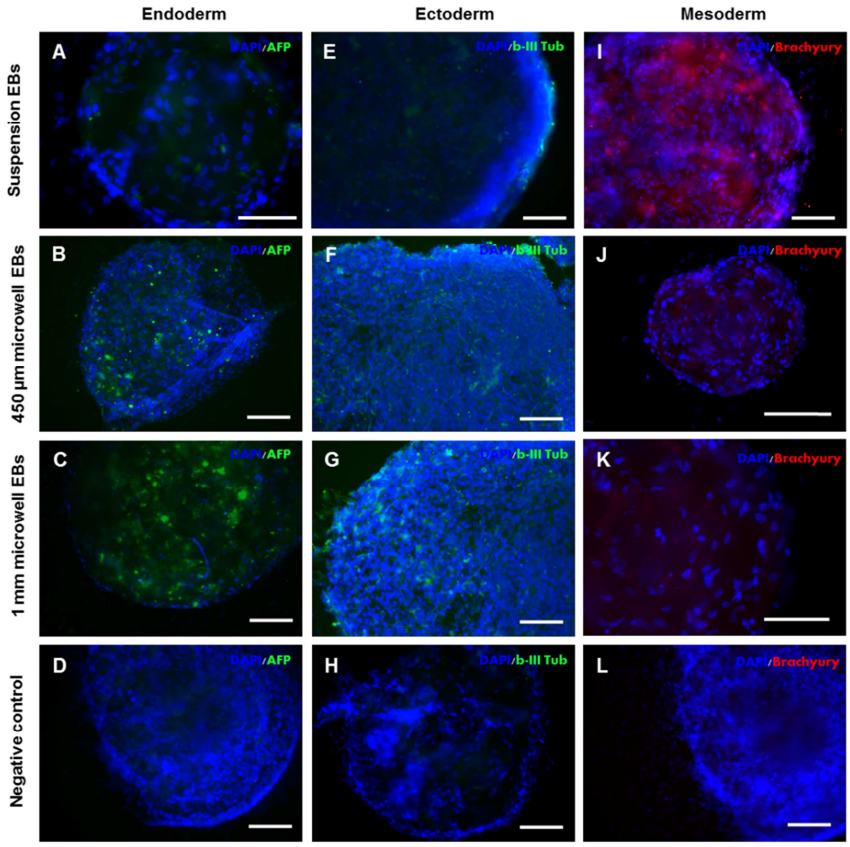

Figure 7. *Immunofluorescence analysis of the three germ layers on adhered (for 16 h) hiPS-derived EBs (8 days) cultured in the three conditions. Panels (**A–D**) show immunolabeling with alpha-fetoprotein (green), and nuclei are stained with DAPI (blue). A major expression of this marker is shown by the microwell culture conditions. Panels (**E–H**) show the expression of beta-III tubulin (green), which results more expressed in the microwell conditions. Panels (**I–L**) show labeling for Brachyury T (red). This marker is more expressed in EBs cultured in suspension. Scale bar is 250 µM.*

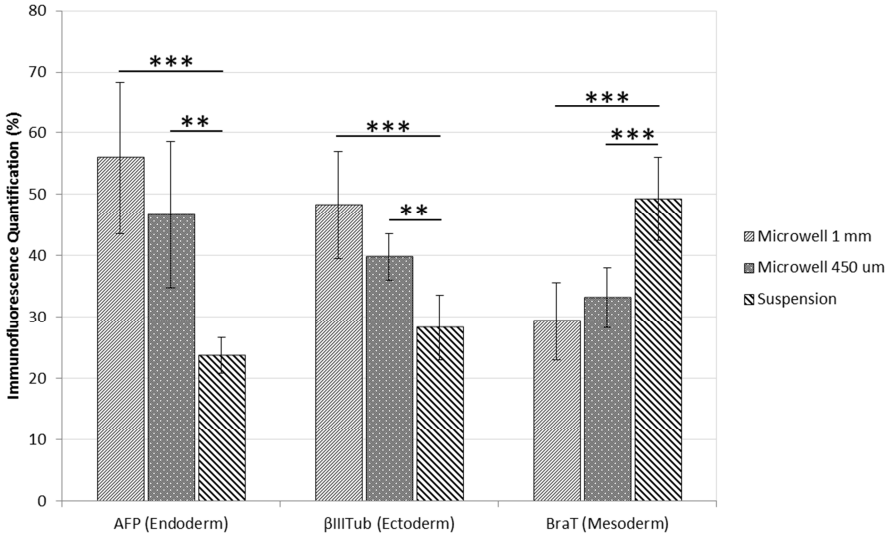

Figure 8. *The graph shows the immunofluorescence quantification by cytospin counts of 8 days hES-disaggregated EBs. Alpha-fetoprotein and beta-III tubulin are more expressed in the two microwell conditions, and show high significant difference compared to suspension culture. Brachyury T is higher expressed in suspension culture with high significant difference from 450 µm and 1 mm microwell cultures. Error bars are ±SD. Significativity is calculated with unpaired t-test. ***P < 0.001, **P < 0.01, *P < 0.05.*

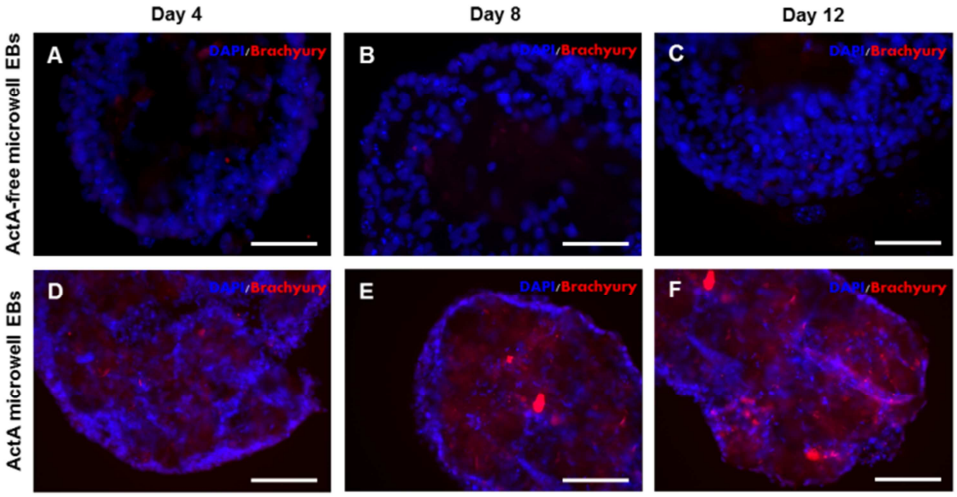

Figure 9. *Immunofluorescence analysis on adhered hES-derived EBs. Panels (**A**–**C**) show immunofluorescence of Brachyury T in 1 mm microwell EBs non-treated with exogenous factors. Panels (**D**–**F**) show immunolabeling with Brachyury T in 1 mm microwells EBs treated with Activin A (5 ng mL^{-1}), at three different time points, 4, 8, and 12 days. Treatment with exogenous ActA show induction of mesoderm germ layer in microwells culture of embryoid bodies. Scale bar is 300 µM.*

Discussion

The aim of the present work is to investigate the influence of a confined three-dimensional microenvironment on hPSC differentiation. Unlike monolayer cell cultures, in which specific aspects of the microenvironment can be more easily investigated, a 3D organization of cells like the EB is more difficult to examine. Differentiation of EBs is directed by exogenous molecules present in the culture media, and endogenous factors produced by differentiating embryonic stem cells. In order to investigate the confined microenvironment influence on differentiation, we used simple culture media, without addition of external growth factors, which could induce specific patterns. We created narrowed niches where EBs can grow and differentiate. The polyacrylamide hydrogel was chosen because it is highly stable and equilibrated with surrounding medium, and therefore permits the creation of hydrated niches suitable for cell cultures. It is a biocompatible polymer easily moldable with UV light and characterized by a non-adhesive surface, which allows the formation of EBs, and it is selectively permeant to soluble molecules of defined dimensions. It is evident that the larger the molecule then the lower the permeability of the PA hydrogel to this molecule (Williams et al., 1998). This property of the biomaterial permits the accumulation of molecules with molecular weights higher than the polymer cutoff. Therefore, it is reasonable to suppose that factors produced by embryoid bodies can accumulate in the microwell microenvironment, when their MW exceeds the hydrogel cutoff of 40–70 kDa.
The culture of hPSC into microstructured polyacrylamide hydrogels allowed the obtainment of homogenous batches of embryoid bodies compared to the standard suspension culture conditions. EBs grown in suspension tend to form aggregates with one other, having therefore more dispersed sizes. This can eventually lead to more heterogeneous results in any repeated analysis carried out in different batches. With microstructured hydrogels we obtained EBs with the same mean size as suspension, but with more homogenous dimensions. This culture

condition also permits to obtain physically separated embryoid bodies, avoiding undesired aggregates.
To evaluate gene expression differences, EBs were cultured until primitive stage of the three germ layers, when specific markers of early differentiation are expressed and therefore recognizable (Keller, 2005). In the microarray experiments there is no significant difference between the two types of hydrogel, and for this reason microwell EBs gene expressions have been grouped and statistically compared to suspension EBs. It is possible that 1:1 ratio of the microwells is sufficient for an accumulation of factors and the geometry 1:2 does not influence anymore the microenvironment. To have a robust analysis of genes expression, we used the same batch of hES cells in all the experiments, and we used three replicates for each culture condition. The heat map shows clearly the homogeneity among the replicates, therefore the experiment is highly repeatable. Functional analysis of the significantly differentially expressed genes shows that confinement of EBs in the microwells lead to specification into ectoderm and endoderm, and to formation of spatial patterns in developing EBs. The culture in conventional dishes, on the other hand, promotes the expression of genes involved in mesoderm germ layer and heart development.
This robust data analysis agrees with data obtained in the immunofluorescence experiments. The proteomic analyses confirm the upregulation of endoderm and ectoderm markers in microwell EBs, and mesoderm marker in suspension culture. These results are consistent for two different stem cell lines with different origins, hES and hiPS. Both microarrays and immunostaining analyses suggest that EBs confinement does influence cell differentiation. The fact that there is no difference between the two microwell conditions could indicate that the microenvironment is not significantly influenced by our chosen depths of the microwells, but it significantly influences differentiation compared to standard suspension conditions.
These outcomes on differentiation marker expression and gene expression can be correlated with an analysis of the relative dimensions (according to UniProt Database http://www.uniprot.org/) of the main secreted factors by the EBs, which are involved in the regulation of the differentiation patterns (Aberger et al., 1998; Clark et al., 2003; Germain and Littlefield, 1986; Stennard et al., 1997). The data of the molecular weights of the endogenous factors are shown in Figure 10. From our data, we can see that mesoderm is more expressed in suspension culture, therefore it can be hypothesized that mesoderm-inducing factors are relatively small compared to the cutoff of the polyacrylamide, so that they diffuse away from the cell niche in the microwells. At the same time, mesoderm-inhibiting factors should be relatively larger molecules that overstay in the microwells and diffuse slowly from the EBs. These hypotheses have a confirmation in the dimensions of secreted factors that influence or inhibit mesoderm formation (see Fig. 10). In the same table the data of the endogenous factors referring to ectoderm and endoderm are shown. Endoderm factors are not clearly defined in number and molecular weight, and not much can be discussed for this germ layer, even though immunofluorescence and microarray experiments confirm that these factors are more expressed in the microwell EBs. Ectoderm-inducing factors have higher molecular weight compared to mesoderm-inducing factors, and therefore have lower diffusional times through the PA mesh and remain longer in the EBs microenvironment. In fact, ectoderm result more expressed in embryoid bodies cultured in the microwells. Interestingly, our results show that a mesoderm-inducing factor could override the effect of endogenous factors in 1 mm microwell culture, restoring mesodermal commitment.
These findings could indicate that the locally controlled availability of endogenous factors elicits significant differences in hPSC differentiation and may provide new insights into the mechanisms involved in cell differentiation.

Secreted Factor	Molecular Weight [kDa]	Regulation			References
		Endoderm	Mesoderm	Ectoderm	
Egf	6.4		Induction		(Stennard et al., 1997)
b-Fgf	18		Induction		(Stennard et al., 1997)
Ecdgf	18	Induction			(Germain et al., 1986)
Dkk-1	28		Induction	Inhibition	(Clark et al., 2003)
Noggin	30			Induction	(Aberger et al., 1998)
Scgf	33.9	Induction			(Germain et al., 1986)
FrzB	37		Inhibition		(Stennard et al., 1997)
Follistatin	39			Induction	(Aberger et al., 1998)
Wnt	40 - 46		Inhibition	Induction	(Aberger et al., 1998)
Tgf-b	50 (dimer)		Induction		(Stennard et al., 1997)
Bmp-4	60 (dimer)		Induction	Inhibition	(Germain et al., 1986)
Chordin	120			Induction	(Aberger et al., 1998)

Figure 10. *The chart shows some of the main germ layers secreted factors involved in embryogenic processes. The red parenthesis at the left side of the chart indicates the molecular weight cutoff of the PA hydrogel (around 40–70 kDa). The factors are ordered by growing molecular weight to show the correlation between dimensions and effect on the germ layers, to correlate with the data shown in the microarray and immunofluorescence analyses. Data referred to UniProt Database http://www.uniprot.org/.*

Conclusions

With FRAP experiments we have shown, in an innovative way, the properties that make polyacrylamide hydrogels one of the most suitable materials for chromatographic purposes. We have evidenced the possibility of building a polymeric and biocompatible substrate with high selective diffusional properties. Our present results demonstrate that homogeneous-size EBs can be produced within a microstructured hydrogel. This technique can be used for homogenously initiating the formation of EBs, which is critical for obtaining standardized and separated cell aggregates. It can be hypothesized that EBs with similar dimensions have comparable uptake of soluble factors on their surfaces, and it is more probable that they follow similar differentiation patterns, increasing homogeneity within the obtained cell populations. This potential improvement in homogeneity may be beneficial to the reproducibility of differentiation protocols into a specific lineage for potential tissue engineering and organ regeneration applications.
Furthermore, hPSC cultured in the three-dimensional system synthesize their own endogenous repertoire of factors and contribute to create a microenvironment suitable for cell growth and differentiation. Our results show that the accumulation of endogenous factors has a deep effect on hPSC differentiation. This study could provide insights to the relationship between the confined cell niche and stem cell behavior during differentiation. In addition it sheds light on the potential effects of the diffusion of soluble factors and related effects on differentiation patterns in microenvironments, relevant to the emerging use of microstructured culture systems. Further experiments are required in order to study the regionalization process in the EBs. It would be challenging to analyze and compare the distribution of specific markers of hPSC differentiation.
Coupling three-dimensional microwell technologies to obtain size-controlled EBs and modulating the availability of endogenous factors, can contribute to the understanding of stem cell differentiation processes, and make this approach a useful tool to consider when developing in vitro differentiation protocols.

Acknowledgements

This research has been supported by the FSE “Fondo Sociale Europeo,” “Progetti di Eccellenza Cariparo,” and the Università degli Studi di Padova.

References

Aberger F, Weidinger G, Grunz H, Richter K. 1998. Anterior specification of embryonic ectoderm: the role of the Xenopus cement gland-specific gene XAG-2. Mechanisms of Development 72(1-2):115-130.

Ashburner M, Ball CA, Blake JA, Botstein D, Butler H, Cherry JM, Davis AP, Dolinski K, Dwight SS, Eppig JT and others. 2000. Gene Ontology: tool for the unification of biology. Nature Genetics 25(1):25-29.

Bauwens CL, Peerani R, Niebruegge S, Woodhouse KA, Kumacheva E, Husain M, Zandstra PW. 2008. Control of human embryonic stem cell colony and aggregate size heterogeneity influences differentiation trajectories. Stem Cells 26(9):2300-2310.

Benjamini Y, Hochberg Y. 1995. Controlling the False Discovery Rate - a Practical and Powerful Approach to Multiple Testing. Journal of the Royal Statistical Society Series B-Methodological 57(1):289-300.

Bratt-Leal AM, Carpenedo RL, McDevitt TC. 2009. Engineering the Embryoid Body Microenvironment to Direct Embryonic Stem Cell Differentiation. Biotechnology Progress 25(1):43-51.

Choi YY, Chung BG, Lee DH, Khademhosseini A, Kim J-H, Lee S-H. 2010. Controlled-size embryoid body formation in concave microwell arrays. Biomaterials 31(15):4296-4303.

Cimetta E, Pizzato S, Bollini S, Serena E, De Coppi P, Elvassore N. 2009. Production of arrays of cardiac and skeletal muscle myofibers by micropatterning techniques on a soft substrate. Biomedical Microdevices 11(2):389-400.

Clark HF, Gurney AL, Abaya E, Baker K, Baldwin D, Brush J, Chen J, Chow B, Chui C, Crowley C and others. 2003. The Secreted Protein Discovery Initiative (SPDI), a large-scale effort to identify novel human secreted and transmembrane proteins: A bioinformatics assessment. Genome Research 13(10):2265-2270.

Dennis G, Jr., Sherman BT, Hosack DA, Yang J, Gao W, Lane HC, Lempicki RA. 2003. DAVID: Database for Annotation, Visualization, and Integrated Discovery. Genome biology 4(5):P3.

Dvash T, Benvenisty N. 2004. Human embryonic stem cells as a model for early human development. Best Practice & Research in Clinical Obstetrics & Gynaecology 18(6):929-940.

Germain EL, Littlefield JW. 1986. Endoderm-Secreted Factor Stimulates Growth of Embryonal Carcinoma Stem-Cells. In Vitro Cellular & Developmental Biology 22(2):107-112.

Huang DW, Sherman BT, Lempicki RA. 2009. Systematic and integrative analysis of large gene lists using DAVID bioinformatics resources. Nature Protocols 4(1):44-57.

Hwang Y-S, Chung BG, Ortmann D, Hattori N, Moeller H-C, Khademhosseini A. 2009. Microwell-mediated control of embryoid body size regulates embryonic stem cell fate via differential expression of WNT5a and WNT11. Proceedings of the National Academy of Sciences of the United States of America 106(40):16978-16983.

Itskovitz-Eldor J, Schuldiner M, Karsenti D, Eden A, Yanuka O, Amit M, Soreq H, Benvenisty N. 2000. Differentiation of human embryonic stem cells into embryoid bodies comprising the three embryonic germ layers. Molecular Medicine 6(2):88-95.

Karp JM, Yeh J, Eng G, Fukuda J, Blumling J, Suh K-Y, Cheng J, Mahdavi A, Borenstein J, Langer R and others. 2007. Controlling size, shape and homogeneity of embryoid bodies using poly(ethylene glycol) microwells. Lab on a Chip 7(6):786-794.

Keller G. 2005. Embryonic stem cell differentiation: emergence of a new era in biology and medicine. Genes & Development 19(10):1129-1155.

Kurosawa H. 2007. Methods for inducing embryoid body formation: In vitro differentiation system of embryonic stem cells. Journal of Bioscience and Bioengineering 103(5):389-398.

Lee LH, Peerani R, Ungrin M, Joshi C, Kumacheva E, Zandstra PW. 2009. Micropatterning of human embryonic stem cells dissects the mesoderm and endoderm lineages. Stem Cell Research 2(2):155-162.

Moeller H-C, Mian MK, Shrivastava S, Chung BG, Khademhosseini A. 2008. A microwell array system for stem cell culture. Biomaterials 29(6):752-763.

Mohr JC, Zhang J, Azarin SM, Soerens AG, de Pablo JJ, Thomson JA, Lyons GE, Palecek SP, Kamp TJ. 2010. The microwell control of embryoid body size in order to regulate cardiac differentiation of human embryonic stem cells. Biomaterials 31(7):1885-1893.

Odorico JS, Kaufman DS, Thomson JA. 2001. Multilineage differentiation from human embryonic stem cell lines. Stem Cells 19(3):193-204.

Park J, Cho CH, Parashurama N, Li Y, Berthiaume F, Toner M, Tilles AW, Yarmush ML. 2007. Microfabrication-based modulation of embryonic stem cell differentiation. Lab on a Chip 7(8):1018-1028.

Park JY, Lee DH, Lee EJ, Lee S-H. 2009. Study of cellular behaviors on concave and convex microstructures fabricated from elastic PDMS membranes. Lab on a Chip 9(14):2043-2049.

Peerani R, Onishi K, Mahdavi A, Kumacheva E, Zandstra PW. 2009. Manipulation of Signaling Thresholds in "Engineered Stem Cell Niches'' Identifies Design Criteria for Pluripotent Stem Cell Screens. Plos One 4(7).

Peerani R, Rao BM, Bauwens C, Yin T, Wood GA, Nagy A, Kumacheva E, Zandstra PW. 2007. Niche-mediated control of human embryonic stem cell self-renewal and differentiation. Embo Journal 26(22):4744-4755.

Pekkanen-Mattila M, Pelto-Huikko M, Kujala V, Suuronen R, Skottman H, Aalto-Setala K, Kerkela E. 2010. Spatial and temporal expression pattern of germ layer markers during human embryonic stem cell differentiation in embryoid bodies. Histochemistry and Cell Biology 133(5):595-606.

Reubinoff BE, Pera MF, Fong CY, Trounson A, Bongso A. 2000. Embryonic stem cell lines from human blastocysts: somatic differentiation in vitro. Nature Biotechnology 18(4):399-404.

Schuldiner M, Yanuka O, Itskovitz-Eldor J, Melton DA, Benvenisty N. 2000. Effects of eight growth factors on the differentiation of cells derived from human embryonic stem cells. Proceedings of the National Academy of Sciences of the United States of America 97(21):11307-11312.

Stennard F, Ryan K, Gurdon JB. 1997. Markers of vertebrate mesoderm induction. Current Opinion in Genetics & Development 7(5):620-627.

Tekin H, Anaya M, Brigham MD, Nauman C, Langer R, Khademhosseini A. 2010. Stimuli-responsive microwells for formation and retrieval of cell aggregates. Lab on a Chip 10(18):2411-2418.

Thomson JA, Itskovitz-Eldor J, Shapiro SS, Waknitz MA, Swiergiel JJ, Marshall VS, Jones JM. 1998. Embryonic stem cell lines derived from human blastocysts. Science 282(5391):1145-1147.

Tian XH, Morris JK, Linehan JL, Kaufman DS. 2004. Cytokine requirements differ for stroma and embryoid body-mediated hematopoiesis from human embryonic stem cells. Experimental Hematology 32(10):1000-1009.

Tusher VG, Tibshirani R, Chu G. 2001. Significance analysis of microarrays applied to the ionizing radiation response. Proceedings of the National Academy of Sciences of the United States of America 98(9):5116-5121.

Wang LS, Li L, Shojaei F, Levac K, Cerdan C, Menendez P, Martin T, Rouleau A, Bhatia M. 2004. Endothelial and hematopoietic cell fate of human embryonic stem cells originates from primitive endothelium with hemangioblastic properties. Immunity 21(1):31-41.

Williams JC, Mark LA, Eichholtz S. 1998. Partition and permeation of dextran in polyacrylamide gel. Biophysical Journal 75(1):493-502.

Supplementary material

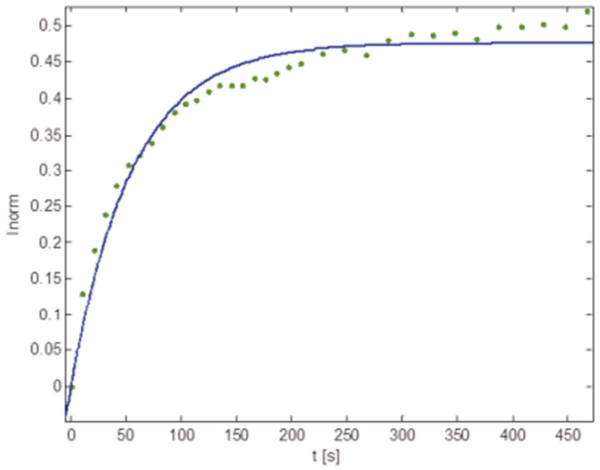

Fig. 1. Supplementary. *Fitting of a normalized FRAP recovery curve.*

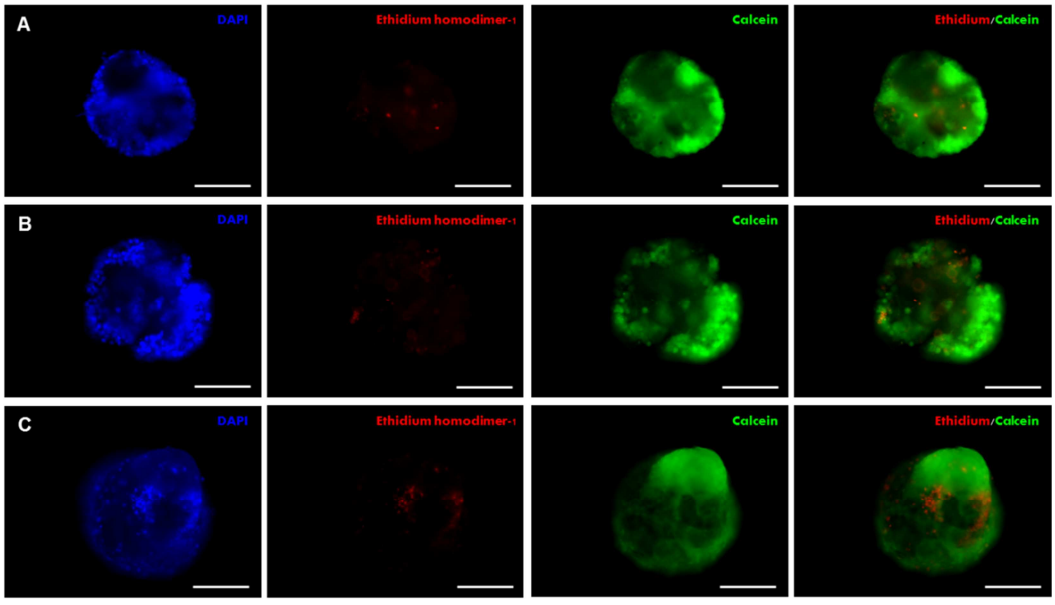

Fig. 2. Supplementary. *Live/dead assay on hES-EBs in standard cell culture conditions, in A) ultra-low adhesive cell culture dishes, B) 450µm deep microwells, C) 1mm deep microwells, 10 days after cell seeding. Cells in the microstructured hydrogel are viable, thus indicating that the PA hydrogel and the confinement do not negatively affect cell viability. Scale bars are 250 µm.*

Group1 vs. Group2	Group1 vs. Group3	Group2 vs. Group3	N° of selected probes
p	p	p	4
m	m	m	10
p	p	m	7
m	m	p	2
p	p	-	189
m	m	-	203
p	-	m	1
m	-	p	2

Fig. 3. Supplementary. *Selection shows how many of the 388 genes are significantly differentially expressed in the two-class comparison and the sign of the differential expression. "Group 1" correspond to genes expressions of EBs cultured in suspension. "Group 2" correspond to genes expressions of EBs cultured in 450 µm microwells. "Group 3" correspond to genes expressions of EBs cultured in 1 mm microwells. "p" indicates upregulation in the first group of comparison compared to the second. "m" indicates downregulation in the first group of comparison compared to the second. "-" indicates genes non-significantly differentially expressed between the two compared groups.*

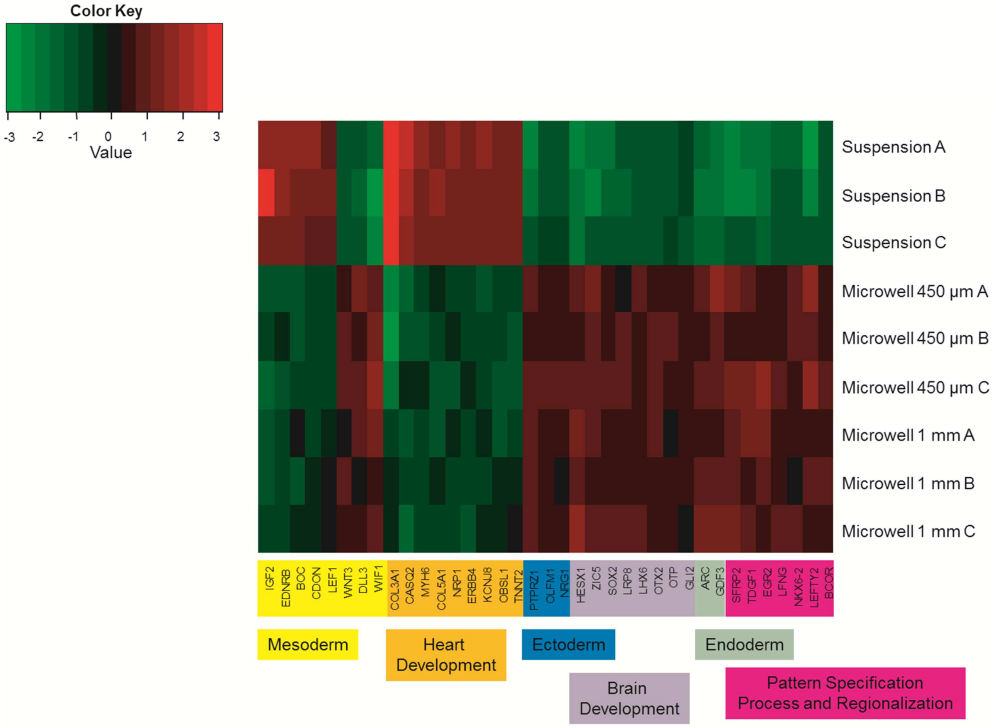

Fig. 4. Supplementary. *Microarray analysis. The panel shows the heat map of the gene expression values of a subset of genes associated to "mesoderm", "heart development", "ectoderm", "brain development", "endoderm", "pattern specification process and regionalization", in the different growing conditions and replicates. Values are scaled with respect to genes average value (log expression value of the gene minus the average log expression value of the gene across the experiments).*

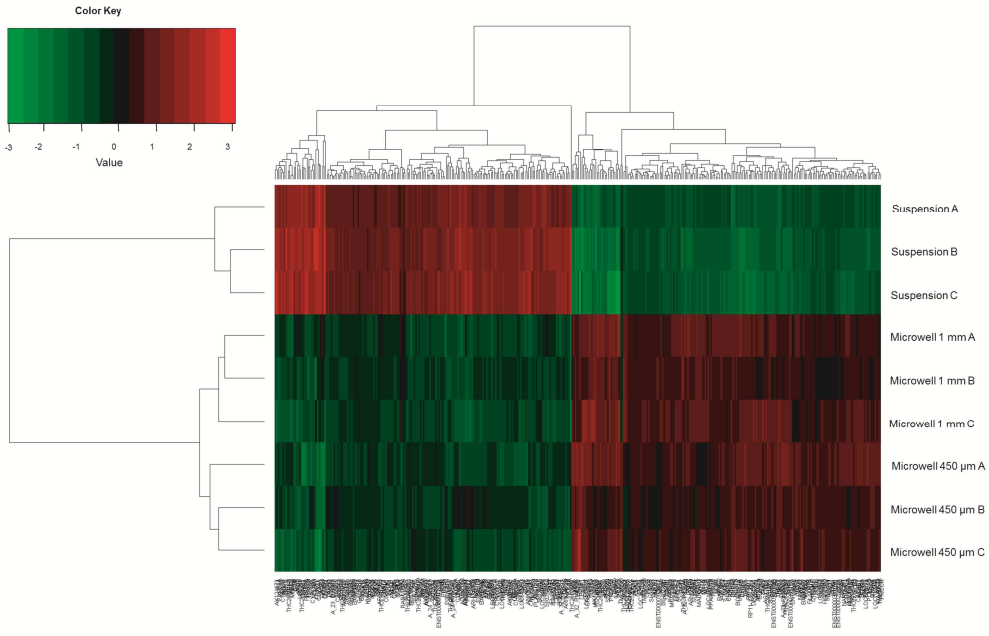

Fig. 5. Supplementary. *Microarray analysis. The panel shows the results of the clustering of all the 388 differentially expressed genes with a significant difference between the suspension culture condition and the microwell culture condition.*

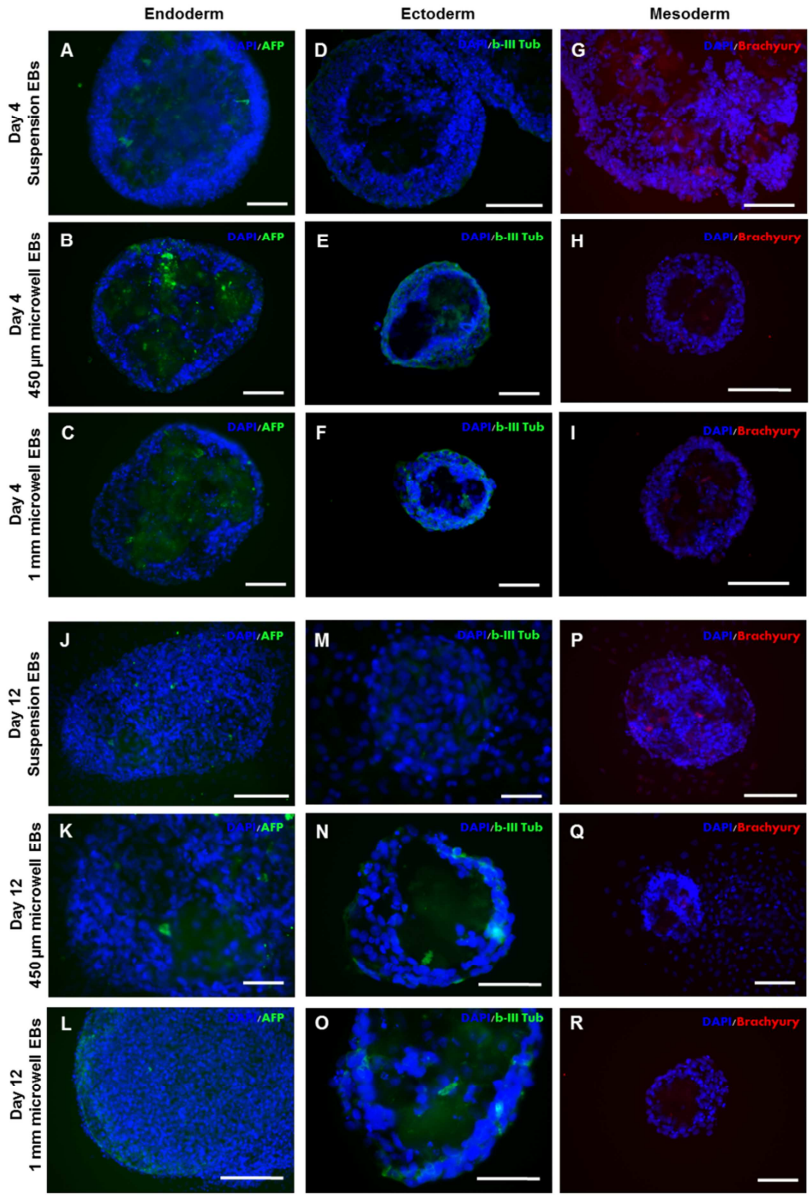

Fig. 6. Supplementary. *Immunofluorescence analysis of the three germ layers on adhered (for 16 h) hESC-derived EBs cultured in the three conditions at two different time points, 4 and 12 days. Panels A-C and J-L show immunolabeling with alpha-fetoprotein (green), and nuclei are stained with DAPI (blue). At both time points AFP is more expressed in the two microwell culture conditions. Panels D-F and M-O show the expression of the ectoderm marker beta-III tubulin (green), which results more expressed in the 450 µM and 1 mm microwell conditions. Panels G-I and P-R show labeling for Brachyury T (red), which recognizes the mesoderm. This marker is more expressed in EBs cultured in suspension, at both time points. Scale bar is 150 µM.*

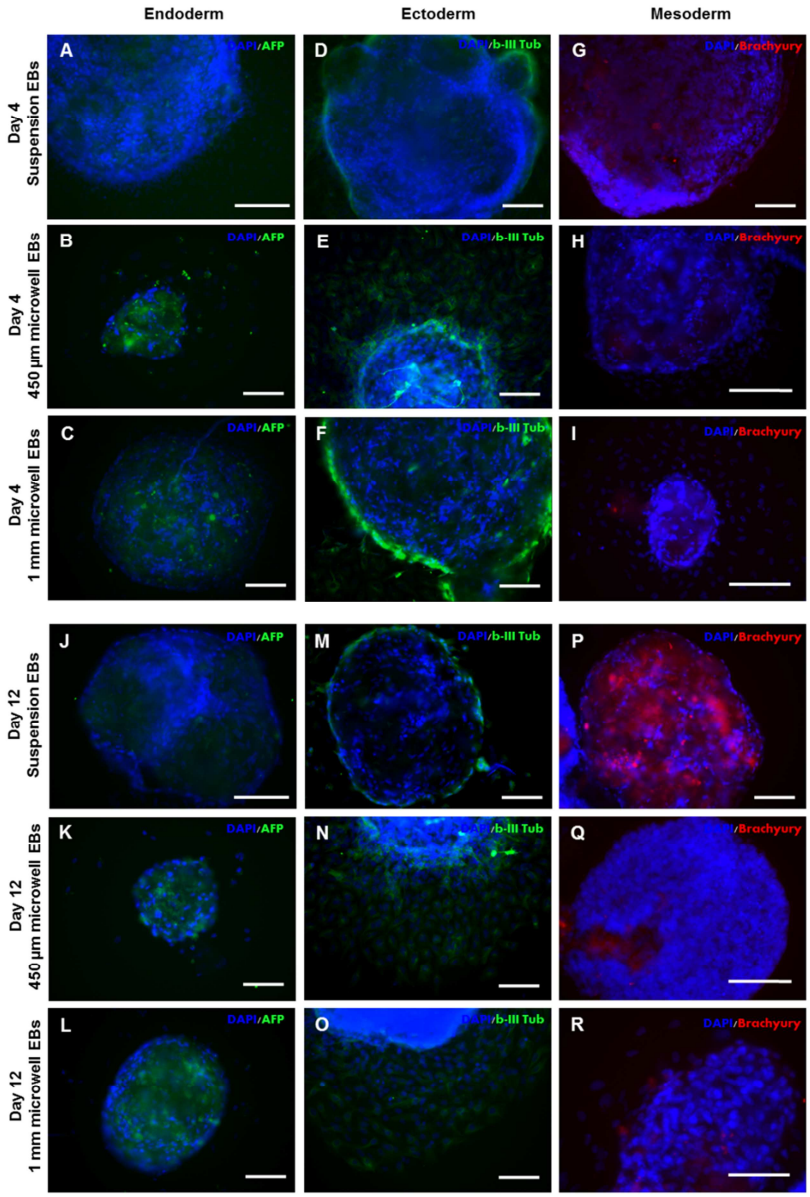

Fig. 7. Supplementary. *Immunofluorescence analysis of the three germ layers on adhered hiPSC-derived EBs cultured in the three conditions at two different time points, 4 and 12 days. Panels A-C and J-L show immunolabeling with alpha-fetoprotein (green). At both time points AFP is more expressed in the two microwell culture conditions. Panels D-F and M-O show the expression of the ectoderm marker beta-III tubulin (green), which results more expressed in the two microwell conditions. Panels G-I and P-R show labeling for Brachyury T (red). This marker is more expressed in EBs cultured in suspension, at both time points. Scale bar is 100 µM.*

APPENDIX B

INTEGRATED MULTI-STAGE TISSUE ON A CHIP GENERATION FROM HUMAN PLURIPOTENT STEM CELLS

Giovanni G. Giobbe[1,2,3,4], Federica Michielin[1,2,4], Sebastian Martewicz[1,2], Stefano Giulitti[1,2], Camilla Luni[1,2], Annarosa Floreani[3], Nicola Elvassore[1,2]

[1]Department of Industrial Engineering (DII), University of Padova, Via Marzolo 9, 35131 Padova, Italy; telephone: +39-049-8275469; fax: +39-049-8275461; e-mail: nicola.elvassore@unipd.it
[2]Venetian Institute of Molecular Medicine (VIMM), Via Orus 2, 35129 Padova, Italy
[3]Department of Surgery, Oncology and Gastroenterology (DiSCOG), University of Padova, Via Giustiniani 2, 35124 Padova, Italy
[4]**These authors contributed equally to this work:** Giovanni G. Giobbe and Federica Michielin

Nature Methods
brief communication under revision

Key words: Microfluidics; Tissue-on-a-chip; Human pluripotent stem cells; Differentiation; Endogenous factors; Exogenous factors; Hepatocytes; Cardiomyocytes.

Abstract

Micro-engineering human tissues and "organs-on-chips" remains an open challenge from both scientific and technological points of view. Here, we described a robust and efficient microfluidic-based approach for the differentiation of human pluripotent stem cells into functional cells. Specific frequency of periodic medium perfusion enhances the selectiveness of early germ layer differentiation and cell commitment through extrinsic microfluidic signal perturbations. Human cardiomyocytes and hepatocytes generated on chip from human pluripotent stem cells through multi-stage approach show functional differentiation, which opens a new perspective for multi-parametric and large scale human organ-based screening assays.

Text

The development of human organs-on-chips, in which the microscale engineering technologies are combined with cultured human cells to recapitulate whole living organ microenvironment, offers a unique opportunity to study human physiology and pathophysiology in an organ-specific context[1,2,3]. This technological perspective could provide an effective solution to the limitations of conventional cell culture models that fail to recapitulate complex, organ-level disease processes in humans and it could overcome the use of costly and time-consuming animal testing, which often shows poor predictive power of human physiology. Moreover, the scientific community, the major pharmaceutical companies and the government agencies are recognizing the paramount importance of developing new technologies, which allow to perform cost effective and multi-parametric assay for *ad hoc* studies in development, disease and pathogenesis, or for screening specific therapeutic strategies.
Recently, successful examples of organs-on-chips development have been provided[4,5,6,7], however, they were obtained from primary animal cells and, in few cases, from primary human cells. The possibility of developing direct organogenesis-on-chip from human pluripotent stem cells (hPSCs) could overcome the limited availability of human primary cells, such as human hepatocytes or cardiomyocytes. Human embryonic stem cells (hESCs) and induced pluripotent stem cells (hiPSCs) grown in culture have the potential to give rise to any fetal and adult cell type, but they also show intrinsic and unexpected levels of emergent self-organization for generating

highly ordered structures and tissues[8,9,10], thus opening a wide perspective for multi-organ generation on a chip.

Organogenesis and tissue generation are complex developmental processes starting from germ layer specification and phenotypic differentiation to tissue morphogenesis. Biomimetic scale down of this multi-stage developmental process could take advantage of the intrinsic properties of micro-technologies and microfluidics that allow accurate control of cell culture microenvironment, of temporal evolution of chemical gradients and of mechanical features, which support specific tissue differentiation[11,12,13]. Few studies reported on mouse embryonic stem cell cultures using microfluidic systems and highlight the importance of accurate soluble microenvironment regulation to maintain pluripotency and self-renewal[14,15,16]. We reported for the first time on hESCs culture on a chip[17] and few other works dealt with hESCs modulating flow perfusion, mainly for maintaining pluripotency[18,19]. Integrated functional hPSC differentiation on a chip, which certainly requires step-by-step control of hPSCs programming for resembling early stages of organogenesis, has not yet been developed.

Here, we explored whether we can control stem cell expansion, selective germ layer commitment and derive functional tissue-specific cells on a chip from both hESCs and hiPSCs through a multi-stage microfluidic-based technology. The different developmental stages required cell niche specification in terms of accurate balance between extrinsic and intrinsic cell signaling, through optimal in vitro delivery of exogenous factors and removal of endogenous cell-secreted factors. Continuous microfluidic flow perfusion has been recently shown to generate soluble factor spatial gradients along the microfluidic channel that lead to heterogeneous cell phenotype. Here, we showed that a discontinuous periodic medium delivery with stage-dependent frequency (number of cycles of medium change per day) is an effective strategy for modulating stem cell niche specification *in vitro*.

Identification of the essential role of extrinsic autocrine-paracrine factors in pluripotency and self-renewal and germ layer commitment[20], suggests a synergic mechanism of specific exogenous and endogenous factors in promoting transcriptional activity of pluripotency genes (**Fig. 1a**). The computational investigations on extrinsic signaling model (**Supplementary Methods** for model details) revealed that frequency of periodic medium delivery strongly affects accumulation of exogenous and endogenous factors, thus regulating transcriptional activity of target genes. A frequency increase reduces the amplitude of temporal fluctuations of both exogenous and endogenous factors (**Fig. 1b**), thus maintaining sustained transcriptional activity of the associated target genes. However, higher frequencies of medium change produce decreased expression of gene transcript, due to continuous endogenous secreted factors wash-out. This simple schematic modeling reveals high correlation between frequency of medium change and extrinsic signaling regulation.

First, we investigated the best condition for both hESC and hiPSC expansion in microfluidic channels to maintain high stemness and homogeneous morphology among colonies at different regions along the channels. HPSCs were injected into multiple microfluidic platforms, each containing 8 independent channels and connected to a multi-port syringe pump (**Fig. 1c**), were cultured with different frequencies up to 6 days (**Fig. 1d**). Immunofluorescence staining revealed that both hESCs and hiPSCs (ADHF#1) homogeneously express pluripotency markers such as Oct-4, Sox2, Tra-1-60 and Tra-1-81 (**Fig. 1e**). We optimized the hESC microfluidic culture to maintain high pluripotency in the channels, comparable to standard static conditions. The qRT-PCR analysis of pluripotency marker Oct-4 after 6 days of culture, showed an optimal frequency of f=2d^{-1} (**Fig. 1f**). Significant three-fold higher expression compared to lower (f=1d^{-1}) and higher frequencies (f=4d^{-1} and f=8d^{-1}) was observed. These results are consistent with the initial hypothesis that an appropriate balance of exogenous molecules and endogenous cell-secreted factors has to be provided. The presented data show a crucial effect of medium change frequency on hPSCs pluripotency maintenance and homogeneity in microfluidics, to allow proper factor supply, while avoiding up/downstream effects throughout the channels (**Supplementary Fig. S1**).

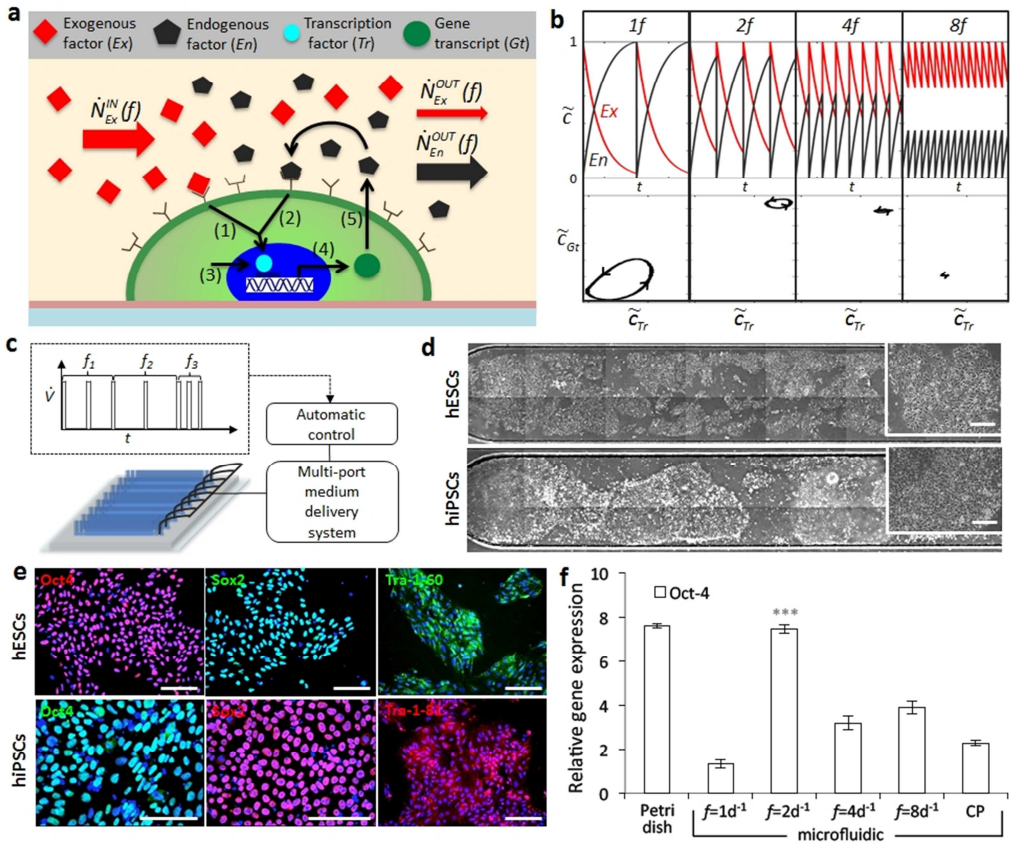

Figure 1 *| Pluripotent stem cell culture on-a-chip. (**a**) Pluripotency signaling model in microfluidic stem cell culture. Both exogenous (Ex) and endogenous (En) factors contribute to transcriptional activity of pluripotency genes through activation of target transcription factors (Tr). (**b**) Signaling model output. Temporal profiles of normalized Ex and En factor concentrations in the microfluidic channel at increasing frequencies (up). Gene transcript (Gt) concentration profile plotted versus corresponding Transcription factor (Tr) variation during a single medium perfusion at increasing frequencies. (**c**) Experimental set-up. Periodic medium delivery in microfluidic channels (200 μm high, 1.5 mm width, 1.8 mm length and 6 μL volume) is controlled through a multi-port delivery system. Different frequencies sequences are automatically programmed through Labview software. (**d**) Microfluidic hPSCs culture. Half channel views showing hESCs and hiPSCs expanded for 6 days in microfluidic conditions with f=2d^{-1}. Insets show typical morphology of stem cells colonies. Scale bar 50 μm. (**e**) Immunofluorescence analysis of pluripotency markers Oct-4, Sox2, Tra-1-60 and Tra-1-81 for hESCs and hiPSCs after 6 days in microfluidic channels. (**f**) Frequency-dependent Oct4 expression. QRT-PCR analysis of pluripotency marker Oct-4 expression of hESCs at different frequencies, f, compared to standard static culture control and continuous perfusion (CP). Student's t-test p-value ***P≤0.001. Data are shown as mean ± s.d. (n=3).*

We next investigated whether the frequency of periodic perfusion could be used for directing early germ layer commitment according to extrinsic endogenous and exogenous factors concentration (as schematized in **Fig. 2a**). HESCs were expanded for 3 days and differentiated for 4 days at different frequencies in spontaneous differentiating conditions (**Supplementary Methods**). Expression levels of early germ layers markers were analyzed through qRT-PCR analysis of β-III tubulin (ectoderm), brachyury T (mesoderm) and alpha-fetoprotein (endoderm). Under these conditions, the static culture showed ectoderm and mesoderm expression but not endoderm. On the other hand, frequency-dependent germ layer enrichment was observed in microfluidic culture (**Fig. 2a**). Ectoderm resulted highly expressed at lower frequencies (f=1d^{-1} and f=2d^{-1}) and it is completely down regulated at higher frequency (f=8d^{-1}) whereas mesoderm and endoderm expression are enhanced at higher frequency (f=8d^{-1}). Interestingly, pluripotency

markers are down regulated as the frequency increases. Gene expression is associated with cell morphology changes. These experimental observations are consistent with the hypothesis that ectoderm differentiation requires high accumulation of extrinsic endogenous factors[14,20], whereas strong endoderm enrichment is only possible with specific exogenous factor delivery. All together, these results suggest that periodic perfusion frequency is an additional player in directing early germ layer commitment.

To verify whether an efficient and selective induction of the three germ layers could be achieved, hESCs were induced to ectoderm, mesoderm and endoderm by specific differentiation media and with *ad hoc* frequency (**Fig. 2b**). Particularly, according to previous results, f=1d^{-1} was used for ectoderm specification whereas f=2d^{-1} and f=3d^{-1} for mesoderm and endoderm, respectively. Selective germ layer commitment was successfully obtained as reported by qRT-PCR analysis, which showed high expression of specific germ layer genes for each differentiation protocol. All other non-specific germ layer genes are strongly down regulated. Interestingly, endoderm has significantly higher expression in microfluidic conditions compared to conventional differentiation in Petri dish. It seems that microfluidic environment effectively washed out the endogenous factors that inhibit endoderm differentiation, and efficiently delivered the exogenous pro-endoderm factors. Immunofluorescence analyses (**Fig. 2c**) confirmed that highly selective commitment for all germ layers, with extremely low contamination from the others, is achievable also at the protein level in each specific differentiation protocol.

Next, we examined if perfusion frequency can be further adjusted for optimizing germ layer microfluidic induction when specific differentiation protocols are used. As proof of concept, results in **Fig. 2d** showed how selective induction of mesoderm was achieved by adjusting frequency of periodic perfusion. In particular, we found a 3 fold higher brachyury T expression at f=2d^{-1} and 3d^{-1}, compared to f=1d^{-1} and almost null expression at f=12d^{-1}.

Collectively, our findings indicate that the frequency of periodic perfusion is an additional parameter to enhance robustness and efficiency of early germ layer specification, even when specific protocols are adopted. In particular, we found major advantages for endoderm differentiation, because it requires large quantities of exogenous molecules (e.g. activin A) and washing out of endogenous inhibiting factors. On the other hand, mesoderm differentiation seems to require a proper balance between exogenous and endogenous molecules that can be achieved by frequency optimization, although dependent on cell culture density and media composition. Ectoderm commitment is mainly driven by endogenous stimulations and microfluidic differentiation can reproduce the results obtained with conventional cell culture methods. From technological point of view, small-scale microfluidic volume leads to extremely reduced medium consumption (few microliter per day per channel) and rapid and accurate perturbation of medium composition that is an important prerequisite for multi-stage differentiation process.

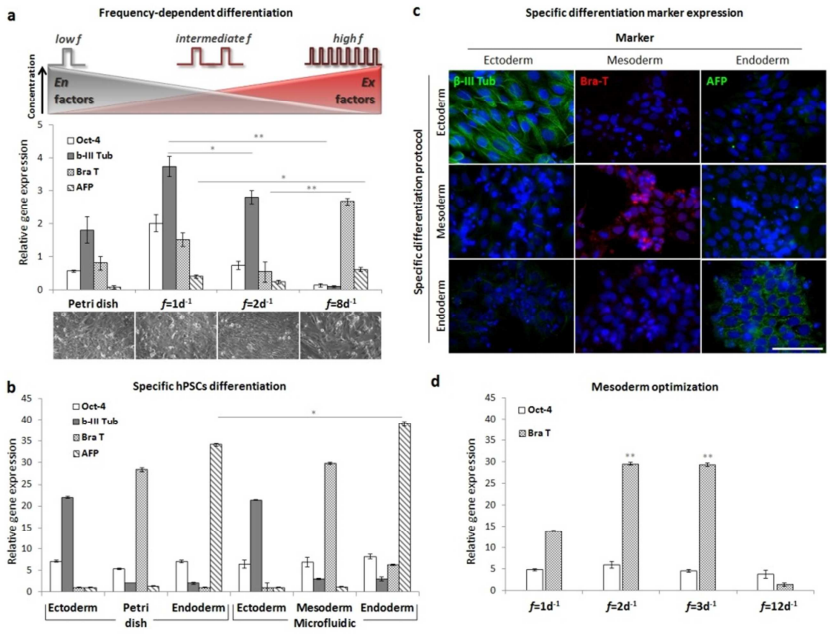

Figure 2 *| Early germ layer induction of hESC on-a-chip. (**a**) Frequency-dependent differentiation. Schematic of frequency, f, relation to En and Ex factors balance (up). The qRT-PCR analysis (gene expression normalized on glyceraldehyde 3-phosphate dehydrogenase) of Oct-4, β-III tubulin, brachyury T and alpha-fetoprotein in hESC spontaneous differentiation on chip, under different f. Cell morphology in phase contrast for each differentiation condition. Scale bar 50 µm. Data are shown as mean ± s.d. (n=3). (**b**) Early germ layer induction with specific media. The qRT-PCR analysis of Oct-4, β-III tubulin, brachyury T and AFP, and comparison between standard static control and microfluidic differentiation. Data are shown as mean ± s.d. (n=3). (**c**) Specific differentiation marker expression. Differentiation protocols applied on hESC line cultured on matrigel-coated channels. Immunofluorescence analysis of each differentiation protocol, with high expression of β-III tubulin in ectoderm, brachyury T in mesoderm and AFP in endoderm. Scale bar 50 µm. (**d**) Mesoderm optimization. The qRT-PCR analysis of Oct-4 and brachyury T expression in different frequencies of medium change for germ layer commitment optimization. brachyury T expression is comparable between $f=3d^{-1}$ and $f=2d^{-1}$, while there is a significantly lower expression at high and low frequencies. Student's t-test p-values *P≤0.05 **P≤0.01. Data are shown as mean ± s.d. (n=3).*

Therefore, we then demonstrated whether functional tissue-specific cell generation on chip can be achieved. We focused on cardiac and hepatic cells that are derived from mesoderm and endoderm germ layers, respectively, are extremely relevant for organ-on-a-chip applications. Cell differentiation was achieved by combining *ad hoc* hPSCs differentiation stages, germ layer specification and mature differentiation with proper frequencies of periodic perfusion and chemical regulation of soluble microenvironment. Cardiac and hepatic cell differentiation protocols are described in **Supplementary Methods**.

We first showed how cardiac cells on chip were derived after 15 days of frequency-dependent multi-stage differentiation protocol (**Fig. 3a**), consisting on mesoderm induction (by Wnt induction), early cardiac commitment (by Wnt inhibition) and functional cardiac maturation (by pro-cardiac factors supply). Typically 5 to 10 thousands cells per channel were obtained. We robustly achieved spontaneous contractile activity from both hES (HES2) and hiPS (ADHF#1)-derived cardiomyocytes (**Supplementary Videos1** and **2**, respectively), 60% of cardiac troponin-T positive cells showing defined cardiac sarcomeric organization (**Fig. 3b**). HPSC-derived cardiomyocytes show spontaneous calcium transients and excitation contraction coupling. In the line scan magnification in **Fig. 3c** both calcium transients and spark-like spontaneous activity are presented. Analyzing calcium handling of hPSC-cardiomyocytes in microchannels, we observed cardiomyocyte functional response to 0,5 µM Verapamil with reduced calcium release after L-

type channel inhibition, and response to 10 mM caffeine with cytosolic calcium increase after ryanodine channel activation (**Fig. 3d**). We successfully showed that it is possible to generate functional cardiac cells on chip and to directly perform dynamic biochemical stimulations taking advantage of the microfluidic environment, which allows robust, accurate, fast, and cost-effective spatio-temporal control of cell microenvironment[11].

We next applied our methodology to derive hepatocyte on chip consistently with the previously endoderm-optimized conditions, which showed higher efficiency in endoderm differentiation than conventional cell culture. Hepatic cells were obtained from both hESCs and hiPSCs by early endoderm commitment, definitive endoderm specification and hepatocyte-like cell maturation steps, driven by specific periodic medium delivery (**Fig. 3e**). In order to prove the robustness of our method, in addition to hESCS (HES2) and retrovirus-derived hiPSCs (ADHF#1), we generated 3 different hiPSC lines by non-integrating methods: Sendai viruses (Send#8) and modified mRNAs (mRNA#2, mRNA#5).

Characteristic polygonal-shaped hepatocyte-like cells are obtained, with presence of bi-nucleate cells at the late stage, showing high expression of the specific hepatic markers albumin and cytochrome P450 3A (**Fig. 3e-f**). Similar results were obtained for all other 4 different hiPSCs lines (Supplementary Fig. S4). Quantification of immunofluorescence of late stage albumin and CYP-3A in hESCs shows higher expression in microfluidic differentiated cells compared to differentiation control on Petri dish (**Fig. 3g** and **Supplementary Fig. S3b**). The hepatic cells show functional activity by high glycogen storage capacity (75% of total cells) and indocyanine green uptake and clearance (**Fig. 3h**), which is extremely relevant for hepatic drug metabolism studies. As expected from prior results, compared to static conditions, we obtained a shortening of the time required for differentiation (from 16d to 14d) and 40% greater albumin secretion rate on the last day of maturation (**Fig. 3i**). An albumin production rate comparable with hESCs-derived hepatocytes was obtained with different hiPSCs lines (ADHF#1, Send#8, mRNA#2 and mRNA#5), confirming the robustness of the method (**Fig. 3j**). The microfluidic environment together with optimized periodic perfusion frequency provides an effective methodology for generating hepatic-like tissues on a chip with remarkable functional differentiation also compared to conventional cell culture methods.

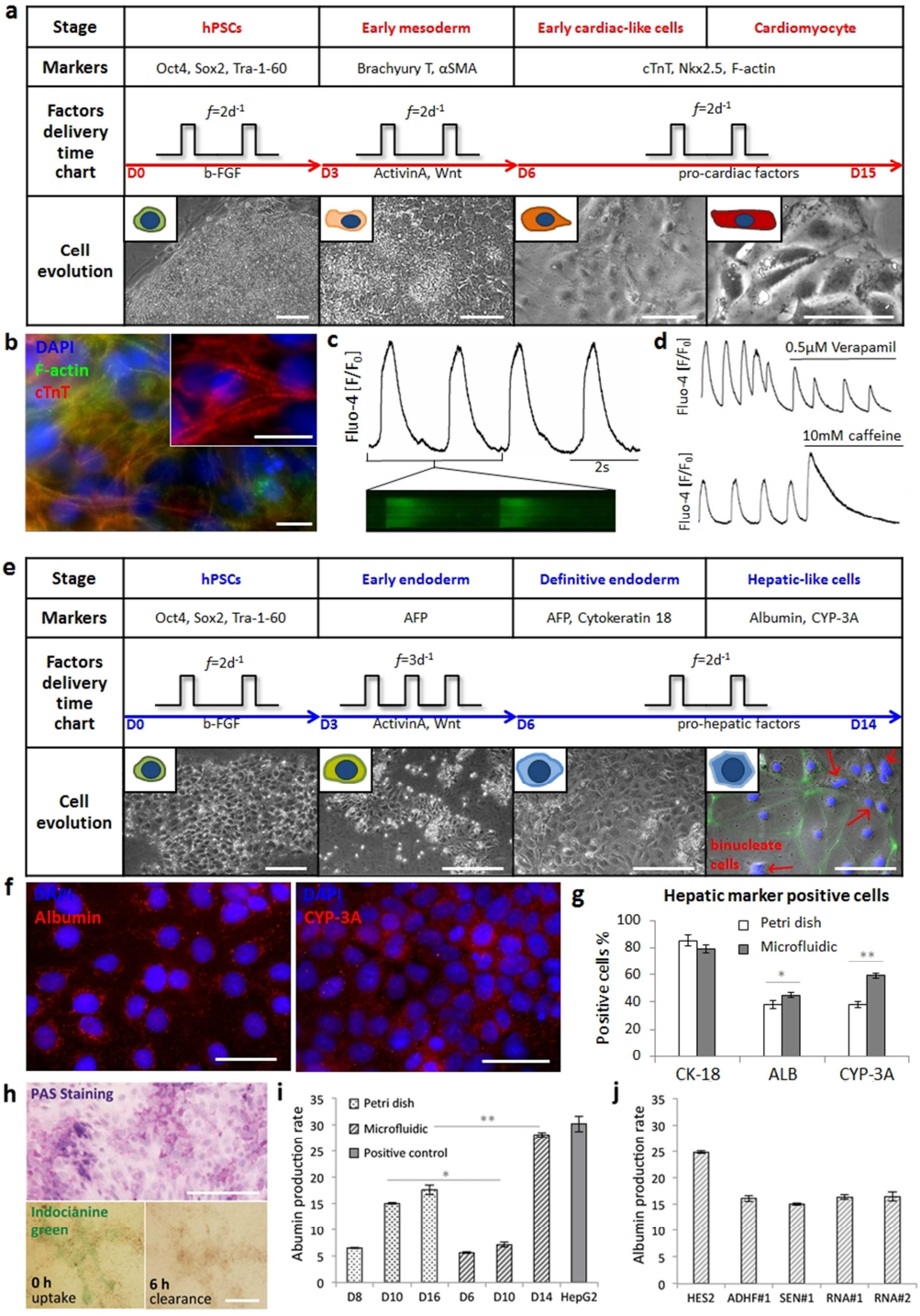

Figure 3 *| Cardiac and hepatic functional differentiation on-a-chip from both hESCs and hiPSCs. (**a**) Microfluidic cardiomyocyte differentiation protocol and morphology changes from pluripotent state to differentiated cell type. Scale bars 200 μm. (**b**) Immunofluorescence of hES-derived CM showing f-actin and cardiac troponin-t organization. Scale bars 20 μm (**c**) Microfluidic calcium dynamics. Spontaneous calcium transients in hPSC-cardiomyocytes recorded with Fluo-4 indicator. (**d**) Functional cardiomyocytes response to 0,5 μM verapamil with reduction in calcium release, and to 10 mM caffeine with increase in cytosolic calcium. (**e**) Hepatic differentiation protocol and cell change in morphology up to hepatocyte-like cells. Red arrows indicate binucleate cells in late stages. Scale bars 200 μm. (**f**) Immunofluorescence stain for hepatocyte-like markers albumin and cytochrome P450 3A from hESCs. Scale bars 30 μm. (**g**) Quantification of immunofluorescence markers. Microfluidic hepatic cells show significant higher expression of ALB*

*and CYP-3A compared to static control. Data are shown as mean ± s.d. (n=10). (**h**) PAS staining of hepatic cells derived on chip; nuclei are stained in blue, pink-violet colored cells show glycogen storage. Indocyanine green staining of live hepatic cells; colorant is absorbed and metabolized in 6 h by functional hepatocyte-like cells. (**i**) ELISA albumin secretion quantification. Microfluidic-derived hepatocyte-like cells secrete 40% more albumin compared to static control at the last day of differentiation. Student's t-test p-values *P≤0.05 **P≤0.01. Data are shown as mean ± s.d. (n=3). (**j**) Comparison of Albumin production at Day 14 for different hiPSCs derived cell lines differentiated into hepatocytes-like cells. Levels of albumin secretion comparable to HES2-hESC line-derived hepatocytes were obtained for hiPSCs lines ADHF#1, derived with retroviruses, Send#8, derived with Sendai viruses and mRNA#2-5, derived with mRNA technology (albumin production rate is expressed as ng/mL/day/2x10^5 cells).*

In conclusion, we derived functional tissue-specific cells on a chip through a robust multi-stage microfluidic technology, which allows accurate spatio-temporal control of cell soluble microenvironment through regulation of periodic-perfusion frequencies. Moreover, functionally differentiated cells derived in the microfluidic channels can be directly used for dynamic multi-parametric and large-scale drug screening or for developing micro-engineered human organ models. This technology opens a new perspective in generating organs-on-chips from hPSCs overcoming the issues related to the limited availability of human primary cell sources. This last aspect will require strong scientific and technological efforts for further mimicking the organogenesis *in vitro*.

References

1. *Huh, D., Torisawa, Y., Hamilton, G. A., Kim, H. J. & Ingber, D. E. Lab. Chip 12, 2156–2164 (2012).*
2. *Huh, D. et al. Sci. Transl. Med. 4, 159ra147–159ra147 (2012).*
3. *Ghaemmaghami, A. M., Hancock, M. J., Harrington, H., Kaji, H. & Khademhosseini, A. Drug Discov. Today 17, 173–181 (2012).*
4. *Huh, D. et al. Science 328, 1662–1668 (2010).*
5. *Lee, S.-A. et al. Lab. Chip (2013). doi:10.1039/C3LC50197C*
6. *Jang, K.-J. et al. Integr. Biol. Quant. Biosci. Nano Macro (2013). doi:10.1039/c3ib40049b*
7. *Grosberg, A., Alford, P. W., McCain, M. L. & Parker, K. K. Lab. Chip 11, 4165–4173 (2011).*
8. *Sasai, Y. Nature 493, 318–326 (2013).*
9. *Eiraku, M. et al. Nature 472, 51–56 (2011).*
10. *Eiraku, M. et al. Cell Stem Cell 3, 519–532 (2008).*
11. *Discher, D. E., Mooney, D. J. & Zandstra, P. W. Science 324, 1673–1677 (2009).*
12. *Dupont, S. et al. Nature 474, 179–183 (2011).*
13. *Wan, C., Chung, S. & Kamm, R. D. Ann. Biomed. Eng. 39, 1840–1847 (2011).*
14. *Przybyla, L. M. & Voldman, J. Proc. Natl. Acad. Sci. 109, 835–840 (2012).*
15. *Przybyla, L. & Voldman, J. Annu. Rev. Anal. Chem. Palo Alto Calif 5, 293–315 (2012).*
16. *Moledina, F. et al. Proc. Natl. Acad. Sci. 109, 3264–3269 (2012).*
17. *Figallo, E. et al. Lab. Chip 7, 710–719 (2007).*
18. *Korin, N., Bransky, A., Dinnar, U. & Levenberg, S. 64160N–64160N (2006). doi:10.1117/12.695558*
19. *Villa-Diaz, L. G. et al. Lab. Chip 9, 1749 (2009).*

20. Giobbe, G. G. et al. Biotechnol. Bioeng. 109, 3119–3132 (2012).

Acknowledgments

This research was supported by Progetti di Eccellenza CARIPARO and Progetti di Eccellenza Giovani Ricercatori of Ministero della Salute. We acknowledge Miltenyi Biotech for kindly providing mmRNA reprogramming kit.

Author contributions

G.G.G., F.M. and N.E. designed the research; G.G.G. and F.M. performed the experiments; S.M. performed cardiac functional tests; S.G. helped in microfluidic platform set-up and microfluidic cell culture; S.G. and C.L performed the reprograming experiments; A.F. supervised hepatic differentiation experiments; N.E. coordinated the project; G.G.G., F.M. and N.E. wrote the manuscript.

Supplementary figures

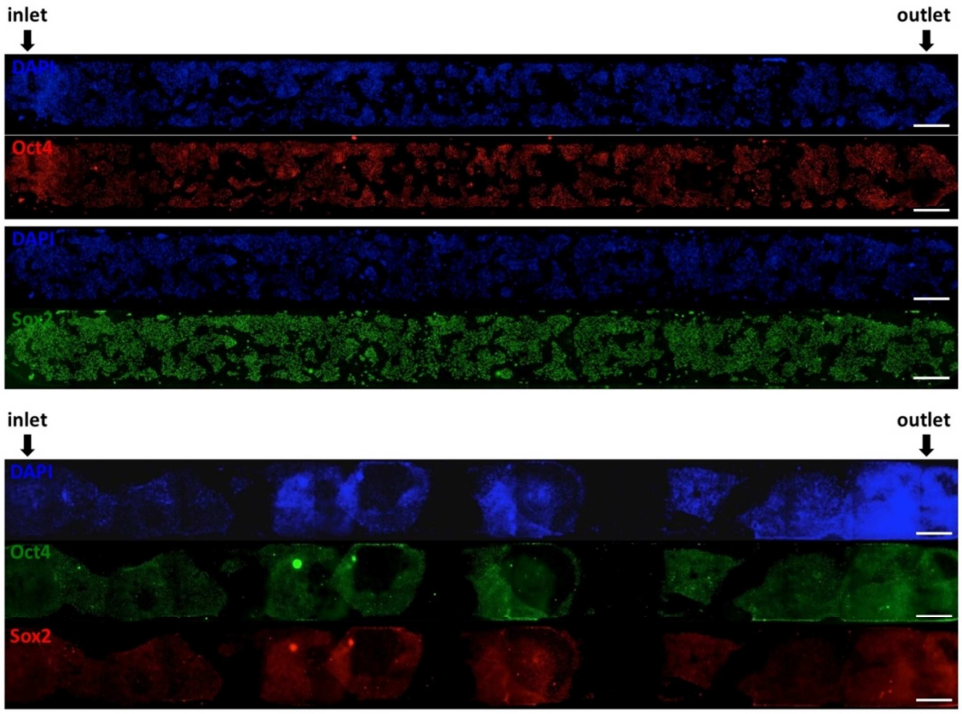

Supplementary Figure 1 | *Pluripotency marker expression in human pluripotent stem cells cultured in microchannels with f=2d^{-1}. (a) "HES2" hES cell line showing oct-4 and sox2 expression. (b) "ADHF#1" hiPS cell line showing oct-4 and sox2 expression. High homogeneity in expression is shown along the microchannels with no upstream and downstream effects.*

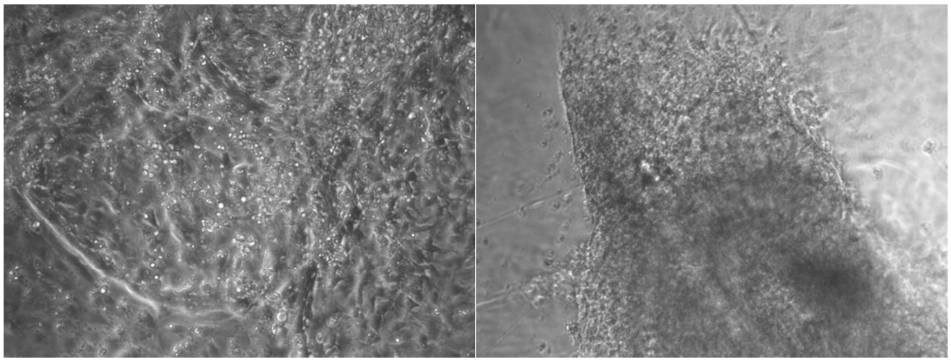

Supplementary Video 2 *| Cardiac monolayer differentiation on chip of hPSCs. (**a**) Beating cardiomyocytes derived from hESCs. (**b**) HiPSCs-derived beating cardiomyocytes in microchannels.*

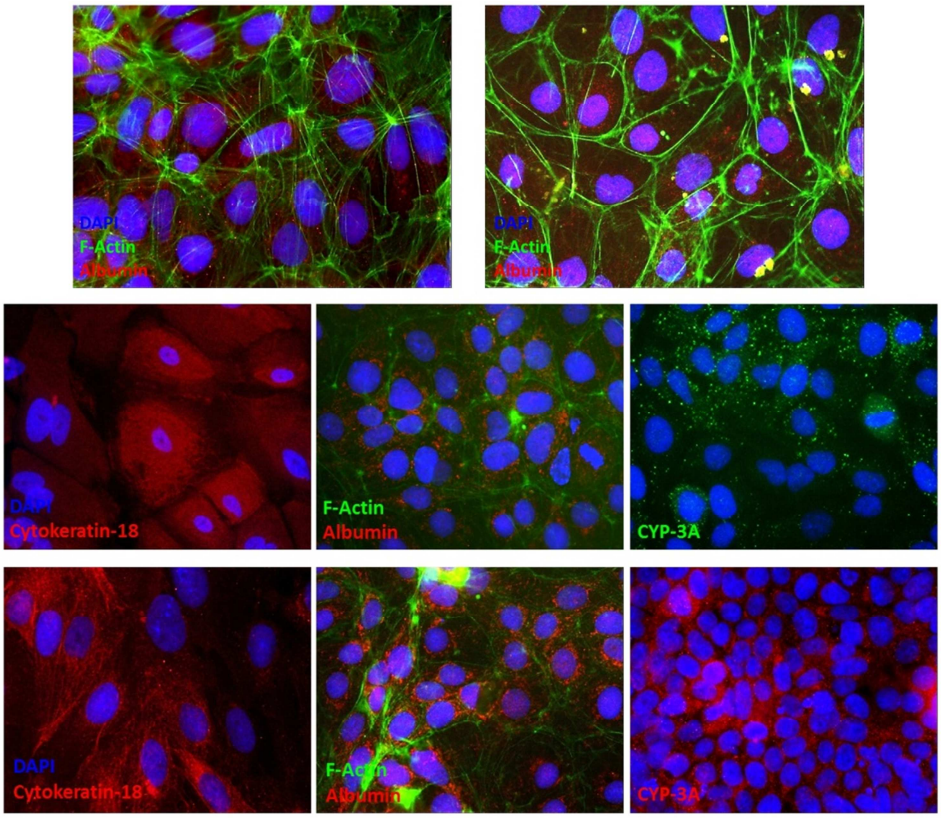

Supplementary Figure 3 | *(**a-b**) HES and hiPSC-derived hepatocyte-like cells. Cells from both cell lines show comparable differentiation into polygonal hepatocyte-like cells with similar albumin secretion. (**c-d**) Comparison between standard static (**c**) and microfluidic (**d**) hepatic differentiation of hPSC. Cells show similar expression of CK-18 hepatic endoderm marker. Microfluidic hepatocyte-like cells show higher expression of albumin and Cyp-3A compared to standard static differentiated cells.*

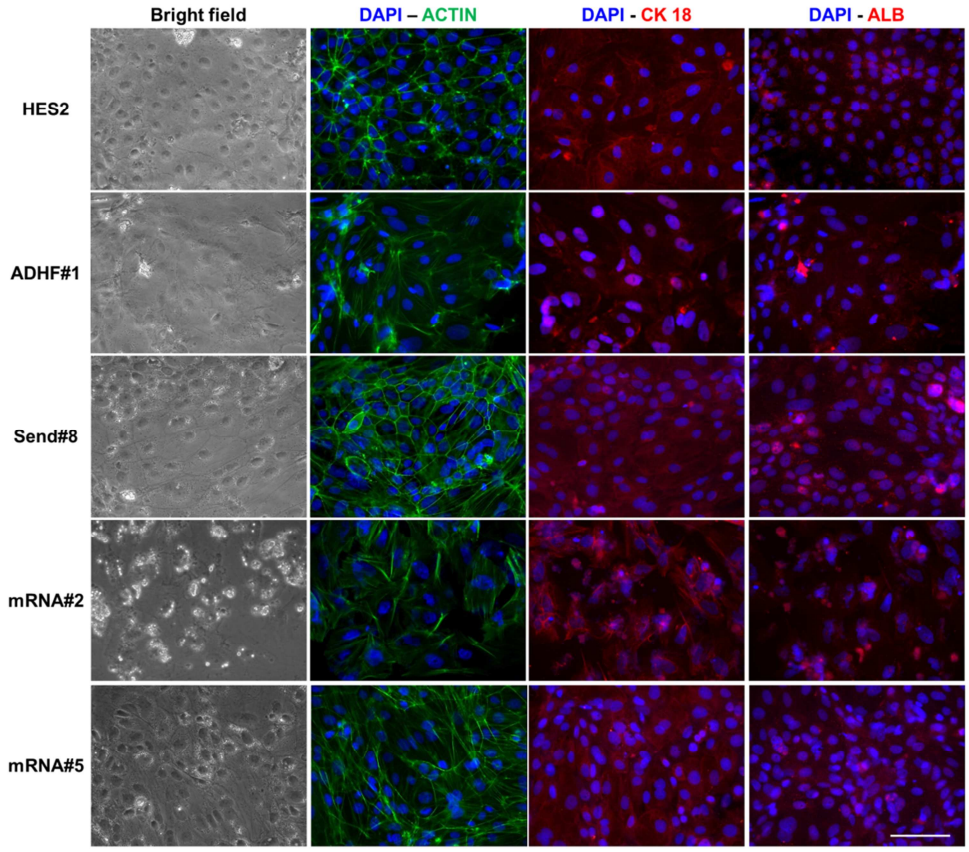

Supplementary Figure 4 | *Multiple pluripotent cell lines differentiated into hepatocyte-like cells. Human embryonic stem cell line HES2. Human induced pluripotent stem cell line ADHF#1 retrovirus-derived. HiPSC line Send#8 Sendai virus-derived. HiPSC lines mRNA#2 and mRNA#5 mRNA-derived. Panel show cells in bright field and F-actin for cell morphology and polygonal-epithelial shape structure. Hepatocyte-like cells derived from each line have been marked for Cytokeratin 18, marking late hepatic endoderm epithelium. All cell have been marked also for Albumin, marking hepatocyte-like cell producing human albumin.*

Supplementary methods

Computational Model

Mathematical model of signaling pathway describing gene transcriptional activity promoted by synergic positive effect of extrinsic exogenous and endogenous factors is shown in **Fig. 1a**. The model takes into account only relevant phenomena to highlight the effect of dynamic changes in extrinsic factors modulated by medium delivery frequency, *f*, on a hypothetic transcriptional activity. Black arrows in **Fig. 1a** indicate chemical reactions involved in the pathway. In particular, reactions (1) and (2) describe the coupling of exogenous, *Ex*, and endogenous, *En*, factors to specific membrane receptors, which promotes the activation of transcriptional factor, *Tr*. In addition, *Tr* is activated at a basal level through reaction (3) and induces expression of pluripotency-associated genes through reaction (4). Gene transcripts, *Gt*, in turn, produce newly *En*, as indicated by reaction (5). The model consists of four ordinary differential equations describing dynamic mass balance equation for the involved species *Ex*, *En*, *Tr* and *Gt*:

$$\begin{cases} \dfrac{d\tilde{c}_{Ex}}{dt} = \dot{N}_{Ex}^{IN} - \dot{N}_{Ex}^{OUT} - V_1 \\ \dfrac{d\tilde{c}_{En}}{dt} = -\dot{N}_{En}^{OUT} - V_2 + V_5 \\ \dfrac{d\tilde{c}_{Tf}}{dt} = V_1 V_2 + V_3 \\ \dfrac{d\tilde{c}_{Gt}}{dt} = V_4 - V_5 \end{cases} \quad (1)$$

c are concentrations of species involved in the pathway (*Ex*, *En*, *Tr* and *Gt)*; ~ symbol indicates adimensional concentration normalized for the initial concentration value c^0. *N* is the molar flux, given from the product between the medium flow rate and the concentration of each species, at the inlet and outlet of the microfluidic channel. Exogenous inlet flux is constant, as exogenous factors are continuously supplied with medium, whereas outlet fluxes are time-dependent. All chemical reaction rates are assumed first order kinetics as follows:

$$V_1 = k_1 \tilde{c}_{Ex}$$
$$V_2 = k_2 \tilde{c}_{En}$$
$$V_3 = k_3$$
(2)
$$V_4 = k_4 \tilde{c}_{Tf}$$
$$V_5 = k_5 \tilde{c}_{Gt},$$

where k_i are constant of reaction with arbitrary value and dimension [t^{-1}].

As an intermittent flow perfusion for medium delivery will be used, system of equations (1) can be solved throughout an interval time equivalent to the reciprocal of the frequency, 1/*f*, and for a defined number of cycles, N_{tot}. Consequently, null inlet and outlet fluxes and opportune initial periodic conditions were set. Time for medium change in the microfluidic channel was assumed negligible and periodic concentration values of *Ex* and *En* were set equal to 1 and 0 respectively after every time period (1/*f*). The system was solved for different values of *f* with periodic initial conditions written as follows:

$$\begin{cases} \dfrac{d\tilde{c}_{Ex}}{dt} = -k_1 \tilde{c}_{Ex} & \tilde{c}_{Ex}(t = \dfrac{i}{f}) = 1 \\ \dfrac{d\tilde{c}_{En}}{dt} = -k_2 \tilde{c}_{En} + k_5 \tilde{c}_{Gt} & \tilde{c}_{En}(t = \dfrac{i}{f}) = 0 \\ \dfrac{d\tilde{c}_{Tf}}{dt} = k_1 k_2 \tilde{c}_{Ex} \tilde{c}_{En} + k_3 & \tilde{c}_{Tf}(t = 0) = 0.1 \\ \dfrac{d\tilde{c}_{Gt}}{dt} = k_4 \tilde{c}_{Tf} - k_5 \tilde{c}_{Gt} & \tilde{c}_{Gt}(t = 0) = 0.1 \\ & i = 0, 1, \ldots, N \end{cases} \quad (3)$$

System of ordinary equations (3) was computationally solved with MATLAB, by using *ode15s function*. Constant rates k_1, k_2, k_4 and k_5 were arbitrarily set equal to 1, whereas k_3 was taken equal to 0.1. N_{tot} was chosen in order to achieve a pseudo-stationary of all species concentrations.

Microfluidic device micro-fabrication and protein functionalization

The microfluidic chip was fabricated by standard soft-lithographic techniques[1]. The master was photo-lithographically patterned by using SU8-2100 negative photoresist (MicroChem, Newton, MA) to obtain a final thickness of 200 micron, according to manufacturer's indications. A premixed 10:1 ratio of polydimethylsiloxane, PDMS, pre-polymer and curing agent solution (Sylgard 184 kit; Dow Corning, Midland, MI) was casted on the silicon wafer and cured at 70 C° for 2 h. The PDMS mold was cut, peeled off, and punched with a 21G stainless steel needle (Small Part Inc., Logansport, IN) to obtain inlet/outlet holes. The PDMS mold was assembled and sealed to a 50×75 mm cleaned glass slide by plasma bonding. Eight independent medium reservoirs

(3mm diameter and 4mm height for about 30microL volume), one for each channel, were obtained by sealing an additional PDMS block to the top of the device by plasma bonding. The assembled device was cleaned with isopropanol (Sigma-Aldrich, St. Louis, MO) and sterilized in an autoclave.
Microfluidic channels were filled with Matrigel Reduced Factor, MRF (BD) diluted in IMDM (Invitrogen) to a final concentration of 20% and incubated overnight at 4°C. Coating solution was aspirated and microfluidic device was incubated at 37°C and 5% CO_2 atmosphere for 1 h.

Sendai viruses-mediated hiPSCs generation

Human fibroblasts derived from skin-biopsy were plated and cultured in a 24-well plate and cultured to 70% confluence in fibroblast medium (DMEM supplemented with 10% FBS). CytoTune iPS Sendai Reprogramming Kit (Invitrogen) based on replication incompetent Sendai virus was used to deliver the four transcription factors Oct4, Sox2, Klf4 and c-Myc and induce reprogramming to iPSc, according to manufacturer instructions. After 24h transduction, cells were fed every other day for 7 days. Transduced cells were then transferred onto inactivated MEF feeder cells at a density of 1 x 10^4 cells on a 6-well plate and expanded as reported below.

Human induced pluripotent stem cell generation by modified mRNA

Human iPS reprogramming using modified mRNA (mmRNA) was performed following the protocol in Warren et al (2010)[2]. Briefly, inactivated human newborn foreskin fibroblast feeders (NuFF-RQ, AMS Biotechnology) were seeded in 6-well tissue culture plates, coated with gelatin 0.2%, at a density of 260 cell/mm^2, and cultured in Dulbecco's modified Eagle medium (DMEM, Life Tecnologies) supplemented with 10% fetal bovine serum (FBS, Life Tecnologies). Cells were always incubated at 37°C and 5% CO_2. After 24 h, human foreskin BJ fibroblasts (Miltenyi Biotec) were seeded at 10 cell/mm^2 and cultured in Eagle's minimal essential medium (EMEM, Life Tecnologies) with 10% FBS. After another 24 h, medium was switched to Pluriton reprogramming medium (Miltenyi Biotec) supplemented with B18R interferon inhibitor (Prodotti Gianni) at a final concentration of 200 ng/mL, and transfections using mmRNA (Miltenyi Biotec) were started and repeated for 18 days, 4 hours prior to daily medium changes. The transfection mix was prepared pooling two solutions: the first obtained diluting 5X 100 ng/µL mmRNA of Oct4, Sox2, Klf4, c-Myc, Nanog, Lin28, and nuclear GFP in OptiMEM (Life Technologies), and the second diluting 10X lipofectamine RNAiMAX (Life Technologies) in Opti-MEM. After mixing, the final solution was incubated for 15 min and then added to the culture medium. At day 6 after the first transfection, Pluriton reprogramming medium was replaced with B18R-supplemented NuFF-conditioned Pluriton medium, which was produced culturing in parallel NuFF cells in T75 flasks with Pluriton medium supplemented with bFGF (Peprotech) at 4 ng/mL. Two days after the last transfection, iPS colonies were picked and passaged to MEF-coated 12-well plates and expanded as reported below.

Human pluripotent stem cell expansion and microfluidic culture

HiPSCs (cell line ADHF#1, obtained from Center for iPS Cell Research and Application, iCeMS, Kyoto University; cell line Send#8, generated with Sendai viruses; cell lines mRNA#2 and mRNA#5, generated with mmRNA technology) and hESCs (cell line HES2, from National Stem Cell Bank, Madison, WI) were cultured in gelatin-coated multiwells with mitomycin C-treated mouse embryonic fibroblasts (MEF; Chemicon) co-culture, in expansion medium DMEM F-12 (Invitrogen), 20% KO serum (Invitrogen), 10% MEF conditioned medium (not used for hiPSCs), 20 ng/mL basic fibroblast growth factor for hESCs, 10 ng/mL for hiPSCs (b-FGF; Invitrogen), 0.1 mM β-mercaptoethanol (Invitrogen), 1% non-essential amino acid (Invitrogen) and 1% Pen/Strep (Invitrogen). HPSCs were passaged to new feeder using CTK solution (trypsin 0.25% - collagenase IV - Ca^{2+}) for hiPSCs and trypsin 0.25% for hESCs (Invitrogen). For MEFs depletion and cell expansion and differentiation, cells were passaged on matrigel-coated microchannels.
The hPSC suspension was injected into each channel and the microfluidic chip was incubated overnight at 37°C and 5% CO_2 atmosphere without perfusion, to allow cell adhesion to substrate.

We used proper cell seeding concentration to achieve 70% confluence cell culture at 24 h after seeding.
A 9-port pump (Cavro® XR Rocket pump, TECAN, San Jose, CA) was used to independently deliver the medium from the reservoirs into each microfluidic channels. 0.5 ID Tygon tubings (Cole-Parmer, Vernon Hills, IL) and 21G stainless-steel needles with a polypropylene luer (Microtest, Taipei, Taiwan) were used to connect the microfluidic chip to the pump. Discontinuous medium delivery with defined temporal frequencies was achieved by automatically controlling the multi-channel syringe pump through LabView 8.2 (National Instruments, Austin, TX). For pluripotency maintenance, hPSCs were cultured with a 2-cycles/day expansion medium change.
A minimum of 3 independent microfluidic channles were used for each experimental conditions.

HPSCs early germ layer microfluidic differentiation

For spontaneous differentiation, no exogenous factors and cytokines were used, and the basal medium is composed of KnockOut DMEM, FBS 20%, NEAA 1%, L-glutamine 0,5% and P/S 1% (all from Invitrogen). Ectoderm differentiation was induced with DMEM F-12 and Neurobasal medium (both from Invitrogen), 1:1 ratio, supplemented with B27 1% (Invitrogen), N2 1% (Invitrogen) and β-met 0.1 mM[3,4]. Mesoderm differentiation was induced with StemPro-34 (Invitrogen) supplemented with 2 mM L-glutamine (Invitrogen), transferrin 200 ng/mL, 0.5 mM ascorbic acid (Sigma), activin A 0.3 ng/mL (R&D), BMP-4 3 ng/mL (R&D)[5]. Endoderm differentiation was induced with RPMI1640 containing 1X B27 (both from Invitrogen), 1mM sodium butyrate (Sigma), 100 ng/ml activinA (Peprotech) and 50 ng/mL Wnt3a (R&D)[6] for the first 2 days. The second endoderm medium was KO DMEM with KO serum 20%, L-glutamine 1 mM, NEAA 1%, DMSO 1%, β-met 0.1 mM, P/S 1% for other 2 days. HPSCs specification was induced for 4 days in all three germ layers. A minimum of 3 independent microfluidic channles were used for each experimental conditions.

Microfluidic cell maturation

For cardiac differentiation cells were cultured with in RPMI/B27-insulin. After 24 h, the medium was changed to RPMI/B27-insulin supplemented with 5 ng/mL BMP4 (R&D) for another 4 days. At day 5, the medium was changed to RPMI/B27-insulin. At day 7 the cells were transferred to RPMI/B27[7].
For hepatic differentiation cells were treated with 100 ng/ml activin A and 0.5mM NaB for 3 days in RPMI/B27. Medium was changed to KO-DMEM, 20%SR (both from Invitrogen), 1 mML-glutamine, 1% NEAA, 0.1 mMβ-met, 1% DMSO (Sigma) for 6 days. Hepatic-like cells were maturated with L15 medium (Sigma) supplemented with 8.3% FBS, 8.3% tryptose phosphate broth, 10 μM hydrocortisone 21-hemisuccinate, 1 μM insulin (all from Sigma) and 2 mML-glutamine containing 10 ng/ml hepatocyte growth factor and 20 ng/ml oncostatin M (both from R&D) for 6 days[8]. For adult specification and maturation, cells were cultured with f=2d^{-1} maturation medium change.
The functional differentation of cardiac and hepatic cells were performed in 30 and 50 independent microfluidic experiments, respectively.

Functional tests

For cardiac functional tests, cardiomyocytes were analyzed at confocal microscopy (Leica SP5) for calcium transient, and caffeine and verapamil treatments[9].
For hepatic functional tests, hepatocyte-like cells were stained with PAS staining (Sigma) according to manufacturer's instructions, for glycogen storage revelation. Indocyanine green test (ICG from Sigma) was performed on living tissue on chip by incubating living tissue for 15 min with dye solution. Green cells retaining ICG were photographed. After 6 hours, same fields were photographed in order to see complete clearance of ICG by functional hepatocyte-like cells. Albumin production and excretion was assessed by collection spent medium (10 μL from each micro-channel) and performing enzyme linked immunosorbent assay ELISA (Immunology

Consultants Laboratory, Inc.) following manufacturer's instructions. Secreted albumin levels were detected at 450 nm by using plate reader Ininite F2000 PRO (Tecan).

Immunofluorescence and qRT-PCR

Immunofluorescence analyses were performed on paraformaldehyde 4% fixed cells for 15 min. Blocking and permeabilization was performed with heat inactivated serum 5%, TritonX-100 (Sigma) 0.1% for 1h. Cells were stained using primary antibodies in blocking buffer 1 h room T, or overnight 4°C, depending on the antibody. Immunostaining was done with secondary antibodies Alexa Fluor 488, 594 (Invitrogen) and Hoechst nuclear staining incubation for 1 h at 37°C. Videos, bright fields and immunofluorescence images and merges were taken on Leica DMI 6000 B.
The qRT-PCR was performed with TaqMan gene expression assay probes (Invitrogen) according to manufactures instructions using GAPDH (glyceraldehyde 3-phosphate dehydrogenase), POU5F1 (oct4), TUBB3 (beta-III tubulin), AFP (alpha-fetoprotein), T (brachyury) probe sets (all from TaqMan Invitrogen). Reaction was done on ABI Prism 7000 machine and results were analyzed with ABI Prism 7000 SDS software. GAPDH expression was used to normalize values of gene expression, and data are shown as relative fold change.

Supplementary citations

1. *Luni, C., Michielin, F., Barzon, L., Calabrò, V. & Elvassore, N. Biophys. J. 104, 934–942 (2013).*
2. *Warren, L. et al. Cell Stem Cell. 7, 618 (2010).*
3. *Camnasio, S. et al. T Neurobiol. Dis. 46, 41–51 (2012).*
4. *Chambers, S. M. et al. Nat. Biotechnol. 27, 275–280 (2009).*
5. *Kouskoff, V., Lacaud, G., Schwantz, S., Fehling, H. J. & Keller, G. Proc. Natl. Acad. Sci. U. S. A. 102, 13170–13175 (2005).*
6. *Hay, D. C. et al. Proc. Natl. Acad. Sci. U. S. A. 105, 12301–12306 (2008).*
7. *Lian, X. et al. Proc. Natl. Acad. Sci. 109, E1848–E1857 (2012).*
8. *Hay, D. C. et al. Stem Cells Dayt. Ohio 26, 894–902 (2008).*
9. *Martewicz, S. et al. Integr. Biol. Quant. Biosci. Nano Macro 4, 153–164 (2012).*

APPENDIX C

COMPLETE RESTORATION OF MULTIPLE DYSTROPHIN ISOFORMS IN GENETICALLY CORRECTED DUCHENNE MUSCULAR DYSTROPHY PATIENT–DERIVED CARDIOMYOCYTES

Susi Zatti[1,2], Sebastian Martewicz[1,2], Elena Serena[1,2], Narumi Uno[3], Giovanni Giobbe[1,2], Yasuhiro Kazuki[3], Mitsuo Oshimura[3] and Nicola Elvassore[1,2]

[1]Department of Industrial Engineering, University of Padova, Padova, Italy;
[2]Venetian Institute of Molecular Medicine (VIMM), Padova, Italy;
[3]Department of Biomedical Science, Institute of Regenerative Medicine and Biofunction, Graduate School of Medical Science, Tottori University, Yonago, Japan.
Correspondence: N Elvassore (nicola.elvassore@unipd.it)

Received 14 August 2013; accepted 3 September 2013
Molecular Therapy — Methods & Clinical Development (2014)
xx, xx; doi:10.1038/mtm.2013.1; published online 08 January 2014
Article in press

Abstract

Duchenne muscular dystrophy (DMD)–associated cardiac diseases are emerging as a major cause of morbidity and mortality in DMD patients, and many therapies targeted to skeletal muscle failed to improve cardiac function. The reprogramming of patients' somatic cells into pluripotent stem cells, combined with technologies for correcting the genetic defect, possesses great potential for the development of new treatments for genetic diseases. In this study, we obtained human cardiomyocytes from DMD patient– derived, induced pluripotent stem cells genetically corrected with a human artificial chromosome carrying the whole dystrophin genomic sequence. Stimulation of cytokines was combined with cell culturing on hydrogel with physiological stiffness, allowing an adhesion-dependent maturation and a proper dystrophin expression. The obtained cardiomyocytes showed remarkable sarcomeric organization of cardiac troponin T and α-actinin, expressed cardiac-specific markers, and displayed electrically induced calcium transients lasting less than 1 second. We demonstrated that human artificial chromosome carrying the whole dystrophin genomic sequence is stably maintained throughout the cardiac differentiation process and that multiple promoters of the dystrophin gene are properly activated, driving expression of different isoforms. These dystrophic cardiomyocytes can be a valuable source for in vitro modeling of DMD-associated cardiac disease. Furthermore, the derivation of genetically corrected, patient-specific cardiomyocytes represents a step toward the development of innovative cell and gene therapy approaches for DMD.

Introduction

Duchenne muscular dystrophy (DMD) is one of the most common and severe inherited neuromuscular disorders, affecting 1 in 3,500 newborn males. DMD is caused by mutations in the dystrophin gene encoding a key structural protein of the dystrophin glycoprotein complex, which connects the contracting cytoskeletal machinery of skeletal and cardiac muscle fibers to the extracellular matrix scaffold.1 The absence of dystrophin in DMD patients causes a broad spectrum of physical consequences, eventually leading to a premature death.2 Approximately 20% of deaths are the result of cardiomyopathies and/or cardiac conduction abnormalities. The increased life span of patients affected by DMD allowed by the improvements in treatments of respiratory muscle disease made cardiomyopathies (present in ~90% of patients) emerge as a

major cause of morbidity and mortality.3 In addition, many experimental therapies have mainly focused on skeletal muscle, aiming at the restoration of dystrophin expression in myofibers, and have failed to improve cardiac function.4 Derivation of DMD patient–specific cardiomyocytes (CMs) and the correction of their genetic defect could provide a valuable cell source for in vitro modeling and for studying DMD-related cardiac dysfunctions, in addition to potentially representing a significant advancement toward an effective therapy for DMD-associated cardiomyopathies. The efficient reprogramming technology pioneered by Yamanaka and colleagues5 opened the perspective of deriving large numbers of disease-specific human cells in vitro. Human induced pluripotent stem (hiPS) cells are recently emerging as an ideal cell source for the generation of clinically relevant cardiac disease models.6 Several recent studies demonstrate how hiPS cell–derived CMs can be used for modeling the pathological phenotype of inherited cardiac disorders, such as the LEOPARD syndrome,7 type 1 and 2 long QT syndrome, 8–10 catecholaminergic polymorphic ventricular tachycardia, 11 arrhythmogenic right ventricular dysplasia/cardiomyopathy,12 and the dilated cardiomyopathy.13 However, to our knowledge, CMs from DMD patient–derived hiPS cells have never been obtained so far. Moreover, disease-specific hiPS cell–derived cells could represent a platform for studying in vitro the pathological dystrophic phenotype and for testing and validating the therapeutic approaches and their efficiency in restoring the normal phenotype.14 In addition, it has been recently demonstrated that hiPS cell–derived CMs can efficiently integrate in injured hearts of a guinea pig,15 providing a proof of principle for the application of these cells in regenerative medicine aiming at the treatment of cardiac dysfunctions. In the perspective of a therapeutic application, the genetic defect of CMs derived from inherited disease–specific hiPS cells should be corrected before these cells are reengrafted in the patient. DMD is among the most difficult genetic diseases to treat, and the dystrophin gene is the largest gene described in the human genome. Promising results have been obtained in rodent models of Duchenne cardiomyopathy using adeno-associated viruses carrying minimized synthetic dystrophin genes (mini- and microdystrophin).16 These approaches do not allow the insertion of a complete functional version of the dystrophin gene. On the other hand, exon-skipping approaches,17 which redirect the gene processing bypassing the mutation, can be applied only to defined ranges of patients, based on their specific mutations. Several studies suggest that utrophin may help in the preservation of heart function in young adult mdx mice and heterozygous mdx mice.18,19 However, similar to dystrophin, the large size of the utrophin gene also presents a significant challenge to gene delivery.16 Other approaches for the treatment of Duchenne cardiomyopathy include the forced expression of sarcoendoplasmic reticulum calcium-ATPase via adeno-associated virus gene transfer, aimed at restoring calcium homeostasis and improving cardiac contractility,20 without correction of the genetic defect. A highly promising gene delivery tool for the correction of the DMD gene is represented by human artificial chromosomes (HACs). HAC is an artificially created exogenous minichromosome having the ability to replicate and segregate autonomously in target human cells and to be stably maintained at episomal level, without integration into the host genome. In addition, HACs have the capacity to carry large genomic loci with all their regulatory elements.21 An HAC vector carrying, for the first time, the whole dystrophin genomic locus including the associated regulatory elements (DYSHAC) was developed by Hoshiya et al.22 Furthermore, Kazuki et al.23 have demonstrated the complete correction of hiPS cells derived from a DMD patient, using the DYS-HAC, pioneering an innovative and promising therapeutic approach for the treatment of DMD and DMD-associated cardiac diseases. The first preclinical proof of safety and efficacy of DYS-HAC– mediated therapy has been provided by Tedesco et al.24 In this study, the authors showed a significantly ameliorated phenotype in the mdx dystrophic mouse model after the transplantation of mdx
mesoangioblasts genetically corrected with the DYS-HAC. In addition, the same group recently reported the differentiation in mesoangioblast- like stem/progenitor cells from DMD patient–derived hiPS cells, carrying the genetic correction with the DYS-HAC.25

In this article, we aim to differentiate DMD patient–derived, genetically corrected hiPS cells into CMs with a mature phenotype and to assess the maintenance of the DYS-HAC during the differentiation of hiPS cells. In particular, we aim at investigating the correct activation, at HAC level, of the complex mechanisms regulating dystrophin expression, such as multiple promoter activities, which should be finely regulated in a development- and tissue-specific way.

An ad hoc cardiac differentiation procedure, combining the delivery of cytokines with mechanical stimulation, by culturing cells on hydrogel with physiological stiffness, has been designed to allow full CM maturation. DYS-HAC–mediated dystrophin expression restoration has been assessed at different stages of the differentiation process. The dystrophic CMs established in this work could potentially represent a valuable cell source to be used for in vitro modeling of DMD-associated cardiomyopathies, and at the same time, the genetically corrected dystrophic CMs possess a promising therapeutic potential for the treatment of DMD.

Results

Differentiation of hiPS cells toward the cardiac lineage

To obtain DMD-specific CMs, their genetic correction, and a positive control of dystrophin expression, the hiPS following cell lines that differentiated toward the cardiac lineage were used: (i) hiPS cells derived from a DMD patient with deletion of exons 4–43 of the muscle isoform Dp427m (DMD hiPS cells); (ii) DMD patient–specific hiPS cells genetically corrected by an HAC carrying the full-length genomic dystrophin sequence (DYS-HAC hiPS cells); and (iii) hiPS cells derived from a healthy individual (healthy hiPS cells), carrying a normal genotype with a wild-type copy of the dystrophin gene. First, DMD, DYS-HAC, and healthy hiPS cell lines were cultured and expanded in their undifferentiated state for up to 10 passages. During expansion, hiPS cell colonies maintained the expression of pluripotency markers such as Oct4, Sox2, c-Myc, Tra-1-60, and Tra-1-81, as evaluated by immunofluorescence (see Supplementary Figure S1a). In addition, DYS-HAC hiPS cells were monitored for the expression of the enhanced green fluorescent protein, a marker contained in the DYS-HAC (see Supplementary Figure S1b). The expanded colonies were then used for embryoid body (EB) generation. DMD, DYS-HAC, and healthy hiPS cell–derived EBs were differentiated toward the cardiac lineage through an ad hoc optimized procedure. Overall outline of this procedure is shown in Figure 1a. Remarkably, the enhanced green fluorescent protein gene, driven by a CAG promoter contained in the DYS-HAC,23 was expressed during all the stages of the differentiation procedure, in DYS-HAC hiPS cells (Figure 1b), in DYS-HAC hiPS cell–derived EBs (Figure 1c), and in cultured cells after EB adhesion (Figure 1d), indicating the stable maintenance of the DYS-HAC. During the first 16 days of the differentiation procedure, EBs were cultured in suspension and subjected to a staged protocol, adapted from the one developed by Kattman et al.,26 based on the addition of specific cytokines known to play a key role in cardiogenesis during embryonic development to the culture medium. This 16-day differentiation procedure resulted in a relevant percentage of spontaneously contracting EBs (see Supplementary Videos S1 and S2), ranging from a minimum of 14% for DMD hiPS cell–derived EBs to a maximum of 44% for healthy hiPS cell– derived EBs (Table 1).

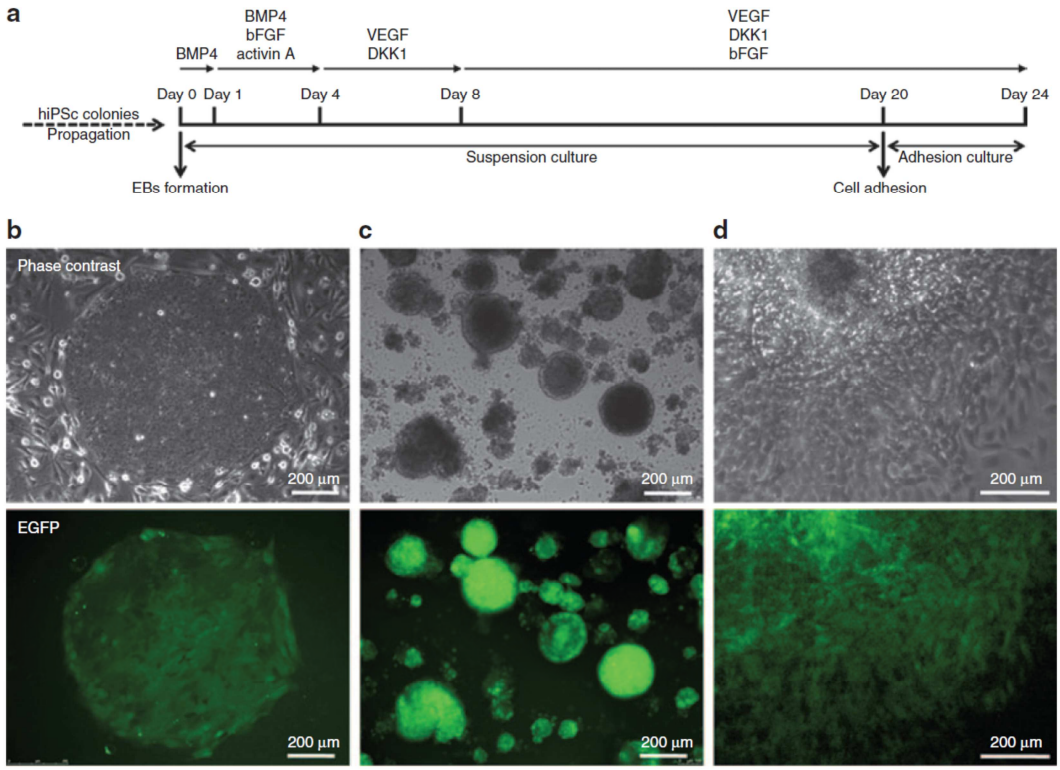

Figure 1. *Differentiation of hiPS cells. (a) Schematic representation of the differentiation procedure. (b) Undifferentiated colonies of DYS-HAC hiPS cells cultured on murine embryonic fibroblast feeder cells. (c) EBs generated from DYS-HAC hiPS cell colonies on day 4 of the differentiation procedure. (d) Cultured cells 2 days after EB adhesion. Epifluorescence images show the expression of EGFP in each condition, indicating the presence of the DYSHAC. BMP4, bone morphogenetic protein 4; DYS-HAC, human artificial chromosome carrying the whole dystrophin genomic sequence; EBs, embryoid bodies; EGFP, enhanced green fluorescent protein; hiPS cells, human induced pluripotent stem cells; VEGF, vascular endothelial growth factor; bFGF, basic fibroblast growth factor.*

Table 1. Percentage of spontaneously contracting EBs and cTnT-positive cells obtained for each cell line used

hES/hiPS cell lines	*Contracting EBs obtained (% ± SD): day16*	*cTnT-positive cells (% ± SD): day 24*
DMD hiPS cells	14 ± 4	7,6 ± 0,7
DYS-HAC hiPS cells	19 ± 5	8,2 ± 1,5
Healthy hiPS cells	44 ± 2	9,8 ± 4,6

cTnT, cardiac troponin T; DMD, Duchenne muscular dystrophy; DYS-HAC, human artificial chromosome carrying the whole dystrophin genomic sequence; EBs, embryoid bodies; hiPS cells, human induced pluripotent stem cells; SD, standard deviation calculated on data obtained from 5 independent analyses.

Our recent data demonstrated that a proper cardiac differentiation requires cell–substrate interactions to promote functional and structural maturation of hiPS cell–derived CMs.36 For this reason, contracting EBs were cultured in suspension up to day 20 and then seeded on hydrogel substrate with a physiological stiffness for additional 4 days. Following adhesion, a remarkable maturation of CMs was observed in terms of both cytoskeletal architecture and cardiac marker

expression (Figure 2). CMs obtained on day 24 were characterized by a remarkable sarcomeric organization, as revealed by immunofluorescence of α-actinin, cardiac troponin T (cTnT), and F-actin, and GAP junction formation, as revealed by immunofluorescence of connexin 43 (Figure 2a). The percentage of cTnT-positive CMs obtained on the overall population was ~10% (Table 1). The same percentage increased to 44 ± 2% when only contracting EBs were selected. Expression of sarcomeric cardiac-specific proteins, in particular cTnT and ventricular myosin light chain, in adhered CMs, was also confirmed by reverse transcription–polymerase chain reaction (RT-PCR) (Figure 2b). For DMD hiPS cell–derived CMs, expression of ML2v, a marker of terminally differentiated ventricular CMs, was not observed before CM adhesion but was observed only after adhesion. Mesoderm- and cardiac-specific transcription factors GATA4 and NKX2.5 were also expressed in all conditions tested, as revealed by RT-PCR (Figure 2b) and immunofluorescence (Figure 2a), respectively. CMs cultured in adhesion displayed both spontaneous and electrically induced calcium transients lasting less than 1 second, typical of calcium cycling during contraction (Figure 2c), together with a diffuse intracellular distribution of cardiac-specific sarcoendoplasmic reticulum calcium-ATPase (Figure 2a), a key element of the calcium handling machinery needed for calcium reuptake after contraction.

Taken together, these results show that functionally differentiated CMs were derived from DMD, DYS-HAC, and healthy hiPS cells. The observed differences in terms of percentage of spontaneously contracting EBs and cTnT-positive CMs on the overall population (Table 1) can be due to the intrinsic variability related to the use of different hiPS cell lines and the efficiency of the cardiogenic protocol itself. HAC-driven expression of dystrophin sequences originally deleted in the DMD patient We then focused on the genetically corrected CMs, testing the restoration of HAC-mediated dystrophin expression. DYS-HAC is the first vector carrying the whole dystrophin genomic locus, including all the associated regulatory elements.22 This potentially allows proper activation of the complex mechanism regulating dystrophin expression, for instance, the activities of seven different promoters driving transcription of tissue-specific isoforms and exon-skipping and exon-scrambling events, which are finely regulated in both development- and tissue-specific manner.1 The possibility to restore dystrophin expression in a tissue-specific manner, following native regulation mechanisms, makes DYS-HAC a promising tool for the treatment of DMD also at cardiac muscle level.

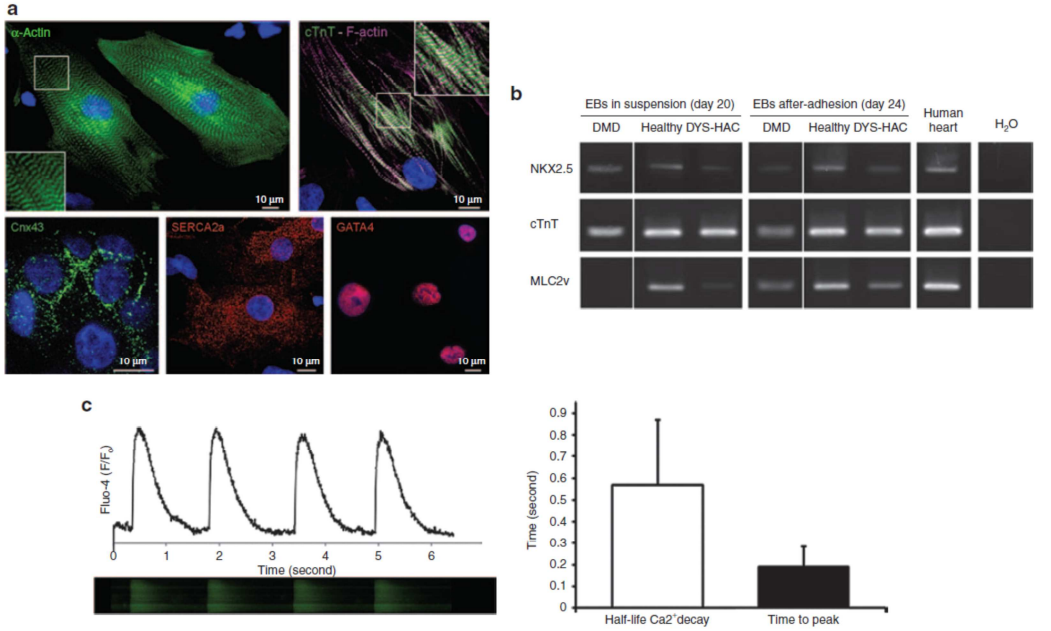

Figure 2. *Characterization of hiPS cell–derived CMs. (a) Immunofluorescence of α-actinin; cardiac troponin T (cTnT) and F-actin; connexin 43 (Cnx43); sarcoendoplasmic reticulum calcium-ATPase (SERCA2a); and GATA4 in adhered CMs on day 24 of the differentiation procedure. Nuclei are counterstained with DAPI. (b) RT-PCR shows the expression of NKX2.5, cTnT, and MLC2v in EBs obtained from DMD, healthy, and DYS-HAC hiPS cells cultured in suspension (on day 20) and on the EB-derived adhered cells on day 24 of the differentiation procedure. (c) Typical calcium*

transients displayed by hiPS cell–derived CMs on day 24 of the differentiation procedure. The histogram reports quantitative evaluation of calcium reuptake rate by the half-life of calcium decay and the calcium release phase as the time to peak. Data are presented as SD. CMs, cardiomyocytes; DAPI, 4',6-diamidino-2-phenylindole; DMD, Duchenne muscular dystrophy; DYS-HAC, human artificial chromosome carrying the whole dystrophin genomic sequence; hiPS cells, human induced pluripotent stem cells; MLC2v, ventricular myosin light chain; RT-PCR, reverse transcription–polymerase chain reaction.

First, dystrophin expression was analyzed on healthy, DMD, and genetically corrected DYS-HAC hiPS cells during the cardiac differentiation procedure, by RT-PCR using specific primers designed to span exon–exon junctions localized inside the deleted genomic sequence of the DMD patient (from exon 4 to 43 of the muscle dystrophin isoform) (Figure 3a). mRNA from human heart and skeletal muscle was used as positive control. As expected, healthy hiPS cell–derived EBs displayed dystrophin expression both when cultured in suspension and after adhesion, whereas, as expected, in DMD hiPS cell–derived EBs, no dystrophin expression was observed in any condition (Figure 3b). In DYS-HAC hiPS cell–derived EBs, dystrophin expression was restored both when cultured in suspension and after adhesion. A positive result was obtained for each of the five exon junctions checked, distributed on the whole deleted genomic region. HAC-driven expression of multiple dystrophin isoforms In vivo, CMs are known to express the full-length muscle dystrophin isoform (Dp427m), together with other isoforms, such as the Dp260 (ref. 27) and Dp71, the smallest but multifunctional product of the DMD gene expressed in many tissues, including cardiac muscle. Dp71 has been shown to contribute to the proper clustering and anchoring of structural and signaling proteins to the plasma membrane and of nuclear envelope proteins to the inner nuclear membrane.28

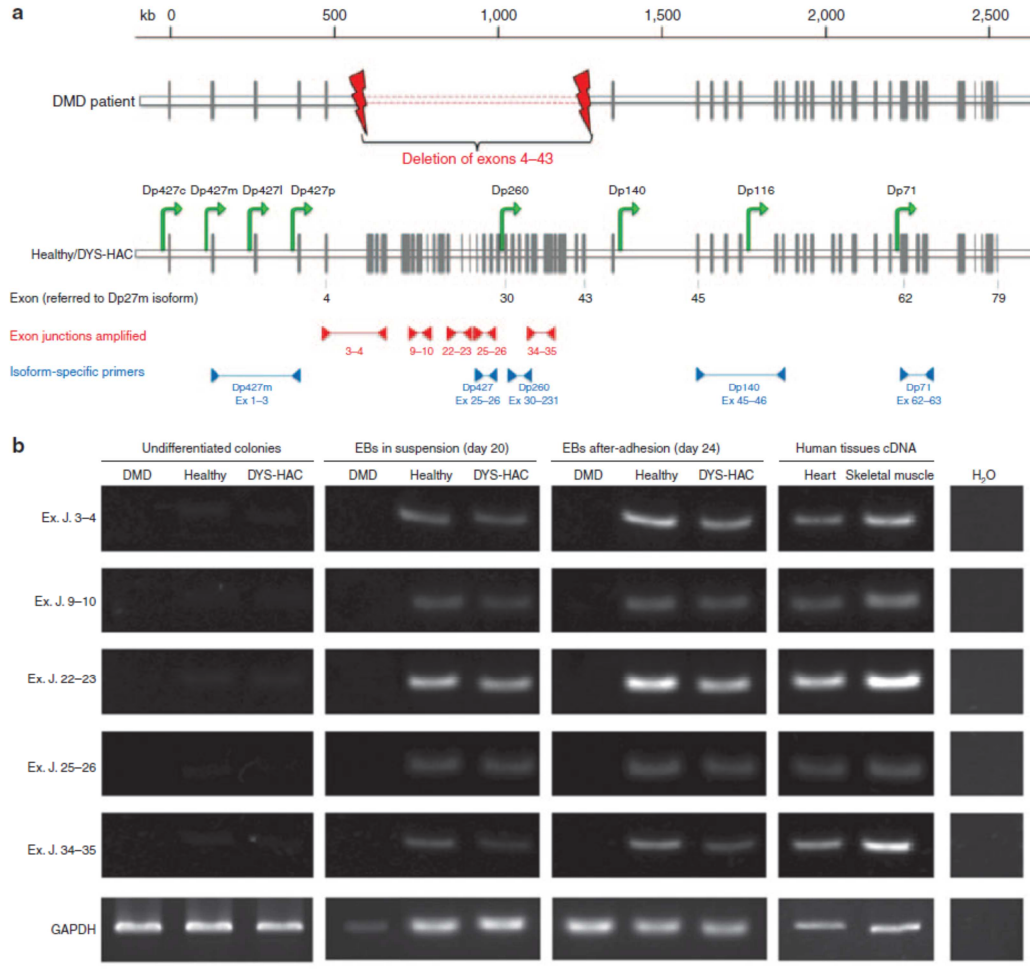

Figure 3. *HAC-driven expression of dystrophin sequences originally deleted in DMD patients. (a) The genomic organization of the dystrophin gene: the gray vertical bars represent the exons; the green arrows indicate the promoters driving the expression of the different dystrophin isoforms within the gene1,2; primer pairs used to amplify exon–exon junctions inside the deleted region are indicated by red arrowheads, and those used to amplify specific isoforms are indicated by blue arrowheads. Exon number is referred to exons composing the muscle dystrophin isoform Dp427m. (b) RT-PCR of specific dystrophin sequences localized inside the patient with deletion of exons (Ex) 4–43. Primers were constructed to spam five different exon–exon junctions (Ex. J.). cDNA from human heart and skeletal muscle was used as positive control. Analyses were performed at three different stages of the differentiation process: undifferentiated colonies, differentiated EBs cultured in suspension (day 20), and adhered cells (day 24), for each hiPS cell lines (DMD, healthy, and DYS-HAC hiPS cells). cDNA from human tissues was used as positive control. cDNA, complementary DNA; DMD, Duchenne muscular dystrophy; DYS-HAC, human artificial chromosome carrying the whole dystrophin genomic sequence; EBs, embryoid bodies; HAC, human artificial chromosome; hiPS cells, human induced pluripotent stem cells; RT-PCR, reverse transcription–polymerase chain reaction.*

The expression of different dystrophin isoforms such as Dp427m, Dp260, Dp140, and Dp71 was analyzed by RT-PCR during the cardiac differentiation procedure on healthy, DMD, and DYS-HAC hiPS cells (Figure 4a). mRNA from human tissues was used as positive control. As expected, healthy hiPS cell–derived EBs (both in suspension and after adhesion) displayed the expression of all the four different dystrophin isoforms. The expression of isoform Dp140 indicates the presence of other cell types in addition to CMs, which are expected in this type of differentiation procedures.29 In DMD hiPS cell–derived EBs, the expression of the Dp260 isoform, the promoter of which stands within the large genomic deletion (exons 4–43), was not observed, whereas isoforms Dp140 and Dp71 were still detectable as their promoters are downstream of the deleted area (intron 44 and intron 62, respectively). The amplicon relative to isoform Dp427m is still present, as the primers specific for this isoform are designed on the first transcribed exons (exons 1–3), upstream of the deletion, testifying a proper initiation of dystrophin transcription. On DYS-HAC hiPS cell–derived EBs (both in suspension and after adhesion), expression of all isoforms can be observed, notably with the restoration of Dp260 isoform transcript. To assess the efficiency of HAC-driven recovery of dystrophin mRNA levels, we performed RT-PCR experiments targeted at the isoforms expressed in the cardiac tissue (Figure 4b). A set of primers targeting exons 25–26 identifying all Dp427 isoforms was used in addition to the Dp427m-specific one to assess the relative expression of Dp427 transcripts inside the deleted genomic region. Confirming the previous results of the RT-PCR, DMD hiPS cell–derived EBs did not display at all the expression of transcripts from inside the deleted genomic region, both in regard to Dp427 isoforms, the transcription of which is truncated after exon 4, and in regard to Dp260 isoform, the transcription of which cannot be initiated. The expression of the truncated Dp427m isoform and the short Dp71 isoform was variable among the different experiments, not reaching statistical significance (n = 3). Differentiated healthy and DYS-HAC hiPS cell–derived CMs displayed similar amounts of all transcripts tested, highlighting the proper function of the HAC in driving and regulating the transcription of different dystrophin isoforms.

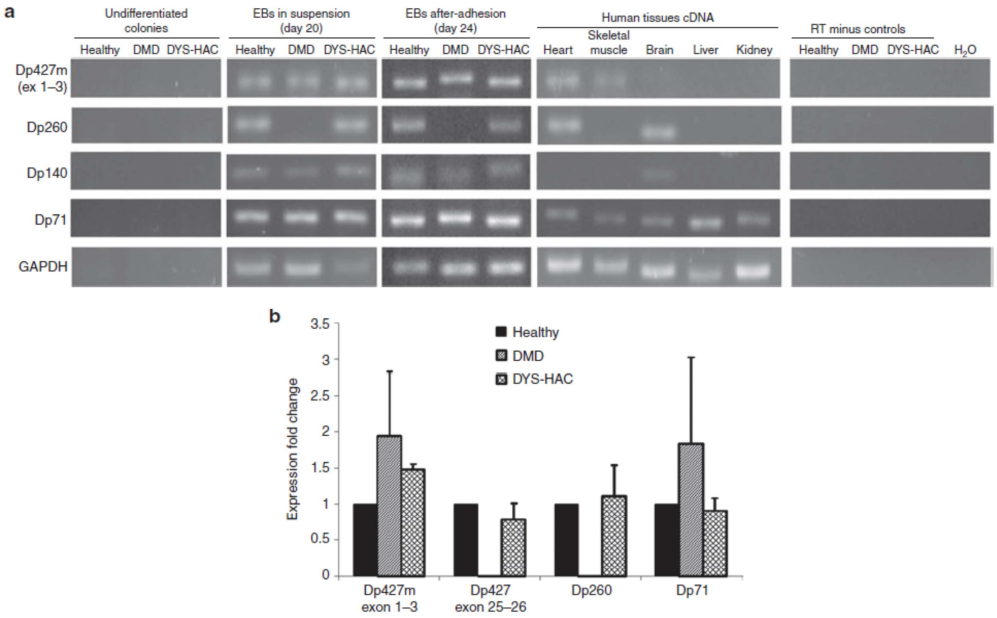

Figure 4. *HAC-driven expression of multiple dystrophin isoforms. (a) RT-PCR of dystrophin isoforms Dp427m, Dp260, Dp140, and Dp71 at three different stages of the differentiation process: undifferentiated colonies, differentiated EBs cultured in suspension (day 20), and adhered cells (day 24), for each hiPS cell lines (DMD, healthy, and DYS-HAC hiPS cells). cDNA from human tissues was used as positive control. (b) Realtime PCR for dystrophin isoforms present in cardiac tissue. Muscle-specific Dp427m is double checked with Dp427m-specific primer set spanning exons 1–3 and an all Dp427 isoform-specific primer set spanning exons 25–26. Data are presented as mean ± SD. cDNA, complementary DNA; DYS-HAC, human artificial chromosome carrying the whole dystrophin genomic sequence; EBs, embryoid bodies; HAC, human artificial chromosome; hiPS cells, human induced pluripotent stem cells; RT-PCR, reverse transcription–polymerase chain reaction; DMD, Duchenne muscular dystrophy.*

Taken together, these analyses on mRNA transcripts show that, during the cardiac differentiation protocol, dystrophin expression is correctly restored by the DYS-HAC and multiple dystrophin isoforms are expressed.

HAC-mediated restoration of dystrophin protein expression and correct subcellular localization In vivo, in physiological conditions, dystrophin is a key structural protein creating a bridge across the sarcolemma, which provides a flexible connection between the basal lamina of the extracellular matrix and the inner cytoskeleton. For this important role, dystrophin should be correctly folded and localized under the plasma

membrane of skeletal and cardiac muscle cells. For this reason, we verified the proper restoration of dystrophin expression at protein level and its subcellular localization by immunofluorescence and confocal microscopy. Analyses were performed 4 days after EB adhesion on substrate with a physiological stiffness

of 15 kPa (Figure 5a). DYS-HAC hiPS cell–derived EBs displayed a clear dystrophin expression at membrane localization, drawing the boundaries of cTnT-positive CMs. A similar dystrophin staining was observed in healthy hiPS cell–derived EBs. On the other hand, as expected, in DMD hiPS cell–derived EBs, any dystrophin staining was observed. These results were confirmed by western blot analysis, in which full-length dystrophin was not observed in DMD hiPS cell– derived CMs, whereas its expression was perfectly restored in CMs corrected with the DYS-HAC (Figure 5b). Although much less abundant, other dystrophin isoforms were also detectable in the DYS-HAC–corrected cells (see Supplementary Figure S2). These results demonstrate that the DYS-HAC restores the expression of dystrophin at protein level, which can correctly localize at membrane localization in genetically corrected, hiPS cell–derived CMs.

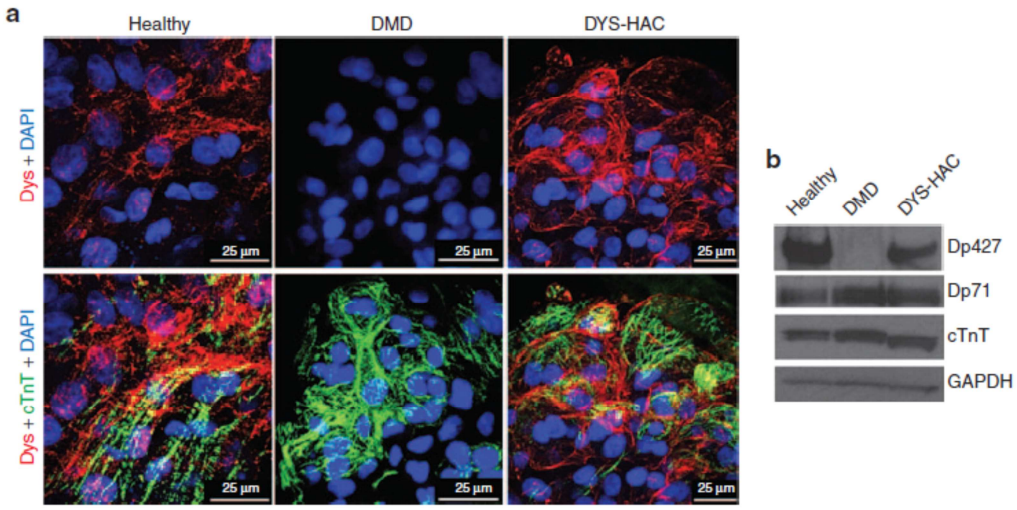

Figure 5. *HAC-mediated restoration of dystrophin protein expression and correct subcellular localization. (a) Confocal microscopic analysis of dystrophin and cardiac troponin T expression on CMs obtained on day 24 of the differentiation procedure from DMD, healthy, and DYS-HAC hiPS cells. Nuclei are counterstained with DAPI. (b) Western blot analysis for dystrophin isoforms with a polyclonal antibody and for cardiac marker troponin T detected in two isoforms in the samples from human hiPS cell–derived cardiomyocytes. CMs, cardiomyocytes; DAPI, 4',6-diamidino-2-phenylindole; DMD, Duchenne muscular dystrophy; DYS-HAC, human artificial chromosome carrying the whole dystrophin genomic sequence; HAC, human artificial chromosome; hiPS cells, human induced pluripotent stem cells.*

Discussion

The derivation of genetically corrected, patient-specific hiPS cells has been recently shown to be a promising strategy for modeling genetic diseases. In particular, An et al.30 reported the derivation of hiPS cells from Huntington's disease patients' fibroblasts that were genetically corrected by an homologous recombination approach and differentiated into DARPP-32–positive neurons. Tedesco et al.25 reprogrammed fibroblasts and myoblasts from limb-girdle muscular dystrophy patients in hiPS cells and developed a protocol for the derivation of mesoangioblast-like cells that were genetically corrected in vitro with a lentiviral vector carrying the human α-sarcoglycan gene. The huge potential of hiPS cell technology has also been demonstrated in modeling human cardiovascular diseases. Some pioneering proof-of-concept studies on patients with inherited arrhythmogenic diseases, most notably different subtypes of long QT syndrome, reported the derivation of hiPS cell–derived cardiac cells to reproduce the clinical phenotype "in the petri dish."14,31 In this work we derived, for the first time to our knowledge, human CMs (hCMs) from DMD patient–specific hiPS cells and genetically corrected hCMs from DYS-HAC–containing hiPS cells. Different procedures for the cardiac differentiation of pluripotent stem cells have been reported in literature, mainly reproducing in vitro the processes of embryonic development through the stimulation of soluble cytokines, driving pluripotent stem cells toward early mesoderm specification until the derivation of cardiac progenitor cells.26,32,33 However, the major drawback of their application, both in vitro and in vivo, is their immature phenotype. To study the restoration of dystrophin expression and its correct localization in cardiac cells, the derivation of hCMs characterized by a functionally and structurally mature phenotype is of paramount importance. We developed an ad hoc optimized differentiation procedure integrating a cytokine-based EB differentiation with a subsequent step of adhesion-dependent maturation. Increasing evidence demonstrate that adhesion and substrate sensing are key requirements for the process of muscle cell functional differentiation. In our previous work, we have shown that the development of sarcomeric structures of human striated muscles is influenced by the substrate on which the cells are cultured.34 Furthermore, in our group, it has been recently demonstrated that adhesion on substrate with a physiological stiffness promotes functional

maturation of hCMs, allowing a shortening of calcium transients.36 Using the procedure developed, we derived hCMs presenting expression of cardiac-specific markers, a defined sarcomeric organization, and calcium transients lasting less than 1 second. In these conditions, dystrophin has been observed to correctly localize at membrane level on both healthy and genetically corrected hCMs. Certain variability has been observed in the expression of cardiac muscle markers along the differentiation process, for the different hiPS cell lines. This could be explained since, as widely reported in literature, hiPS cell lines derived from different cells and different clones can have a different ability to differentiate toward the cardiac lineage. In addition, it has been recently demonstrated that in vitro cultured DMD skeletal muscle cells display a delay in the appearance of typical myogenic markers.35 Similarly, we observed a delay in the expression of the late cardiac differentiation marker ventricular myosin light chain in DMD-derived cardiac cells, compared with the healthy and genetically corrected (DYS-HAC) ones. Further analyses could be performed to specifically address this issue in cardiac muscle. hiPS cell–derived CMs represent a unique platform for testing in vitro the efficiency of the DYS-HAC in restoring a proper dystrophin expression at cardiac level, in a patient-specific manner. DYS-HAC is a potential tool for use in DMD gene correction, and its ability to properly restore dystrophin expression on differentiated human cells has been recently reported.25 However, its efficiency in restoring different isoforms' expression on differentiated hCMs has not been extensively investigated so far. For the first time, we demonstrated that DYS-HAC (i) does not hinder and is stably maintained during cardiac differentiation of hiPS cells; (ii) allows a proper dystrophin expression restoration during the cardiac differentiation procedure of hiPS cells (in particular, the expression of specific sequences deleted in the patient was observed); (iii) drives the transcription of multiple dystrophin isoforms in CMs at similar expression levels compared with healthy hiPS cell–derived CMs, in particular, the full-length muscle isoform Dp427m and the cardiac isoform Dp260, which are not expressed in the DMD patient with deletion of exons 4–43; and (iv) allows the recovery of full-length dystrophin protein that localizes properly at the cell membrane. These results highlight DYS-HAC as a potential tool for use in gene correction of DMD patient cells.

Finally, the coupling of DMD CMs with specific technologies for testing cardiac functionality, such as measurement of force generation or performance under stressed condition, will provide a unique platform for studying in vitro the pathogenesis of DMD-associated cardiac disease and its correction.

Materials and methods

hiPS cell culturing and cardiac differentiation

hiPS cells, obtained as previously reported,23 were cultured on a feeder layer of mitomycin-C–inactivated murine embryonic fibroblasts. Composition of the culture medium was as follows: Dulbecco's modified Eagle medium/F12 (Life Technologies) containing 20% knockout serum (Life Technologies), 2 mmol/l of l-glutamine (Life Technologies), 0.1 mmol/l of nonessential amino acids (Life Technologies), 0.1 mmol/l of 2-mercaptoethanol (Life Technologies), 50 units and 50 mg/ml of penicillin and streptomycin (Life Technologies), and 4 ng/ml of basic fibroblast growth factor (Peprotech). To maintain the pluripotent state for a high number of passages and avoid chromosomal aberrations, the colonies were passed as described
below—usually once a week. hiPS cells were washed with phosphate-buffered saline (PBS) and treated with 1 ml of CTK solution for 30 seconds. CTK solution was prepared as follows: 5 ml of 2.5% trypsin (Life Technologies), 5 ml of 1 mg/ml collagenase IV (Sigma-Aldrich), 0.5 ml of 0.1 mol/l CaCl2 (Sigma-Aldrich), and 10 ml of knockout serum were all added to 30 ml of distilled water. The mechanical separation of colonies was performed with the use of a stereomicroscope to dissect the undifferentiated colonies into several pieces using a cutting pipette. These selected pieces were then replated for expansion onto dishes containing fresh murine embryonic fibroblast feeders or moved to ultralow adhesion plates to be cultured in suspension for EB generation. The obtained EBs were differentiated in suspension using a protocol adapted from Kattman et al.26 Briefly, for EB formation, the detached and separated colonies were maintained for 24 hours in basal medium (StemPRO-34; Life Technologies), 2 mmol/l of l-glutamine (Life

Technologies), 150 µg/ml of transferrin (Roche), 50 µg/ml of ascorbic acid (Sigma-Aldrich), 0.4 mmol/l of monothioglycerol (Sigma-Aldrich), 50 units and 50 mg/ml of penicillin and streptomycin (Life Technologies) supplemented with 10 ng/ml of human bone morphogenetic protein 4 (R&D). From day 1 to day 4, EBs were cultured in basal medium with 10 ng/ml of human bone morphogenetic protein 4, 5 ng/ml of human basic fibroblast growth factor (R&D), and 6 ng/ml of hActivin A (R&D). From day 4 to day 8, the EB culture medium consisted of basal medium and 10 ng/ml of human vascular endothelial growth factor (R&D) and 150 ng/ml of hDKK (R&D). Finally, from day 8 to day 14, the EB culture medium consisted of basal medium and 10 ng/ml of human vascular endothelial growth factor and 5 ng/ml of human basic fibroblast growth factor. Cultures were maintained in a 5% CO2, 5% O2, and 90% N2 environment for the first 16 days and then transferred to a 5% CO2 air environment. The obtained EBs were maintained in suspension using the last medium described until day 20 and then seeded on hydrogel substrates with a physiological stiffness of 15 kPa (prepared as previously described)34,36,37, functionalized with 100 µg/ml of laminin (BD), and cultured in these conditions for additional 4 days.

Immunofluorescence

A standard immunohistochemistry protocol was used. Briefly, cells were fixed with PBS containing 2% paraformaldehyde (Sigma-Aldrich) for 7 minutes, permeabilized with PBS containing 0.5% Triton X-100 (Sigma-Aldrich), and blocked in PBS containing 2% horse serum for 45 minutes, at room temperature. Primary antibodies were applied for 1 hour at 37 °C. Cells were washed in PBS (Life Technologies) and incubated with fluorescence-conjugated secondary antibodies against mouse, rabbit, or goat, depending on primary antibody used, for 45 minutes at 37 °C. Finally, nuclei were counterstained with 4’,6-diamidino-2-phenylindole (Sigma-Aldrich), and samples were mounted with Elvanol and viewed under Leica TCS SP5 fluorescence confocal microscope (Leica). Primary antibodies used were the following: mouse monoclonal anti-cTnT (Thermo Scientific; #MS-295-P; 1:100 dilution), mouse monoclonal anti-α-actinin (Sigma-Aldrich; #A7811; 1:100 dilution), rabbit polyclonal antidystrophin (Abcam; #ab15277; 1:200 dilution), mouse monoclonal anti-Cx43 (Millipore; #MAB3067; 1:100 dilution), goat polyclonal anti-SERCA2a (Santa Cruz; #SC 8094; 1:200 dilution), and goat polyclonal anti-GATA4 (Santa Cruz; #SC 1237; 1:200 dilution). Secondary antibodies used were the following: goat anti-mouse (Invitrogen; #A11005 and #A11001; 1:200 dilution), goat anti-rabbit (Invitrogen; #A11012 and A1108; 1:200 dilution), and donkey antigoat (Jackson ImmunoLab; #705-165-003; 1:300 dilution). All antibodies were diluted in 3% bovine serum albumin (Sigma-Aldrich).

Calcium measurements

Confocal calcium measurements were performed as previously reported in Martewicz et al.38 Briefly, CMs were loaded in serum-free 25 mmol/l HEPES Dulbecco's modified Eagle medium (Life Technologies) supplemented with 2,5 mmol/l of fluorescent calcium dye Fluo-4 AM (Life Technologies) for 20 minutes at 37 °C in the presence of 2 mmol/l of Pluronic F-127 (Life Technologies) and 20 mmol/l of sulfinpyrazone (Sigma-Aldrich), then incubated for additional 10 minutes at 37 °C without Fluo-4 AM, and added with 0.2 mmol/l of di-8-ANEPPS (Life Technologies). Cell dynamics were obtained in recording solution: NaCl, 125 mmol/l; KCl, 5 mmol/l; Na3PO4, 1 mmol/l; MgSO4, 1 mmol/l; HEPES, 20 mmol/l; CaCl2, 2 mmol/l; and glucose, 5.5 mmol/l, to pH 7.4 with NaOH. Line scans were acquired with a Leica TCS SP5 fluorescence confocal microscope using a 63× oil immersion objective, with 488-nm Ar laser line as an excitation source and 400-Hz acquisition frequency. Line scans were then analyzed using ImageJ software (version number 1.46) to obtain calcium transient profile. For evaluating the calcium reuptake rate after contraction, the half-life of the calcium decay was considered. Half-life of the calcium decay was calculated by fitting a first-order exponential decay to the calcium reuptake phase of the calcium transient profile. For the calcium release phase, the time to peak value was calculated considering the time from baseline to a minimum of the second derivative of the calcium transient. All numerical data were manipulated with Origin 8.1 software.

Reverse transcription–polymerase chain reaction.

Total RNA from hiPS cell colonies and differentiated EBs was purified with RNeasy Mini Kit (Qiagen), in accordance with the manufacturer's instructions, or with TRIzol reagent (Invitrogen) and treated using a Turbo DNA-free kit (Applied Biosystems) to remove genomic DNA contamination. For the cardiac marker analyses, first strand complementary DNA (cDNA) synthesis was performed using an oligo- (dT)20 primer and the cDNA Reverse Transcription Kit (Applied Biosystems). PCR was performed with cDNA using AmpliTaq Gold (Applied Biosystems). Amplifications were performed with an annealing temperature of 55 or 58 °C for 30–35 cycles. For the dystrophin isoform analyses, cDNA retrotranscription was carried out with High Capacity cDNA Reverse Transcription Kit (Invitrogen), followed by RT-PCR using Platinum Taq Polymerase (Invitrogen) with annealing temperature of 60 °C for 35 cycles. All the amplicons were resolved by electrophoresis on a 2% agarose gel, followed by staining with SYBR Safe Gel. Primer sequences are given in Table 2.

Real-time PCR

Real-time PCR on cDNA retrotranscribed with High Capacity cDNA Reverse Transcription Kit was carried out with Power SYBR Green PCR Master Mix (Applied Biosystems) in a 7000 System thermal cycler platform (Applied Biosystems). Annealing temperature for all primer sets was 60 °C (sequences reported in Table 2). Relative amount of transcripts was calculated with Pfaffl method relative to healthy hiPS cell–derived EB expression levels. Amplification efficiency for all primer sets was >1.9.

Western blot analyses

Detection of dystrophin (antibody 1:500; o/n + 4 °C; Abcam; #ab15277), cTnT (antibody 1:500; 60 minutes at room temperature; Thermoscientific #MS-295-P), and GAPDH (antibody 1:2,000; 60 minutes at room temperature; Abcam; #ab8245) was carried out after protein lysates were resolved in a NuPAGE 3–8% Tris-acetate polyacrylamide gel (Invitrogen) and transferred for 6 hours at 4°C on a polyvinylidene difluoride membrane (Invitrogen) with a BioRad cassette. Detection was performed with Novex ECL Kit (Invitrogen). Anti-rabbit (Invitrogen) and anti-mouse (BioRad) secondary horseradish peroxidase–conjugated antibodies were used.

Conflicts of interest

The authors declare no conflict of interest.

Acknowledgments

This work was supported by Fondazione Ing. Aldo Gini, Fondazione CaRiPaRo, and Fondazione Citta della Speranza. We thank Motonobu Katoh (Department of Biomedical Science, Institute of Regenerative Medicine and Biofunction, Tottori University, Yonago, Japan) for helping with experimental work.

References

1 Muntoni, F, Torelli, S and Ferlini, A (2003). Dystrophin and mutations: one gene, several proteins, multiple phenotypes. Lancet Neurol 2: 731–740.

2 Blake, DJ, Weir, A, Newey, SE and Davies, KE (2002). Function and genetics of dystrophin and dystrophin-related proteins in muscle. Physiol Rev 82: 291–329.

3 Spurney, CF (2011). Cardiomyopathy of Duchenne muscular dystrophy: current understanding and future directions. Muscle Nerve 44: 8–19.

4 Fayssoil, A, Nardi, O, Orlikowski, D and Annane, D (2010). Cardiomyopathy in Duchenne muscular dystrophy: pathogenesis and therapeutics. Heart Fail Rev 15: 103–107.

5 Takahashi, K, Tanabe, K, Ohnuki, M, Narita, M, Ichisaka, T, Tomoda, K et al. (2007). Induction of pluripotent stem cells from adult human fibroblasts by defined factors. Cell 131: 861–872.

6 Robinton, DA and Daley, GQ (2012). The promise of induced pluripotent stem cells in research and therapy. Nature 481: 295–305.

7 Carvajal-Vergara, X, Sevilla, A, D'Souza, SL, Ang, YS, Schaniel, C, Lee, DF et al. (2010). Patient-specific induced pluripotent stem-cell-derived models of LEOPARD syndrome. Nature 465: 808–812.

8 Moretti, A, Bellin, M, Welling, A, Jung, CB, Lam, JT, Bott-Flügel, L et al. (2010). Patientspecific induced pluripotent stem-cell models for long-QT syndrome. N Engl J Med 363: 1397–1409.

9 Itzhaki, I, Maizels, L, Huber, I, Zwi-Dantsis, L, Caspi, O, Winterstern, A et al. (2011). Modelling the long QT syndrome with induced pluripotent stem cells. Nature 471: 225– 229.

10 Matsa, E, Rajamohan, D, Dick, E, Young, L, Mellor, I, Staniforth, A et al. (2011). Drug evaluation in cardiomyocytes derived from human induced pluripotent stem cells carrying a long QT syndrome type 2 mutation. Eur Heart J 32: 952–962.

11 Novak, A, Barad, L, Zeevi-Levin, N, Shick, R, Shtrichman, R, Lorber, A et al. (2012). Cardiomyocytes generated from CPVTD307H patients are arrhythmogenic in response to ß-adrenergic stimulation. J Cell Mol Med 16: 468–482.

12 Ma, D, Wei, H, Lu, J, Ho, S, Zhang, G, Sun, X et al. (2013). Generation of patient-specific induced pluripotent stem cell-derived cardiomyocytes as a cellular model of arrhythmogenic right ventricular cardiomyopathy. Eur Heart J 34: 1122–1133.

13 Sun, N, Yazawa, M, Liu, J, Han, L, Sanchez-Freire, V, Abilez, OJ et al. (2012). Patient-specific induced pluripotent stem cells as a model for familial dilated cardiomyopathy. Sci Transl Med 4: 130ra47.

14 Zeevi-Levin, N, Itskovitz-Eldor, J and Binah, O (2012). Cardiomyocytes derived from human pluripotent stem cells for drug screening. Pharmacol Ther 134: 180–188.

15 Shiba, Y, Fernandes, S, Zhu, WZ, Filice, D, Muskheli, V, Kim, J et al. (2012). Human ES-cellderived cardiomyocytes electrically couple and suppress arrhythmias in injured hearts. Nature 489: 322–325.

16 Lai, Y and Duan, D (2012). Progress in gene therapy of dystrophic heart disease. Gene Ther 19: 678–685.

17 Lu, QL, Yokota, T, Takeda, S, Garcia, L, Muntoni, F and Partridge, T (2011). The status of exon skipping as a therapeutic approach to duchenne muscular dystrophy. Mol Ther 19: 9–15.

18 Bostick, B, Yue, Y, Long, C and Duan, D (2008). Prevention of dystrophin-deficient cardiomyopathy in twenty-one-month-old carrier mice by mosaic dystrophin expression or complementary dystrophin/utrophin expression. Circ Res 102: 121– 130.

19 Janssen, PM, Hiranandani, N, Mays, TA and Rafael-Fortney, JA (2005). Utrophin deficiency worsens cardiac contractile dysfunction present in dystrophin-deficient mdx mice. Am J Physiol Heart Circ Physiol 289: H2373–H2378.

20 Shin, JH, Bostick, B, Yue, Y, Hajjar, R and Duan, D (2011). SERCA2a gene transfer improves electrocardiographic performance in aged mdx mice. J Transl Med 9: 132.

21 Kazuki, Y, Hoshiya, H, Takiguchi, M, Abe, S, Iida, Y, Osaki, M et al. (2011). Refined human artificial chromosome vectors for gene therapy and animal transgenesis. Gene Ther 18: 384–393.

22 Hoshiya, H, Kazuki, Y, Abe, S, Takiguchi, M, Kajitani, N, Watanabe, Y et al. (2009). A highly stable and nonintegrated human artificial chromosome (HAC) containing the 2.4 Mb entire human dystrophin gene. Mol Ther 17: 309–317.

23 Kazuki, Y, Hiratsuka, M, Takiguchi, M, Osaki, M, Kajitani, N, Hoshiya, H et al. (2010). Complete genetic correction of ips cells from Duchenne muscular dystrophy. Mol Ther 18: 386–393.

24 Tedesco, FS, Hoshiya, H, D'Antona, G, Gerli, MF, Messina, G, Antonini, S et al. (2011). Stem cell-mediated transfer of a human artificial chromosome ameliorates muscular dystrophy. Sci Transl Med 3: 96ra78.

25 Tedesco, FS, Gerli, MF, Perani, L, Benedetti, S, Ungaro, F, Cassano, M et al. (2012). Transplantation of genetically corrected human iPSC-derived progenitors in mice with limb-girdle muscular dystrophy. Sci Transl Med 4: 140ra89.

26 Kattman, SJ, Witty, AD, Gagliardi, M, Dubois, NC, Niapour, M, Hotta, A et al. (2011). Stage-specific optimization of activin/nodal and BMP signaling promotes cardiac differentiation of mouse and human pluripotent stem cell lines. Cell Stem Cell 8: 228–240.

27 D'Souza, VN, Nguyen, TM, Morris, GE, Karges, W, Pillers, DA and Ray, PN (1995). A novel dystrophin isoform is required for normal retinal electrophysiology. Hum Mol Genet 4: 837–842.

28 Tadayoni, R, Rendon, A, Soria-Jasso, LE and Cisneros, B (2012). Dystrophin Dp71: the smallest but multifunctional product of the Duchenne muscular dystrophy gene. Mol Neurobiol 45: 43–60.

29 Shiba, Y, Hauch, KD and Laflamme, MA (2009). Cardiac applications for human pluripotent stem cells. Curr Pharm Des 15: 2791–2806.

30 An, MC, Zhang, N, Scott, G, Montoro, D, Wittkop, T, Mooney, S et al. (2012). Genetic correction of Huntington's disease phenotypes in induced pluripotent stem cells. Cell Stem Cell 11: 253–263.

31 Oh, Y, Wei, H, Ma, D, Sun, X and Liew, R (2012). Clinical applications of patient-specific induced pluripotent stem cells in cardiovascular medicine. Heart 98: 443–449.

32 Mummery, C, Ward-van Oostwaard, D, Doevendans, P, Spijker, R, van den Brink, S, Hassink, R et al. (2003). Differentiation of human embryonic stem cells to cardiomyocytes: role of coculture with visceral endoderm-like cells. Circulation 107: 2733–2740.

33 Laflamme, MA, Chen, KY, Naumova, AV, Muskheli, V, Fugate, JA, Dupras, SK et al. (2007). Cardiomyocytes derived from human embryonic stem cells in pro-survival factors enhance function of infarcted rat hearts. Nat Biotechnol 25: 1015–1024.

34 Serena, E, Zatti, S, Reghelin, E, Pasut, A, Cimetta, E and Elvassore, N (2010). Soft substrates drive optimal differentiation of human healthy and dystrophic myotubes. Integr Biol (Camb) 2: 193–201.

35 Martone, J, De Angelis, FG and Bozzoni, I (2012). U1 snRNA as an effective vector for stable expression of antisense molecules and for the inhibition of the splicing reaction. Methods Mol Biol 867: 239–257.

36 Serena, E, Cimetta, E, Zatti, S, Zaglia, T, Zagallo, M, Keller, G et al. (2012). Micro-arrayed human embryonic stem cells-derived cardiomyocytes for in vitro functional assay. PLoS ONE 7: e48483.

37 Zatti, S, Zoso, A, Serena, E, Luni, C, Cimetta, E and Elvassore, N (2012). Micropatterning topology on soft substrates affects myoblast proliferation and differentiation. Langmuir 28: 2718–2726.

38 Martewicz, S, Michielin, F, Serena, E, Zambon, A, Mongillo, M and Elvassore, N (2012). Reversible alteration of calcium dynamics in cardiomyocytes during acute hypoxia transient in a microfluidic platform. Integr Biol (Camb) 4: 153–164.

APPENDIX D

HUMAN PLURIPOTENT STEM CELL NUCLEAR SELF-DEFORMATION IN PLURIPOTENCY AND DIFFERENTIATION

Eleonora Grespan[1,2,3,5], Giovanni G. Giobbe[1,2,5], Florent Badique[4], Karine Anselme[4], Jürgen Rühe[3], Nicola Elvassore[1,2]

[1]Department of Industrial Engineering (DII), University of Padua, via Marzolo 9, 35131 Padua, Italy; telephone: +39-049-8275469; fax: +39-049-8275461; e-mail: nicola.elvassore@unipd.it
[2]Venetian Institute of Molecular Medicine (VIMM), via Orus 2, 35129 Padua, Italy
[3]Institut für Mikrosystemtechnik, Chemie und Physik von Grenzflächen, Georges-Koehler-Allee 103, 79110 Freiburg, Germany
[4]Institut de Science des Matériaux de Mulhouse, Université de Haute-Alsace, Mulhouse, France
[5]**These authors contributed equally to this work:** Eleonora Grespan and Giovanni G. Giobbe

Manuscript under preparation

Introduction

Nuclear shape and structure in eukaryotic cells are recognized to be deeply related with cell function during developmental, physiological and pathological modifications (Lombardi et al. 2010, De Vos et al. 2010, Dahl et al. 2010,). The nucleus, while regulating cell division and transcription processes, is exposed to mechanical stimuli from inside and outside the cell. Mechanical stimuli are transmitted by the cytoskeleton to the highly specialized nuclear membrane. The nuclear envelope connects to and interacts with the inner nucleus through the nuclear lamina, a dense protein network also connected to chromatin structure and gene regulatory complexes, which is crucial for structural support of the nucleus. Mechanics of the interphase cell nucleus is of paramount importance for the biological function of healthy cells and it is related to several pathologies (Lee et al. 2007, Hale et al. 2008, Lammerding et al. 2004,).
A growing number of studies try to analyze nuclear mechanics behavior, and there is an emergent topic in scientific research, which investigates the possible relationship between nuclear properties and cancer, pluripotency and mechanotransduction responses (Zink et al. 2004, Davidson et al. 2009 and 2010, Chalut et al. 2012).
Nuclear stiffness has been evaluated and compared in healthy and pathological cells, and a connection between disease and nuclear stiffness was reported (Lombardi et al. 2010, De Vos et al. 2010). Nuclear stiffness seems to increase from human embryonic stem cells to differentiated cells and chromatin is shown to be less condensed in the pluripotent stage (Pajerowski et al. 2007). Few studies consider nuclear mechanics as a property of the nucleus in the cell in connection with the cytoskeleton. Studies on cancer cells show a strong deformation of the cell, and in particular of the nucleus, which adapts to the surrounding micro-topography. Despite such large nuclear deformation, cancer cells are still capable to divide, proliferate and differentiate. It has been demonstrated that this capability to self-deform depends on substrate topography, cell phenotype and cytoskeleton organization (Badique et al. 2013). Interestingly, cancer and stem cells seem to have a comparable nuclear behavior. However, nuclear plasticity and self-nuclear arrangement due to geometric constraints on human pluripotent stem cells during differentiation has never been reported and the comparison between pluripotent cells and cancer cells has not yet been performed.
In this part of the project, the aim was to study human pluripotent stem cell nuclear capacity to self-deform under defined geometrical constraints, meant as the spontaneous nuclear response to the morpho-topological environment. Here is reported how nuclei of human pluripotent stem cells have a high capability to deform and adapt their shape to the geometry of the substrate. Give this, the interest focused on understanding if this strong nuclear deformability could affect

pluripotency and it was shown that pluripotency is not affected by a highly deformed nucleus. Furthermore, we investigate if an highly deformed nucleus can have an influence in the process of early germ layer differentiation. Our results show that the strong nuclear deformation of the nuclei when seeded in microstructured substrates affects the process of differentiation. Studies on stem cells can represent an effective model to evaluate transitions in nuclear plasticity from the pluripotent to the differentiated stage and to elucidate the underlying mechanisms.

Results

Pluripotency maintenance in micropillar cell cultures

To evaluate how nuclear deformability changes in different cell lines, osteosarcoma cells (SaOs-2), hESCs, hiPSCs, cord blood mesenchymal stem cells (CBMSCs) and human epithelial renal cells (hERC) were seeded on matrigel-coated microstructured polymeric substrates characterized by square micropillars with a width of 7 micrometers, an inter-axial distance of 14 micrometers and a height of 7 micrometers. The substrates were fabricated both in polydimethylsiloxane (PDMS) and poly-l-lactic acid (PLLA). PDMS substrates were fabricated through replica molding technique and PLLA substrates through hot embossing technique. Substrate morphology was then characterized by SEM measurements (Fig. 1B). The geometrical structure of the substrates has been designed in order to impose a geometrical constrain to cell body and nucleus: the available space among micropillars is smaller than the average diameter both of cells and cell nuclei.
HOECHST stained cell nuclei of all cell lines were observed through fluorescent microscopy after two days of culture (Fig. 1A). A qualitative analysis of nuclear morphology show how SaOs-2, hESC and hiPSC nuclei strongly deform and assume very unusual shapes, to adapt to the morphology of the environment. HERCs keep a rounder shape, while CBMSCs are characterized by an intermediate behavior, with some nuclei showing concave shape. For each cell line the distribution of the number of concavities (N_c) was also evaluated (Figure 1D): cells that have a lot of concave nuclei that present only one concavity have to be considered less deformable than cells where high number of nuclei show three or four concavities. Lightly deformable cells as CBMSC and hERCs are characterized by nuclei that never present three or four concavities. To quantify this deformability we calculated two parameters, which are related respectively to nuclear penetration below pillar height and to nuclear shape: nuclear deformability (ND) and nuclear concavity (NC). ND has been calculated as the percentage of the nuclear volume that lies below pillar height (Fig. 1C). NC is the percentage of nuclei that present at least one concavity. A concavity is defined as a concave curvature in cell nucleus: concave shapes appear only in deformable nuclei to adapt to pillar interspaces. The calculation of ND show a higher degree of deformability of SaOs-2, hESCs and hiPSCs compared to CBMSCs. HERCs show low deformability (Fig. 1D). These data are consistent with results obtained through the calculation of NC (Fig. 1E). Again, SaOs-2, hESCs and hiPSCs are the cells whose nuclei adapt the most to the morphological environment.
All together these results show that hPSCs have highly deformable nuclei, and this behavior can be compared to results found for cancer cell line SaOs-2. Nuclear deformability is much lower in mesenchymal cells and very strongly reduced in adult somatic cells.

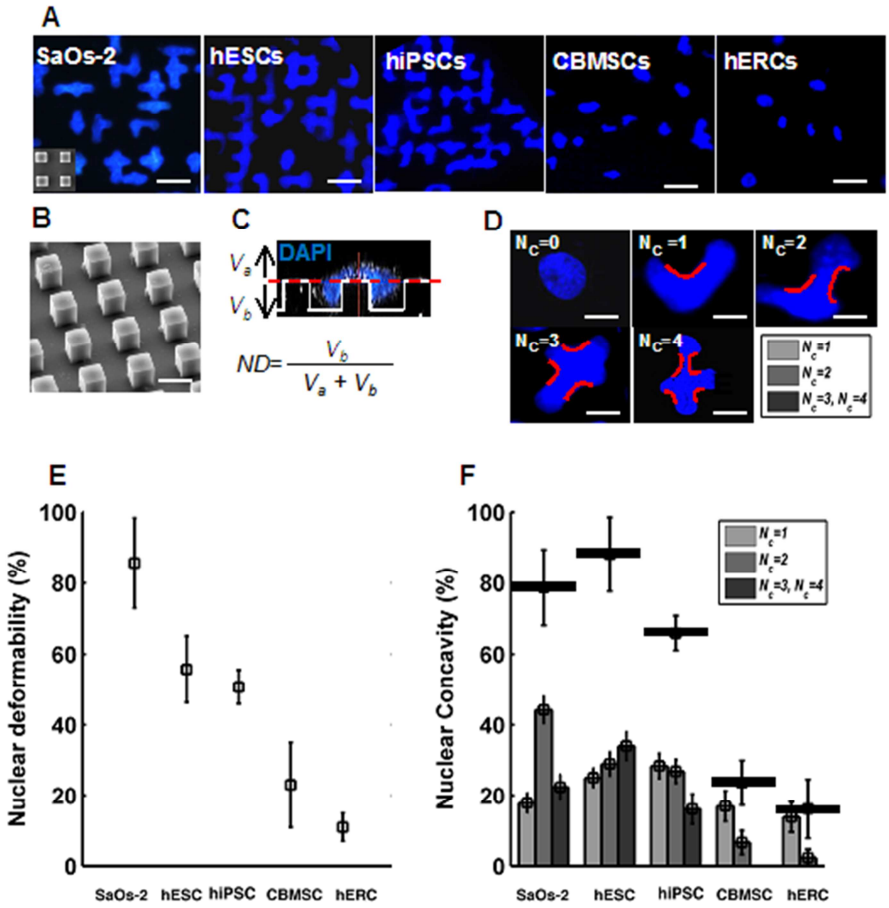

Figure 1. *Evaluation of nuclear deformability for different cell lines.* ***A:*** *HOECHST stained nuclei of SaOs-2, hiPSCs, hESCs, and CBMSCs acquired through fluorescent microscopy at day 2. Images show very deformed nuclei that assume unusual concave and sometimes branched shapes in hESCs, hiPSCs and SaOs-2. hERCs keep a round shape and CBMSCs show an intermediate behavior.* ***B:*** *SEM image of the PDMS microstructured substrates were cells are seeded.* ***C:*** *Confocal image of a fluorescent labeled deformed nucleus: V_b (volume below) is the part of the nucleus which penetrates among pillar interspaces; V_a (volume above) is the part of the nucleus which stays above pillar height. Nuclear deformability (ND) is defined as ND=(V_b/(V_a+V_b))*100.* ***D:*** *Examples of nuclei with 0 concavities (Number of concavities=N_c=0), 1 concavity (Nc=1), 2 concavities (N_c=2), 3 concavities (Nc=3) and 4 concavities (N_c=4). The presence of such concavities in the nucleus is related to nuclear capability to deform.* ***E:*** *Plot of the nuclear deformability values calculated respectively for SaOs-2, hESCs, hiPSCs, CBMSCs and hERCs after fixing the cells at day 2. hESCs , hiPSCs and SaOs-2 present a nuclear deformability above 50%.* ***F:*** *Plot of nuclear concavity, meant as the percentage of cells having N_c>= 1. The histograms show the distribution of the number of nuclear concavities (1 concavity N_c=1, 2 concavities N_c=2, 3 or more concavities N_c=3, N_c=4) calculated among all the concave nuclei for each cell line. This graph show that hESCs, hiPSCs and SaOs-2 present the more deformable nuclei, in particular hESCs and SaOs-2 cell lines.*

After assessing how hESCs have a highly deformable nucleus, we investigated if morphologically deformed nuclei can affect pluripotent cell behavior. First, we evaluated the possible effects on maintenance of pluripotency. HESCs were seeded both in flat (Ctrl) and microstructured (µP) matrigel-coated PDMS substrates, and cultured in expansion medium. After 6 days cells were fixed and immunofluorescence analysis of pluripotency markers Oct-4, Nanog and SSEA4 was performed (Fig. 2A). The analysis shows a comparable expression of the markers between cells expanded in Ctrl and µP substrates. To confirm these data, quantitative real time PCR of pluripotency markers Nanog and Oct-4 was also performed (Fig. 2B). The results from qRT-PCR demonstrate that there is not a significant difference of marker expression between cells

expanded on Ctrl and on µP. Pluripotency is maintained by hPSCs also when the expansion is performed in µP substrates, where cell nuclei present very deformed shapes. Consequently, self-deformation does not affect maintenance of pluripotency. The same experiments were performed on PLLA flat (Ctrl-PLLA) and microstructured (µP-PLLA) substrates and the same results were obtained (data not shown).

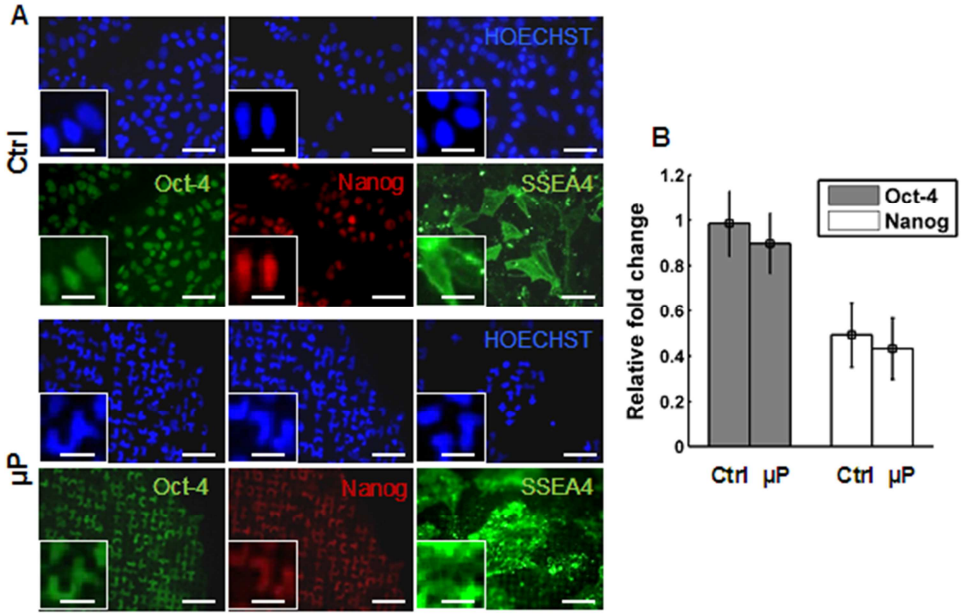

Figure 2. *HESC pluripotency maintenance on microstructured substrates.* ***A:*** *Immunofluorescence panel of cells cultured on flat PDMS substrates (Ctrl), showing pluripotency marker expression of Oct-4, Nanog and SSEA4. Cells cultured on PDMS microstructured substrates (µP). Marker expression between Ctrl and µP is similar. These panels show how nuclear deformation have no effect on pluripotency maintenance.* ***B:*** *qRT-PCR of Oct-4 and Nanog expression in hESCs cultured on flat PDMS (Ctrl) and pillar PDMS substrates (µP), which show comparable expression of pluripotency transcripts between the two conditions. Relative fold expression normalized on GAPDH (n=3).*

Effects of self-deformation during early differentiation

Next, we analyzed if the reorganization of the nuclei morphology can influence the process of differentiation into the three germ layers. Again, we seeded hESCs both in flat (Ctrl) and microstructured (µP) matrigel-coated PDMS substrates. The scheme in Figure 3A shows all the steps that lead to the commitment of the cells into early germ layers. Cells were first expanded for two days in expansion medium to achieve 70-80% cell confluence. Early germ layer specification was induced for 5 days, after which fluorescent labeled nuclei were observed through fluorescent microscopy. Interestingly, nuclei from ectoderm germ layer tend to escape from pillar interspaces and assume a round shape, whereas nuclei from mesoderm and endoderm germ layers still lies among the microstructures keeping deformed shapes. To understand if early germ layer specification took place, we immunolabeled a specific marker for each germ layer: β-III tubulin for ectoderm, brachyury T for mesoderm and α-fetoprotein for endoderm (Fig. 3B). Immunofluorescence early differentiation markers seems normally expressed in µP cells, compared to flat controls, and both in deformed nuclei (meso, endo) and de-deformed nuclei (ecto). To quantitatively assess changes in gene expression due to nuclear deformation, we performed q-PCR to quantify the expression of β-III Tub, Bra-T and AFP for each germ layer, both for ctrl and µP substrates (Fig. 3C). Our analysis shows that the expression of β-III Tub and AFP is comparable between ctrl and µP substrates, whereas there is a significant difference between Bra-T expression in ctrl and µP substrates. Bra-T is very lowly expressed both

in ectoderm and endoderm early germ layers when the protocol of early germ layers specifications are applied on cells cultured on flat substrates (ctrl) whereas there is an usual and significant expression of Bra-T on endoderm germ layer obtained from cells cultured and differentiated on microstructured substrates (μP).

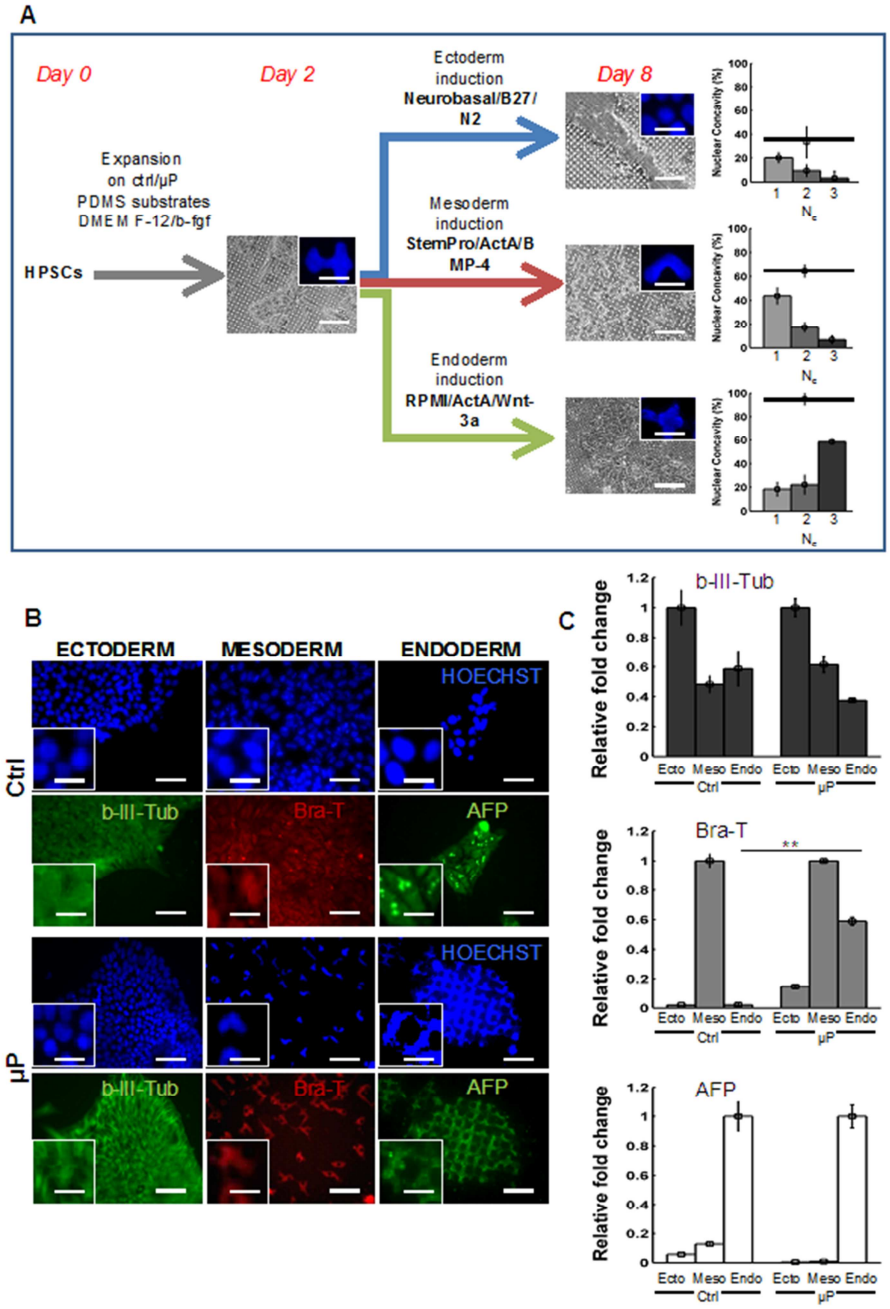

Figure 3. *HESC differentiation on microstructured substrates.* ***A:*** *Schematic showing experimental procedure of early germ layer commitment in hESCs with self-deformed nuclei. Cell are passaged on microstuctured PDMS substrates and expanded for 2 days. Different replicates are then induced with specific media into 3 germ layers for 5 days.* ***B:*** *Immunofluorescence panel showing differentiated hESCs on flat PDMS substrates (Ctrl) and on PDMS substrates (μP). Cells are marked with beta III tubulin for ectoderm, brachyury for mesoderm and alpha-fetoprotein for endoderm. Notably, ectoderm cell nuclei tend to homogeneously emerge from the pillars and gain round shape. Mesoderm and endoderm cells tend to differentiate while maintaining highly deformed nuclei.* ***C:*** *qRT-PCR of early germ layer markers, β-III tub, bry and AFP in the 3 differentiation*

protocols in both flat (Ctrl) and microstructured substrates (μP) . β-III tub is significantly higher expressed in ectoderm flat and pillar differentiation. Bry is significantly higher expressed in mesoderm flat and pillar differentiation, and notably, in endoderm pillar differentiated cells. AFP is significantly high in endoderm flat and pillar differentiation. Relative fold expression normalized on GAPDH (n=3). Student t test p-values P ≤ 0.01 (**).

The nuclear deformation induced by microstructured substrates does not affect mesoderm specification, despite cell nuclei keep a high level of deformation during the all process of differentiation. Ectoderm specification can also take place when cells are seeded on microstructured substrates, but is associated to a strong loss of nuclear deformability by the cells. Endoderm germ layer specification is characterized by strongly deformed nuclei that do not lost their deformability, but this nuclear reorganization hinders the physiological process of differentiation.
Being ectoderm the only germ layer showing major nuclear morphological changes, we decided to further investigate nuclear behavior during differentiation. In Figure 4A is shown a time-course of live-stained HES2 nuclei from pluripotent state at day 0, with highly deformed shapes, to ectodermal commitment ad day 4, with almost entirely round-shaped nuclei. Figure 4B shows nuclear concavity quantification following a day by day measure of percentage concavity. Notably, major shape changes happen between day 1 and day 2, with almost all cells losing self-deformation capacity. It will be necessary to further analyze this results, mainly studying what happens when cells start changing morphology during ectodermal commitment. This will be done through cytoskeletal analyses, with chemical and biological selective inhibitors of specific proteins though to be involved in nuclear and cytoskeletal organization. New results will help to understand how important is nuclear deformation during differentiation and if these properties have specific relevant applications.

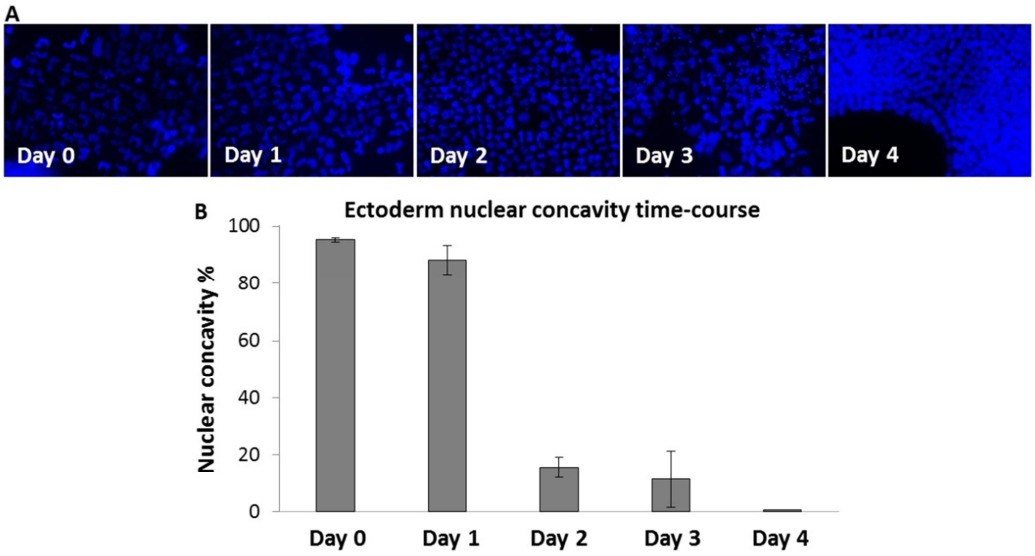

Figure 4. *HESC ectoderm differentiation on microstructured substrates.* ***A:*** *Nuclear morphology evolution from pluripotent state (Day 0) to ectoderm germ layer (Day 4). Nuclei progressively pass from deformed shapes to rounder morphology. B: Nuclear concavity time-course of pluripotent cells (Day 0) induced to ectoderm commitment (Day 4). Major drop of NC % in between day 1 and day 2 of differentiation.*

These first results on pluripotent nuclei self-deformation capacity are important to understand the mechanisms of nuclear properties and plasticity. Further and detailed work has to be done in order to understand how this intrinsic property is important for pluripotency, early germ layer commitment and functional maturation, and to understand if there is a strict connection between pluripotent cells and cancer cells properties.

Material and methods

Substrate fabrication

Polydimethylsiloxane (PDMS, Sylgard 184, Dow-Corning. Midland, MI) microstructurated substrates were fabricated through a replica-molding process. As first step, the negative pattern was prepared through standard photolithography technique: Si-wafers were spin coated with AZ-1518 negative photoresist (MicroChemicals, Germany) for 30 seconds at 2000 rpm and for 5 minutes at 80°C. The photoresist was illuminated with UV light (λ=365 nm) through a chrome-etched mask that consisted of a square lattice (7 µm width) with a lattice constant of 7 µm. Uncross-linked resist was removed rinsing the wafer in an AZ-1518 developer (MicroChemicals, Germany) for 20 s. The obtained microstructurated Si-wafers were subsequently silanized by exposure to the vapor of (tridecafluoro-1,1,2,2-tetrahysrooctyl)-1-trichlorosilane in vacuum for 30 minutes, to facilitate PDMS removal during the replica-molding step. PDMS elastomer was thoroughly mixed with the silicone elastomer curing agent in a 10:1 ratio, poured over the microstructured Si-master and kept under vacuum for 1 h to allow the complete filling of the pattern and air bubbles removal. The sample was then cured at 80°C for 3 hours and subsequently peeled off the Si-wafers. The final micropillar topography was characterized by confocal microscopy and scanning electron microscopy (SEM) (fig. 1). The height of the microstructures was fixed at around 6 µm.

Image analysis

Nuclear deformability

Nuclear deformability is defined here as the capability of the nuclei to penetrate among pillar inter-spaces and it was quantitatively evaluated as the percentage of the nuclear volume which lies below pillar height. The quantification was performed through the use of a MATLAB algorithm that analyzes a set of z-stack confocal images fluorescent labeled(HOECHST) nuclei. The algorithm counts the number of blue pixels in each image and sum all of the pixel from z-stack images above pillar height: this sum represents an approximation of the nuclear volume above pillar height (V_a). Subsequently the algorithms evaluate through the same method the volume below pillar height (V_b). As final step, nuclear deformability (ND) is evaluated as:
$ND=(V_b/(V_a+V_b))*100$
ND was evaluated for at least 50 nuclei for each cell line. The final value is given by the mean and the error bars are the standard deviation among all the analyzed nuclei.

Nuclear concavity

Nuclear concavity (NC) is defined as the capability of cell nucleus to assume unusual concave shapes when it penetrates among pillar interspaces in order to adapt to the available area, and it was quantitatively evaluated as the percentage of nuclei having at least one concavity. A set of confocal images of DAPI stained nuclei (5 to 8 images for each cell line) which were acquired at a height of 3.5 micrometers have been analyzed by a suite of MATLAB algorithms. Nuclear images are first of all turned into black and white, then the contour of the nuclei is found. In the following step a function that calculates the smallest convex area surrounding the nucleus is applied ("convex hull"). Afterwards, the area defined by the nuclear contour is subtracted to the area defined by the convex hull. In presence of nuclear concavities the result of this subtraction is not zero because the convex hull includes also one or more zones that don't belong to the nucleus. In order to avoid to consider as concavity some very small curvatures in the nucleus or some artifacts due to image acquisition, we considered as concavities only the areas with a size equal or bigger than the 10% of the nuclear area. The algorithm also displays were these concave areas are located and it was possible to make a statistics of how many nuclei have just one concavity, two concavities or three or more concavities for each cell line. NC was evaluated for at

least 120 nuclei for each cell line. The final value is given by the mean and the errors bar are the standard deviation among all the analyzed nuclei.

Human pluripotent stem cell expansion and culture on substrates

HESCs (line HES2; National Stem Cell Bank, Madison, WI) and hiPSCs (line ADHF#1; Center for iPS Cell Research and Application, Kyoto University) were cultured in gelatin-coated multiwells with mitomycin C-treated mouse embryonic fibroblasts (MEF; Chemicon) co-culture. Cells were expanded in expansion medium DMEM F-12 (Invitrogen), 20% KO serum (Invitrogen), 10% MEF conditioned medium (not used for hiPSCs), 20 ng/mL basic fibroblast growth factor for hESCs, 10 ng/mL for hiPSCs (b-FGF; Invitrogen), 0.1 mM β-mercaptoethanol (Invitrogen), 1% non-essential amino acid (Invitrogen) and 1% Pen/Strep (Invitrogen). HPSCs were passaged to new feeder using trypsin 0.25% for hESCs (Invitrogen) and CTK solution (trypsin 0.25% - collagenase IV - Ca^{2+}) for hiPSCs. For MEFs depletion, cell expansion and differentiation, cells were passaged on matrigel-coated PLLA and PDMS substrates, both flat and micropillar structured. The hPSC suspension was seeded on each well containing functionalized substrate, and the plates were incubated at 37°C and 5% CO^2 atmosphere, to allow cell adhesion to substrate. For pluripotency maintenance and analysis, we used proper cell seeding concentration to achieve 80-90% confluence cell culture after 4-5 days. HPSCs were cultured with expansion medium changed every day.

HPSCs early germ layer microfluidic differentiation

For early germ layer induction and analysis, we used proper cell seeding concentration to achieve 70-80% cell confluence after 2 days. Ectoderm differentiation was induced with DMEM F-12 and Neurobasal medium (both from Invitrogen), 1:1 ratio, supplemented with B27 1% (Invitrogen), N2 1% (Invitrogen) and β-met 0.1 mM[1,2]. Medium was changed every 2 days. Mesoderm differentiation was induced with StemPro-34 (Invitrogen) supplemented with 2 mM L-glutamine (Invitrogen), transferrin 200 ng/mL, 0.5 mM ascorbic acid (Sigma), activin A 0.3 ng/mL (R&D), BMP-4 3 ng/mL (R&D)[3]. Medium was changed every 2 days. Endoderm differentiation was induced with RPMI1640 containing 1X B27 (both from Invitrogen), 1mM sodium butyrate (Sigma), 100 ng/ml activin A (Peprotech) and 50 ng/mL Wnt3a (R&D)[4] for the first 2 days. The second endoderm medium was KO DMEM with KO serum 20%, L-glutamine 1 mM, NEAA 1%, DMSO 1%, β-met 0.1 mM, P/S 1% for other 3 days. HPSCs specification was induced for 5 days in all three germ layers. A minimum of 6 independent microstructured substrates were used for each experimental conditions.

Immunofluorescence and Real Time PCR

Immunofluorescence analyses were performed on paraformaldehyde 4% fixed cells for 15 min. Blocking and permeabilization was performed with heat inactivated serum 5%, TritonX-100 (Sigma) 0.1% for 1h. Cells were stained using primary antibodies in blocking buffer 1 h room T for pluripotency markers, or overnight 4°C for differentiation markers, depending on the antibody. Immunostaining was done with secondary antibodies Alexa Fluor 488, 594 (Invitrogen) and Hoechst nuclear staining incubation for 1 h at 37°C. Bright fields, immunofluorescence images and merges were taken on Leica DMI 6000 B. The qRT-PCR was performed with TaqMan gene expression assay probes (Invitrogen) according to manufactures instructions, using GAPDH (glyceraldehyde 3-phosphate dehydrogenase), POU5F1 (oct4), NANOG (Nanog), TUBB3 (beta-III tubulin), AFP (alpha-fetoprotein), T (brachyury) probe sets (all from TaqMan Invitrogen). Reaction was done on ABI Prism 7000 machine and results were analyzed with ABI Prism 7000 SDS software. GAPDH expression was used to normalize values of gene expression, and data are shown as relative fold change, with a minimum replicates of n=3 for each experimental condition.

Bibliography

Lombardi ML, Lammerding J. Altered mechanical properties of the nucleus in disease. Nuclear Mechanics and Genome Regulation. 2010;98:121-41.

Dahl KN, Booth-Gauthier EA, Ladoux B. In the middle of it all: Mutual mechanical regulation between the nucleus and the cytoskeleton. J Biomech. 2010 JAN 5;43(1):2-8.

De Vos WH, Houben F, Hoebe RA, Hennekam R, van Engelen B, Manders EM, et al. Increased plasticity of the nuclear envelope and hypermobility of telomeres due to the loss of A-type lamins. Biochim Biophys Acta. 2010 Apr;1800(4):448-58.

Lee JSH, Hale CM, Panorchan P, Khatau SB, George JP, Tseng Y, et al. Nuclear lamin A/C deficiency induces defects in cell mechanics, polarization, and migration. Biophys J. 2007 OCT;93(7):2542-52.

Hale CM, Shrestha AL, Khatau SB, Stewart-Hutchinson PJ, Hernandez L, Stewart CL, et al. Dysfunctional connections between the nucleus and the actin and microtubule networks in laminopathic models. Biophys J. 2008 DEC 1;95(11):5462-75.

Lammerding J, Schulze P, Takahashi T, Kozlov S, Sullivan T, Kamm R, et al. Lamin A/C deficiency causes defective nuclear mechanics and mechanotransduction. J Clin Invest. 2004 FEB;113(3):370-8.

Zink D, Fischer A, Nickerson J. Nuclear structure in cancer cells. Nature Reviews Cancer. 2004 SEP;4(9):677-87.

Davidson PM, Ozcelik H, Hasirci V, Reiter G, Anselme K. Microstructured surfaces cause severe but non-detrimental deformation of the cell nucleus. Adv Mater. 2009 SEP 18;21(35):3586.

Davidson PM, Fromigue O, Marie PJ, Hasirci V, Reiter G, Anselme K. Topographically induced self-deformation of the nuclei of cells: Dependence on cell type and proposed mechanisms. Journal of Materials Science-Materials in Medicine. 2010 MAR;21(3):939-46.

Chalut KJ, Hopfler M, Lautenschlager F, Boyde L, Chan CJ, Ekpenyong A, et al. Chromatin decondensation and nuclear softening accompany nanog downregulation in embryonic stem cells. Biophys J. 2012 Nov 21;103(10):2060-70.

Pajerowski JD, Dahl KN, Zhong FL, Sammak PJ, Discher DE. Physical plasticity of the nucleus in stem cell differentiation. Proc Natl Acad Sci U S A. 2007 OCT 2;104(40):15619-24.

Badique F, Stamov DR, Davidson PM, Veuillet M, Reiter G, Freund J, et al. Directing nuclear deformation on micropillared surfaces by substrate geometry and cytoskeleton organization. Biomaterials. 2013 4;34(12):2991-3001.